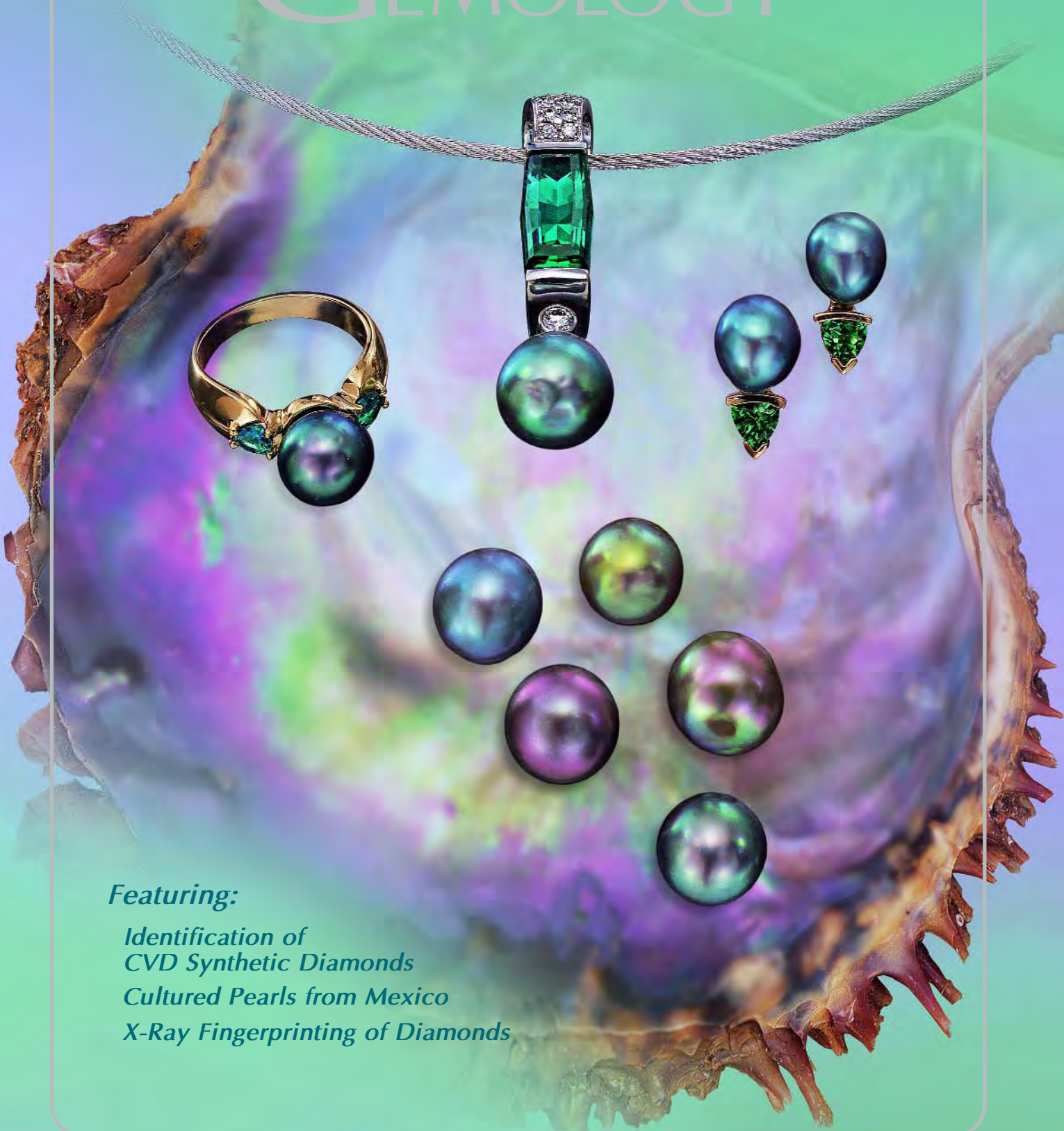


VOLUME XL

SPRING 2004

GEMS & GEMOLOGY



Featuring:

- Identification of
CVD Synthetic Diamonds*
- Cultured Pearls from Mexico*
- X-Ray Fingerprinting of Diamonds*

THE QUARTERLY JOURNAL OF THE GEMOLOGICAL INSTITUTE OF AMERICA



pg. 6



pg. 27

EDITORIAL

- 1 **Gems & Gemology Celebrates Its 70th Anniversary with Recognition by ISI**

Alice S. Keller

FEATURE ARTICLES

- 2 **Identification of Synthetic Diamond Grown Using Chemical Vapor Deposition (CVD)**



Phillip M. Martineau, Simon C. Lawson, Andy J. Taylor, Samantha J. Quinn, David J. F. Evans, and Michael J. Crowder

Presents the results of the DTC Research Centre's studies of more than 1,000 CVD synthetic diamond research samples and the properties that differentiate them from natural diamond.

- 26 **Cultured Pearls from the Gulf of California, Mexico**

Lore Kiefert, Douglas McLaurin Moreno, Enrique Arizmendi, Henry A. Hänni, and Shane Elen

Reports on the production and properties of multicolored cultured pearls harvested from the *Pteria sterna* oyster in Guaymas, Sonora, Mexico.

- 40 **X-Ray Fingerprinting Routine for Cut Diamonds**

Roland Diehl and Nikolaus Herres

Presents an X-ray topographic technique for generating a unique "fingerprint" that can be used to confirm the identity of a faceted diamond.

REGULAR FEATURES

- 58 **Lab Notes**

Feathers in copal • Rare type IIa pink diamond, with green radiation stains • Two yellow synthetic diamonds • Herderite update • Large opal doublet • Three rutilated quartz cat's-eyes • Spurrite • Bicolored cat's-eye tourmaline

- 66 **Gem News International**

2004 Tucson report • Yellow cat's-eye beryl from Brazil • Update on demantoid and cat's-eye demantoid from Iran • Blue omphacite from Guatemala • Black cultured pearls from Japan • New ruby production from Malawi • Pink to pink-orange spinel from Tanzania • Large tsavorite and green grossular from Tanzania • Color-change glass, imitating alexandrite • Commercial production of HPHT-treated diamonds showing a color shift • Update on proprietary diamond cuts • Diamond exhibiting a spectacular phantom • Black horn coral coated with artificial resin • Petroleum inclusions in quartz from Pakistan • New Swarovski triplet loupe • Conference reports • Announcements

- 87 **The Dr. Edward J. Gübelin Most Valuable Article Award**

- 89 **2004 Gems & Gemology Challenge**

- 91 **Book Reviews**

- 94 **Gemological Abstracts**



pg. 51



pg. 61

Celebrates Its 70th Anniversary with Recognition by ISI



his colleagues from the De Beers DTC Research Centre present the results of their study of more than a thousand synthetic diamonds grown by chemical vapor deposition (CVD), and the properties that differentiate them from natural diamonds. Drs. Roland Diehl and Nikolaus Herres describe an X-ray topographic method for “fingerprinting” a cut diamond so that its identity may be confirmed later in the event of loss or theft (or even recutting), while Dr. Lore Kiefert and co-authors shed light on the new cultured pearls from Mexico’s Gulf of California. These feature articles are well complemented by the regular Lab Notes and Gem News International sections, and much more.

When GIA founder Robert M. Shipley released the first issue of *Gems & Gemology* in January 1934, his aim, stated on the first of 32 loose-leaf pages, was to “increase the gem merchant’s knowledge and ability in order that he may protect more thoroughly his customers’ best interests.” Though not the first gemological publication to appear—Great Britain’s *The Gemmologist* began in 1931—*G&G* was introduced at a time when such information was desperately needed. For the most part, jewelry trade magazines of the day did not delve into gemology, and many jewelers and dealers knew very little about the gems they were handling.

Although its early staff was perennially low on budget and manpower, *G&G* was fortunate to enjoy contributions from some of the world’s most distinguished gemologists and mineralogists. Such legends as Basil Anderson, Sydney Ball, Dr. Edward Gübelin, Dr. Edward Kraus, Dr. Karl Schlossmacher, Robert Webster, and Shipley himself, regularly wrote for the journal during its first two decades. That torch eventually was passed to G. Robert Crowningshield, Richard Liddicoat, Dr. Kurt Nassau, and Dr. John Sinkankas, among others, and today it rests in a number of equally capable hands worldwide.

So, despite the many changes in cosmetics and content over the years, the scientific tradition built by the likes of Shipley and Liddicoat continues. In this 285th issue (for those of you doing the math, *G&G* was bimonthly rather than quarterly during its first two years), our contributors represent gemological research from around the world—the United Kingdom, Switzerland, Germany, Mexico, and the U.S.—and report on a range of meaningful topics. In the lead article, Dr. Philip Martineau and

As we celebrate our 70th anniversary, I am delighted to announce another significant milestone. *Gems & Gemology* has been accepted into the database of the Institute for Scientific Information. ISI (www.isinet.com) is widely recognized as the premier database of scientific publications, and its print and online resources are used by libraries and researchers worldwide. This nomination provides *G&G* with a mark of recognition within the scientific community for publishing quality research. Just as important, it raises the visibility and stature of gemology as a scientific discipline, since *G&G* is the first gemological journal to be included in the ISI database. We are very grateful to the authors and reviewers who wrote letters to ISI on behalf of *G&G*, and to those whose contributions over the years have made the journal a vital component of the scientific literature.

Gems & Gemology will be included in the following ISI media, beginning with last year’s Spring issue (Vol. 39, No. 1, 2003): *Current Contents—Physical, Chemical & Earth Sciences*; *Science Citation Index—Expanded*, including the *Web of Science*; and ISI’s current awareness alerting services.

ISI’s recognition is a fitting tribute to gemology, a science that—like *G&G*—has come a long way in the last 70 years.

Alice S. Keller
Editor-in-Chief

IDENTIFICATION OF SYNTHETIC DIAMOND GROWN USING CHEMICAL VAPOR DEPOSITION (CVD)

Philip M. Martineau, Simon C. Lawson, Andy J. Taylor,
Samantha J. Quinn, David J. F. Evans, and Michael J. Crowder

Studies carried out at the DTC Research Centre have shown that single-crystal CVD synthetic diamond is clearly distinguishable from natural diamond. This article presents information about the CVD process, the history of its development, the different kinds of CVD synthetic diamond material that can be produced, and properties that differentiate them from natural diamond. The authors studied more than a thousand CVD synthetic diamond samples that were grown for research purposes using a range of different process conditions. Absorption, photoluminescence, and cathodoluminescence spectra of these CVD synthetic diamond samples showed a range of different impurity-related features not seen in natural diamond. Photoluminescence imaging is also useful in identifying CVD synthetic diamond, and X-ray topography may give supportive evidence. The effectiveness of the Diamond Trading Company Diamond Verification Instruments for identifying CVD synthetic diamond is also described.

Synthetic diamond has occasionally been encountered by the gem trade, but until recently attention has focused almost exclusively on the kind produced by exposing carbon-containing solids to high pressures and temperatures (HPHT-grown synthetic diamond; see, e.g., Shigley et al., 1986, 1987). For many years, however, scientists have known that it is also possible to synthesize diamond at low pressures from carbon-containing gases, using chemical vapor deposition (CVD) techniques. Although the gem trade has been relatively unaware of CVD, over the last two decades this method of diamond synthesis has been the subject of intense worldwide research because of the many potential technological applications of CVD synthetic diamond material.

Apollo Diamond Inc. of Boston, Massachusetts, has spent many years developing CVD synthetic diamond material for use in technological applications and jewelry. In August 2003, this company announced plans to begin selling limited quantities

of faceted material starting in the fourth quarter of 2003 (Pridy, 2003).

Butler et al. (2002) presented analytical results for one faceted sample of single-crystal CVD synthetic diamond produced by Apollo Diamond. Preliminary notes on examination of several Apollo samples appeared in the Gem News International section of the Fall 2003 issue of this journal. Then, in the Winter 2003 issue, Wang et al. gave a thorough description of the results of their study of 13 samples provided by Apollo Diamond, offering useful indicators to aid identification of CVD synthetic diamond of the kind proposed for commercial jewelry production.

Since the late-1980s, the Diamond Trading Company, a De Beers Group company, has carried out proactive research to investigate the implications

See end of article for About the Authors and Acknowledgments.
GEMS & GEMOLOGY, Vol. 40, No. 1, pp. 2–25.
© 2004 Gemological Institute of America

Figure 1. These faceted CVD synthetics (0.21–1.04 ct) range from colorless to brown. Diamond Trading Company faceted CVD synthetics are not commercially available; they have been produced solely for research and education. Photo by M. Crowder.



of CVD diamond synthesis for the gem trade. The purpose of this research has been to develop understanding of the properties of CVD synthetic diamond, so that an effective and practical methodology for distinguishing it from natural diamond could be developed ahead of the marketing of CVD synthetics for jewelry by companies such as Apollo Diamond. As part of these experiments, faceted stones have been produced from some of the synthetic diamond samples (see, e.g., figure 1). As with HPHT-grown synthetic diamond, scientists at the DTC Research Centre in Maidenhead (UK) have developed an advanced understanding of the growth and properties of CVD synthetic diamond. Information from this research program can now be disseminated to help the gem trade in the identification of material of the kind being commercially produced.

The aim of the present article is to provide gemologists with a broader understanding of the CVD process, the history of its development, the different kinds of CVD synthetic diamond material that can be produced, and the properties that differentiate them from natural diamond. Information is presented that will further help gemologists identify the kind of CVD synthetic diamond that is being offered commercially, including the use of Diamond Verification Instruments that have been developed by the Diamond Trading Company.

CVD DIAMOND SYNTHESIS

In contrast to the more widely known HPHT-grown synthetic diamond, CVD synthetic diamond is produced at low pressures, typically in the region of one-tenth of atmospheric pressure, from carbon-con-

taining gases such as methane (see, e.g., Bachmann, 1998; Goodwin and Butler, 1998). This method of synthesis involves breaking up gas molecules into reactive species from which diamond can be grown. This can be done in a number of ways, resulting in a family of related growth techniques.

In perhaps the most common CVD method, the gas molecules (usually methane and hydrogen) are broken apart in a high-temperature plasma generated using microwaves in a reactor of the kind shown schematically in figure 2. Grotjohn and Asmussen (2002) described this method—microwave plasma-assisted CVD—in a recent review. Yehoda (2002), Wolden (2002), and Heberlein and Ohtake (2002) have reviewed other techniques that involve the use of a hot filament, flame, or plasma jet.

CVD synthetic diamond is generally grown on a substrate held at a temperature in the region of 800–1000°C. For many industrial applications, silicon or metal substrates are used and the material grown is polycrystalline, because multiple crystals nucleate with different crystallographic orientations in different positions on the substrate (see, e.g., Wild et al., 1993). It is extremely difficult to polish such material into anything resembling a traditional gemstone. A single-crystal diamond substrate can, however, be used as a template for further single-crystal growth in which synthetic diamond grows with the same crystallographic orientation everywhere on the substrate. This is termed *homoepitaxy*. If grown to a great enough thickness, CVD synthetic diamond produced in this way can be polished into faceted stones for jewelry applications.

HPHT diamond synthesis is typically carried out at temperatures and pressures (in the region of

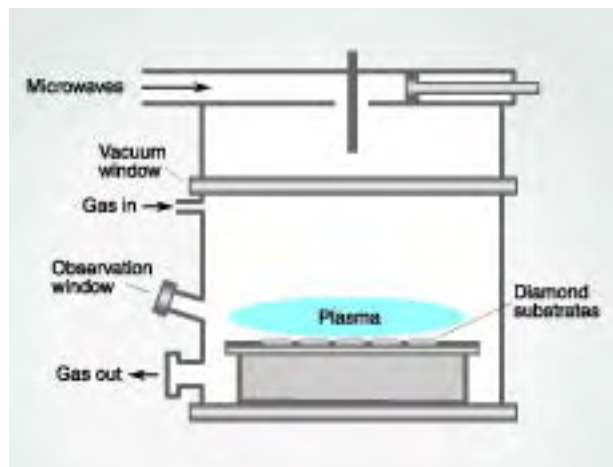


Figure 2. This schematic diagram depicts a microwave CVD reactor of the kind used to grow CVD synthetic diamond. The molecules of the starting gases, usually methane and hydrogen, are dissociated in a plasma that is generated using microwaves. The chemical species created react at the surface of seed crystals (substrates) mounted at the base of the reactor to form CVD diamond material. The diameter of the usable growth area may range between approximately 2 and 20 cm.

1400°C and 55 kbar) at which diamond is the most stable form of carbon. Under the low-pressure conditions used in CVD synthesis, diamond is metastable. This means that it does not spontaneously convert to graphite, although steps must be taken to prevent graphite from forming. Standard CVD processes use a hydrogen-rich gas mixture, and the atomic hydrogen generated in the CVD process has an important role in suppressing the formation of graphite (see, e.g., Goodwin and Butler, 1998).

HISTORICAL BACKGROUND

In 1952, William Eversole, of U.S.-based Union Carbide Corp., demonstrated homoepitaxial growth of diamond at low pressures from a carbon-containing gas (Kiffler, 1956; Eversole, 1962a,b; Angus, 2002). This predates the synthesis of diamond at high pressures and high temperatures (in February 1953) at ASEA in Sweden (see, e.g., Davies, 1984) and (in December 1954) at General Electric Co. in the U.S. (Bundy et al., 1955). Eversole is therefore believed to have been the first person to synthesize diamond by any method.

The CVD growth rates, however, were initially

extremely low, and there was considerable skepticism that they could ever be increased enough to make the process commercially viable. Russian research into low-pressure diamond synthesis, initiated in 1956, led to higher growth rates and demonstrated that CVD synthetic diamond could be nucleated on materials other than diamond (Angus, 2002).

In the early 1980s, a major breakthrough was made in Japan. Matsumoto et al. (1982a,b), researchers at the National Institute for Research in Inorganic Materials (NIRIM), reported CVD synthetic diamond growth rates of over 1 $\mu\text{m}/\text{hour}$ (1 $\mu\text{m} = 0.001 \mu\text{m}$). This development led to worldwide interest in CVD synthesis, stimulated by the various potential industrial applications of CVD synthetic diamond that many scientists believed to be within reach, exploiting diamond's superlative optical, mechanical, thermal, and electronic properties.

In the late 1980s, Element Six (then the De Beers Industrial Diamond Division) started research into CVD diamond synthesis and rapidly became a leader in the field (Valentine et al., 1994; Wort et al., 1994; Sussmann et al., 1994; Coe and Sussmann, 2000), with a substantial portfolio of polycrystalline CVD synthetic diamond industrial products (see, e.g., figure 3). Since the late 1980s, the Diamond Trading Company has made good use of these capabilities to explore the significance of CVD synthetic diamond for the gem trade. Today, through contract research, it continues to use the growth expertise of Element Six in its Consumer Confidence Technical Research Program.

Although the increased growth rates demonstrated at NIRIM represented an important breakthrough for the production of the relatively thin diamond layers necessary for some industrial applications, production of faceted CVD synthetics for jewelry required growth of thick layers of single-crystal diamond material. A 0.5 ct round brilliant has a depth of over 3 mm and, at 1 $\mu\text{m}/\text{hour}$, a CVD layer of this thickness would take almost 18 weeks to grow. Production of thick single-crystal CVD synthetic diamond was therefore still hindered by the low growth rates.

Importantly, there was also a tendency for anything but very thin layers to crack during growth, and some researchers found that the overgrowth often contained rogue crystallites (see, e.g., Tsuno et al., 1994). Some people believed these problems and the low growth rates made CVD synthesis an impractical route for production of single-crystal material thick enough for jewelry applications. Initially, discussion of CVD synthetic diamond in the gem trade

was limited to possible coating of polished natural stones to affect their color. For example, boron-doped CVD synthetic diamond coatings can add a blue color. Surface finish is, however, badly affected and such coated diamond is easily detected (Fritsch et al., 1989). In the 1990s, E. Fritsch reported on the use of polycrystalline diamond to produce novel kinds of jewelry (Johnson and Koivula, 1997), distinct from single-crystal diamond jewelry.

Most research into single-crystal CVD synthetic diamond has involved very thin layers, usually less than 0.1 mm. Beginning in the early 1990s, however, a number of research groups published studies of the growth of somewhat thicker CVD synthetic diamond. For example, researchers at Nijmegen University, the Netherlands, reported flame and hot filament growth of layers up to 0.5 mm thick (Janssen et al., 1990, 1991; Schermer et al., 1994, 1996). In the U.S., Crystallume (Landstrass et al., 1993; Plano et al., 1994) used microwave CVD to produce layers of similar thickness, and Badzian and Badzian (1993) described a layer of single-crystal synthetic diamond that was 1.2 mm thick.

More recently, Linares and Doering (1999) and Yan et al. (2002) described the properties of layers of single-crystal CVD synthetic diamond, and—as

noted above—both Butler et al. (2002) and Wang et al. (2003) presented results of investigations of faceted material produced by Apollo Diamond. Isberg et al. (2002) reported measurements on single-crystal CVD synthetic diamond produced by Element Six that indicated dramatic improvements in the electronic properties, suggesting that this material may have a future in electronic devices. For the remainder of this article, the term *CVD synthetic diamond* should be understood to refer to single-crystal CVD synthetic diamond.

MATERIALS AND METHODS

Materials. There are many process variables that can influence the properties of the CVD material produced. Over the last 15 years, researchers at Element Six have varied the growth process in many different ways to gain a general understanding of the relationship between growth conditions and material properties. The results reported here have been gathered from studies of over a thousand CVD synthetic diamond samples grown by Element Six since the early 1990s as part of the Diamond Trading Company's proactive research program aimed at identifying methods to distinguish CVD synthetics from natural diamond. This research has focused on developing an understanding of how growth conditions affect the properties of the material produced, particularly those that can be useful for identifying CVD synthetic diamond.

The single-crystal CVD synthetic samples for which results are presented here were grown on single-crystal diamond substrates (predominantly HPHT-grown synthetics) processed into plates with the dominant faces being within a few degrees of a cube {100} plane. They may be divided into four categories. First, several hundred samples were grown with nitrogen added to the growth process; for many of these, the nitrogen concentration in the process gases was altered during growth to investigate the effect of such changes. Approximately 50 of these N-doped samples, which were predominantly brown, were given high pressure/high temperature treatments in a belt-type press, under diamond stable conditions, to investigate the effect on their color and other properties. Samples belonging to the third category were grown with small concentrations of diborane (B_2H_6), a source of boron, added to the growth gases in order to produce boron-doped material. The focus of our research has been on looking for any weaknesses in detection methodologies, and

Figure 3. The polycrystalline CVD synthetic diamond optical window shown here was manufactured by Element Six and has a thickness of 0.68 mm. Polycrystalline material has a range of technical uses, but it is extremely difficult to polish into anything resembling a traditional gemstone. Photo courtesy of Element Six Ltd.





Figure 4. High-purity CVD material is colorless, as illustrated by the 0.44 ct ($D-SI_1$) rose cut and 0.82 ct ($E-VVS_1$) round brilliant shown here (left and center), but it is technically more difficult to grow than brown material, such as the 0.85 ct pinkish brown (VVS_1) round brilliant on the right. For relatively thin layers of CVD synthetic diamond, flat cuts give the highest yield, but the ability to grow thicker layers makes brilliant cuts more feasible. Photos by M. Crowder and P. Martineau.

we have therefore moved our process in directions that remove potential detection features. Thus, for the final category of samples, strenuous efforts were made to eliminate all sources of nitrogen and boron impurities from the growth process to produce colorless CVD material of high purity. We believe that categorizing the material we have grown in terms of impurities will bring out the most relevant information for gemologists.

Various samples were processed in three principal ways. More than 200 samples were polished as free-standing CVD plates from which the substrate was removed. Approximately 200 polished cross-sectional slices through CVD layers and their substrates were also produced. Twenty-seven samples were faceted in order to test proposed detection

methods, give information on the grades that are achievable for various kinds of CVD synthetic material, and help educate gemologists. The faceted samples ranged from 0.21 to 2.64 ct and, with the exception of those produced from boron-doped CVD material, from colorless to dark brown (see, e.g., figures 1 and 4). B-doped faceted samples ranged from light blue to intense blue (see, e.g., figure 5).

Methods. Birefringence microscopy was carried out for all the free-standing plates and cross-sectional slices with a Wild M420 microscope equipped with a pair of polarizers.

X-ray topographs (Lang et al., 1992) were recorded, with a 0.25 mm slit width, on Ilford L4 nuclear emulsion using $Mo\ K\alpha_1$ radiation (wavelength: 0.070926 nm) from a Marconi GX20 rotating anode X-ray generator. With this wavelength, use of the $\langle 533 \rangle$ reflection allowed diamond samples to be set up so that the plane sampled by the X-ray beam was very close to a cube $\{100\}$ plane. It also allowed topographs to be recorded with relatively little projection distortion because, at 81.37° , 2θ for the Bragg condition was fairly close to 90° . We recorded X-ray

Figure 5. This 1.03 ct Fancy Deep blue square-cut CVD synthetic (VS_2 clarity, type IIb) was grown with diborane added to the process gases. Photo by M. Crowder.



TABLE 1. Laser and spectrometer systems used in Raman and photoluminescence studies of CVD synthetic diamond.

Wavelength	Laser	Spectrometer system
325 nm	HeCd (60 mW)	JY Horiba Labram Raman system
488 nm and 514 nm	Ar ion (300 mW)	Spex 1404
633 nm	HeNe (27 mW)	JY Horiba Labram Raman system
785 nm	NIR diode (25 mW)	Renishaw 1000 Raman system



Figure 6. The Diamond Trading Company's Diamond Verification Instruments are effective for identifying both HPHT-grown and CVD synthetics. From left to right, this picture shows the DiamondSure, DiamondView, and DiamondPlus instruments. Photo by C. Alderman.

topographs for approximately 150 CVD synthetic diamond samples (both faceted and unfaceted). Of these, approximately a hundred were nitrogen-doped, 20 were boron-doped, and 30 were of high purity. We recorded X-ray topographs in such a way that the beam sampled a cross-sectional slice through the CVD layer and its substrate, using the $\langle 533 \rangle$ X-ray reflection. We also obtained $\langle 533 \rangle$ X-ray section topographs parallel and perpendicular to the growth direction for faceted synthetic samples.

Absorption spectra were recorded for almost all the free-standing plates and many of the cross-sectional slices. Perkin Elmer Lambda 9 and Lambda 19 spectrometers were used to record absorption spectra in the ultraviolet, visible, and near-infrared regions of the spectrum. A Nicolet Magna-IR 750 FTIR spectrometer was used to cover the range between $11,000 \text{ cm}^{-1}$ and 400 cm^{-1} .

Photoluminescence and Raman spectra were recorded for five different laser excitation wavelengths (table 1). At each wavelength of excitation, at least 10 samples were investigated for each of the four categories of CVD synthetic diamond material mentioned above. Observations of luminescence excited by ultraviolet radiation were made for all of the faceted stones in a darkened room using conventional long-wave (365 nm) and short-wave (254 nm) Ultraviolet Products lamps.

Cathodoluminescence (CL) topographs were recorded using a CLmk4 (Cambridge Image Technology Ltd.) and a Wild M420 microscope equipped with a digital camera. CL spectra were recorded using a Cambridge Instruments 336 SEM equipped with an Oxford Instruments MonoCL spectrometer. For each

of the four categories of CVD synthetic diamond material mentioned above, at least 10 samples were investigated using CL topography and spectroscopy.

All of the faceted stones were tested on all three Diamond Trading Company Diamond Verification Instruments (figure 6). Earlier versions of DiamondSure and DiamondView, which were developed for identification of HPHT-grown synthetics, were described in a *Gems & Gemology* article by Welbourn et al. (1996) and are in use in gemological laboratories worldwide. These instruments have now been significantly improved and are commercially available from GIA Instruments UK Ltd. A third instrument, DiamondPlus, has been developed to help with the detection of HPHT-treated type II diamond (Welbourn and Williams, 2002).

DiamondSure is a compact instrument that produces a "Pass" or "Refer" result on the basis of an absorbance measurement across the visible and ultraviolet regions of the spectrum. "Pass" indicates that the stone is a natural diamond that requires no further testing. "Refer" means that further testing is required to determine whether the stone is synthetic or natural. Tests on more than 300,000 natural diamonds and several hundred HPHT-grown synthetic diamonds have indicated that DiamondSure refers only 1–2% of natural diamonds, but it refers *all* HPHT-grown synthetics.

Photoluminescence (PL) images were recorded with a DiamondView that has been improved in a number of ways that will be detailed in a future article. This instrument exposes polished stones to short-wave UV radiation and records a digital image of the resulting surface luminescence. It may also be used to

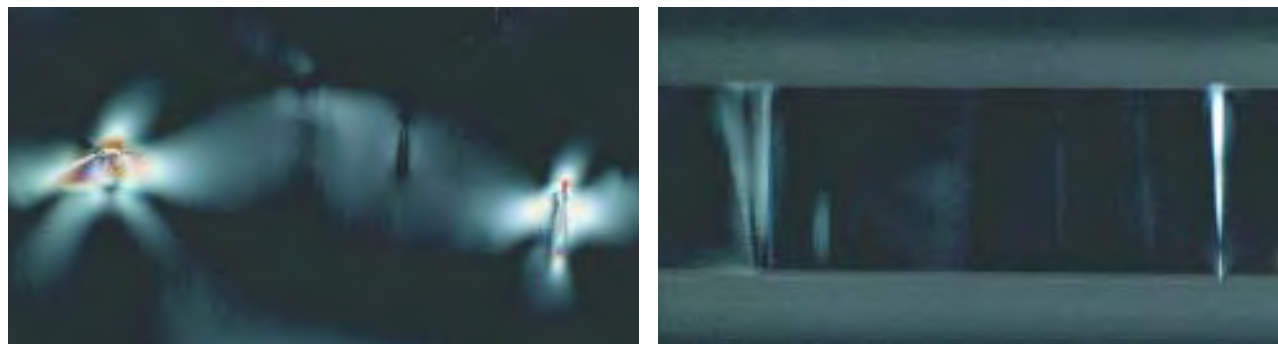


Figure 7. These photomicrographs of a free-standing tabular plate of CVD synthetic diamond (1.06 mm thick) were recorded with crossed-polarizers in a viewing direction parallel (left) and perpendicular (right) to the growth direction. The optical path lengths were 1.06 mm and 4.02 mm, respectively. The regions of anomalous birefringence run through the sample in a direction parallel to the growth direction. Such birefringence is believed to result when bundles of dislocations nucleate at or near the interface with the substrate and propagate in the growth direction as the layer grows. Photos by A. Taylor.

record phosphorescence images. The DiamondView was used to investigate the spatial distribution of both PL and phosphorescence for all but a small number of the samples produced for this study.

The new DiamondPlus is a compact instrument designed to make high-sensitivity, low-temperature photoluminescence measurements on polished stones immersed in liquid nitrogen. It contains two solid-state lasers and two miniature spectrometers. Each measurement takes about 20 seconds, and a result is then displayed on the screen.

RESULTS

Most of our results are presented under headings of the four main categories of CVD synthetic diamond material that we investigated. We start, however, with two general sections. The first describes results relating to gemological features that we observed using microscopy in some samples from each of the four varieties of material. It is important to stress, however, that many of the samples we investigated showed none of these features. The second summarizes results from X-ray topography studies in which characteristic contrast features were seen for all the samples in all four categories that we investigated.

General Gemological Features. Birefringence. The samples of CVD synthetic diamond we investigated often showed characteristic birefringence features. The photomicrographs in figure 7 show views of a free-standing plate of CVD synthetic diamond, with six cube {100} faces, seen with crossed polarizers from perpendicular directions. Characteristic birefringence features showing higher-order colors can be seen in the micrograph recorded with the view-

ing direction parallel to the growth direction. The strongest birefringence occurs with this viewing direction even though it gives the shortest path length. From the cross-sectional view, it can be seen that the corresponding regions of strain run all the way through the sample along the growth direction.

Figure 8. In this X-ray section topograph of a 2-mm-thick layer of CVD synthetic diamond on a type Ib HPHT-grown synthetic substrate, a cross-sectional slice parallel to the growth direction has been sampled. The columnar texture is caused by dislocations and is typical of CVD synthetic diamond, but it is not always seen in such an extreme form. The interface between the substrate and the CVD layer is clearly evident from the abrupt change in contrast. Features such as these in X-ray topographs may be used as evidence to support identification.



Crystallographic Orientation. We have found that, in CVD processes, growth on octahedral {111} faces is problematic because there is a tendency for twins to form. Regions of samples that contained one or more twins were difficult to polish, had a tendency to crack, and were generally of lower optical quality. Most of the CVD synthetic diamond material that we investigated was grown on substrates with faces in near-cubic orientation, and octahedral growth faces had a tendency to form at the four corners. The resulting four regions of lower-quality diamond often limited the yield and clarity grade of faceted stones. Cracks, graphitic inclusions, or poor surface finish were sometimes seen in one or more of the four positions, typically near the girdle.

Layers with Different Colors. In many of the samples we investigated, we observed layers with different colors. When present, such layers were easily seen in cross-sectional slices or free-standing plates with polished faces. They were more difficult to discern for faceted CVD synthetic stones. In our experience, layers with different brown colors were most common but, for samples doped with boron, we also observed layers with different blue colors. For the most part, such layers formed parallel to the plane presented by the substrate, with deviations near the edges resulting from the formation of additional growth faces.

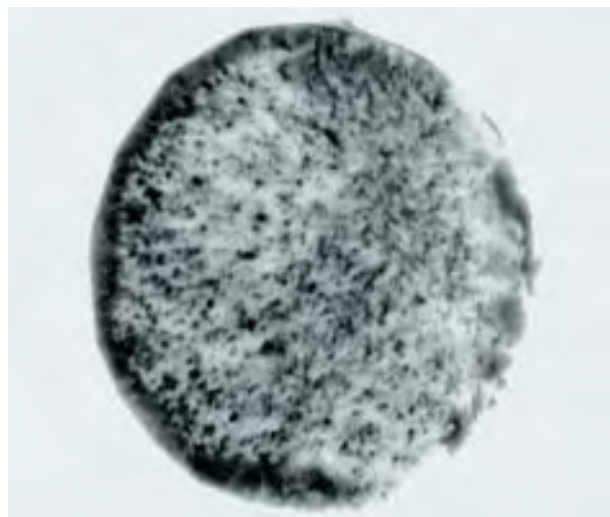
Figure 9. The columnar texture is also evident in this X-ray section topograph of a faceted CVD synthetic (girdle diameter 5.5 mm), in which a cross-sectional slice parallel to the growth direction was sampled by the X-ray beam.



Inclusions. We observed inclusions in only a few of our samples. In those rare cases, for the most part they appeared as groups of pinpoint inclusions lying in planes parallel to the interface between the CVD layer and the substrate on which it was grown. On the basis of Raman scattering, these pinpoint inclusions could generally be associated with non-diamond carbon.

X-ray Topography. X-ray topographs for samples from each of the four categories of CVD synthetic diamond material showed striking similarities, and the results are therefore reported together here. Cross-sectional topographs through a CVD layer and its substrate showed contrast features similar to those seen in figure 8, but not generally in such an extreme form. A change in contrast relating to the position of the interface between the substrate and the CVD layer was clearly visible. All the cross-sectional topographs recorded parallel to the growth direction showed contrast streaks similar to those observed in figure 9. Within each of the four categories of samples, the plan-view topographs revealed different kinds of contrast, ranging from the type of features seen in figure 10 to a more poorly defined cross-hatch pattern.

Figure 10. In this X-ray section topograph of the faceted CVD synthetic shown in figure 9, the X-ray beam sampled a plan-view slice through the girdle and perpendicular to the growth direction. The dark spots are believed to be caused by bundles of dislocations aligned close to perpendicular to the plane sampled by the X-ray beam.



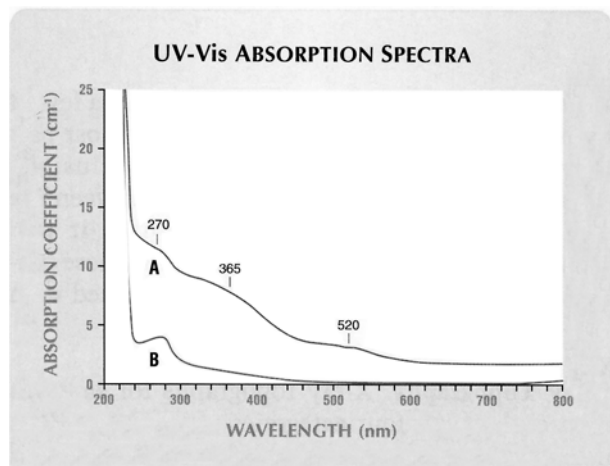


Figure 11. Absorption spectrum A, of an initially brown layer of nitrogen-doped CVD synthetic diamond, is typical of the spectra recorded at room temperature for this material. It shows broad features at 270 nm and approximately 365 and 520 nm. After an HPHT treatment that removed the brown color from this same specimen, the spectrum (B) shows no evidence of the features at about 365 and 520 nm.

Samples Grown with Added Nitrogen. After removal of their substrates, samples grown with added nitrogen were found to range from faint brown to dark brown (or black in extreme cases). For a given sample thickness, there was a strong correlation between the nitrogen concentration in the process gases and the saturation of the brown color. Moreover, when the nitrogen concentration in the process gases was changed during a growth run, examination of polished cross-sections produced from the samples grown showed that layers with different brown colors resulted, as described above. For most of the samples that we investigated, no nitrogen-related absorption could be detected in the one-phonon region of the infrared spectrum and the material was therefore classified as type II (for details of diamond classification by type, see Shigley et al., 1986). In rare cases, absorption features were observed at 1344 cm^{-1} and 1130 cm^{-1} , indicating the presence of isolated nitrogen atoms (see, for example, Clark et al., 1992). In these rare cases, the material was classified as type Ib.

UV-visible absorption spectrum A in figure 11 was recorded at room temperature for a typical free-standing plate of CVD synthetic diamond grown with nitrogen added to the gas mixture. Broad features may be seen at 270 nm and approximately 365 and 520 nm. In addition to these, there is a general rise in absorption coefficient toward shorter wavelengths. Table 2 lists features that we

have observed in the optical absorption spectra of samples grown with added nitrogen. Many of these lines have been reported previously for samples produced by Apollo Diamond (Butler et al., 2002; Wang et al., 2003). However, we observed an additional absorption feature at 3323 cm^{-1} in the spectra of dark brown samples that was not reported by either of the above studies.

Figure 12 shows the photoluminescence spectrum of a brown CVD synthetic diamond sample excited at liquid nitrogen temperature with a 514 nm Argon ion laser. It exhibits PL systems with zero-phonon lines at 575 and 637 nm that were present in the spectra of all the nitrogen-doped samples we investigated. It also shows a pair of sharp lines at 596 and 597 nm that we have observed only for nitrogen-doped samples. Samples grown early in our research program showed a line at 737 nm (also reported for Apollo Diamond's CVD synthetic material [Wang et al., 2003]), but this feature was absent from the spectra of samples grown more recently.

Spectrum A in figure 13 is the PL spectrum of an as-grown nitrogen-doped CVD synthetic diamond sample excited using a 325 nm HeCd laser at 77 K. It shows lines at 467, 533, and 575 nm. The 533 nm and 575 nm lines were observed for all nitrogen-doped

Figure 12. This photoluminescence spectrum of a nitrogen-doped CVD synthetic diamond sample, excited at 77 K with 514 nm argon ion laser radiation, shows zero-phonon lines at 575 and 637 nm. The spectrum also contains a pair of lines at 596 and 597 nm. First reported by Wang et al. (2003), to the best of our knowledge these two lines have never been detected for natural diamond or HPHT-grown synthetic diamond.

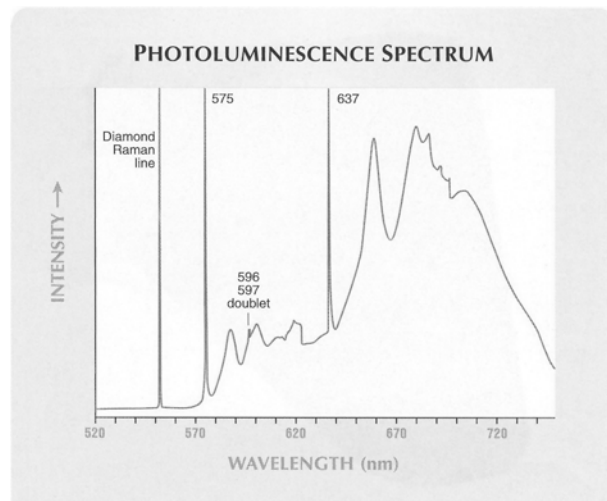


TABLE 2. Common features observed in the spectra of some as-grown and HPHT-treated nitrogen-doped CVD synthetic diamond.^{a,b}

Feature	Method	Notes/comments
270 nm	UV-Vis-NIR absorption spectroscopy	Associated with isolated nitrogen; also seen in type Ib HPHT-grown synthetic diamond and in some HPHT-treated type IIa natural diamond.
Ramp	UV-Vis-NIR absorption spectroscopy	Gradual rise in absorbance toward shorter wavelengths. Seen across the UV, visible, and NIR regions of the spectrum. Removed by HPHT treatment. A similar rise is sometimes seen in type IIa natural diamond.
365 nm	UV-Vis-NIR absorption spectroscopy	Broad band not seen in natural diamond or HPHT-grown synthetic diamond. Removed by HPHT treatment.
389 nm	PL spectroscopy (325 nm excitation) and CL spectroscopy	Removed by HPHT treatment. Also seen in some HPHT-grown synthetic diamond and in radiation-damaged N-containing diamond.
415 nm	CL and PL spectroscopy (325 nm excitation)	HPHT-treated CVD synthetic diamond. N3 center associated with nitrogen; also observed in natural diamond.
451–459 nm series of lines	PL spectroscopy (325 nm excitation)	Observed only in HPHT-treated CVD synthetic diamond.
467 nm	PL spectroscopy (325 nm excitation) and CL spectroscopy	Not seen in natural or HPHT-grown synthetic diamond; removed by HPHT treatment.
503 nm	PL spectroscopy (325 nm excitation)	HPHT-treated CVD synthetic diamond. H3 center associated with nitrogen; also observed in some natural diamond and HPHT-grown synthetic diamond.
520 nm	UV-Vis-NIR absorption spectroscopy	Broad band not seen in natural diamond or HPHT-grown synthetic diamond. Removed by HPHT treatment.
533 nm	PL spectroscopy (325 nm excitation) and CL spectroscopy	Not seen in natural or HPHT-grown synthetic diamond. Removed or substantially reduced by HPHT treatment.
575 nm	PL spectroscopy (325, 488, and 514 nm excitations) and CL spectroscopy	NV ⁰ center; reduced but still readily detectable after HPHT treatment. Also seen in some HPHT-grown synthetic diamond and some natural type IIa diamond.
596 nm	UV-Vis-NIR absorption spectroscopy	Observed in absorption spectra of some brown CVD synthetic diamond and not seen in natural diamond. Removed by HPHT treatment. Line-width comparison indicates that this has a different origin from the 596 nm PL line.
596/597 nm doublet	PL spectroscopy (488 and 514 nm excitations)	Narrow PL lines not seen in natural or HPHT-grown synthetic diamond. Not observed after HPHT treatment.
625 nm	UV-Vis-NIR absorption spectroscopy	Observed in some brown CVD synthetic diamond and not seen in natural or HPHT-grown diamond. Removed by HPHT treatment.
637 nm	UV-Vis-NIR absorption spectroscopy and PL spectroscopy (488 and 514 nm excitations)	NV ⁻ center; seen in absorption and PL spectra of some natural and HPHT-grown synthetic diamond.
737 nm	UV-Vis-NIR absorption spectroscopy and PL spectroscopy (488, 514, & 633 nm excitations)	Si-related; not seen in more recently grown (Element Six) samples of CVD synthetic diamond, and not seen in natural diamond; seen in HPHT-grown synthetic diamond when silicon is deliberately added to the growth capsule. Not removed by HPHT treatment.
8753, 7354, 6856, 6524, 5564 cm ⁻¹	FTIR (or NIR) absorption spectroscopy	H-related; not seen in natural or HPHT-grown synthetic diamond. Removed by HPHT treatment.
3323 cm ⁻¹	FTIR absorption spectroscopy	H-related; seen in some brown CVD synthetic diamond. Not seen in natural or HPHT-grown material. Removed by HPHT treatment.
3123 cm ⁻¹	FTIR absorption spectroscopy	H-related; not seen in natural or HPHT-grown synthetic diamond. Removed by HPHT treatment.
3107 cm ⁻¹	FTIR absorption spectroscopy	H-related. Appeared after HPHT treatment. Seen in some natural diamond.
2800–3000 cm ⁻¹	FTIR absorption spectroscopy	C-H stretch vibrational modes (see, for example, Fuchs et al. [1995]); not seen in natural diamond and rarely seen in HPHT-grown synthetics. ^c
1540 cm ⁻¹	Raman/PL spectroscopy (785 nm excitation)	Non-diamond carbon; removed by HPHT treatment.

^aNone of these features is present in the spectra of all CVD synthetic diamond, and it is possible to grow CVD synthetic material that does not show any of these features.

^bMore information on many of these spectroscopic features is given by Zaitsev (2001).

^cAll type IIb diamond, whatever its origin, shows B-related lines at 2802 and 2928 cm⁻¹. For a typical example, see King et al. (1998), p. 252.

samples. The 467 nm line was observed for some, but not all, nitrogen-doped samples. When present in the PL spectrum of a sample, the lines at 467, 533, and 575 nm were also observed in the cathodolumines-

cence spectrum. Table 2 also lists the PL features observed most commonly for the nitrogen-doped CVD synthetic diamond samples we studied.

Cross-sectional slices through layers on HPHT-

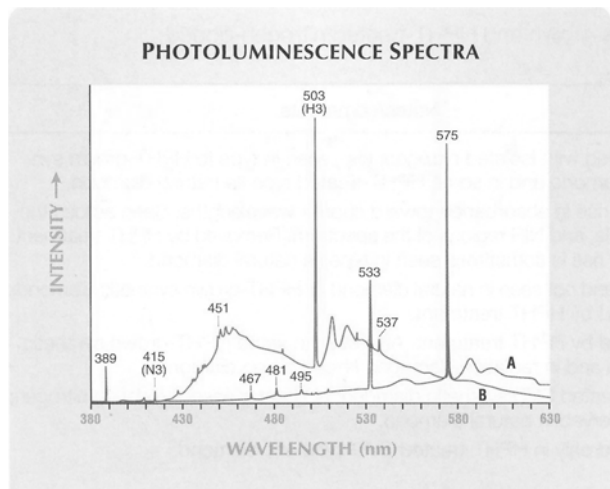
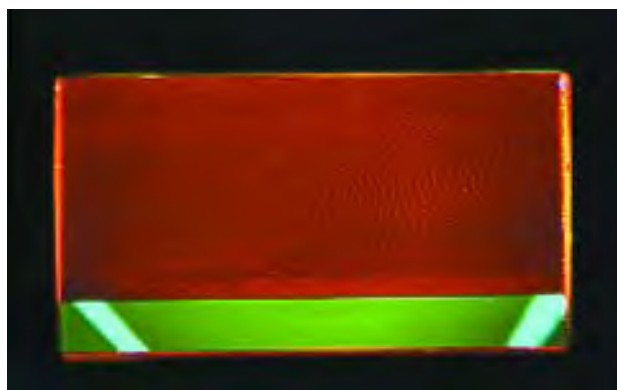


Figure 13. These photoluminescence spectra, excited at 77 K using 325 nm HeCd laser radiation, were collected from an initially brown N-doped CVD synthetic diamond sample. Spectrum A, of the as-grown sample, shows zero-phonon lines at 467 and 533 nm, which to the best of our knowledge have never been detected for natural or HPHT-grown synthetic diamond. These are also commonly seen in the cathodoluminescence spectrum of CVD synthetic diamond. Spectrum B, recorded after HPHT treatment removed the sample's brown color, shows H3 and N3 luminescence at 503 and 415 nm, respectively. It also shows a group of features between 451 and 459 nm that we believe have not been previously reported.

grown type Ib substrates showed clear color zoning (see figure 14, left). Orange to orangy red luminescence was observed in the DiamondView images of

Figure 14. Color zoning is obvious in this polished cross-sectional slice through a CVD synthetic diamond layer on its HPHT-grown synthetic substrate (left). Although predominantly yellowish green, the type Ib HPHT-grown substrate has two sectors with less color. The sample is 6 mm long, and CVD growth beyond the edges of the substrate has been removed. In a DiamondView image of the same slice (right), the CVD layer shows the orange to orangy red luminescence typically seen for N-doped samples, as well as the characteristic striations (the circular pattern is from the vacuum holder). These striations are a result of different uptake of defects on the risers and terraces of steps on the growth surface. Photos by A. Taylor.



all the nitrogen-doped samples that we investigated (see, e.g., figure 14, right). In addition, all samples were observed to have striations (which run diagonally in figure 14, right) that were seen most easily in cross-sectional slices. In some samples, the striations were spaced too closely to be visible in the DiamondView images, but they were always evident in CL topographs recorded at higher magnification. The spacing between striations was fairly constant within a given sample, but it ranged from approximately 0.001 mm to 0.2 mm between samples.

The growth surface of nitrogen-doped samples invariably showed sequences of growth steps with terrace regions separated by inclined risers. There was a correspondence between the striation spacing for a given sample and the spacing between steps that formed on the growth surface during the CVD process. When traced to the growth surface, the striations observed in cross-sectional slices were found to terminate at the risers and terraces of such growth steps. Figure 15 illustrates schematically how these striations are formed.

Table 3 lists the weight, color, and clarity grades (as determined in our laboratory using the GIA grading scales) and fluorescence to long- and short-wave UV of our 14 faceted nitrogen-doped CVD synthetics. All the samples tested with the DiamondSure gave a "Refer" result. In the DiamondView, all those tested showed orange to orangy red luminescence. In eight cases, striations were observed in the DiamondView images (figure 16). In all cases, the 575 and 637 nm

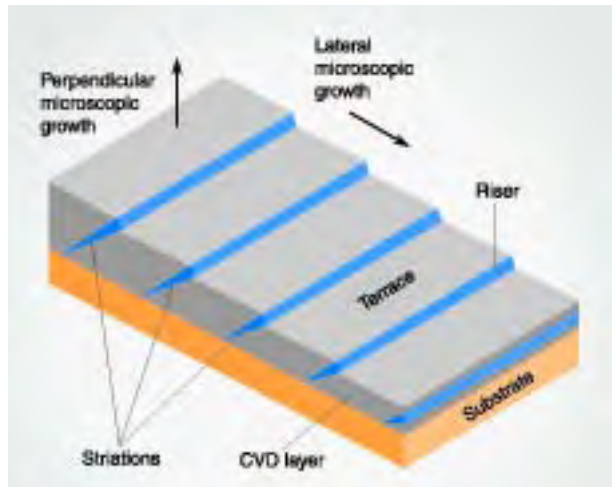


Figure 15. This schematic diagram shows part of a CVD synthetic diamond layer polished to reveal cross-sectional views. It illustrates the early development of striations caused by differential uptake of impurity-related defects on the risers and terraces (here blue and gray, respectively) of surface steps.

luminescence features were observed in PL spectra excited at 77 K with a 514 nm argon ion laser and were also detected by the DiamondPLus.

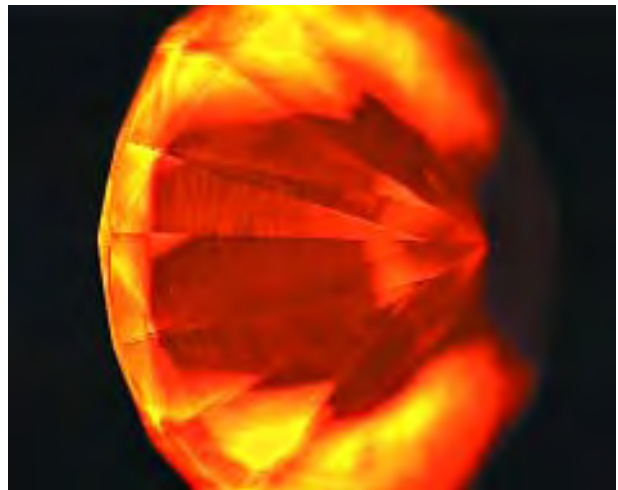


Figure 16. The orange luminescence and striations were also seen in the faceted CVD synthetics, as evident in this DiamondView image of a 0.85 ct CVD synthetic round brilliant. Photo by P. Martineau.

HPHT-Treated CVD Synthetic Diamond. In all the cases investigated, UV-visible absorption spectroscopy revealed that HPHT treatment of brown nitrogen-doped CVD synthetic diamond under diamond stable conditions reduced the overall

TABLE 3. Weights, grades, and fluorescence reactions of 14 faceted nitrogen-doped CVD synthetic diamond samples (produced for research and education only).

Sample number	Carat weight	Cut	Color	Clarity	UV fluorescence	
					Long-wave	Short-wave
N1	0.63	Round brilliant	Brown	I ₁	Weak orange	Weak orange
N2	0.90	Round brilliant	Fancy pinkish brown	I ₃	Orange	Orange ^a
N3	0.34	Square cut	G	VS ₁	Weak orange	Weak orange
N4	0.50	Square cut	H	VS ₂	Weak orange	Weak orange
N5	1.04	Square cut	Fancy Dark brown	SI ₁	Orange	Orange ^a
N6	1.10	Square cut	Fancy Light pinkish brown	VS ₁	Orange	Orange ^a
N7	1.04	Square cut	Fancy pinkish brown	I ₁	Orange	Orange ^a
N8	0.85	Round brilliant	Fancy brownish pink	VVS ₁	Orange	Orange ^a
N9	0.50	Square cut	Fancy Light pinkish brown	VS ₁	Orange	Orange
N10	0.38	Emerald cut	Fancy Light pinkish brown	VVS ₁	Orange	Orange
N11	0.50	Round brilliant	Brown	VS ₁	Weak orange	Weak orange ^a
N12	0.55	Round brilliant	Brown	SI ₂	Weak orange	Weak orange ^a
N13	0.39	Princess cut	Brown	SI ₁	Weak orange	Weak orange ^a
N14	2.23	Rectangular step cut	Pinkish brown	I ₁	Orange	Orange

^aStriations were observed in DiamondView images of these samples.



Figure 17. These photographs illustrate how two N-doped CVD synthetic diamond samples that started as brown (top left, $3.06 \times 2.06 \times 0.86 \text{ mm}^3$) and black (bottom left, $1.52 \times 1.34 \times 0.94 \text{ mm}^3$) responded to HPHT treatment (right). Photos by A. Taylor.

absorption in the visible and ultraviolet regions of the spectrum. All of these samples showed a corresponding reduction or change in color. Figure 17 shows how HPHT treatment affected the color of two samples: one brown and the other black. After treatment, the brown sample was nearly colorless and the black sample had become a pale greenish brown.

We recorded UV-visible absorption spectra for the same region of a brown sample before and after HPHT treatment (again, see figure 11). Note that the broad features at approximately 365 nm and 520 nm were removed by the treatment, and there was also a substantial reduction in the general rise in absorption toward shorter wavelengths. The shape of the post-treatment spectrum is very similar to that for the absorption caused by a low concentration of isolated nitrogen atoms.

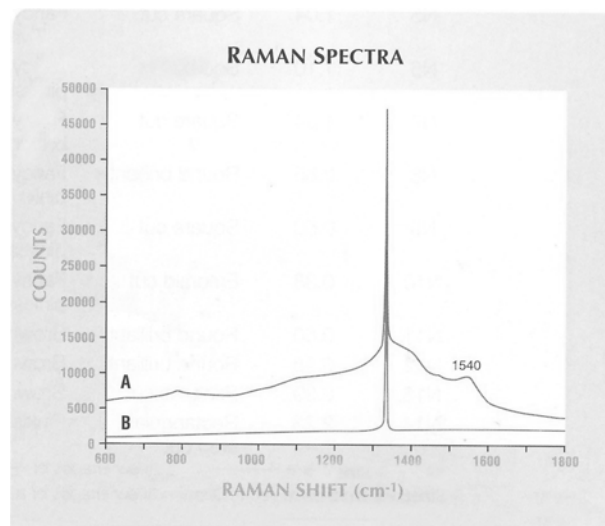
HPHT treatment of brown CVD synthetic samples also caused a change in the hydrogen-related features in their infrared absorption spectra (again, see table 2). For example, it removed the hydrogen-related absorption lines in the near-infrared region of the spectrum and at 3123 cm^{-1} and 3323 cm^{-1} . In most cases, a hydrogen-related line at 3107 cm^{-1} ,

seen in the absorption spectra of some natural diamonds (Woods and Collins, 1983), was observed after HPHT treatment.

We also recorded Raman/photoluminescence spectra (at room temperature, with 785 nm excitation; figure 18) for the same region of a sample before and after HPHT treatment that substantially reduced the absorption in the visible and ultraviolet regions. The feature at approximately 1540 cm^{-1} in the spectrum recorded before treatment indicates the presence of non-diamond carbon. The spectrum of the post-treatment sample contains only the diamond Raman line and shows no evidence of non-diamond carbon.

Figure 13 shows PL spectra for this sample as recorded at liquid nitrogen temperature with 325 nm excitation before and after HPHT treatment. Although substantially reduced by the treatment, the 575 nm luminescence feature remained readily detectable. Other features in the initial spectrum, such as the line at 467 nm, were removed during annealing. The features at 503 nm and 415 nm are the H3 and N3 centers respectively (see, e.g., Zaitsev, 2001, pp. 262–272 and 320–323), which are very commonly observed in natural nitrogen-containing diamond. In addition, the post-treatment spectrum contains a series of lines in the 451–459

Figure 18. The feature at approximately 1540 cm^{-1} that was present in the Raman spectrum of this brown N-doped CVD synthetic diamond sample before treatment (A) was completely absent (B) after HPHT treatment removed the brown color. These spectra were recorded at room temperature with 785 nm excitation.



nm region that we have only observed for HPHT-treated CVD synthetic diamond. In all cases where the starting material showed the 737 nm luminescence feature with 633 nm excitation, this was still readily detectable after HPHT treatment, as noted by Wang et al. (2003). We never observed the pair of lines at 596 and 597 nm for HPHT-treated samples.

Whereas DiamondView images of as-grown samples showed orangy red luminescence, the images recorded after annealing were dominated by green luminescence (see, e.g., figure 19). Striations similar to those observed in DiamondView images of as-grown material were still visible after treatment.

Boron-Doped CVD Samples. All the CVD synthetic diamond samples grown from gas mixtures containing diborane showed colors equivalent to a range from Fancy Light grayish blue to Fancy Deep blue (again, see figure 5). All had optical absorption properties typical of type IIb diamond (see King et al., 1998). The color arose from boron-related absorption extending into the visible part of the spectrum, with decreasing absorption from the red to the blue. None of the samples we examined showed any of the impurity-related (i.e., N, H, or Si) features we observed in the absorption or PL spectra of nitrogen-doped CVD synthetic diamond.

As-grown samples exhibited octahedral {111} growth faces and, for any given sample, the resulting {111} growth sectors showed a more intense blue color than {100} sectors formed above the cube {100} surface of the substrate. SIMS analysis of approximately 40 samples indicated that the concentration of boron in the {100} sector ranged from a few parts per billion to a few parts per million.

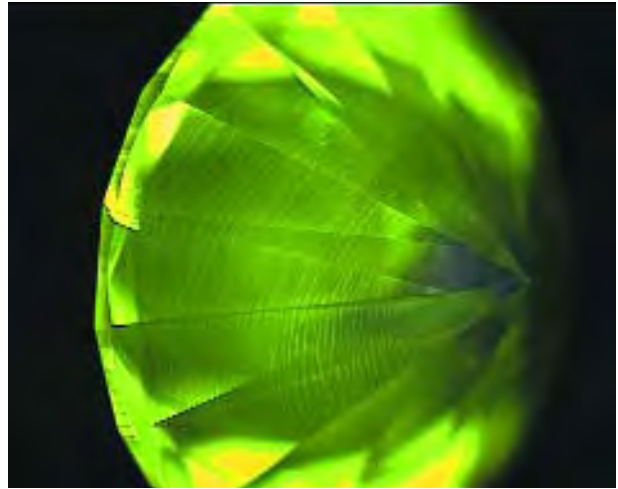


Figure 19. In this DiamondView image of a formerly brown 0.50 ct faceted CVD synthetic that has been made more colorless by HPHT annealing, the dominant component of the luminescence is now green but growth striations indicative of CVD synthetic diamond are still clearly seen. Photo by P. Martineau.

The weights, grades, and fluorescence properties (as obtained with a typical gemological UV lamp unit) of the five blue faceted stones we produced from CVD synthetic material are given in table 4. When tested with the DiamondSure, all were referred.

When exposed to short-wave UV radiation in the DiamondView, all the boron-doped CVD synthetic diamond samples showed bright blue luminescence with some regions of light greenish blue luminescence. After such exposure, they showed blue phosphorescence that decayed over a period ranging from a few seconds to several tens of seconds.

DiamondView images of cross-sectional slices of as-grown boron-doped samples indicated that differ-

TABLE 4. Weights, grades and fluorescence reactions of five faceted boron-doped CVD synthetic diamond samples (produced for research and education only).

Sample number	Carat weight	Cut	Color	Clarity	UV fluorescence	
					Long-wave	Short-wave
B1	1.05	Round brilliant	Fancy Light grayish blue	VS ₁	Inert	Greenish blue, and blue phosphorescence
B2	1.53	Round brilliant	Fancy Light blue	IF	Inert	Greenish blue, and blue phosphorescence
B3	1.85	Cushion cut	Fancy Intense blue	SI ₁	Inert	Greenish blue, and blue phosphorescence
B4	1.03	Square cut	Fancy Deep blue	VS ₂	Inert	Greenish blue, and blue phosphorescence
B5	2.64	Square cut	Fancy Deep blue	VS ₁	Inert	Greenish blue, and blue phosphorescence

ently oriented growth faces showed different luminescence properties. The luminescence from the octahedral {111} and cube {100} growth faces was generally greenish blue and blue, respectively. These different luminescence properties conform to the edges and corners of the substrate, where the differently oriented growth faces started to form, just as HPHT-grown synthetics show growth sectors radiating from the seed (Welbourn et al., 1996).

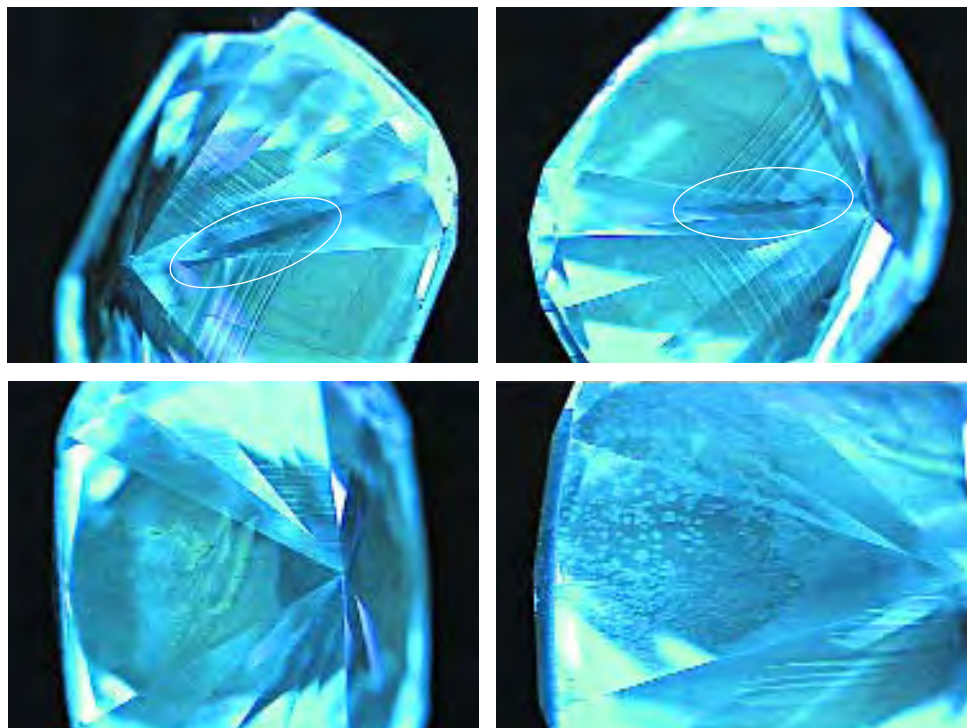
The final growth surface of all boron-doped samples showed growth steps, shallow pits, or a combination of both of these. DiamondView images of these surfaces revealed that the luminescence properties (color and intensity) of these steps and pits were different from those of adjacent regions where the surface was flat. After the original growth surface was removed during the preparation of free-standing CVD plates, we imaged the polished surface in the DiamondView. In every case, a pattern of features closely resembling that of the original growth surface was observed. DiamondView images clearly delineated the regions where growth had taken place on the differently oriented surfaces of steps and pits.

In the samples that were faceted, the intersection of the polished surface with growth sector boundaries showed up in DiamondView images. Jagged growth sector boundaries can be seen adjacent to the linear, step-related features in the upper two images

of figure 20. The linear and bubble-like features also visible in figure 20 correspond to regions where growth has taken place on risers and in pits, respectively. We have never seen such features in DiamondView images of natural type IIb diamond; nor have they been reported in the literature. Similar features were observed in DiamondView images of all the boron-doped CVD synthetics we examined.

CVD Samples Grown in the Absence of Impurities other than Hydrogen. Samples grown under conditions created by exhaustive efforts to remove all impurities other than hydrogen from the growth environment were investigated using the DiamondView and cathodoluminescence topography. DiamondView and cathodoluminescence images of such samples showed only lines emitting blue luminescence. It is well known that dislocations in diamond tend to produce blue luminescence when excited by an electron beam or short-wave UV radiation. (For natural diamond, Kiflawi and Lang [1976] have demonstrated a one-to-one correspondence of CL-emitting lines and dislocations mapped using X-ray topography.) We also studied these samples using absorption and photoluminescence spectroscopy. Apart from localized regions showing blue dislocation luminescence under short-wave ultraviolet excitation, we observed no spectroscopic features

Figure 20. The characteristic linear and bubble-like features seen in these DiamondView images of a 1.85 ct faceted boron-doped CVD synthetic relate to the effect of growth surface steps (highlighted) and pits, respectively. Other features relate to growth sector boundaries.



associated with either impurities or extended defects in the crystal structure.

When a polished high-purity CVD synthetic round brilliant was examined with the DiamondView, none of the orange luminescence characteristic of the N-doped material was observed. Even when recorded with a long integration time on the instrument's high-gain setting and with the aperture fully open, as in figure 21, the image is dark except where blue dislocation luminescence is seen from regions of high dislocation density. We did not observe arrays of dislocations in mosaic patterns or in slip bands, as are typically seen in type IIa natural diamond (Lang, 1979), in any of the high-purity CVD synthetic diamond samples we investigated. Instead, the CL topographs and DiamondView images of high-purity CVD synthetic diamond showed blue dislocation luminescence as either individual or clustered streaks. Correlation of birefringence and luminescence images for free-standing plates showed that each region of anomalous birefringence was centered on a cluster of dislocations. Cross-sectional X-ray topographs showed contrast features similar to those seen in figure 9.

Table 5 lists the grade equivalents and other relevant information for eight faceted stones produced from high-purity CVD synthetic diamond. When tested with the DiamondSure, all of these were referred. Examination with a DiamondView allowed them all to be identified as outlined above.

DISCUSSION

The Origin of Gemological Features. As a result of our experience with the CVD process and many different samples of CVD synthetic diamond, we have built up a general understanding of the origin of gemological features that may help in the identification of CVD synthetic diamond. Our experience is that, while such features cannot be relied on for definitive identification of CVD synthetics, if present they can be important clues. The most common features were described at the beginning of the Results section: birefringence, crystallographic orientation, different-colored layers, and inclusions.

In an HPHT synthesis process, growth proceeds outward from a small seed crystal that acts as a template for diamond formation (see, e.g., Welbourn et al., 1996). In the production of CVD synthetic diamond, the substrate serves the same purpose as a seed, but it generally has the form of a horizontally



Figure 21. DiamondView images of this 0.30 ct high-purity CVD synthetic round brilliant did not show orange luminescence. The blue luminescence emanates from bundles of dislocations in arrangements not seen in natural diamond. High-purity CVD synthetics of this kind are not initially expected to be produced commercially. Photo by P. Martineau.

mounted diamond plate. The dominant faces of this plate have a chosen crystallographic orientation, often close to the cube orientation. Instead of growing out from a central seed crystal, CVD synthetic diamond will therefore initially form with one dominant growth face, with smaller growth faces forming at its edges, as illustrated in figure 22.

In CVD synthetic diamond that is of high enough quality to be polished for jewelry purposes, like the material studied for this article, we have found that dislocations are the dominant kind of extended defect. Understanding the nature of these disloca-

TABLE 5. Weights and grades of eight faceted high-purity CVD synthetic diamond samples (produced for research and education only).^a

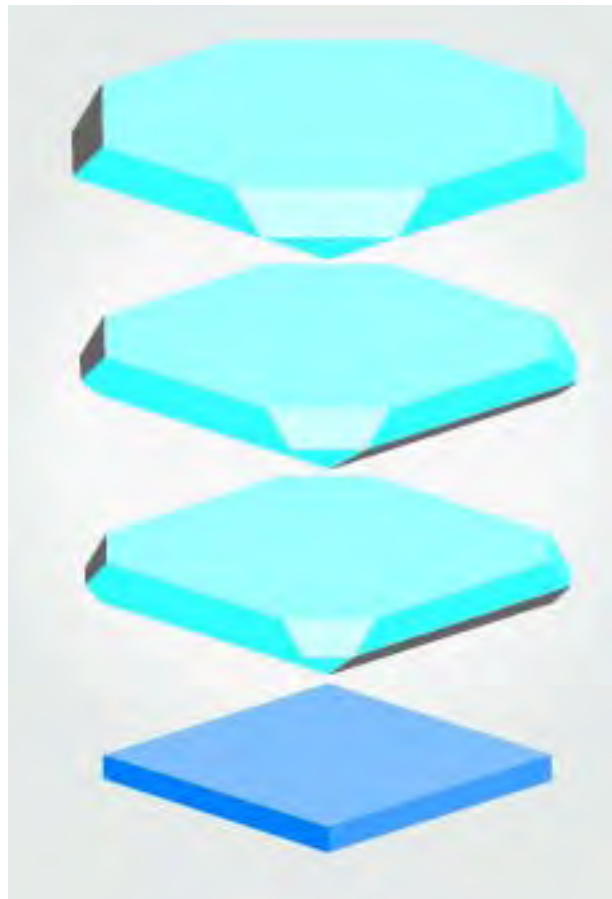
Sample number	Carat weight	Cut	Color	Clarity
HP1	0.31	Round brilliant	F	I ₃
HP2	0.30	Round brilliant	E	VS ₁
HP3	0.44	Rose cut	D	SI ₁
HP4	0.30	Rose cut	D	VVS ₁
HP5	0.21	Rose cut	D	SI ₁
HP6	0.50	Round brilliant	G	SI ₁
HP7	0.44	Round brilliant	D/E	VVS ₂
HP8	0.82	Round brilliant	E	VVS ₁

^aAll were inert to long- and short-wave UV radiation.

tions not only provides clues useful to the identification of CVD synthetic diamond, but it also aids interpretation of the birefringence shown by this material.

The results of cross-sectional X-ray topography suggest that dislocations tend to lie close to perpendicular to the growth surface and often originate at or near the interface between the CVD layer and its substrate. When a sample is viewed along the growth direction, dislocations will therefore tend to lie along the line of sight and, as a result, the effect of the strain field of the entire length of a particular dislocation is seen in one position in the field of view. This means that, when it is possible to view a sample along the growth direction using crossed

Figure 22. These diagrams show the morphological development of single-crystal CVD synthetic diamond for one particular set of growth conditions, starting from a substrate with six faces in cubic orientation. Four octahedral growth faces form in the corners, but the major cube {100} growth faces are enlarged and cube {100} edge growth faces can also be seen.



polarizers, localized birefringence may be observed in positions relating to sources of dislocations. Bundles of dislocations originating from individual point sources at or near the interface with the substrate give rise to characteristic birefringence patterns, such as those in figure 7. Wang et al. (2003, p. 278, figure 13) observed similar localized birefringence features in the CVD synthetic diamond samples they investigated. Such birefringence patterns are not generally seen in natural diamonds.

In our experience, the table-to-culet axis of a polished CVD synthetic stone will usually be almost parallel to the growth direction. Although it often will be impossible to observe birefringence with this viewing direction, it may be feasible for particularly flat cuts or when the culet is large. CVD synthetic diamond will generally have low birefringence compared to type IIa natural diamond, which is usually highly strained, as commented by Wang et al. (2003).

We have often observed lower-quality growth on octahedral growth faces, leading to four regions of defective material when a CVD layer is formed on a substrate that has a dominant face with cubic orientation. For a faceted stone, four-fold symmetry in the distribution of regions of lower quality may therefore raise suspicions that the item is a CVD synthetic.

We have found that it is relatively simple to change the composition of the gas mixture used during CVD growth. If this is done sequentially, a series of layers with different optical absorption or luminescence properties may be formed. In unstable processes, the growth conditions may temporarily change and this can lead to the formation of one or more growth event bands lying normal to the local growth direction. Wang et al. (2003, p. 277, figure 10) found evidence of such banding in at least one of the samples they investigated and explained it in terms of changes in growth conditions.

As CVD processes do not involve metal catalysts, CVD synthetic diamond does not generally contain metallic inclusions, but material grown using the hot filament technique may contain remnants of filament metals such as tungsten or tantalum. We have found that CVD synthetic diamond may contain inclusions of non-diamond carbon. When several inclusions have been incorporated at a given stage of the growth process, they will lie in a growth event band.

X-ray Topography of CVD Synthetic Diamond. Black et al. (1995) reported plan-view X-ray topography results for thin free-standing samples of CVD syn-

thetic diamond. The layers investigated were of relatively low quality and only 70 to 80 μm thick. Butler et al. (2002) presented a plan-view X-ray topograph of a thicker CVD sample grown by Apollo Diamond. It showed interesting cross-hatched contrast, but no cross-sectional topograph was presented.

X-ray topography can be used to detect the interface between a CVD layer and its substrate (again, see figure 8). The V-shaped features above the interface suggest that dislocations nucleated at particular sites at or near the interface early in the growth process. In general, as a CVD layer grows, dislocations propagate in a direction almost perpendicular to the growth surface, leaving a record of the direction of growth. In our experience, X-ray topographs of natural diamond do not show the columnar texture that we have observed for CVD synthetic diamond (again, see figures 8 and 9). We therefore believe that X-ray topography can give supporting evidence that may help identification of CVD synthetic diamond.

Impurities in the CVD Process. In CVD processes, impurities can be eliminated or added in a controlled way to produce doped CVD synthetic diamond material for a range of different technical applications. This also means that it is possible to produce various kinds of CVD synthetics for jewelry, which differ in impurity-related properties such as color and spectroscopic features. Because many potential identification features are impurity related, we investigated four growth processes involving different concentrations of impurities with the aim of developing a broad identification methodology for CVD synthetic diamond.

The results of our research indicate that, depending on the growth process and the impurities present in the growth environment, nitrogen, boron, hydrogen, and silicon may be present in detectable concentrations in CVD synthetic diamond (see, e.g., table 2). Hydrogen plays an important role in the CVD process (see, e.g., Goodwin and Butler, 1998), and because it is typically the most abundant gas in the growth environment, it is likely to be found in the resulting material. Nitrogen and boron content may result from deliberate or accidental sources in the growth process (see, e.g., Muller-Sebert et al., 1996; Locher et al., 1995), and silicon is often present as an unintentional impurity (see, e.g., Zaitsev, 2001, pp. 174–181). In attempts to produce diamond with novel electronic properties, some researchers have experimented with doping CVD synthetic diamond with other impurities, such as phosphorus

and sulfur (see, e.g., Koizumi et al., 1998; Nishitani-Gamo et al., 2000). From a gemologist's point of view, nitrogen, boron, hydrogen, and silicon are likely to remain the most common impurities.

Samples Grown with Added Nitrogen. CVD synthetic diamond can be classified according to its impurity content in the same way as natural diamond and HPHT-grown synthetic diamond. It may be type IIa, type Ib, or type IIb. When there is no boron present during growth, type IIa diamond will generally result, but in rare cases sufficient singly substitutional nitrogen may be incorporated for CVD synthetic diamond to be classified as type Ib.

Our experience has indicated that nitrogen is difficult to eliminate entirely from the growth environment. It may be present because of unintentional leaking of air into a CVD reactor or because it is an impurity in gases used in the CVD process. It is incorporated into CVD synthetic diamond in various kinds of defects that give characteristic spectroscopic signatures that can be useful as indicators of CVD synthetic diamond. It is known that even small concentrations of nitrogen in the starting gas can increase the growth rate (Muller-Sebert et al., 1996), and this may lead producers of CVD synthetic diamond to add nitrogen deliberately.

In terms of concentration, isolated nitrogen was one of the dominant nitrogen-related defects in the nitrogen-doped CVD synthetic diamond samples that we investigated. This corresponds to an isolated single nitrogen atom substituting for a carbon atom at a site in the diamond crystal with no other neighboring impurities or vacancies (missing carbon atoms). This defect causes a monotonic rise in absorption from about 500 nm into the blue and ultraviolet regions of the spectrum, with a broad absorption feature at 270 nm (see, for example, Zaitsev, 2001, pp. 343–344).

Wang et al. (2003) reported that many of the Apollo CVD synthetic diamond samples they investigated showed lines at 8753, 7354, 6856, 6425, 5564, and 3123 cm^{-1} , which is consistent with what Butler et al. (2002) also reported for an Apollo sample. These lines were identified as being hydrogen-related by Fuchs et al. (1995a,b). They can be considered strong indicators of CVD synthetic diamond, because they have never been seen in any other kind of diamond. Note that we observed these lines only in the spectra of the as-grown CVD synthetic diamond samples doped with nitrogen. Like Wang et al. (2003), we found that they were

removed by HPHT treatment.

The line we observed at 3323 cm^{-1} for some dark brown samples was also identified as being hydrogen-related by Fuchs et al. (1995a,b). Although it has been seen only in CVD synthetic diamond, it is not considered an important indicator because, even among nitrogen-doped samples, we observed it in relatively few cases and it, too, is removed by HPHT treatment.

Some CVD synthetic diamond contains hydrogen in paramagnetic defects that have been detected and characterized using electron paramagnetic resonance (EPR). Recent studies of nitrogen-doped single-crystal CVD synthetic diamond (Glover et al., 2003, 2004) have identified two such defects that have never been observed in other kinds of diamond. Both of these were found to be present in the faceted CVD synthetic (M. E. Newton, pers. comm., 2004) investigated by Butler et al. (2002).

The nitrogen-vacancy (N-V) center is a very important defect in CVD synthetic diamond. It consists of an isolated single nitrogen atom, again at a site normally occupied by a carbon atom, but with one of its nearest-neighbor carbon atoms missing. It occurs in two different charge states: neutral and negatively charged. The latter gives rise to the photoluminescence system with a zero-phonon line at 637 nm (see, e.g., Zaitsev, 2001, pp. 197–203), and it is now generally believed that the neutral N-V center is responsible for the PL system with a zero-phonon line at 575 nm (Lawson et al., 1998). Together they cause the orange or orangy red luminescence seen in DiamondView images of nitrogen-doped CVD synthetic diamond. Nitrogen-vacancy centers are responsible for the orange luminescence that was observed when the N-doped CVD synthetic diamond samples were exposed to UV radiation (254 nm or 365 nm). Consequently, observation of predominantly orange luminescence should therefore trigger gemologists to study a stone in more detail.

The lines at 467 nm and 533 nm that we observed in the cathodoluminescence and PL spectra of nitrogen-doped CVD synthetic diamond have only been seen for CVD synthetic diamond (Zaitsev, 2001, pp. 245–246 and p. 300). We have shown, however, that HPHT treatment may remove them or substantially reduce their intensity.

All the Apollo synthetic diamond samples tested by Wang et al. (2003), and the one examined by Butler et al. (2002), showed a moderately strong PL line at 737 nm. The 737 nm line has never been detected for natural diamond, and it has only been

found in the spectra of HPHT-grown synthetic diamond in cases where silicon was deliberately added to the starting materials (Clark et al., 1995). Much of the CVD synthetic material that we have studied, however, does not show the 737 nm feature, and therefore it should not be relied on too heavily for identification. The center responsible is known to be very stable and is not likely to be altered by HPHT treatment (Clark et al., 1995).

The surface of CVD synthetic diamond has a tendency to show growth steps (van Enckevort et al., 1995), and our results indicate that differential uptake of impurity-related defects on the risers and terraces of these steps is responsible for the striations observed in luminescence images of polished samples. We have never observed such striations in luminescence (including DiamondView) images of non-CVD samples; nor have they been reported in the literature. The presence of such striations can, therefore, be considered a strong indicator of CVD synthetic diamond.

HPHT-Treated Nitrogen-Doped CVD Synthetic

Diamond. It is now well known that the optical absorption properties of brown natural type IIa diamond can be changed by HPHT annealing (see, e.g., Fisher and Spits, 2000; Smith et al., 2000). Butler et al. (2003) reported that the brown color of CVD synthetic diamond can be reduced by HPHT annealing. Wang et al. (2003) reported results for HPHT annealing of three samples of CVD synthetic diamond but did not observe a color change in every case. We noted different responses to HPHT treatment depending on the starting material, but in every case we did observe a distinct reduction in ultraviolet and visible absorption (and a corresponding color change), with the absorption spectra of treated samples being dominated by absorption caused by isolated nitrogen atoms. In our experience, low-nitrogen (type IIa/Ib) natural diamond containing predominantly isolated nitrogen is extremely rare; the low concentrations of nitrogen atoms in type IIa natural diamond are generally in aggregated forms.

Brown color in type IIa natural diamond is associated with plastic deformation. We found no evidence that any of our brown CVD synthetic diamond samples were plastically deformed. Raman spectroscopy indicated that, unlike most brown natural type IIa diamond, brown CVD synthetic diamond contains significant amounts of non-diamond carbon that likely contributes to the absorption spectrum. After HPHT treatment removes the color, the non-diamond carbon is no longer present, almost certainly

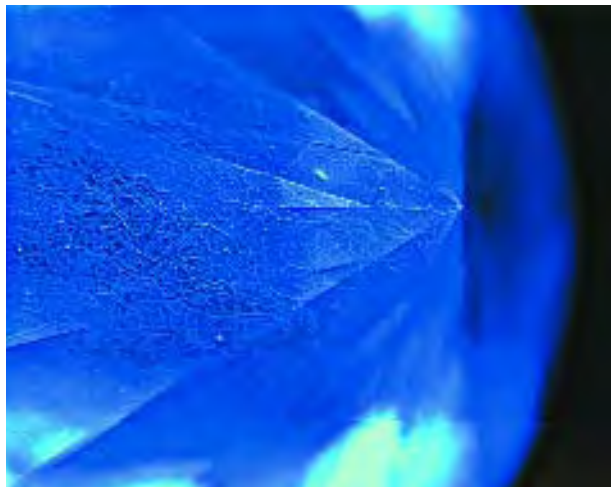


Figure 23. Blue luminescence and “mosaic” networks of polygonized dislocations are evident in this DiamondView image of a typical type IIa natural diamond. Such networks were not seen in any of the CVD samples investigated in this study. (Imaged area: 3.6 mm × 2.7 mm.) Photo by S. Lawson.

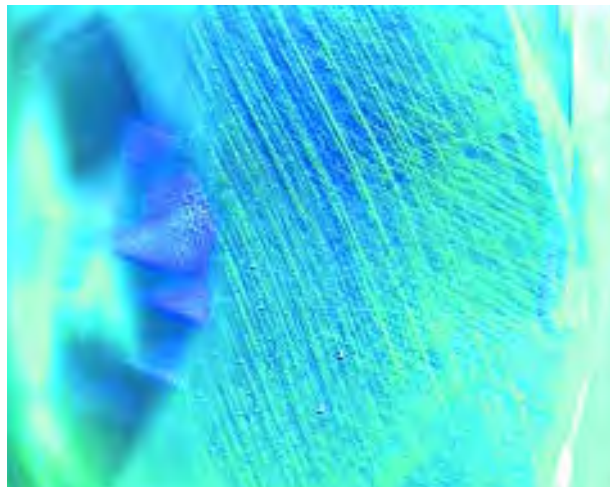


Figure 24. This DiamondView image of part of a plastically deformed natural type IIa diamond shows dislocations lying in slip bands, which were not seen in any of the CVD samples investigated in this study. (Imaged area: 3.6 mm × 2.7 mm.) Photo by P. Martineau.

because it has been converted to diamond. We cannot rule out the possibility that some of the UV-visible absorption of brown CVD synthetic diamond samples is caused by hydrogen-related defects that are removed by HPHT treatment.

It is clear from our results that HPHT annealing not only changes the absorption spectrum of brown CVD synthetic diamond, but it also affects the defects that contribute to PL spectra and images. Although some nitrogen-vacancy luminescence generally remains, DiamondView images of HPHT-treated nitrogen-doped CVD synthetic diamond samples tend to be dominated by green or green-blue luminescence with striations similar in form to those observed for the orange luminescence in as-grown samples.

Boron-Doped CVD Synthetic Diamond. DiamondView images of the B-doped CVD synthetic diamond samples we studied showed the effect of differential incorporation of boron on differently oriented surfaces that formed during growth. This gives rise to features we have never observed in DiamondView images of natural type IIb diamond samples. We believe that these will remain reliable for the identification of boron-doped CVD synthetic diamond. Type IIb natural diamond samples we have investigated show a mosaic pattern of dislocations similar to that seen for natural type IIa diamond. Lang (1979) and Hanley et al. (1977) have described observation of such arrays of dislocations

in cathodoluminescence topographs of type IIb natural diamond. We have never observed such arrays of dislocations in B-doped synthetic diamond, whether CVD or HPHT-grown.

High-Purity CVD Synthetic Diamond. DiamondView images of type IIa natural diamond typically show a high density of streaks of blue luminescence. The corresponding dislocations or bundles of dislocations show a variety of different patterns. In the majority of type IIa natural diamonds, we have found that they form a fairly random “mosaic” pattern (figure 23). In plastically deformed type IIa natural diamonds we have investigated, they tend to lie in slip bands on octahedral planes (figure 24). Some rare natural type IIa diamonds produce orange luminescence of the kind shown by CVD synthetic diamond. In these rare cases, however, DiamondView images show underlying dislocation structures that are characteristic of natural type IIa diamond (figure 25). We did not observe such arrays in any of the CVD synthetic diamond samples we studied, nor have they been reported in the literature to date. We therefore believe that, for type IIa diamond, the absence of such arrays of dislocations is a strong indicator of synthetic diamond.

It is possible to produce high-purity CVD synthetic diamond that shows no detectable impurity-related luminescence. This is technically very difficult, and growth rates are significantly lower than for nitrogen-doped CVD synthetic diamond. It is, therefore,



Figure 25. There are rare instances in which DiamondView images of a natural type IIa diamond will show orange luminescence throughout. In such cases, we have observed underlying networks of dislocations of a kind that we have not seen for CVD synthetic diamond. (Imaged area: 3.6 mm × 2.7 mm.) Photo by S. Lawson.

unlikely that CVD synthetics of this kind will be commercially produced in the immediate future. The absence of detectable impurity-related luminescence would be very unusual for natural diamond; thus, in combination with the absence of dislocations in the mosaic or slip band arrays found in natural type IIa diamond, it would be a strong indicator of high-purity CVD synthetic diamond.

IDENTIFICATION

The key characterization results of this work are summarized in table 6. Nitrogen-doped CVD synthetic diamond shows a number of spectroscopic features not exhibited by either natural diamond or HPHT-grown synthetic diamond. When present, these are useful indicators of CVD synthetic material. However, our results show that it is possible to grow high-purity or boron-doped CVD synthetic diamond samples that show none of these features. In addition, many of the features of N-doped material can be removed by HPHT treatment.

The Apollo Diamond samples provided to GIA for study contained low but significant concentrations of nitrogen. Their spectroscopic properties were almost identical to those we observed for samples grown with nitrogen added to the process gas. In particular, they showed H-related absorption features, in the NIR (8753, 7354, 6856, 6425 and 5564 cm^{-1}) and at 3123 cm^{-1} , which have never been

reported for natural diamond. We concur with Wang et al. (2003) that these features represent a strong indicator of CVD synthetic diamond.

We also observed the 596/597 nm photoluminescence doublet reported by Wang et al. (2003), and this is another potentially useful indicator. One significant difference was that, whereas few of our samples showed the silicon-related 737 nm PL feature, Wang et al. (2003) observed this for every Apollo sample they investigated. This feature has never, to our knowledge, been reported for natural diamond and is therefore another useful indicator. It should, however, be emphasized that the absence of the 737 nm feature from the spectra of our more recently grown samples suggests that it may eventually be absent for material from other sources. Thus, the 737 nm feature, the 596/597 nm doublet, and the hydrogen-related absorption lines are useful only when present. Their absence is not a reliable indicator of natural or synthetic origin.

Following post-growth HPHT treatment, nitrogen-doped samples exhibited UV-visible absorption features that were caused predominantly by low concentrations of isolated nitrogen atoms. Low-nitrogen natural diamond containing predominantly isolated nitrogen (type IIa/Ib) is extremely rare. Our treated CVD synthetic diamond samples also showed green or green/blue luminescence accompanied by PL features in the region of 451–459 nm, with 325 nm excitation, that have not been observed in any other kind of diamond.

Although the DiamondSure was originally developed to screen for HPHT-grown synthetics, it refers all type IIa stones. We therefore feel confident that it will refer the CVD synthetic diamond currently being commercially produced, because Wang et al. (2003) have reported that it is type IIa. Some CVD synthetic diamond samples may contain high enough concentrations of isolated nitrogen to be classified as type Ib, but the DiamondSure also refers all type Ib stones.

CVD synthetic diamond material of the kind that Apollo Diamond currently is producing commercially shows orangy red luminescence (Butler et al., 2002; Wang et al., 2003) from nitrogen-related defects that generate spectral lines at 575 nm and 637 nm. This luminescence is clearly visible in DiamondView images and, when seen, should alert the user. In very rare cases, natural type IIa diamond may show orange luminescence. Identification of CVD material therefore requires the observation of

TABLE 6. The key characterization results for the four kinds of CVD synthetic diamond material studied.

Property	Nitrogen-doped	HPHT- annealed nitrogen-doped	Boron-doped	High purity
Color	Faint brown to brown	Near-colorless or green-brown ^a	Fancy Light blue to Fancy Intense blue	Near-colorless or colorless
UV-visible absorption	270 nm 360 nm 520 nm 624 nm 637 nm 737 nm	270 nm and associated absorption	Decreasing absorbance from red to blue regions of spectrum	Intrinsic absorption only
IR absorption	8753, 7354, 6856, 6425, 5564, 3323, 3123 cm ⁻¹	3107 cm ⁻¹	Boron-related	Intrinsic absorption only
Photoluminescence spectroscopy	467 nm 533 nm 575 nm 596 nm 597 nm 637 nm	415 nm 451–480 nm region 503 nm 575 nm 637 nm	Broad luminescence band in the blue region of the spectrum	Only intrinsic and dislocation luminescence
DiamondView images	Orange to orangy red with striations sometimes visible	Green to blue-green with striations sometimes visible	Blue with characteristic features relating to growth-surface morphology	Dark except for blue dislocation luminescence
Cathodoluminescence spectroscopy	467 nm 533 nm 575 nm	415 nm 503 nm 575 nm	Broad CL band in the blue-green region of the spectrum	Only intrinsic and dislocation luminescence
Cathodoluminescence topography	Orange with striations	Green or blue-green with striations	Blue-green with features relating to surface morphology	Only intrinsic and dislocation luminescence
X-ray topography (cross-sectional)	Streaks nearly parallel to growth direction	Streaks nearly parallel to growth direction	Streaks nearly parallel to growth direction	Streaks nearly parallel to growth direction

^aThese represent the results for the majority of samples tested.

additional features indicative of CVD synthetic diamond, such as the striations described earlier, or the absence of the dislocation networks found in type IIa natural diamond.

Although DiamondPlus was primarily designed for rapid screening for HPHT-treated type II diamonds, it will detect a range of spectroscopic features associated with CVD synthetic diamond of the kind currently being commercially produced. Wang et al. (2003) reported that all the Apollo Diamond samples they investigated showed 575, 637, and 737 nm photoluminescence features. Based on this information, we are confident that DiamondPlus would give a “refer CVD” result for these samples. In our experience, the 737 nm feature is not removed by HPHT annealing.

In cases where doubt remains after a stone has been studied in a DiamondView and DiamondPlus, X-ray topography also can provide a useful indication of the mode of growth. The directional contrast streaks of the kind that we have observed in cross-sectional topographs are a strong indicator of CVD synthetic diamond.

CONCLUSIONS

Our research has shown that it is possible to produce a variety of CVD synthetic diamond materials with differing properties. We have described the properties of nitrogen-doped, annealed nitrogen-doped, boron-doped, and high-purity CVD synthetic diamond. Comparison of our results with those of Butler et al. (2002) and Wang et al. (2003) indicates that the Apollo Diamond samples they studied fit into the category we have called nitrogen-doped. Such material shows a range of spectroscopic features that can be used to identify it, as we summarized in the last section.

Although there are useful gemological clues (such as observation of characteristic birefringence or orange fluorescence) and some CVD material shows spectroscopic features that are not observed for other kinds of diamond (such as the 737 nm photoluminescence feature or the H-related absorption lines), our research has shown that these gemological and spectroscopic indicators cannot be relied on in all cases.

Our results indicate that surface luminescence

images of the kind that can be generated using the DiamondView provide very useful information for identifying all the kinds of CVD synthetics that we have produced in our research, including those that show no gemological or spectroscopic indicators. Luminescence imaging is already used by the major gemological laboratories to study unusual stones, and the results of our research suggest that

it will play a central role in the identification of CVD synthetics in the future.

Apollo Diamond has a stated policy of disclosure and marking (Priddy, 2003). The combination of disclosure and reliable detection methods will help protect consumer confidence that CVD synthetics will not be misrepresented as natural diamond and will facilitate informed jewelry buying.

ABOUT THE AUTHORS

The authors work in the Physics Department of the DTC Research Centre, Berkshire, United Kingdom. Dr. Martineau is a principal scientist, working mainly on CVD synthetic diamond, and Dr. Lawson is project manager for Consumer Confidence Technical Research. Mr. Taylor and Ms. Quinn are senior technicians, Mr. Evans is a senior research assistant, and Mr. Crowder is a principal technician.

ACKNOWLEDGMENTS: The authors thank all the members of

the DTC Research Centre, Maidenhead, who have been involved in the CVD research program. Particular recognition is due to C. J. Kelly and J. A. Jones for carrying out sample processing work, and to M. Cooper, C. M. Welbourn, and D. Fisher for helpful discussions and general guidance over many years. The authors are also grateful to the members of the CVD synthesis team at Element Six for the high level of expertise, commitment, and enthusiasm they have shown throughout this work. Particular recognition is due to G. A. Scarsbrook and D. J. Twitchen.

REFERENCES

- Angus J.C. (2002) A short history of diamond synthesis. In J. Asmussen and D.K. Reinhard, Eds., *Diamond Films Handbook*, Marcel Dekker, New York, pp. 17–26.
- Bachmann P.K. (1998) Microwave plasma chemical vapor deposition of diamond. In M.A. Prelas, G. Popovici, and L.K. Bigelow, Eds., *Handbook of Industrial Diamonds and Diamond Films*, Marcel Dekker, New York, pp. 821–850.
- Badzian A., Badzian T. (1993) Diamond homoepitaxy by chemical vapor deposition. *Diamond and Related Materials*, Vol. 2, No. 2–4, pp. 147–157.
- Black D., Burdette H., Linares R., Doering P., Marchywka M., Pehrsson P. (1995) X-ray diffraction imaging of free-standing single-crystal CVD diamond films. In K.V. Ravi, J.P. Dismukes, J.L. Davidson, K.E. Spear, R.H. Hauge, and B.V. Spitsyn, Eds., *Fourth International Symposium on Diamond Materials*, Electrochemical Society, Reno, Nevada, Vol. 95–4, pp. 467–472.
- Bundy F.P., Hall H.T., Strong H.M., Wentorf R.J. (1955) Man-made diamond. *Nature*, Vol. 176, pp. 51–54.
- Butler J.E., Kennedy T.A., Colton J.S., Quadri S., Linares R., Doering P., Newton M., Glover C., Smith H., Collins A. (2002) Analysis of large single-crystal CVD diamond. *8th International Conference New Diamond Science and Technology*, July 21–26, Melbourne, www.conferences.unimelb.edu.au/icndst-8/Presentations/p1-01-1.pdf [date accessed: 04/13/04].
- Butler J.E., Charles S., Feygelson B., Yan C.-H., Mao H.-K., Hemley R. (2003) Characterization of HPHT annealed single-crystal CVD diamond. *Proceedings of the De Beers Diamond Conference*, July 7–9, Cambridge, U.K., pp. 24.1–24.5.
- Clark C.D., Collins A.T., Woods G.S. (1992) Absorption and luminescence spectroscopy. In J.E. Field, Ed., *The Properties of Natural and Synthetic Diamond*, Academic Press, London, pp. 35–79.
- Clark C.D., Kanda H., Kiflawi I., Sittas G. (1995) Silicon defects in diamond. *Physical Review B*, Vol. 51, No. 23, pp. 16681–16688.
- Coe S.E., Sussmann R.S. (2000) Optical, thermal and mechanical properties of CVD diamond. *Diamond and Related Materials*, Vol. 9, No. 9–10, pp. 1726–1729.
- Davies G. (1984) *Diamond*, Adam Hilger Ltd., Bristol.
- Eversole W.G. (1962a) *Synthesis of Diamond*. U.S. patent 3,030,187, issued April 17.
- Eversole W.G. (1962b) *Synthesis of Diamond*. U.S. patent 3,030,188, issued April 17.
- Fisher D., Spits R.A. (2000) Spectroscopic evidence of GE POL HPHT-treated natural type IIa diamonds. *Gems & Gemology*, Vol. 36, No. 1, pp. 42–49.
- Fritsch E., Conner L., Koivula J.I. (1989) A preliminary gemological study of synthetic diamond thin films. *Gems & Gemology*, Vol. 25, No. 2, pp. 84–90.
- Fuchs F., Wild C., Schwarz K., Muller-Sebert W., Koidl P. (1995a) Hydrogen induced vibrational and electronic transitions in chemical vapor deposited diamond, identified by isotopic substitution. *Applied Physics Letters*, Vol. 66, No. 2, pp. 177–179.
- Fuchs F., Wild C., Schwarz K., Koidl P. (1995b) Hydrogen-related IR absorption in chemical vapour deposited diamond. *Diamond and Related Materials*, Vol. 4, No. 5–6, pp. 652–656.
- Glover C., Newton M.E., Martineau P.M., Twitchen D.J., Baker J.M. (2003) Hydrogen incorporation in diamond: The nitrogen-vacancy-hydrogen complex. *Physical Review Letters*, Vol. 90, No. 18, pp. 185507-1–185507-4.
- Glover C., Newton M.E., Martineau P.M., Twitchen D.J. (2004) Hydrogen incorporation in diamond: The vacancy-hydrogen complex. *Physical Review Letters*, Vol. 92, No. 13, pp. 135502-1–135502-4.
- Goodwin D.G., Butler J.E. (1998) Theory of diamond chemical vapor deposition. In M.A. Prelas, G. Popovici and L.K. Bigelow, Eds., *Handbook of Industrial Diamonds and Diamond Films*, Marcel Dekker, New York, pp. 527–581.
- Grotjohn T.A., Asmussen J. (2002) Microwave plasma-assisted diamond film deposition. In J. Asmussen and D.K. Reinhard, Eds., *Diamond Films Handbook*, Marcel Dekker, New York, pp. 211–302.
- Hanley P.L., Kiflawi I., Lang A.R. (1977) On topographically identifiable sources of cathodoluminescence in natural diamonds. *Philosophical Transactions of the Royal Society of London A*, Vol. 284, pp. 329–368.
- Heberlein J.V.R., Ohtake N. (2002) Plasma torch diamond deposition. In J. Asmussen and D.K. Reinhard, Eds., *Diamond Films Handbook*, Marcel Dekker, New York, pp. 141–210.

- Isberg J., Hammersberg J., Johansson E., Wikstrom T., Twitchen D.J., Whitehead A.J., Coe S.E., Scarsbrook G.A. (2002) High carrier mobility in single-crystal plasma-deposited diamond. *Science*, Vol. 297, No. 5587, pp. 1670–1672.
- Janssen G., van Enckevort W.J.P., Schamnee J.J.D., Vollenberg W., Giling L.J., Seal M. (1990) Rapid single crystalline diamond growth by acetylene-oxygen flame deposition. *Journal of Crystal Growth*, Vol. 104, No. 3, pp. 752–757.
- Janssen G., Vollenberg W., Gilling L.J., van Enckevort W.J.P., Schamnee J.J.D., Seal M. (1991) Rapid growth of single-crystal diamond on diamond substrates. *Surface and Coatings Technology*, Vol. 47, No. 1–3, pp. 113–126.
- Johnson M.L., Koivula J.I., Eds. (1997) Gem News: Synthetic diamond thin film jewelry. *Gems & Gemology*, Vol. 33, No. 2, pp. 143–144.
- Kiffer A.D. (1956) Synthesis of diamond from carbon monoxide. Report, Tonowanda Laboratories, Linde Air Products Co., June 6.
- Kiflawi I., Lang A.R. (1976) On the correspondence between cathodoluminescence images and X-ray diffraction contrast images of individual dislocations in diamond. *Philosophical Magazine*, Vol. 33, No. 4, pp. 697–701.
- King J.M., Moses T.M., Shigley J.E., Welbourn C.M., Lawson S.C., Cooper M.C. (1998) Characterizing natural-color type IIb blue diamonds. *Gems & Gemology*, Vol. 34, No. 4, pp. 246–268.
- Koizumi S., Kamo M., Sato Y., Mita S., Sawabe A., Reznik A., Uzan-Saguy C., Kalish R. (1998) Growth and characterization of phosphorus doped n-type diamond thin films. *Diamond and Related Materials*, Vol. 7, pp. 540–544.
- Landstrass M.I., Plano M.A., Moreno M.M., McWilliams S., Pan L.S., Kania D.R., Han S. (1993) Device properties of homoepitaxially grown diamond. *Diamond and Related Materials*, Vol. 2, No. 5–7, pp. 1033–1037.
- Lang A.R. (1979) Internal structure. In J.E. Field, Ed., *The Properties of Diamond*, Academic Press, London, pp. 425–469.
- Lang A.R., Moore M., Walmsley J.C. (1992) Diffraction and imaging studies of diamond. In J.E. Field, Ed., *The Properties of Natural and Synthetic Diamond*, Academic Press, London, pp. 215–258.
- Lawson S.C., Fisher D., Hunt D.C., Newton M.E. (1998) On the existence of positively-charged single substitutional nitrogen in diamond. *Journal of Physics C: Condensed Matter*, Vol. 10, No. 27, pp. 6171–6180.
- Linares R., Doering P. (1999) Properties of large single crystal diamond. *Diamond and Related Materials*, Vol. 8, No. 2–5, pp. 909–915.
- Locher R., Wagner J., Fuchs F., Maier M., Gonon P., Koidl P. (1995) Optical and electrical characterization of boron-doped diamond films. *Diamond and Related Materials*, Vol. 4, No. 5–6, pp. 678–683.
- Matsumoto S., Sato Y., Kamo M., Setaka N. (1982a) Vapor deposition of diamond particles from methane. *Japanese Journal of Applied Physics*, Vol. 21, No. 4, pp. L183–L185.
- Matsumoto S., Sato Y., Tsutsumi M., Setaka N. (1982b) Growth of diamond particles from methane-hydrogen gas. *Journal of Materials Science*, Vol. 17, pp. 3106–3112.
- Muller-Sebert W., Worner E., Fuchs F., Wild C., Koidl P. (1996) Nitrogen induced increase of growth rate in chemical vapor deposition of diamond. *Applied Physics Letters*, Vol. 68, No. 6, pp. 759–760.
- Nishitani-Gamo M., Yasu E., Xiao C., Kikuchi Y., Ushizawa K., Sakaguchi I., Suzuki T., Ando T. (2000) Sulfur-doped homoepitaxial (001) diamond with n-type semiconductive properties. *Diamond and Related Materials*, Vol. 9, No. 3–6, pp. 941–947.
- Plano M.A., Moyer M.D., Moreno M.M., Black D., Burdette H., Robins L., Pan L.S., Kania D.R., Banholzer W. (1994) Characterization of a thick homoepitaxial CVD diamond film. In C.H. Carter, G. Gildenblat, S. Nakamura, R.J. Nemanich, Eds., *Diamond, SiC and Nitride Wide Bandgap Semiconductors*, Materials Research Society, Warrendale, PA, pp. 307–312.
- Priddy S. (2003) Apollo Diamond to release CVD diamonds in Q4. *Rapaport News*, www.diamonds.net/news/newsitem.asp?num=8374 [date accessed: 04/13/04].
- Schermer J.J., van Enckevort W.J.P., Giling L.J. (1994) Flame deposition and characterization of large type IIa diamond single crystals. *Diamond and Related Materials*, Vol. 3, No. 4–6, pp. 408–416.
- Schermer J.J., de Theije F.K., Giling L.J. (1996) Mosaic growth of diamond: A study of homoepitaxial flame deposition and etching of [001]-oriented diamond layers. *Journal of Crystal Growth*, Vol. 165, No. 4, pp. 387–401.
- Shigley J.E., Fritsch E., Stockton C.M., Koivula J.I., Fryer C.W., Kane R.E. (1986) The gemological properties of the Sumitomo gem-quality synthetic yellow diamonds. *Gems & Gemology*, Vol. 22, No. 4, pp. 192–208.
- Shigley J.E., Fritsch E., Stockton C.M., Koivula J.I., Fryer C.W., Kane R.E., Hargett D.R., Welch C.W. (1987) The gemological properties of the De Beers gem-quality synthetic diamonds. *Gems & Gemology*, Vol. 23, No. 4, pp. 187–206.
- Smith C.P., Bosshart G., Ponahlo J., Hammer V.M.F., Klapper H., Schmetzer K. (2000) GE POL diamonds: Before and after. *Gems & Gemology*, Vol. 36, No. 3, pp. 192–215.
- Sussmann R.S., Brandon J.R., Scarsbrook G.A., Sweeney C.G., Valentine T.J., Whitehead A.J., Wort C.J.H. (1994) Properties of bulk polycrystalline CVD diamond. *Diamond and Related Materials*, Vol. 3, No. 4–6, pp. 303–312.
- Tsuno T., Imai T., Fujimori N. (1994) Twinning structure and growth hillock on diamond (001) epitaxial film. *Japanese Journal of Applied Physics*, Vol. 33, pp. 4039–4043.
- Valentine T.J., Whitehead A.J., Sussmann R.S., Wort C.J.H., Scarsbrook G.A. (1994) Mechanical property measurements of bulk polycrystalline CVD diamond. *Diamond and Related Materials*, Vol. 3, No. 9, pp. 1168–1172.
- van Enckevort W.J.P., Janssen G., Schermer J.J., Giling L.J. (1995) Step-related growth phenomena on exact and misoriented [001] surfaces of CVD-grown single-crystal diamonds. *Diamond and Related Materials*, Vol. 4, No. 4, pp. 250–255.
- Wang W., Moses T., Linares R., Shigley J.E., Hall M., Butler J.E. (2003) Gem-quality synthetic diamonds grown by a chemical vapor deposition (CVD) method. *Gems & Gemology*, Vol. 39, No. 4, pp. 268–283.
- Welbourn C.M., Cooper M., Spear P.M. (1996) The De Beers natural versus synthetic diamond verification instruments. *Gems & Gemology*, Vol. 32, No. 3, pp. 156–169.
- Welbourn C.M., Williams R. (2002) DTC comes to diamonds' defense. *Rapaport Diamond Report*, Vol. 25, No. 17, pp. 46–47.
- Wild C., Koidl P., Muller-Sebert W., Walcher H., Kohl R., Herres N., Locher R., Samlenski R., Brenn R. (1993) Chemical vapour deposition and characterization of smooth [100]-faceted diamond films. *Diamond and Related Materials*, Vol. 2, No. 2–4, pp. 158–168.
- Wolden C.A. (2002) Combustion synthesis of diamond. In J. Asmussen and D.K. Reinhard, Eds., *Diamond Films Handbook*, Marcel Dekker Inc., New York, pp. 303–323.
- Woods G.S., Collins A.T. (1983) Infrared absorption spectra of hydrogen complexes in type I diamonds. *Journal of Chemistry and Physics of Solids*, Vol. 44, No. 5, pp. 471–475.
- Wort C.J.H., Sweeney C.G., Cooper M.A., Scarsbrook G.A., Sussmann R.S. (1994) Thermal properties of bulk polycrystalline CVD diamond. *Diamond and Related Materials*, Vol. 3, No. 9, pp. 1158–1167.
- Yan C.-S., Vohra Y.K., Mao H.-K., Hemley R.J. (2002) Very high growth rate chemical vapor deposition of single-crystal diamond. *Proceedings of the National Academy of Sciences of the United States of America*, Vol. 99, No. 20, pp. 12523–12525.
- Yehoda J.E. (2002) Thermally assisted (hot-filament) deposition of diamond. In J. Asmussen and D.K. Reinhard, Eds., *Diamond Films Handbook*, Marcel Dekker, New York, pp. 119–140.
- Zaitsev A.M. (2001) *Optical Properties of Diamond*. Springer-Verlag, Berlin, 502 pp.

CULTURED PEARLS FROM THE GULF OF CALIFORNIA, MEXICO

Lore Kiefert, Douglas McLaurin Moreno, Enrique Arizmendi,
Henry A. Hänni, and Shane Elen

Black pearls have been found in Mexico's Gulf of California since the area was settled more than 2,000 years ago. Attempts at culturing pearls in this area have met with varying success over the past century. Today, a pearl farm in Guaymas is producing commercial quantities of mabe as well as bead-nucleated full-round cultured pearls from the indigenous pearl oyster *Pteria sterna*. This article provides an overview of the history of natural and cultured pearls from Mexico, describes pearl culturing at the Guaymas farm, and focuses on the properties of bead-nucleated cultured pearls from *P. sterna*. These cultured pearls have a brown or gray to dark gray bodycolor with various interference colors caused by the stacking of platy aragonite crystals and organic matter. One indication of their natural color (and their Mexican provenance) is a red fluorescence to long-wave UV radiation.

The history of pearls from the Gulf of California is as fascinating as the pearls themselves (figure 1) and has been described by various authors over the years (e.g., George, 1971; Cariño and Monteforte, 1995; Strack, 2001; McLaurin Moreno, 2002; McLaurin Moreno and Arizmendi Castillo, 2002). Therefore, only a brief historical summary, based on these sources, is given here.

The first European to visit the "Sea of Pearls" (another name for the Gulf of California) was Captain Fortun Jiménez, a Spanish explorer sent by famed *conquistador* Hernán Cortés, who in 1533 observed native people wearing large dark pearls. From that time until the early 20th century, the history of Baja California was closely connected with the recovery of these pearls, which for decades were more important exports than gold, silver, or spices.

For more than 300 years, European and Mexican entrepreneurs harvested fine dark natural pearls from the Gulf of California with rudimentary diving techniques. The introduction of the diving suit in the late 19th century made it possible to reach new pearl oyster beds at greater depths. Eventually, though, overfishing led to the total depletion of the beds and brought pearl fishing to a halt.

In 1903, Gastón Vivès founded the first pearl farm on the Baja California peninsula in the bay of La Paz. The oysters and equipment were either confiscated or destroyed in July 1914, as a consequence of the Mexican Revolution. The company harvested approximately 1.5 million pearl oysters (*Pinctada mazatlanica*) in each of the last three years of its operation (Cáceres-Martinez and Chávez-Villalba, 1997), 9–11% of which yielded natural pearls.

By the 1930s, the oyster beds in the Gulf of California had recovered sufficiently that pearls could again be found. However, these oysters were not *P. mazatlanica* but rather the rainbow-lipped *Pteria sterna*, which produced smaller pearls of unusual color. Then, in 1936, virtually all the oysters began inexplicably dying off, starting in the north. To protect the remaining beds, the Mexican government banned pearl fishing in 1939, but unfortunately this did not stop the death of the oysters. The die-offs would remain a mystery for another

See end of article for About the Authors and Acknowledgments.
GEMS & GEMOLOGY, Vol. 40, No. 1, pp. 26–38.
© 2004 Gemological Institute of America



Figure 1. Attractive cultured pearls are now commercially available from the Gulf of California. The cultured pearls shown here range from 9.5 to 10.5 mm in diameter. Courtesy of Colombia Gem House; photo © GIA and Harold & Erica Van Pelt.

three decades, until it was suggested that the construction of the Hoover Dam in early 1936 had held back enough of the Colorado River to deplete the nutrients flowing into the Gulf of California and greatly disturb its salinity (Alvarez-Borrego, 1983). In recent years, there have been only a few reports of natural pearls from this area (e.g., Crowningshield, 1991; Hurwit, 1992; Wentzell, 1995).

Around 1966, two pearl farms in the Gulf of California began cultivating both *P. mazatlanica* and *P. sterna* with the aim of producing cultured pearls. However, it is only in the past 10 years that two commercial pearl farms have opened. The more significant of these, Perlas del Mar de Cortez (Pearls from the "Sea of Cortez," as the gulf is also known), is located in Guaymas (see Ladra, 1998). This pearl farm has the larger production and is the more technically advanced. To the best of our knowledge, it is the only facility in Latin America that cultures full-round pearls. One of the authors visited this farm in 2000 (see Kiefert, 2002). With the assistance of two staff members (DMM and EA), we have prepared this description of the farm and, primarily, its full-round cultured pearls, as well as obtained new gemological and spectroscopic data that enable them to be distinguished from Tahitian and treated-color cultured pearls. This study concentrates on the full-round cultured pearls from *P. sterna*, since they are much more valuable than the mabe product and because *P. mazatlanica* production is currently for research purposes only; cultured pearls from this oyster are not available commercially.

BACKGROUND OF THE SEA OF CORTEZ PEARL

Pearl Oyster Biology. Pearl oysters are mollusks belonging to the family *Pteriidae*, which includes two genii capable of producing high-quality mother-of-pearl shell: *Pinctada* and *Pteria*. There are fewer than 40 species of pearl oysters worldwide (Shirai, 1994), and of these just three are responsible for about 99.9% of the world's production of saltwater cultured pearls: the Akoya (*Pinctada fucata martenisii* or *Pinctada imbricate*), the black-lipped oyster *Pinctada margaritifera*, and the silver/gold-lipped oyster *Pinctada maxima*. Another saltwater oyster commonly used for commercial pearl production is the mabe-gai or penguin-wing oyster *Pteria penguin*, which is used solely for the production of mabe or half-round blister pearls.

Pearl oysters have separate sexes (although any individual oyster may change sex, known as *protandric hermaphroditism*) and breed by external fertilization. Clouds of gametes, sperm, and eggs are released into the water, so fertilization occurs randomly. Once fertilization takes place, several free-swimming larval stages develop; eventually, the juvenile will settle on an appropriate hard substrate (rock, coral, or shell). This entire process takes 18–34 days depending on water temperature and other factors. Once the juveniles settle, growth is rapid. During the first year, an oyster can reach 7 cm in length. It takes 18–24 months for the oysters to reach 8.5–10 cm, which is the desired size for pearl seeding (McLaurin Moreno and Arizmendi Castillo, 2002).



Figure 2. The *Perlas del Mar de Cortez* pearl farm in Guaymas, Sonora, is located on Bacochibampo Bay in the Gulf of California.

Pearl oysters usually grow in colonies from the low-tide mark to depths of 20 m and attach themselves to the substrate by a tuft of strong fibers (called the byssus). They feed by continuously filtering minute particles and organisms with their

Figure 3. The pearl farm is situated on coastline owned by the campus of the Instituto Tecnológico y de Estudios Superiores de Monterrey (ITESM) in Guaymas. Buoys mark the location of “long lines,” from which the oyster cages are suspended. Photo by Lore Kiefert, © SSEF.



gills (branchia), which are adapted to both breathing and feeding (McLaurin Moreno and Arizmendi Castillo, 2002).

Within the Gulf of California, there are two species of native pearl oysters: the Panamic black-lipped pearl oyster *Madreperla* (*P. mazatlanica*) and the rainbow-lipped pearl oyster or *Concha Nácar* (*P. sterna*). Both species inhabit the Sonora coastline as a part of their natural distribution, but both can also be found along Mexico’s Pacific coast, except that *P. mazatlanica* is not present on the western side of southern Baja California. *P. mazatlanica* can reach lengths of 20 cm, and has long been considered by many authors to be a variety or subspecies of *P. margaritifera*, the black-lipped oyster of the Indo-Pacific (Shirai and Sano, 1981). *P. sterna* can reach lengths of 16 cm, and has a more concave shell than either *P. mazatlanica* or *P. margaritifera*. The nacre of *P. sterna* has a more iridescent multicolored hue, with a metallic sheen unequalled by any other pearl oyster. It belongs to the “winged oyster” variety, thought by some (e.g., Shirai and Sano, 1981) to be unable to produce full-round (bead-nucleated) cultured pearls. While *Perlas del Mar de Cortez* has produced full-round cultured pearls from both oyster species, the commercial production is entirely from *P. sterna*, which yields richer and more varied colors than *P. mazatlanica*.

Location and Access. The *Perlas del Mar de Cortez* farm is located in Bacochibampo Bay, some 8 km from the port town of Guaymas, Sonora (figure 2), on coastline owned by the Guaymas campus of the Instituto Tecnológico y de Estudios Superiores de Monterrey (ITESM; figure 3). This privately owned and operated technological university has campuses across Mexico. Guaymas may be reached by air (a direct flight from Phoenix, Arizona); by land (a four-hour drive from Nogales, Arizona), or an eight-hour ferry ride from Santa Rosalia, on the Baja California peninsula. Once in Guaymas, any taxi can take the visitor to the university (known locally as “Tec de Monterrey”). The pearl farm is open to visitors, who may take a free tour of the facilities. Eight thousand visitors, most of them from the U.S., come every year.

Bacochibampo Bay is a typical marine bay, with little influence of freshwater (consisting mainly of rainfall runoff). The bay has a diversity of ecological niches: sand, gravel, and rocky bottoms provide a rich environment. Most of the bay is shallow (average depth 7 m), but near its mouth it deepens

abruptly (to 20 m), creating yet another marine environment.

Because of the Gulf of California's subtropical climate, summer months (June to September) are usually hot and dry, with an average water temperature of 29°C (84.2°F), a range of 27–32°C (80.6–89.6°F), with considerable evaporation. Winter months are characterized by much cooler average water temperatures of 19°C (66.2°F), with a range of 15–25°C (59–77°F), due primarily to the strong northwest winds that create upwelling along the Sonoran coastline. This movement of cold, nutrient-rich water masses from the deep ocean to surface levels allows for the high production of chlorophyll, which is necessary for the survival of pearl oysters.

Company Structure and Facilities. In 1993, ITESM researchers Sergio Farell, Manuel Nava, and two of the present authors (DMM and EA) began developing an economically and technically feasible pearl culture methodology. This group subsequently was responsible for the first commercial harvest of cultured mabe pearls in North America (in 1995) and the production of the first bead-nucleated cultured pearls utilizing *P. sterna*. Increased funding from ITESM in 1996 led to a project known as ITESM/Perlas de Guaymas, which served mainly to assist with pearl culture in Mexico and promote the resulting products in the local and world markets. In 2000, this branch of the aquaculture department was converted into a separate private company, Perlas del Mar de Cortez, which is still linked to the university.

The pearl farm encompasses a lagoon of 2 hectares (5 acres) for collecting spat and culturing the pearl oysters. A thatched-roof structure, or *palapa*, houses the land-based operations, and a small pearl-culture structure shelters the seeding operations and an X-ray apparatus. Pearl oyster production depends solely on juveniles gathered from "spat collectors" (mesh bags on which pearl oyster larvae settle) deployed within the bay. The abundance of pearl oyster larvae in Bacochibampo Bay is largely a result of the adult oysters in the pearl farm, since they are able to release their eggs and sperm directly into the sea where fertilization takes place. Thus a positive cycle develops where the more adult pearl oysters there are under culture, the more juveniles can be collected. Wild adult pearl oysters also contribute to larvae production but are never removed from the natural beds, since the 1939 Mexican federal fishing ban (mentioned above) remains in effect.



Figure 4. Juvenile *P. sterna* oysters are cultivated in various types of cages, according to their age. Photo by Lore Kiefert, © SSEF.

The oysters are housed in various cages according to their age and size (figures 4 and 5); these are hung from buoy-supported surface "long-lines." The cages are suspended at depths of 3–4 m. The largest number of oysters being cultivated at any one time is approximately 250,000. At the time of this writing, there were no plans to expand the size of the operation, although short-term plans are to increase the yield of cultured pearls, using the same number of oysters, through technical improvements.

Pearl seeding operations take place from October to early March, when the water temperature is below 25°C. As many as five seeding technicians can work simultaneously, using nuclei made from the shells of *Unionidae* family freshwater mussels from the Tennessee River.



Figure 5. After bead nucleation, the oysters are suspended in flat cages. Photo by Lore Kiefert, © SSEF.

Harvesting and Production. The results of the pearl culturing operation are unpredictable. There are no reliable methods to predetermine quality of the product, although Perlas del Mar de Guaymas uses two methods to monitor it. The first is X-ray examination of all the oysters, eight weeks after implantation. With this method, one can ensure that the oyster has not rejected the bead, and that the bead is located in the correct area of the animal's body. Oysters not meeting these criteria are considered "rejects," but they can be used to culture mabe pearls by opening the shell, pushing back the mantle, and attaching a mabe implant with cyanoacrylate ("super glue"). The second method involves several random samplings in order to better evaluate the development of the cultured pearls.

There is only one harvest per year, which takes place 18–20 months after seeding, typically in June when the water temperature rises. While other pearl oysters are sometimes reseeded with a larger bead, *P. sterna* oysters are shucked (their flesh removed) at the first harvest. This is because reseeded is very difficult and the resulting cultured pearls are, although larger, not as lustrous or colorful (Nava et al., 2000). Natural pearls and "keshi" (beadless cultured pearls formed due to rejected beads or injured mantle tissue) are occasionally found; both are used in jewelry. The shell is fashioned into buttons, while the oyster meat is sold locally.

P. sterna "keshi" are small (2–8 mm) and typically have baroque shapes (figure 6). Natural pearls usually are caused by drill-worms and worm-cysts. These pearls tend to be smaller and rounder than the "keshi." They can be distinguished during harvest because most grow within a very thin and delicate pearl sac found in the oyster's mantle. Typically, a half-dozen to a dozen good-quality natural pearls are obtained yearly.

The first dozen experimental full-round cultured pearls were shown during the February 1996 Tucson gem show. Since then, production has grown to about 4,000 cultured pearls per year, with improvements in size, shape, and surface quality evident each year. In the 2001 harvest, the average size was 7.5 mm, and only 5% were round or near-round; the other 95% were baroque. By 2002, average size had increased to 8.9 mm and some 25% were round or

Figure 6. A variety of shapes is seen in these "keshi" cultured pearls (up to 8 mm long) from the rainbow-lipped oyster *P. sterna*. Photo by Lore Kiefert, © SSEF.



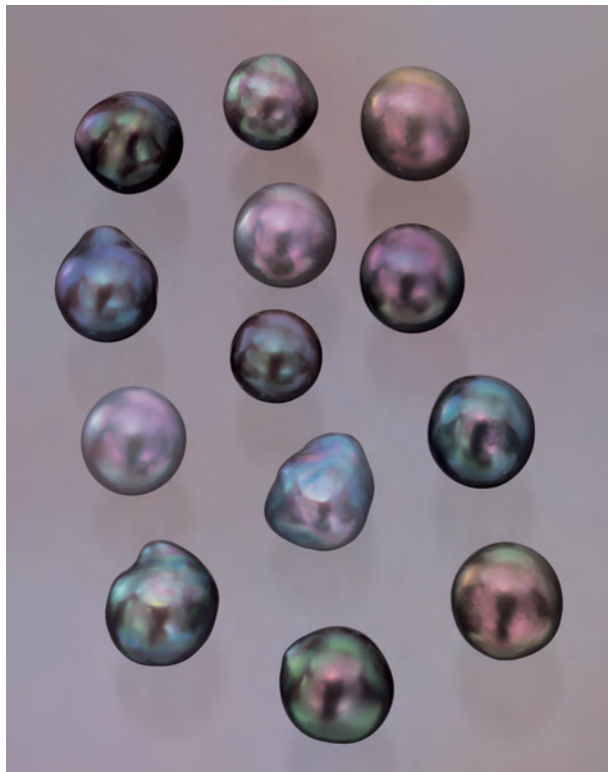


Figure 7. These cultured pearls (9.0–11.5 mm in diameter) illustrate the range of colors and shapes that are commercially available from Mexico's Gulf of California. Courtesy of Columbia Gem House; photo © GIA and Harold & Erica Van Pelt.

near-round. Starting in 2005, production is expected to stabilize at 10,000 cultured pearls (10 kg) per year.

Processing and Marketing of the Sea of Cortez Pearl. After harvesting, the full-round cultured pearls are placed in containers of fresh water, then drained and washed several times under running water. They are patted dry in a soft cotton towel and placed in a receptacle with mineral oil for about six hours, after which they are removed and blotted with a paper towel.

Approximately half of the cultured pearl production is mounted in jewelry by Mexican artisans and sold at the farm site and other tourist destinations. The marketing of these cultured pearls is managed primarily by the producing company, but the main distributor in the U.S., Columbia Gem House (Vancouver, Washington), is becoming a leading participant. The main goal of the marketing effort is to highlight differences between Mexican and Tahitian black cultured pearls. The Mexican product exhibits a greater diversity of color (figure 7), and prevailing colors may vary from year to year. Future goals

include development of a stable price structure with wholesalers, while avoiding overproduction.

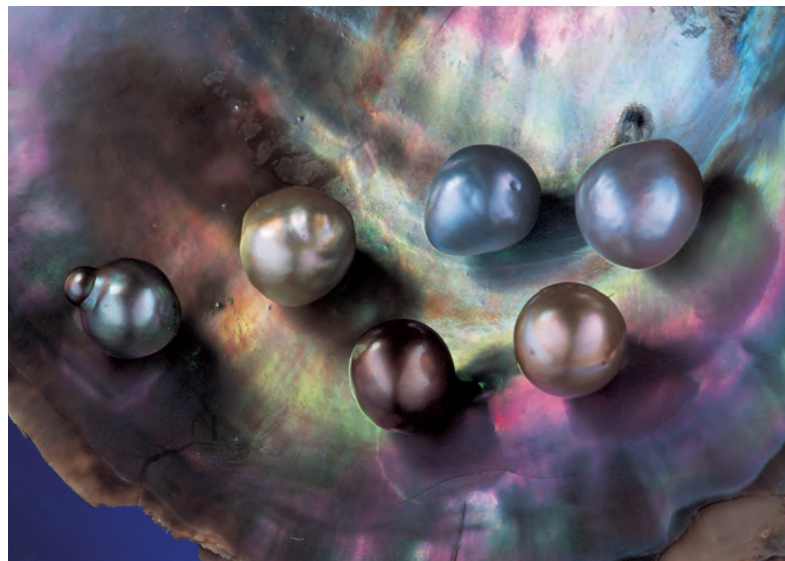
MATERIAL AND METHODS

For this study, 20 shells, 50 full-round cultured pearls (approximately 7–12 mm), and 11 “keshi” (4.5–8.3 mm long), all from *P. sterna* and farmed by Perlas del Mar de Cortez, were examined at SSEF. Additionally, two *P. sterna* shells and three full-round cultured pearls from the same farm were studied at GIA for comparison (figure 8). All of the samples tested were obtained in 2000. The samples consisted of various colors and qualities; 10–15% represented the commercial quality seen in the jewelry trade, whereas the others were rejects due to thin nacre layers and surface blemishes.

Forty-two of the full-round cultured pearls and 10 of the “keshis” were X-rayed using a Hewlett-Packard X-ray unit and Agfa Industrex X-ray film. Specific gravity of 20 cultured pearls was determined hydrostatically. All the cultured pearls were tested for reaction to both long- and short-wave UV radiation with a System Eickhorst UV lamp.

Scanning electron microscopy of five shell sections was performed at the University of Basel

Figure 8. Three of the *P. sterna* cultured pearls shown here were analyzed at GIA (i.e., the “golden,” gray, and dark brown samples in the center, 6.7–8.2 mm in diameter). Note the similarity in their colors to portions of the *P. sterna* shell (GIA Collection no. 30488). Photo by Maha Tannous.



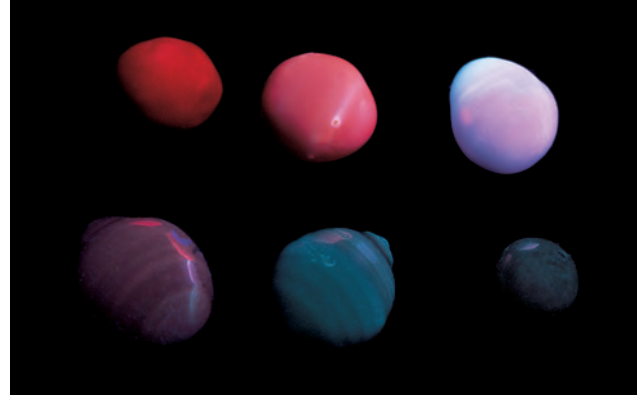
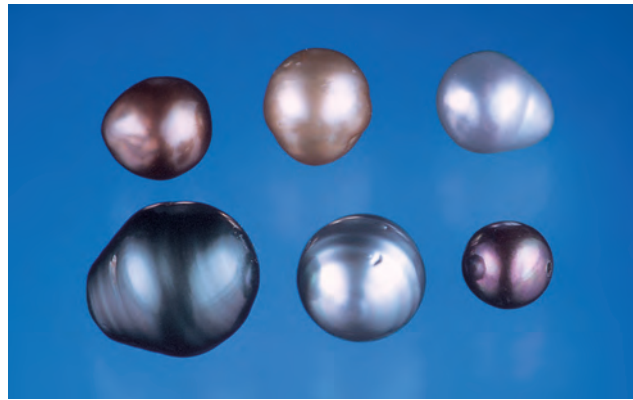


Figure 9. When exposed to long-wave UV radiation, the Mexican cultured pearls (top row; 6.7–8.2 mm in diameter) typically showed a weak to distinct red fluorescence. In contrast, the Tahitian cultured pearls examined (bottom left and center) fluoresced bluish gray and slightly reddish brown, and the dyed Akoya cultured pearl (bottom right) was inert. Natural Mexican pearls have fluorescence reactions similar to their cultured counterparts. Photos by Maha Tannous (left) and Shane Elen (right).

(ZMB SEM laboratory) with a Philips ESEM XL 30 FEG instrument, and the surface of one cultured pearl was imaged with the camera connected to a Raman microscope.

Reflectance spectra of 12 cultured pearls and one piece of shell were acquired in the visible and UV range (between 290 and 800 nm) with a Hitachi U4001 spectrophotometer at SSEF. Three cultured pearls and one piece of shell were characterized at GIA with the same type of instrument; luminescence spectra were also collected at GIA with an SLM Aminco AB2 luminescence spectrometer, using 360 and 400 nm excitation.

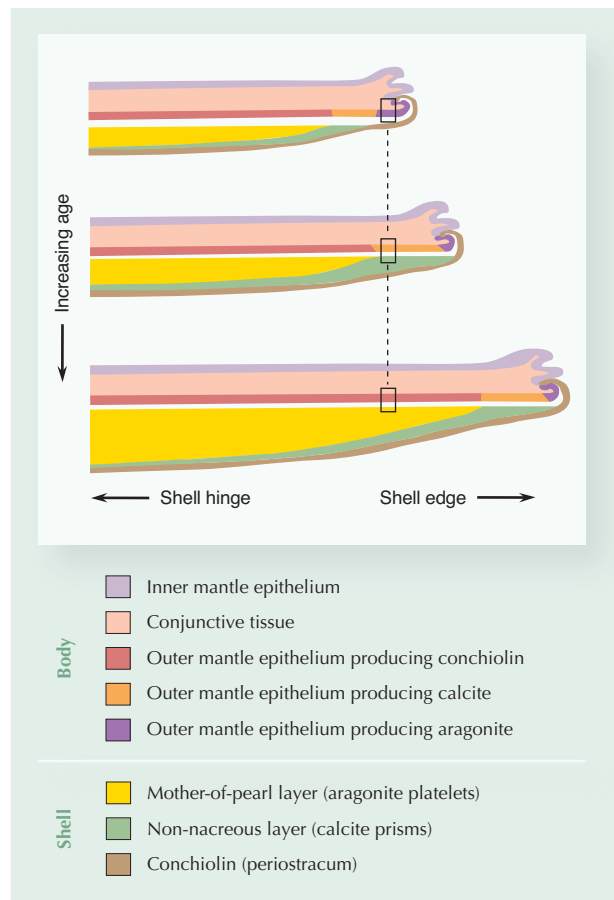
The chemical composition of six cultured pearls was determined qualitatively with a Tracor Spectrace 5000 energy-dispersive X-ray fluorescence spectrometer (EDXRF) at SSEF.

Raman spectra of six other cultured pearls and a piece of shell were recorded at SSEF with a Renishaw Raman System 1000 spectrometer, equipped with a CCD-Peltier detector and argon-ion laser (514 nm).

RESULTS

Physical Properties. The colors observed in the Mexican cultured pearls consisted of a brown or gray to dark gray bodycolor with overtones of violet, blue, yellow, and green, also called orient. The size of the cultured pearls depended mainly on the size of the implanted bead, and varied between approximately 7 and 11 mm. The larger samples often contained a cavity, occasionally with a loose bead. X-ray images showed the same pattern as for Akoya and other cultured pearls (Hänni, 1995, 1997, 2002; Strack, 2001): The round bead, which

Figure 10. This drawing shows the succession of materials (conchiolin, calcite prisms, aragonite platelets) that are deposited by the oyster's mantle tissue. Within a particular location (as indicated by the boxes) the production of the various materials changes with the passage of time. Mother-of-pearl (aragonite platelets) is the last material to form. © SSEF, 2004.



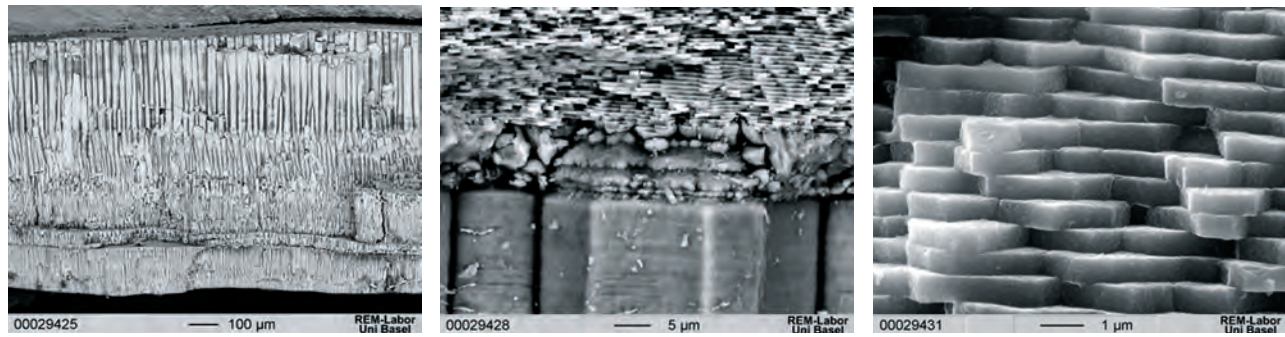


Figure 11. These SEM images show the microstructure of a shell section from *P. sterna*. As seen in the image on the left, most of the shell is composed of columnar calcite with subordinate tabular growth (aragonite). At higher magnification (center) the transition from columnar to tabular growth is plainly visible; the left side of the aragonite shows a more irregular growth pattern than the right side. The image on the right provides a closer look at the stacked aragonite “tiles” of the nacre, which are approximately 500 nm thick.

usually appeared lighter in the image, was surrounded by a concentric, somewhat darker layer of nacre. Nacre thickness of the commercial-quality cultured pearls X-rayed at SSEF varied between 0.8 and 1.2 mm. For the irregular and larger cultured pearls (semi-baroque or baroque), a dark, mostly irregular layer was visible on the X-ray image between the bead and the nacre, which indicated either a cavity or a layer of organic material.

For the most part, the “keshis” were baroque shaped and had a gray bodycolor with vivid overtones of violet, blue, yellow, and green. As with most “keshis,” the X-ray images of these samples frequently showed an irregular cavity in the center, which was surrounded by a relatively thin layer of nacre.

The full-round cultured pearls without a cavity had a specific gravity between 2.45 and 2.76, while the S.G.’s of those with a cavity were much lower, between 1.54 and 2.17. These values are below that of pure aragonite (2.94) and varied according to the presence of organic matter and/or cavities.

The vast majority (about 95%) of the cultured pearls analyzed showed a weak to distinct red fluorescence to long-wave UV radiation (figure 9).

Microstructure. Shell sections from *P. sterna* were used to study the construction of the strongly iridescent nacre in a manner similar to that used later by Liu et al. (2003). SEM images revealed that the shell showed the same succession of CaCO_3 components from outside to inside as other *Pinctada* and *Pteria* shells (Wise, 1970; figure 10): Columnar calcite was overlain by tabular aragonite (figure 11), and this was confirmed by Raman spectroscopy. A transition from columnar calcite to tabular aragonite also could be seen on the surface of the shell’s interior (figure 12), with the arag-

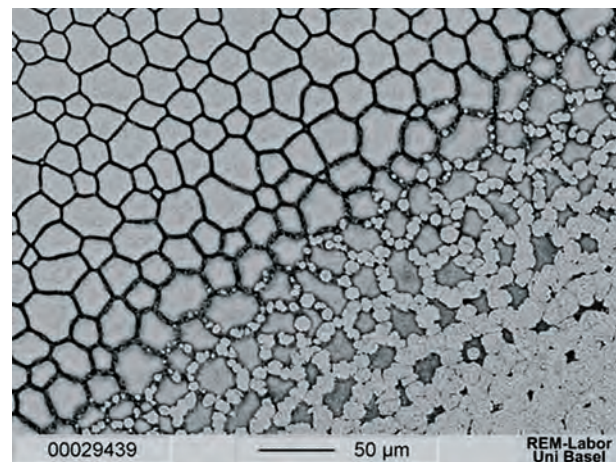
onite tiles initially deposited at the ends of the calcite columns.

The microstructure of *P. sterna* nacre is shown in figure 11 (center and right). The average thickness of the aragonite tablets was 500 nm, which is comparable to the wavelength of green light.

The scales of aragonite tiles that form the nacre surface of a cultured pearl are shown in figure 13. In places, the aragonite scales revealed spiral arrangements (figure 14).

Reflectance Spectroscopy. The top spectrum in figure 15 shows a typical UV-Vis reflectance spectrum of the Mexican *P. sterna* cultured pearls. An absorption band appears at around 400–405 nm, which can be attributed to porphyrins (Britton,

Figure 12. This SEM image of a *P. sterna* shell’s inner surface shows the polygonal pattern created by columnar calcite (upper left), which is overgrown by tabular aragonite (lower right).



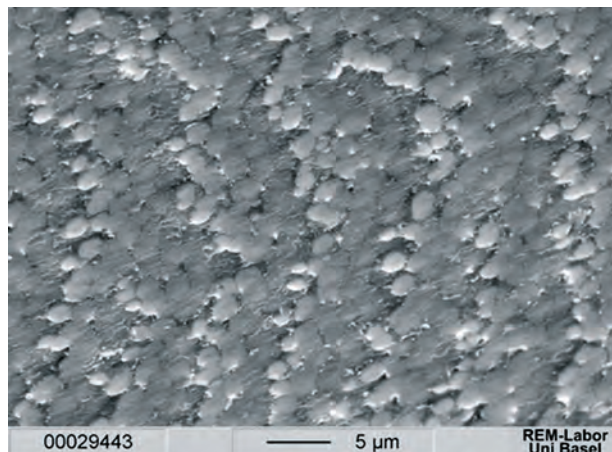


Figure 13. The aragonite tiles shown in this SEM image of the surface of a cultured pearl are responsible for the gritty sensation when it is rubbed against a tooth.

1983). This absorption is also present in black Tahitian cultured pearls (see bottom spectrum in figure 15). However, the distinctive absorption maximum at 700 nm in the Tahitian product is not present in the UV-Vis spectrum of Mexican cultured pearls. There are other more subtle differences in these spectra, as well.

Luminescence Spectrometry. Luminescence spectrometry of a cultured pearl revealed a broad fluorescence feature at 618 nm and a weaker one at 678 nm (figure 16). These features are the source of the red fluorescence, and are stronger than those recorded in dark-colored *P. margaritifera* cultured pearls (Elen, 2001). In the latter, the weaker peak at 678 nm is often not present (again, see figure 16).

Chemical Composition. The chemical composition of the Mexican cultured pearls resembled that of other saltwater cultured pearls, with Ca as the main element and traces of Sr. The Mn content was below the detection limit of EDXRF analysis, which is expected for saltwater cultured pearls (Gutmansbauer and Hänni, 1994).

Raman Spectroscopy. Raman spectra of the *P. sterna* shell and the cultured pearls showed a strong increase in fluorescence from 1000 cm^{-1} toward higher wavenumbers, with aragonite bands at 210, 705, and 1084 cm^{-1} that were weak due to the overall high fluorescence of the samples. Between 1100 and 1800 cm^{-1} were several broad bands centered at approximately 1260, 1320, and 1565 cm^{-1} , which are attributed to various types of organic matter such as conchiolin and porphyrin (figure 17, top).

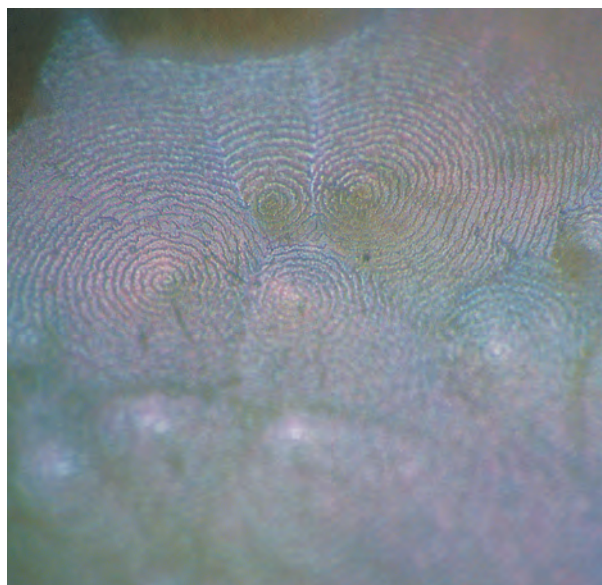
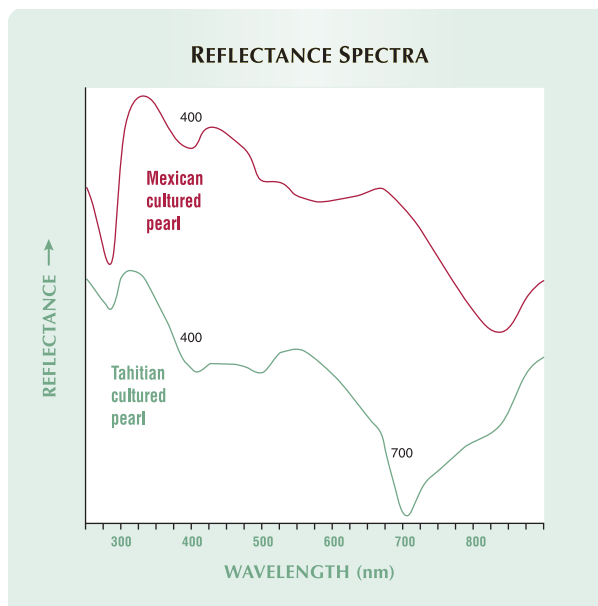


Figure 14. Note the spiral patterns formed by the aragonite layers on the surface of this Mexican cultured pearl. Photomicrograph by Lore Kiefert, © SSEF; magnified 100 \times .

The intensity of these bands increased with the intensity of the color. The Raman spectrum of a black Tahitian cultured pearl shows similar features (figure 17, bottom).

Figure 15. The UV-Vis reflectance spectrum of a Tahitian *P. margaritifera* cultured pearl (bottom) shows a typical absorption feature at 700 nm, which was absent from the Mexican *P. sterna* cultured pearls studied (top).



DISCUSSION

Cause of Color. A dark bodycolor in cultured pearls is produced by layers of conchiolin (and porphyrin) that are found between the layers of aragonite (cf. Wentzell, 1998). The iridescence has been attributed to the microstructure (i.e., layering) of the aragonite tiles and organic matter (Wada, 1981; Gauthier and Ajaques, 1989; Liu et al., 2003). The violet, blue, yellow, and green iridescent overtones seen in the Mexican cultured pearls are produced by interference, as light passes through and is reflected from the alternating thin layers of aragonite and conchiolin (Fritsch and Rossman, 1988). The iridescent colors exhibited by our samples are very similar to those of natural pearls from the Gulf of California (Cariño and Monteforte, 1995) and, in some cases, comparable to the colors of natural abalone pearls (e.g., Wentzell, 1998).

The calcite and aragonite constituents are produced by the same external mantle tissue, but at different times. This observation and explanation is in agreement with Lowenstam and Weiner (1989), Gutmannsbauer and Hänni (1994), and Hänni (2002). Figures 11 and 12 illustrate how the first aragonite tiles were deposited at the ends of the calcite columns. Scanning electron micrographs of the *P. sterna* shell sections revealed that the average thickness of an aragonite tablet was 0.5 μm (or 500 nm), which is comparable to the wavelength of green light. Thus, the layers are spaced appropriately to cause

interference phenomena and produce iridescence. The aragonite layers are mostly parallel, but there are also areas that are slightly irregular (figure 11). This wavy structure has been observed previously in abalone shells, which also show very strong iridescence (Hänni, 2002). It is therefore possible that this structure may provide an additional cause of iridescence in shell and cultured pearl samples from *P. sterna*.

As mentioned above, both the shells and the cultured pearls contained a certain amount of conchiolin and porphyrin. Conchiolin is a fibrous protein, and porphyrins are naturally occurring tetrapyrrole pigments. While such organic network structures are essential for the formation of the individual aragonite tiles, we could observe no traces of them in our SEM images. This is probably due to the high water content of this organic material, which dries out and shrinks when removed from the water. Porphyrin occurrence in mollusk shell can often be detected by a red, pink, or reddish brown fluorescence to long-wave UV radiation or blue light (Comfort, 1949), which also produces a fluorescence emission around 620 nm (Miyoshi et al., 1987a,b). Similar red fluorescence was documented in our samples.

The presence of porphyrin and conchiolin was also evident in the Raman spectra of the cultured pearls, where several broad bands centered at approximately 1260, 1320, and 1565 cm^{-1} can be observed. Reference spectra of one type of porphyrin (i.e., uroporphyrin) taken by one of the authors (SE)

Figure 16. With 365 nm excitation, the luminescence spectrum of a typical *P. sterna* cultured pearl from Mexico shows features at 618 and 678 nm due to porphyrins. The luminescence spectrum of a typical *P. margaritifera* cultured pearl taken under similar conditions reveals a much weaker emission at 618 nm and no evidence of the 678 nm feature.

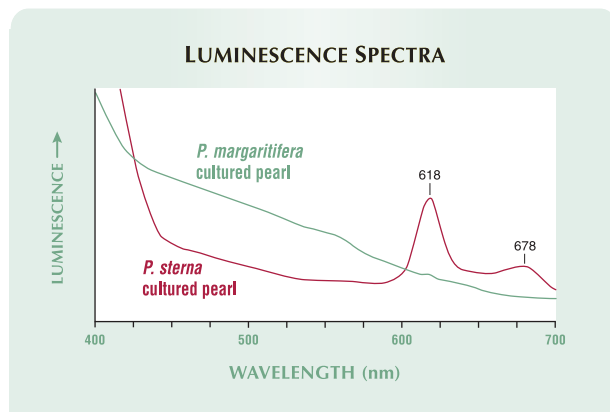


Figure 17. The similarity in the Raman spectra of Mexican cultured pearls (top) and black Tahitian cultured pearls (bottom) is the result of the presence of porphyrin as a coloring pigment in both. The spectra have been baseline-corrected to eliminate the fluorescent effect.

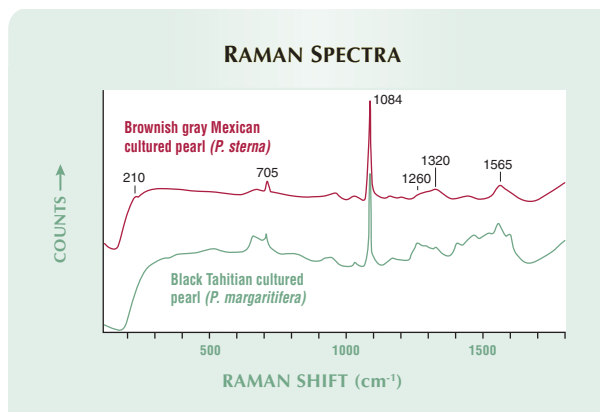




Figure 18. The cultured pearls produced in Mexico by the rainbow-lipped oyster *P. sterna* show brown or gray to dark gray bodycolors and attractive iridescence. Interesting baroque shapes as well as spherical products are available, as shown by these cultured pearls shown loose (up to 12.5 mm long) and in 18K gold jewelry. Courtesy of Columbia Gem House; photo © GIA and Harold & Erica Van Pelt.

contain these bands, but other organic materials also have such features in the same region. The bands attributed to organic matter increased with the intensity of the bodycolor. Porphyrin has been described as a coloring pigment in Tahitian cultured pearls from *P. margaritifera* (Gauthier and Ajaques, 1989; Iwahashi and Akamatsu, 1994) as well as for *P. sterna* (S. Akamatsu, pers. comm., 2003). This explains the similarity between the Raman spectra of these two varieties of cultured pearls (figure 17).

Separation from Tahitian Cultured Pearls. The red long-wave fluorescence shown by the Mexican cultured pearls is not seen in Tahitian cultured pearls, which are typically inert to slightly reddish brown (Elen, 2002; figure 9). Porphyrins are among the most highly fluorescent compounds in nature (Guilbault, 1990), and according to Hurwit (1992; 2000), red fluorescence is a characteristic feature of

pearls from the Gulf of California.

Usually the presence of porphyrins also results in an intense absorption feature between 390 and 425 nm, depending on the exact structure of the porphyrin present. This absorption is known as the B band, or Soret band, after its discoverer (Britton, 1983). In the case of *P. sterna* from Mexico, it was observed that this absorption feature appears around 400–405 nm, and exposure to this wavelength of light will produce strong fluorescence from the porphyrin in the shell or cultured pearls.

The most significant difference in the reflectance spectra of *P. sterna* and *P. margaritifera* is the absence of the 700 nm absorption feature for *P. sterna*. This absorption is characteristic of *P. margaritifera* (figure 15; see also Goebel and Dirlam, 1989; Iwahashi and Akamatsu, 1994; and Elen, 2002).

Separation from Artificially Colored Black Pearls.

Since the full-round cultured pearls from the Sea of Cortez are similar in size to Akoya cultured pearls and are also bead-nucleated (unlike black dyed or irradiated Chinese freshwater cultured pearls), it is important to identify their color authenticity. Attempts to produce black colors in Akoya cultured pearls with silver nitrate were undertaken as early as the 1930s in Japan (Strack, 2001). This treatment is still being done, although a number of other methods of artificial coloration have been developed (McClure and Smith, 2000; Strack, 2001). Silver nitrate treatment is relatively easy to detect, either through X-ray imaging, where a white line due to the absorption of X-rays by the silver nitrate is visible between the bead and the nacre, or through X-ray fluorescence, where silver is detected. Another method of identifying silver nitrate treatment is Raman spectroscopy, which reveals a band at 240 cm^{-1} (Kiefert et al., 2001) that does not occur in black cultured pearls of natural color (see figure 17).

Other treatments, such as irradiation or organic dye, are much harder to identify. One identification tool is the fluorescence to long-wave UV radiation. The red fluorescence typical of natural (Cariño and Monteforte, 1995) and cultured pearls from the Gulf of California is not seen in those artificially colored by organic dye or irradiation, which are either inert or display a weak white fluorescence.

CONCLUSIONS

As a commercial source of black cultured pearls, the Gulf of California is relatively unknown com-

pared to Tahiti. Natural pearls from the Gulf of California have been highly valued since the times of the Spanish conquerors, but they have been extremely rare for many decades. At the end of the 1990s, pearl culturing in the Gulf of California achieved commercial status for the first time. The full-round cultured pearls from this area are produced by the rainbow-lipped oyster *P. sterna*, and possess an attractive brown or gray to dark gray bodycolor with various overtones (figure 18). They are marketed directly through sales offices in Mexico and at the Tucson gem show; the main U.S. distributor is Columbia Gem House. Since these cultured pearls are similar in size to Akoya cultured pearls, which are often artificially colored black, it is important to know their distinguishing features.

As in other dark-colored cultured pearls, the bodycolor of those from the Gulf of California is produced by layers of conchiolin (and porphyrin) between the layers of aragonite, while the various

hues and overtones are a product of light passing through and reflecting from alternating layers of aragonite and organic matter (mostly conchiolin, but also some porphyrin). Compared to black Tahitian cultured pearls, those from the Sea of Cortez have a wider variety of overtones, sometimes similar to colors found in abalone pearls.

The porphyrin present in the *P. sterna* cultured pearls produces a clearly visible red fluorescence when observed with long-wave UV radiation, while such strong red fluorescence is not observed in Tahitian cultured pearls. Another difference lies in the UV-Vis spectrum, with Tahitian cultured pearls exhibiting a strong absorption feature at 700 nm that is absent from Mexican cultured pearls. The presence of conchiolin and porphyrin may be detected with Raman spectroscopy, where bands between 1100 and 1800 cm^{-1} can be observed. These bands, as well as the red fluorescence, are not present in the spectra of artificially colored cultured pearls and therefore are indicative of natural color.

ABOUT THE AUTHORS

Dr. Kiefert (gemlab@sssf.ch) is director of the Coloured Stones Department, and Dr. Hänni is director, at the SSEF Swiss Gemmological Institute, Basel. Mr. McLaurin Moreno is professor at the Guaymas campus of the Instituto Tecnológico y de Estudios Superiores de Monterrey, Mexico. Mr. Arizmendi is managing director at Perlas del Mar de Cortez in Guaymas, Sonora, Mexico. Mr. Elen is a research gemologist at GIA Research in Carlsbad.

ACKNOWLEDGMENTS

The authors thank Dr. K. Schmetzer (Petershausen, Germany) and P. Groenenboom (Amhem, Netherlands) for supplying references. Scanning electron microscopy was carried out by Daniel Mathys of the Centre for Microscopy of Basel University (ZMB), and Peter Giese of SSEF recorded numerous UV-Vis spectra. We thank S. Akamatsu for a critical review of the paper and numerous helpful suggestions.

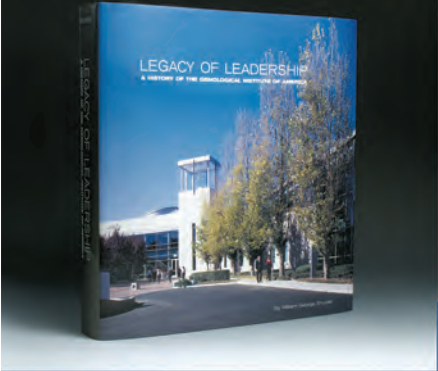

REFERENCES

- Alvarez-Borrego S. (1983) Gulf of California. In B.H. Ketchum, Ed., *Estuaries and Enclosed Seas*, Elsevier Science, Amsterdam, pp. 427–449.
- Britton G. (1983) *The Biochemistry of Natural Pigments*. Cambridge University Press, Cambridge.
- Cáceres-Martínez C., Chávez-Villalba J. (1997) The beginnings of pearl oyster culture in Baja California Sur, Mexico. *World Aquaculture*, Vol. 28, No. 4, pp. 33–38.
- Cariño M., Monteforte M. (1995) History of pearling in La Paz Bay, South Baja California. *Gems & Gemology*, Vol. 31, No. 2, pp. 88–105.
- Comfort A. (1949) Acid-soluble pigments of shells. I. The distribution of porphyrin fluorescence in molluscan shells. *Biochemical Journal*, Vol. 44, pp. 111–117.
- Crowningshield R. (1991) Gem Trade Lab Notes: Pearls from Baja California. *Gems & Gemology*, Vol. 27, No. 1, p. 42.
- Elen S. (2001) Spectral reflectance and fluorescence characteristics of natural-color and heat-treated “golden” South Sea cultured pearls. *Gems & Gemology*, Vol. 37, No. 2, pp. 114–123.
- Elen S. (2002) Identification of yellow cultured pearls from the black-lipped oyster *Pinctada margaritifera*. *Gems & Gemology*, Vol. 38, No. 1, pp. 66–72.
- Fritsch E., Rossman G.R. (1988) An update on color in Gems. Part 3: Colors caused by band gaps and physical phenomena. *Gems & Gemology*, Vol. 24, No. 2, pp. 81–102.
- Gauthier J.P., Ajaques J.M. (1989) La perle au microscope électronique. *Revue de Gemmologie a.f.g.*, No. 99, pp. 12–17.
- George C. D. (1971) The black pearls. History and development. *Lapidary Journal*, Vol. 25, No. 1, pp. 136–147.
- Goebel M., Dirlam D.M. (1989) Polynesian black pearls. *Gems & Gemology*, Vol. 25, No. 3, pp. 130–148.
- Guilbault G.G. (1990) *Practical Fluorescence*, 2nd ed. Marcel Dekker, New York.
- Gutmansbauer W., Hänni H.A. (1994) Structural and chemical investigations on shells and pearls of nacre forming salt- and fresh-water bivalve molluscs. *Journal of Gemmology*, Vol. 24, No. 4, pp. 241–252.
- Hänni H.A. (1995) A short synopsis of pearls: Natural, cultured, imitation. *Journal of the Gemmological Association of Hong Kong*, Vol. 18, pp. 43–46.
- Hänni H.A. (1997) Über die Bildung von Perlmutter und Perlen. *Gemmologie: Zeitschrift der Deutschen Gemmologischen Gesellschaft*, Vol. 46, No. 4, pp. 183–196.
- Hänni H.A. (2002) *Pearls*. SSEF Tutorial 1, Modern Gemmology.

- CD-ROM, SSEF Swiss Gemmological Institute, Basel.
- Hurwit K. (1992) Gem Trade Lab Notes: Black pearl from Baja California. *Gems & Gemology*, Vol. 28, No. 2, p. 126.
- Hurwit K. (2000) Black cultured pearls from Baja California, Mexico. *GIA Insider*, Vol. 2, Issue 6, www.gia.edu/newsroom/issue/2798/1002/insider_newsletter_details.cfm#2.
- Iwahashi Y., Akamatsu S. (1994) Porphyrin pigment in black-lip pearls and its application to pearl identification. *Fisheries Science*, Vol. 60, pp. 69–71.
- Kiefert L. (2002) Zuchtperlen vom Golf von Kalifornien, Mexiko. *Gemmologie: Zeitschrift der Deutschen Gemmologischen Gesellschaft*, Vol. 51, No. 2–3, pp. 121–132.
- Kiefert L., Hänni H.A., Ostertag T. (2001) Raman spectroscopic applications to gemmology. In I.R. Lewis and H.G.M. Edwards, Eds., *Handbook of Raman Spectroscopy*. Marcel Dekker, New York, pp. 469–489.
- Ladra D. (1998) Mexico revives pearl production. *Colored Stone*, Vol. 11, No. 6, pp. 38–41.
- Liu Y., Hurwit K.N., Tian L. (2003) Iridescence of a shell of *Pteria sterna* (Gould 1851): An optical and structural investigation. *Gemmologie: Zeitschrift der Deutschen Gemmologischen Gesellschaft*, Vol. 52, No. 4, pp. 145–150.
- Lowenstam H.A., Weiner S. (1989) *On Biomineralization*. University Press, Oxford.
- McClure S.F., Smith C.P. (2000) Gemstone enhancement and detection in the 1990s. *Gems & Gemology*, Vol. 36, No. 4, pp. 336–359.
- McLaurin Moreno D. (2002) Mexico's pearling history. *Pearl World*, Vol. 10, No. 1, pp. 1–16.
- McLaurin Moreno D., Arizmendi Castillo E. (2002) Five centuries of Mexican pearls. *Australian Gemmologist*, Vol. 21, No. 5, pp. 190–201.
- Miyoshi T., Matsuda Y., Komatsu H. (1987a) Fluorescence from pearls to distinguish between mother oysters used in pearl culture. *Japanese Journal of Applied Physics*, Vol. 26, No. 4, pp. 578–581.
- Miyoshi T., Matsuda Y., Komatsu H. (1987b) Fluorescence from pearls and shells of black-lip oyster, *Pinctada margaritifera*, and its contribution to the distinction of mother oysters used in pearl culture. *Japanese Journal of Applied Physics*, Vol. 26, No. 7, pp. 1069–1072.
- Nava M., Arizmendi E., Farell S., McLaurin D. (2000) Evaluation of success in the seeding of round pearl nuclei in *Pteria sterna* (Gould 1851) a new species in pearl culture. *SPC Pearl Oyster Information Bulletin*, Secretariat of the Pacific Community, New Caledonia, December, pp. 12–16.
- Shirai S. (1994) *Pearls & Pearl Oysters of the World*. Marine Planning Co., Nagano, Japan, 108 pp.
- Shirai S., Sano Y. (1981) Report on the pearl resources, pearl oyster grounds and pearl culture around La Paz in Baja California, Mexico. *Journal of the Pacific Society*, October, pp. 5–23.
- Strack E. (2001) *Perlen*. Rühle-Diebener Verlag GmbH & Co. KG, Stuttgart, 696 pp.
- Wada K. (1981) Pearls. *Journal of the Gemmological Society of Japan*, Vol. 8, pp. 151–158.
- Wentzell C.Y. (1995) Gem Trade Lab Notes: Blister pearl attached to shell. *Gems & Gemology*, Vol. 31, No. 1, pp. 55–56.
- Wentzell C.Y. (1998) Cultured abalone blister pearls from New Zealand. *Gems & Gemology*, Vol. 34, No. 3, pp. 184–200.
- Wise S.W. (1970) Microarchitecture and mode of formation of nacre (mother-of-pearl) in pelecypods, gastropods and cephalopods. *Eclogae Geologicae Helvetiae*, Vol. 63, pp. 775–797.

LEADERSHIP LEGACY OF LEADERS

NOW AVAILABLE!

LEGACY OF LEADERSHIP
A HISTORY OF THE GEMOLOGICAL INSTITUTE OF AMERICA

Prize-winning journalist William George Shuster of JCK magazine tells the story of GIA and the growth of the gemology movement worldwide. Features more than 200 archival images and interviews with dozens of the gem and jewelry industry's history makers.

Yours for only \$49.95

To order, visit www.gia.edu and click on **GIA Gem Instruments and Books**.
Call 800-421-8161 within the U.S., or 760-603-4200.

X-RAY FINGERPRINTING ROUTINE FOR CUT DIAMONDS

Roland Diehl and Nikolaus Herres

X-ray topography is a nondestructive technique that permits the visualization of internal defects in the crystal lattice of a gemstone, especially diamond, which is highly transparent to X-rays. This technique yields a unique “fingerprint” that is not altered by gem cutting or treatments such as irradiation and annealing. Although previously a complicated and time-consuming procedure, this article presents a simplified X-ray topographic routine to fingerprint faceted diamonds. Using the table facet as a point of reference, the sample is crystallographically oriented in a unique and reproducible way in front of the X-ray source so that only one topograph is necessary for fingerprinting. Should the diamond be retrieved after loss or theft, even after recutting or exposure to some forms of treatment, another topograph generated with the same routine could be used to confirm its identity unequivocally.

Diamonds, whether rough or cut (figure 1), are one of the most closely scrutinized commodities in the world. Gemological laboratories routinely evaluate the carat weight, color, clarity, and cut characteristics of faceted diamonds, and record them on a report that serves not only as a basis for the gem’s value, but also as a record that can help in the later identification of a stone. These identifying characteristics may be useful in the event of loss or theft, and for tracking diamonds that may be resubmitted to laboratories for regrading. However, re-identification may become difficult or impossible if the stone has undergone any of the following:

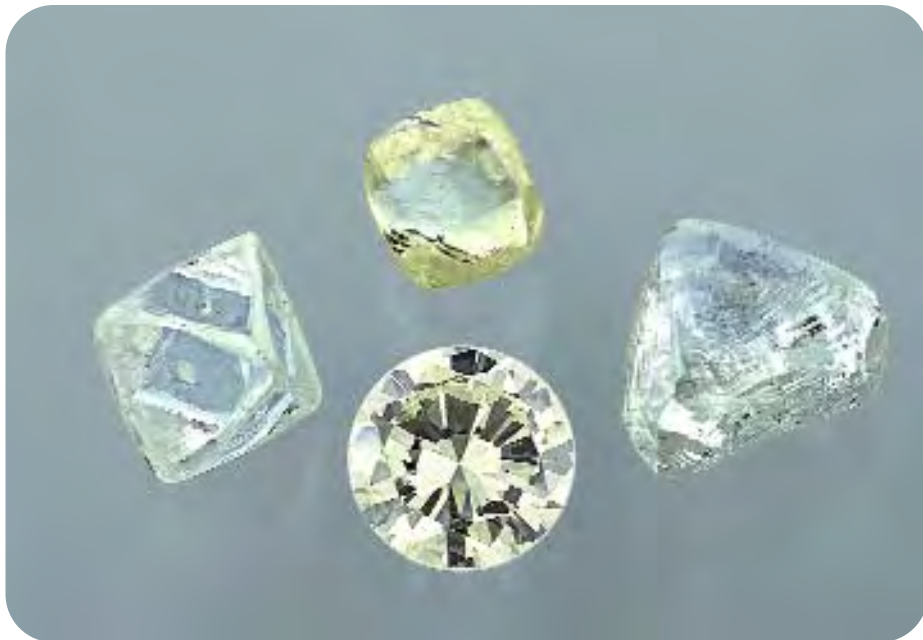
- Re-cutting or re-polishing, which may cause significant deviations in a stone’s proportions and weight, or remove identifying marks such as laser inscriptions
- Laser drilling, which can significantly change the clarity appearance and/or grade
- Treatments to induce a change in color

In the past decade, there have been various attempts to develop characterization methods that

render a faceted diamond uniquely identifiable. One method records the pattern of light reflected from the facets on a cylindrical sheet of film surrounding the stone. Such a *scintillogram* is indeed a “fingerprint,” but minor re-polishing will modify subsequent patterns obtained from the same stone (Wallner and Vanier, 1992). Another approach is to place a mark on the surface of a given stone that does not affect its clarity grade, but is clearly visible under certain viewing conditions. As described in a recent patent (Smith, 1999), this type of feature can be generated by ion-beam milling to “uniquely identify the gemstone by a serial number or as a brand or quality mark.” However, the mark penetrates only about 30 nm, so it can be easily polished away with just a tiny loss in weight. In at least one instance, laser inscriptions were polished off diamonds that had been decolorized by high pressure/high temperature treatment (Moses et al.,

See end of article for About the Authors and Acknowledgments.
GEMS & GEMOLOGY, Vol. 40, No. 1, pp. 40–57.
© 2004 Gemological Institute of America

Figure 1. Diamond crystals show morphological features, such as sharp or resorbed crystal faces, that can be used to find the orientation of their crystal lattice. When faceted, the orientation of the crystal lattice relative to any facet can be described using X-ray topography. This technique also can be used to image various lattice defects, which form a unique “fingerprint” for each diamond. Clockwise from the 7.51 ct round brilliant is a 15.98 ct octahedron, a 9.43 ct yellow crystal, and a 22.32 ct macle (GIA Collection nos. 8992, 11954, 11952, and 11955, respectively). Photo by C. D. Mengason.



1999). In the last few years, advanced methods of fingerprinting diamonds have been researched to support a global certification program to deal with conflict diamonds (see, e.g., Laurs, 2001).

Most promising are X-ray methods, which can nondestructively portray the internal defects of a diamond’s crystal lattice (figure 2), and have already been used to prove that two diamonds were faceted from the same piece of rough (Sunagawa et al., 1998). In this article, we present the concept of an alignment procedure using X-ray topography that routinely enables the unique and virtually unchangeable characterization of cut diamonds. We first described this concept, in German, in the late 1990s (Diehl and Herres, 1997; 1998); it was based on the study of one piece of rough and three faceted diamonds (one of which was cut from the sample piece of rough), from which we collected approximately 50 topographs.

To explain the essentials of this concept here, we have provided some background on crystallography. The first section below describes how the individual faces of crystal forms are named. The next introduces the most important crystal forms of diamond and their symmetry, and the third explains the representation of a crystal’s orientation using a stereographic projection. Then, following an introduction to crystal lattice defects and some basics of X-ray diffraction, we explain how to visualize lattice defects using X-ray topography. Finally, we describe the simplified routine to orient a faceted diamond for fingerprinting.

BACKGROUND

Directions and Faces in a Crystal Lattice. In principle, a crystal is a periodic regular arrangement of atoms in three dimensions. This spatial arrangement of atoms is termed a *crystal lattice*. In diamond, these atoms are carbon. During crystal growth, atoms are deposited layer by layer on lattice planes, causing the crystal to grow as the lattice planes increase in area. When the crystal stops growing, the multitude of lattice planes forms the faces, edges, and corners of the crystal (figure 3).

In crystallography, a system of axial coordinates is used to index the individual faces of a crystal so that it can be described completely. To achieve this, crystallographers denote the faces of a crystal form with numerals in parentheses called *Miller indices*. Crystal forms belonging to the cubic system—such as the cube, octahedron, and dodecahedron—are related to a perpendicular set of coordinate axes *x*, *y*, and *z*, with faces that intersect these axes at equal units *a*, *b*, and *c* (figure 4). The Miller indices (*hkl*) describe the position of a crystal face relative to the distance at which it intersects each of the coordinate axes. The index “*h*” refers to the *x*-axis, “*k*” to the *y*-axis, and “*l*” to the *z*-axis.

Consider face A in figure 4, which intersects the *x*-axis at *1a* and the *y*-axis at *1b*, and is parallel to the *z*-axis (which means that it intersects the *z*-axis at infinity, ∞). As calculations with infinite numbers are inconvenient, the axial intersections “*1 1 ∞* ” are transformed to their reciprocal values to become “(110)” (read “one, one, zero”), which are the Miller

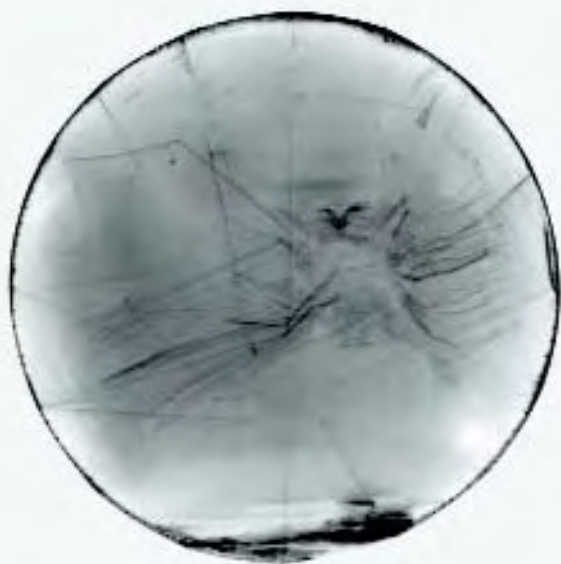


Figure 2. This X-ray topograph of a 0.63 ct round brilliant diamond shows characteristic bundles of dislocation lines and other contrast features that originate from lattice defects. Some of the pavilion edges also are visible as straight lines.

indices of crystal face A. Face B has the Miller indices (001), since it intersects the z-axis but not the x- or y-axes. Face C intersects all axes at the same relative distance, denoted (111). Face D, with its axial intersections of $1a$, $2b$, and $1^{1/2}c$, transforms to “1, $1/2$, and $2/3$.” However, Miller indices are always expressed as whole numbers, so multiplying by the common denominator (in this case 6) yields Miller indices for face D of (634).

Face E intersects the “positive” x-axis, the “negative” y-axis, and the “positive” z-axis, all at unity. Hence, the Miller indices of E are (1 $\bar{1}$ 1), read “one, bar one, one.” Face F intersects the axes at $1a$, $2b$, and $-2c$, with reciprocal values of 1, $1/2$ and $-1/2$, respectively. After multiplication with a factor of 2 (again, the common denominator) to obtain integers, this yields the Miller indices (21 $\bar{1}$).

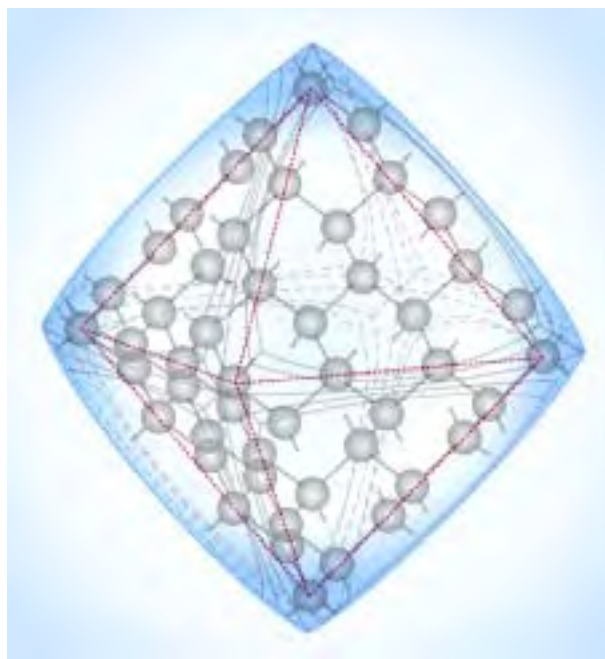
The orientation of vectors within a crystal lattice is expressed within square brackets. The vector direction is defined according to the coordinate axes, starting at their intersection point or origin. For example, [100] denotes the direction parallel to the x-axis, and [111] denotes a diagonal direction (go $1a$ along x, $1b$ along y, and $1c$ along z, and connect this point with the origin of the coordinate axes). In a cubic lattice, a vector given by [hkl] is perpendicular to the (hkl) plane. [For textbooks on crystallography, see, for example, Buerger (1967) and Borchardt-Ott (1997).]

Crystal Forms and Symmetry. An inherent property of regular crystal forms is their symmetry (figure 5). This is recognized by their congruence of shape when viewed from various directions. Thus, when viewed parallel to one of its three coordinate axes, a cube looks like a square (figure 6); the appearance of a square occurs six times (twice for each coordinate axis). This multiplicity is eight-fold for an octahedron and 12-fold for a dodecahedron. The crystal faces of these highly symmetric forms are described as “symmetrically equivalent,” and a single index can be used to express the form of the crystal as a whole. When this is done, the index is placed in braces, for example {100} for a cube.

The cube, also known as a “hexahedron,” has six faces with Miller indices (100), (010), (001), ($\bar{1}$ 00), (0 $\bar{1}$ 0), and (00 $\bar{1}$)—indicating that each face intersects only one of the coordinate axes, but is parallel to the remaining two axes. This ensemble of faces is symbolized by {100} for this crystal form. The octahedron—the crystal form of most diamonds—is represented by {111}, since the axes are intersected at equal length by each of the eight faces.

Each of the 12 faces of the dodecahedron intersects two of the axes at equal length and does not

Figure 3. This schematic illustration shows a diamond octahedron in relation to the underlying crystal lattice. Such octahedra usually have a rounded appearance due to partial dissolution after crystal growth.



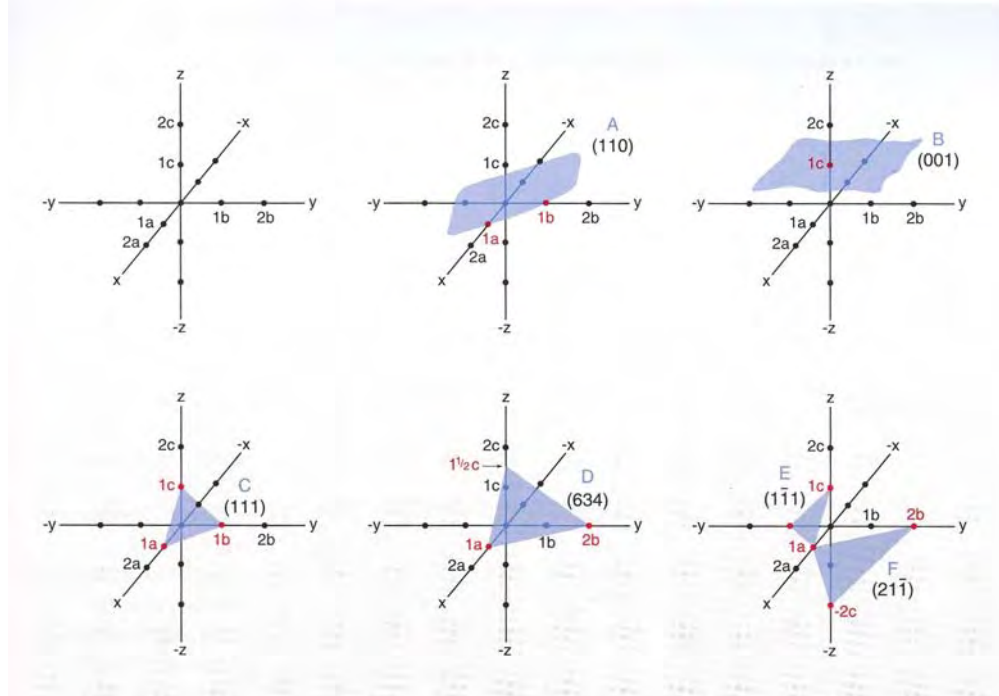


Figure 4. Crystal forms belonging to the cubic system (such as diamond) are related to a perpendicular set of coordinate axes x , y , and z . Crystal faces are described by Miller indices according to their intersection with these axes at unit distances of a , b , and c , respectively. (See text for details.)

intersect the third axis. Hence the Miller index for this crystal form is $\{110\}$. The dodecahedron is another important crystal form of diamond; it is thought to form by post-growth resorption along the edges of an octahedron.

Another way to express symmetry is to relate a crystal form to rotation around imaginary axes that run through the intersection point (or "origin") of the coordinate axes. For a cube, there are three such perpendicular axes, each connecting the center of one square face to the center of the opposite face. With each complete rotation of the cube around one axis, there are four positions of congruence—that is, after each quarter-turn, the cube looks like it did in the previous position. This axis of four-fold symmetry is called a *tetrad*. A cube has three tetrads, which coincide with the three coordinate axes.

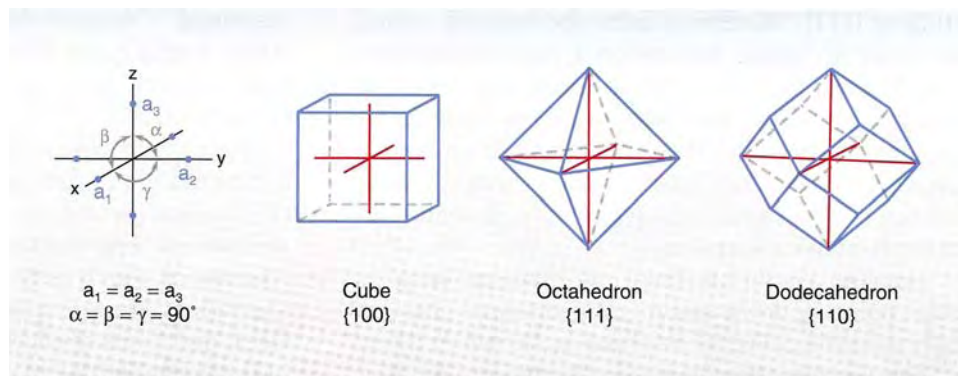
An axis that connects two corners of a cube exhibits three positions of congruence after a full rotation of the cube. This three-fold symmetry axis is termed a *triad*. Since a cube has eight corners, it has four triads.

An axis that connects the centers of opposite cube edges has two-fold symmetry. These are termed *diads* because congruence occurs after each half-turn. A total of six diads connect the 12 edges of a cube.

Octahedra and dodecahedra exhibit the same axial symmetry as a cube. Tetrads connect the corners of the octahedron, triads connect the centers of its opposing faces, and diads connect the centers of its edges. For the dodecahedron, tetrads connect the acute corners, triads connect the obtuse corners, and diads connect the centers of its faces.

Complementing axial symmetry, mirror symme-

Figure 5. The cubic system has the highest degree of symmetry of all the crystal systems. All three axes are perpendicular, and the unit distances a , b , and c are equal and therefore commonly denoted a_1 , a_2 , and a_3 to indicate equality. Three common cubic forms are shown here. Diamond commonly displays octahedral and dodecahedral forms.



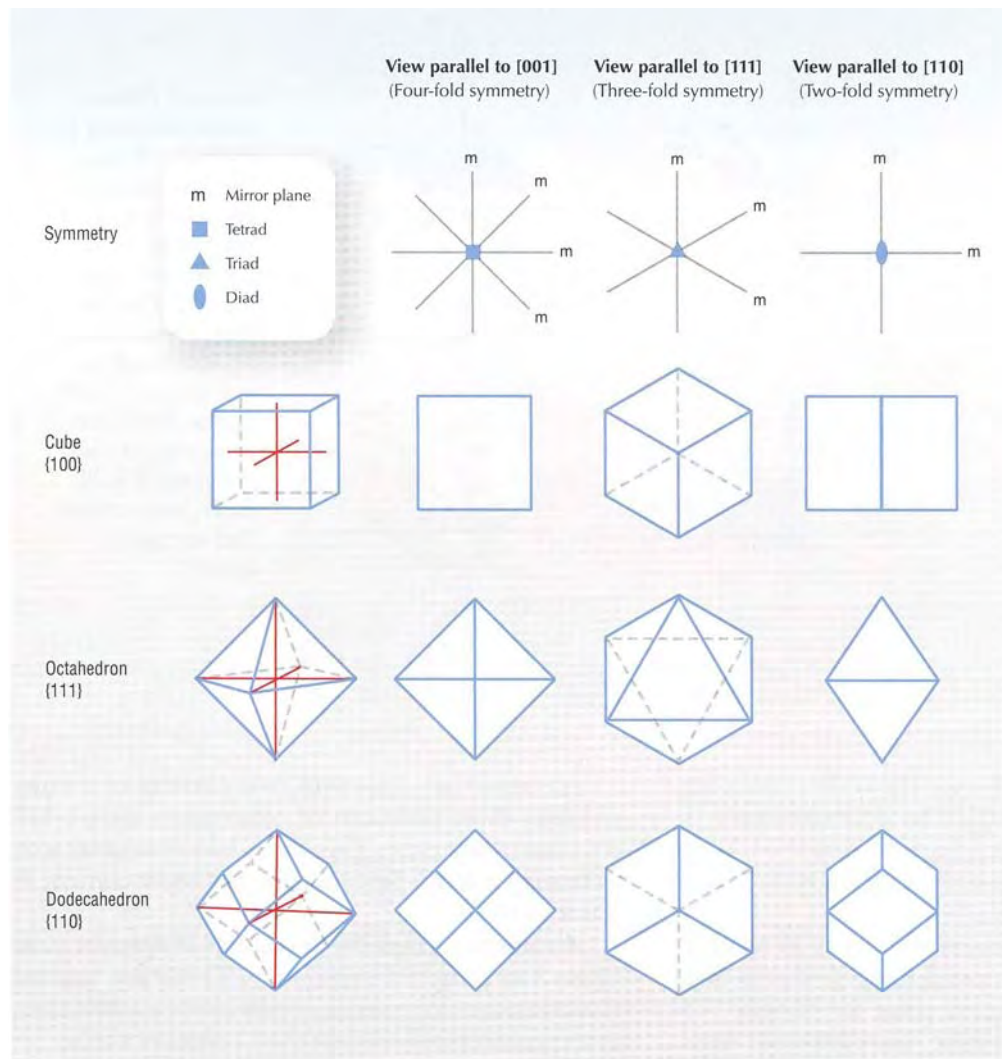


Figure 6. Depending on the viewing orientation, a variety of shapes and symmetries are apparent for these common cubic forms. The symmetry of these forms is shown according to mirror planes and rotational order (i.e., diad, triad, and tetrad for two-, three-, and four-fold rotational symmetry).

try relates two halves of a crystal form by a virtual plane termed a *mirror plane*. A total of nine mirror planes yield congruence of the cubic, octahedral, and dodecahedral crystal forms (again, see figure 6).

Mapping of Orientations Using Stereographic Projection. Most facets of a cut diamond are not parallel to low-index crystal lattice planes such as {100} or {111}. Moreover, since the original crystal faces are no longer present on a faceted diamond, the orientation of the crystal lattice in relation to the cut gemstone is obscured. X-ray techniques may be used to find this orientation, thus revealing the relationship between the polished facets, former crystal faces, lattice planes, and vectors in three-dimensional space.

Imagine a round brilliant cut diamond with its culet pointing down and its table oriented horizontally near the center of a sphere, as shown in figure 7. The vector perpendicular (or *normal*) to an arbi-

trarily chosen low-index crystal face present on the original crystal, such as (111), will point from the center of the diamond to a point (or *pole*) on the sphere's surface. The location of this point can be described using two coordinates: ρ —the polar distance, expressed in degrees, relative to the “north pole” where the vertical diameter line intersects the sphere's surface; and ϕ —the azimuthal angle, measured in degrees along the horizontal diameter circle, starting at a point (“east pole”) on the right side where a horizontal diameter line hits the sphere's surface.

Projecting a pole from the sphere's surface onto a horizontal plane that passes through the center of the sphere (as shown in figure 7) yields a two-dimensional representation of this crystal face, the position of which is given by polar distance ρ and azimuth ϕ . Projecting other crystal features such as faces, directions of edges, and/or vectors and planes in the crystal lattice in a similar fashion results in a

stereographic projection of these elements. The stereographic projection has many useful properties and applications beyond the scope of this article (for more on stereographic projections see, e.g., McKie and McKie, 1974, and Borchardt-Ott, 1997). We use such projections to graphically depict the orientation of a cut diamond (e.g., the diamond's table facet) relative to its crystal lattice.

In fact, it is possible to map the location of every facet of a cut diamond on a stereographic projection. Combined with knowledge of the relationship to crystal vectors within this projection (as acquired, e.g., by X-ray diffraction methods), projecting all of the facets of a particular cut diamond relative to its crystal lattice yields a unique depiction of that stone. However, even a slight repolishing of the stone would destroy the integrity of the data.

Figure 8 shows stereographic projections of {100}, {111}, and {110} faces; the axial symmetry at each crystal face pole is indicated by the shape of the symbols. The symmetry of a crystal is evident in these stereographic projections in much the same way as figure 6 shows this symmetry head-on. Owing to symmetry, a section of the cubic stereographic projection that covers only $1/24$ of the area of the projection plane is sufficient to describe a particular crystal form completely (the rest being possible to generate by symmetry operations), because both crystal form and crystal lattice have the same coordinate system.

This section is called a "standard triangle," denoted "t" in figure 8, which spans between poles generated by the normals to the neighboring faces (100), (111), and (110). The location of a pole (ρ, ϕ) within the frame of the standard triangle allows one to identify the orientation of a particular facet (e.g., the table facet) of a diamond with respect to the crystal lattice. Thus, to fix the orientation of the diamond's table facet with respect to the crystal lattice, the analyst must first determine the location of the pole of the perpendicular T to that facet within the standard triangle. This is accomplished by means of X-rays diffracted by the crystal lattice of the diamond. The diffraction of X-rays by single crystals—whether faceted or not—to yield spatial resolution of peculiarities within the crystal is called X-ray topography (see below for details). In contrast, X-ray powder diffraction is used to identify mineral species based on their specific powder diffraction patterns, which arise from the spacing and other characteristics of their lattice planes.

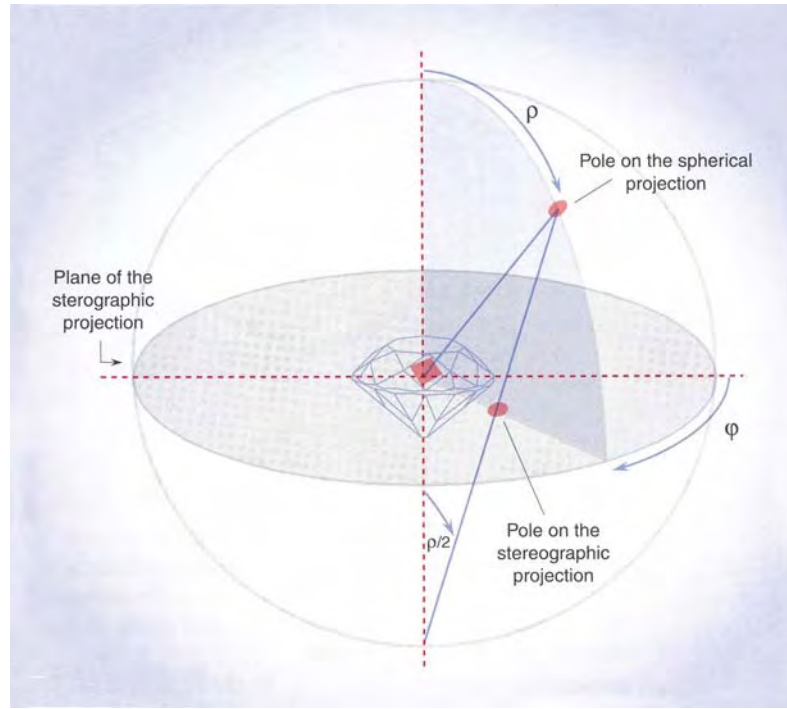
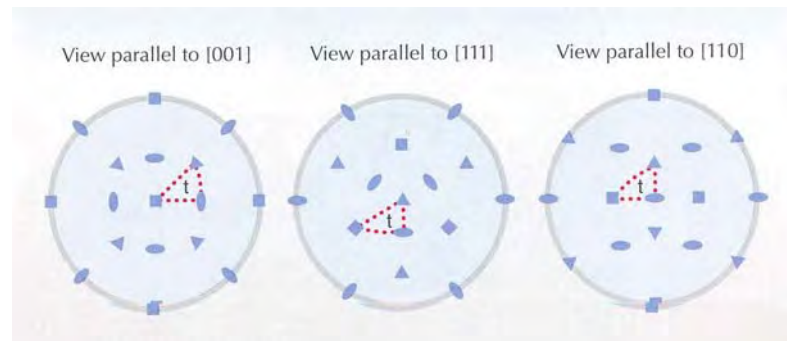


Figure 7. This diagram shows the mechanics of a stereographic projection. The orientation of the diamond crystal lattice is schematically shown within a round brilliant with its table oriented horizontally. A vector perpendicular to a certain crystal face, such as (111), will intersect the sphere's surface at a point called a pole. The location of the pole is described using two angular measurements, the polar distance ρ and the azimuthal angle ϕ . This pole is plotted on a stereographic projection by projecting its intersection with the sphere onto a horizontal plane that passes through the sphere's center.

Figure 8. These stereographic projections show the major cubic system faces projected along [001], [111], and [110] directions. Also shown is the "standard triangle" t (see text). The axial symmetry at each crystal face pole is indicated by the shape of the symbols: ■ = tetrad [100], ▲ = triad [111], and ▣ = diad [110].



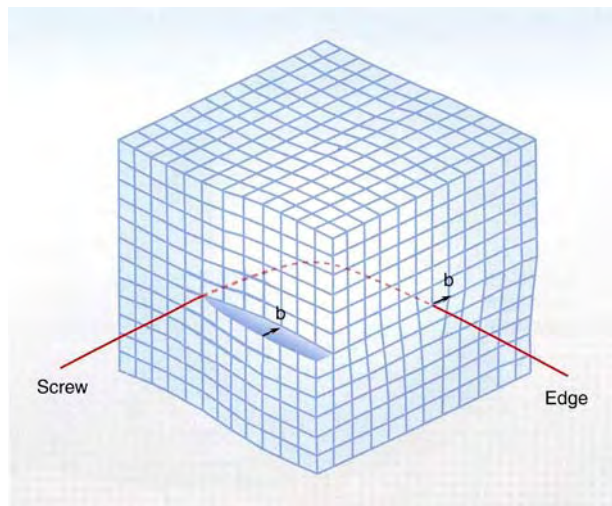
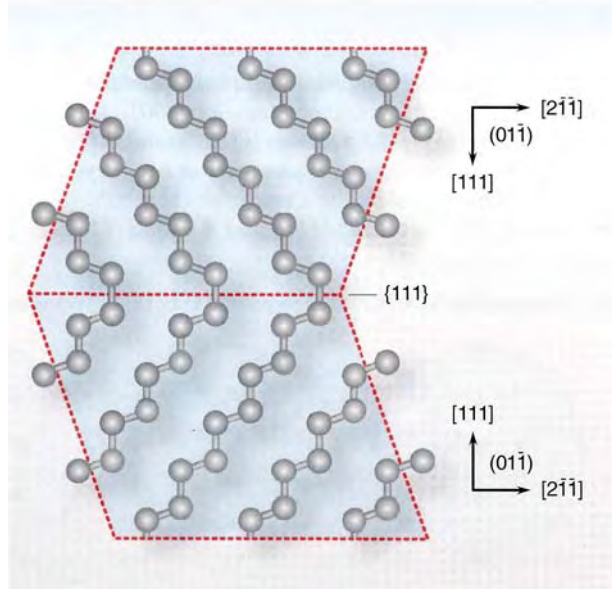


Figure 9. Crystal defects that extend over a relatively large portion of the crystal lattice are termed dislocations. Most common are edge and screw dislocations. An edge dislocation occurs when a lattice plane is displaced by “one step,” characterized by the displacement vector “ b ,” as shown on the right side of the figure. For a screw dislocation, two lattice blocks are displaced against each other by “one step,” again characterized by the displacement vector b , as shown on the left side. Both types of dislocations are accompanied by strain, which is revealed by diffracted X-rays, since the diffraction condition is not satisfied in the strained region of the lattice.

Figure 10. A stacking fault, shown here in a diamond lattice, occurs when one portion of a crystal has a different orientation from the rest of that crystal. This change in the stacking sequence of the lattice planes is often the cause of twinning.



CRYSTAL LATTICE DEFECTS

As crystals grow layer by layer, this process almost never remains undisturbed. In reality, the regular spatial arrangement of atoms in a crystal lattice is locally perturbed by numerous defects of various kinds (Bohm, 1995; Kelly et al., 2000). Missing or additional atoms, atoms in wrong positions, or foreign atoms not belonging to the chemical composition of the crystal, are termed *point defects* or *centers*. Their presence is detected by physical or spectroscopic evidence. Due to lack of resolution, point defects cannot be detected by X-ray topography unless they cause regions of strain in the lattice around the defect. An even higher degree of disorder is caused by clusters of atoms of foreign phases or minerals, such as inclusions. Crystal lattice distortions that affect some local volume of the lattice are termed *extended defects* or *dislocations*. The most common types of extended defects are edge and screw dislocations (figure 9), which can be visualized by X-ray topography.

This is also the case with another extended defect termed a *stacking fault*, which occurs when the stacking sequence of the lattice planes changes and part of the crystal has an orientation different from the rest (figure 10). A stacking fault is often the reason for twinning.

When large blocks of the crystal lattice are tilted slightly with respect to one another, an extended defect termed a *small-angle boundary* (figure 11) results. Similar defects are *growth sector boundaries*, which occur when portions of a crystal lattice growing along different respective lattice planes meet one another so as to generate a rough internal face, which often can be recognized on the crystal's surface as a seam. X-ray topography can depict such internal lattice boundaries.

The assemblage of internal extended lattice defects present is unique to any crystal. Hence, the lattice defect features of a particular diamond, rough or cut, render it unique. Most internal extended lattice defects are not visible in a gemological microscope, but they can be depicted by directing X-rays at the diamond's crystal lattice and recording the resulting diffraction pattern on X-ray sensitive film or with an electronic imaging device.

X-RAY DIFFRACTION

When X-rays are directed toward a crystal, they are diffracted; that is, part of the incident or “primary” X-ray beam is deflected into various directions by

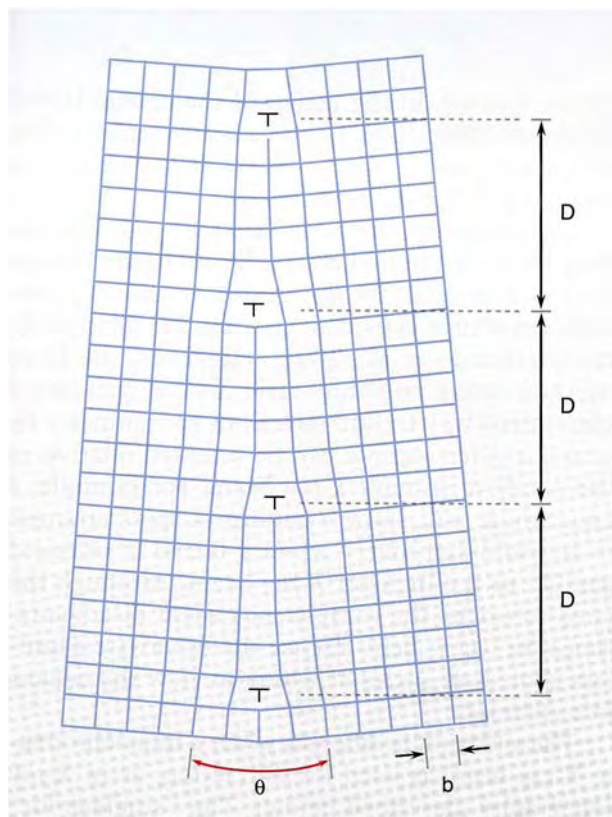


Figure 11. This diagram of a small-angle boundary shows an array of dislocations spaced by an average distance D (which is on the order of 10 nm to 1 μm). The angle θ between the two crystal regions typically measures between 0.01° and 1° . For each dislocation, the lattice planes are displaced by the distance “ b .”

virtue of the crystal lattice (Cullity, 1978). This is because both the crystal-lattice spacings and the wavelength of X-rays are on the order of 0.1 nm. If the primary X-ray beam is composed of many wavelengths (a polychromatic or “white” X-ray beam), the diffracted beams expose an X-ray sensitive film with a pattern that represents the symmetry of the crystal lattice in the direction of the primary beam, a procedure called the *Laue method*.

Each diffracted beam is generated by the reflection of a small portion of the primary beam’s range of wavelengths from a set of parallel lattice planes within a crystal. However, this reflection does not occur for any angle of incidence, but only at certain “glancing angles” (i.e., the angle between the incident X-ray beam and the set of diffracting lattice planes). This condition—“Bragg reflection” or “diffraction condition”—is given by the Bragg equation:

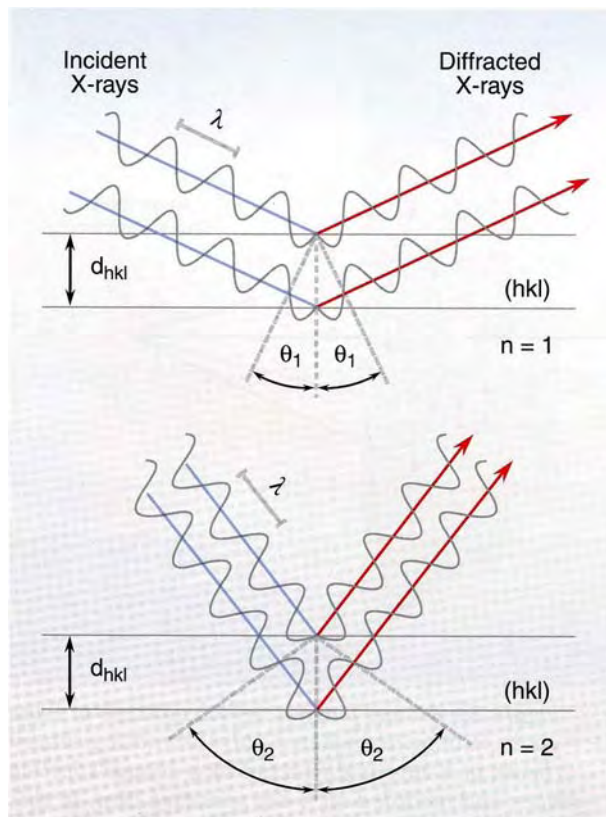


Figure 12. A monochromatic X-ray beam of wavelength λ is diffracted by a set of lattice planes (hkl) according to their spacing d_{hkl} . Different orders of X-ray diffraction can occur at various Bragg angles θ_1 , θ_2 , etc., according to the integer n , which is defined by the difference between the propagation lengths of the X-ray waves. Examples for $n = 1$ and $n = 2$ are shown here.

$$n\lambda = 2d_{hkl}\sin\theta_{hkl}$$

where: n = order of diffraction
 λ = X-ray wavelength
 d_{hkl} = distance between lattice planes
 θ_{hkl} = Bragg angle

A polychromatic X-ray beam will produce many diffracted beams, each with a different wavelength and glancing angle. Therefore, many glancing angles are possible that satisfy the diffraction condition, thus generating a diffraction pattern. At a fixed glancing angle θ , an X-ray beam with a specific wavelength λ is diffracted according to the lattice plane spacing d_{hkl} (figure 12). The diffracting set of lattice planes has Miller indices (hkl) , so the corresponding X-ray reflection is indexed hkl —without parentheses—and termed a *Laue index*. The resulting spot on the film is called a *Laue spot* (figure 13). The intensity of the diffracted X-ray beam is influenced by the lattice

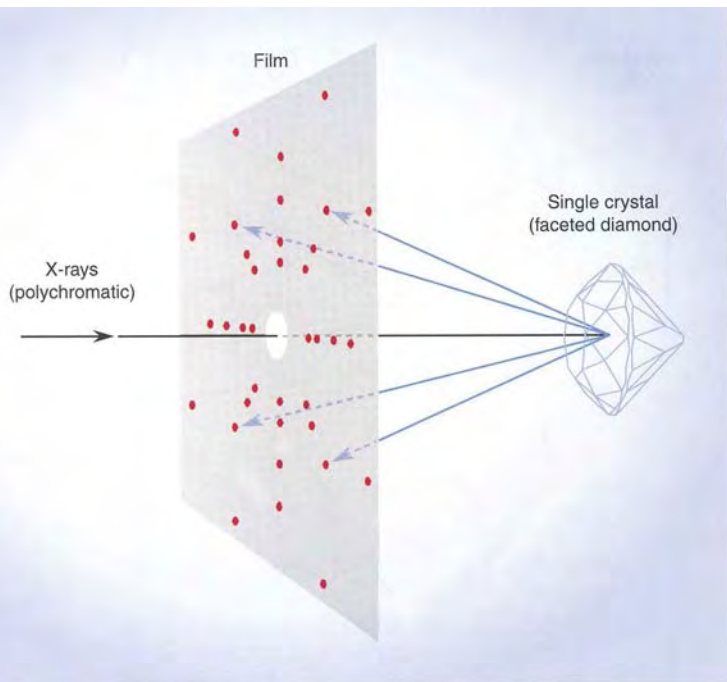
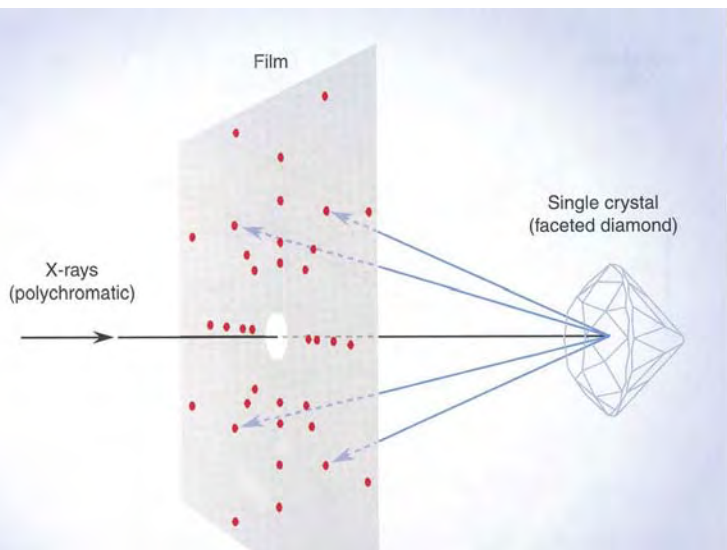


Figure 13. A Laue pattern, which consists of Laue spots, is obtained when a polychromatic primary beam of X-rays is diffracted by a crystal's lattice planes and recorded on X-ray sensitive film. In this "back-reflection" set-up, the film is oriented perpendicular to the primary beam, between the X-ray source and the sample. The primary beam is directed through a central hole in the film.

Figure 14. This diagram shows the diffraction geometry used for X-ray topography that was devised by Lang (1959). The crystal and recording medium are moved at the same time during the procedure, to record the spatial resolution of the lattice defect structure on the topograph.



defects present in the region of the crystal lattice causing the diffraction. Hence, a spot recorded on the film contains information on the lattice defects in the form of intensity modulations.

Unfortunately, due to its limited spatial resolution, the Laue method cannot record lattice defects in sufficient detail for fingerprinting (unless a synchrotron source is used to generate the incident X-rays; Rinaudo et al., 2001). However, the Laue method (using polychromatic X-rays) provides a convenient way to find directions of symmetry by which a given sample can be oriented relative to the incident primary X-ray beam. For example, a Laue image will show a pattern of spots arranged in fourfold symmetry when a tetrad is oriented parallel to the incident X-ray beam. Although the need to orient the sample may seem disadvantageous, in fact it helps reduce the otherwise countless choices of angles at which to view the defects in a diamond.

The situation is different when a monochromatic X-ray beam is used for diffraction, as in X-ray topography (described below). The "single-color" radiation composing this beam has a specific wavelength λ (e.g., X-rays from a copper source have $\lambda=0.154$ nm), so the number of glancing angles under which "reflection" (diffraction) of the primary X-ray beam can occur is greatly reduced. The orientation of the crystal lattice relative to the incident X-ray beam must be carefully positioned to induce diffraction of the X-ray beam (i.e., to satisfy the Bragg equation).

X-ray diffraction occurs when the glancing angle (θ_1) is such that the difference between the propagation lengths of a set of parallel X-ray waves within the incident beam is an integer number "n" of wavelengths also called the *order of diffraction*. The case for $n = 1$ is shown in the upper part of figure 12, where the difference in the propagation lengths between both waves is just one wavelength λ . Diffraction also is observed at another glancing angle (θ_2), if n is a multiple of 1, such as 2—as shown in the lower part of figure 12, where the difference is 2λ . The corresponding Laue index is termed $2h\ 2k\ 2l$ to indicate the second order of diffraction. Thus, although Miller indices always consist of base integers, such as (110), higher-order reflections from the same set of lattice planes carry Laue indices such as 220, 330, etc., from which can be derived the Bragg angle under which diffraction is observed.

The X-rays most commonly employed in industrial laboratory diffraction experiments are generated

Figure 15. In the X-ray topographic apparatus used in this study, the diamond is held in the circular goniometer array (20 cm in diameter) in the top-center of the photo. The X-ray beam enters from the left, and the film is positioned on the right side of the goniometer. Photo by Nikolaus Herres.



using copper ($\lambda=0.154$ nm), molybdenum ($\lambda=0.071$ nm), or silver targets ($\lambda=0.056$ nm) in the X-ray tube. The shorter the wavelength λ is, the more energetic the X-rays are, and the deeper they can penetrate a sample.

X-RAY TOPOGRAPHY

The method of applying X-rays to image crystal lattice defects with local resolution is called *X-ray topography*, and the image recorded on a photographic plate is an *X-ray topograph*. X-ray topography of extended lattice defects in diamond was pioneered by A. R. Lang and co-workers (see, e.g., Frank and Lang, 1965; Lang, 1978b, 1979; Lang et al., 1992). Since diamond is highly transparent to X-rays, X-ray topography is particularly suited to imaging its lattice defects. Topographs can be taken irrespective of the stone's shape, and X-rays do not induce color change in a diamond. Hence, the method is nondestructive.

To obtain the greatest amount of information, the specimen is exposed to monochromatic X-rays according to a method devised by Lang (1959; figures 14 and 15). Slits are used to form the monochromatic X-ray beam into a ribbon-like shape some 10 μm thick and equal in height to that of the sample. The diamond is oriented relative to the incident X-ray beam such that a desired set of lattice planes satis-

fies the Bragg condition. An oscillating mount is used to expose all portions of the sample to the incident X-ray beam.

The image generated by the diffracted beam is recorded on the photographic plate (or on a screen when employing an electronic imaging device with a charged-coupled detector [CCD]). This image shows the locally resolved intensity of the diffracted X-ray beam as modified by the defects in the portion of the crystal lattice that is analyzed. In theory and, so far, in practice, no two diamonds have identical sets of defects (just as no two people have identical fingerprints). An X-ray topograph, therefore, provides a fingerprint that is unique to each particular diamond.

This is demonstrated by the X-ray topographs of a diamond crystal and the round brilliant cut from it (figure 16), and of a rough diamond that was cut first to a round brilliant, then recut to a smaller round brilliant, and ultimately recut again to a totally different shape (figure 17). The unique appearance of the extended lattice defects is clearly preserved through the faceting and recutting processes. Similarly, such defects should remain identifiable in topographs of diamonds taken before and after HPHT processing (as shown by Smith et al., 2000).

Diamonds with a low clarity grade will also show a large number of extended lattice defects, since fissures and inclusions locally destroy the

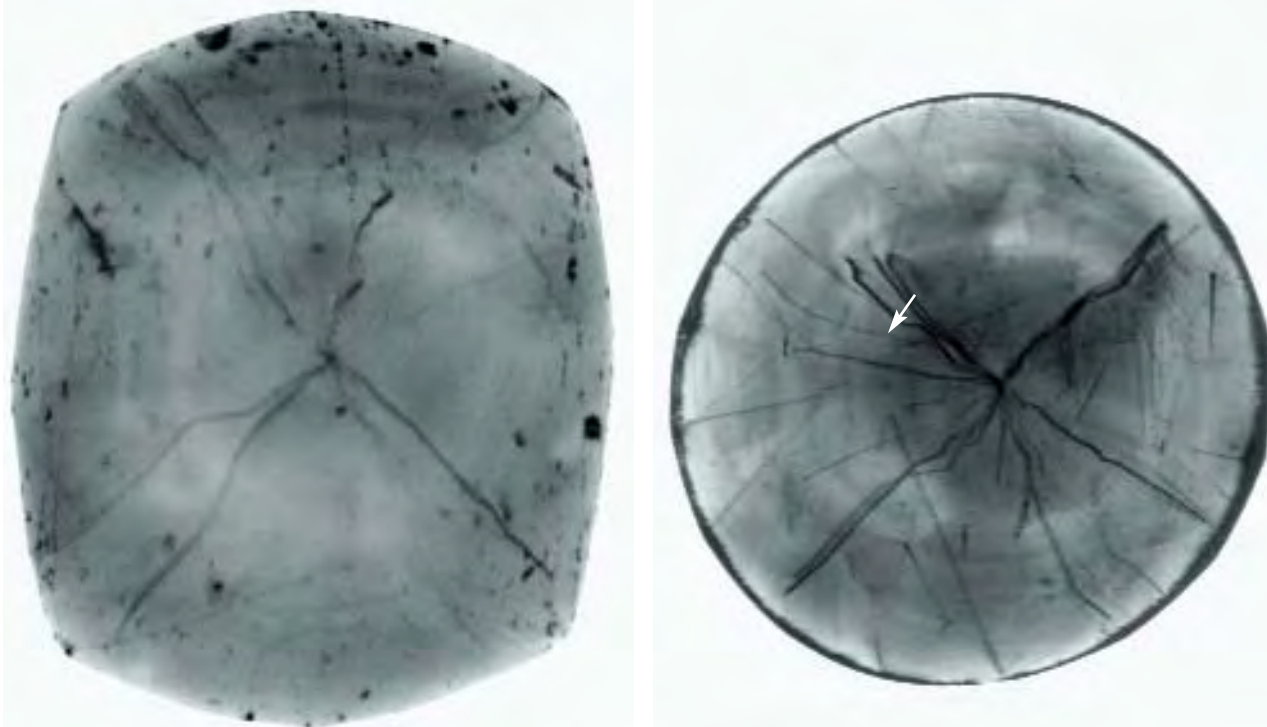


Figure 16. These X-ray topographs were taken of a 1.67 ct rounded diamond octahedron and a 0.75 ct round brilliant that was cut from it. Dislocations are seen as strong irregular lines originating from the center of the diamonds. In the rough sample, shades of gray indicate areas of different lattice strain and minute misorientations (i.e., deviation from the diffraction condition); surface blemishes appear as dark spots. In the faceted sample, the generally darker area that is slightly off-center marks an area of higher X-ray absorption through the stone's pavilion, which is the thickest part of the sample. Rough facet edges are visible as straight dark lines, and the location of the culet is shown with an arrow. The appearance of the dislocations in the two topographs differs somewhat because they would have been projected onto the film from different directions.

integrity of the crystal lattice. If the lattice defects are too abundant, their interference will render a topographic image rather meaningless. Although the image could still provide a fingerprint, it is unlikely that a stone of such low commercial value would be submitted for this procedure.

X-ray topography can also be used to identify natural vs. synthetic diamonds (see, e.g., Lang et al., 1992; Sunagawa, 1995; Martineau et al., 2004). This could become significant in the future, as diamond synthesis techniques are refined to produce larger, high-quality stones with less evidence of a synthetic origin (e.g., inclusions and luminescence features).

TYPICAL METHOD FOR GENERATING A TOPOGRAPH

To record X-ray topographs, one needs a set-up similar to the one diagrammed in figure 14. The diamond is mounted on an adjustable specimen holder that allows for translation and rotation of the sample in front of the X-ray beam. Taking X-

ray topographs also requires proper choice of the Bragg reflection to be used for imaging. This selection is made by practical considerations. First, the cross-section of the stone that is projected onto the film should be as large as possible to minimize superposition of defects; in the case of a round brilliant, the projected image should thus be a circle. Second, the "diffracting power" of the selected set of lattice planes (i.e., the intensity of the diffracted X-ray beam) should be high, to reduce exposure time. In the case of diamond, Bragg reflections of the 220 type satisfy both conditions (Lang and Woods, 1976).

The diamond is oriented according to the desired glancing angle θ_{220} by using X-ray diffraction to locate an appropriate crystallographic reference vector—such as a tetrad or diad. This reference vector can be found through the use of the sample holder, actually a *goniometer*, which has a number of circles that rotate on independent axes. Figure 18 shows a goniometer with five circles, denoted A through E. The desired reference vector is found by

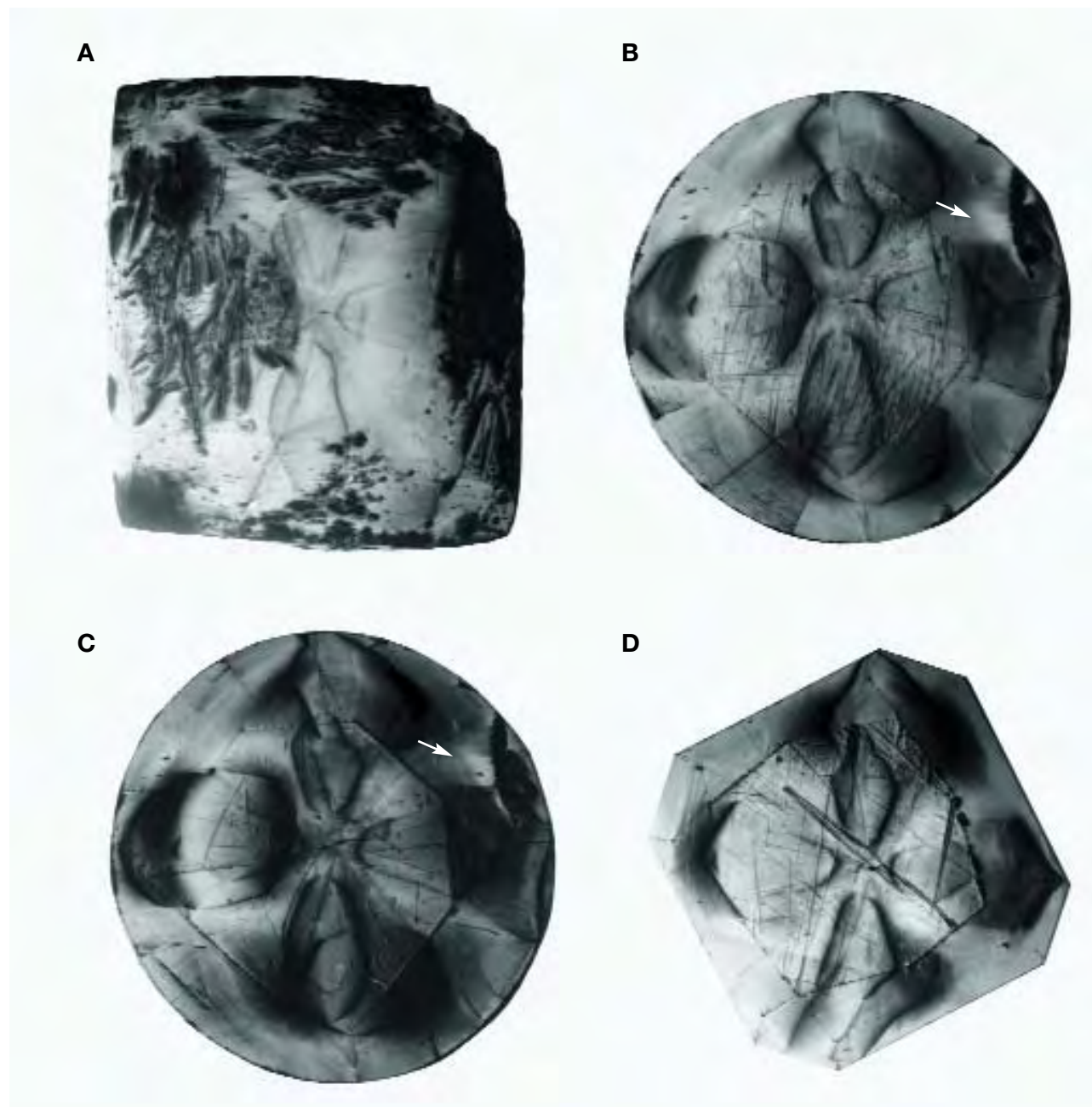


Figure 17. This sequence of topographs was taken from the same diamond in rough, cut, and recut states. Topograph A was taken from a 2.31 ct half-octahedron, which was faceted into the 1.19 ct round brilliant shown in topograph B. A defect structure determined by growth sector boundaries shaped like a four-leaf clover is clearly visible, as is a small inclusion near the upper right edge (marked by an arrow). This stone was then slightly recut to 1.12 ct, which has a nearly identical topograph (C); note the difference in the surface features. The diamond was then completely recut to a 0.88 ct square shape (Sunflower Carré; topograph D), with the inclusion removed in the process. (The diagonal linear feature near the center of topograph D corresponds to a scratch on the table facet.) Even after extensive recutting, the typical internal features in this diamond remain recognizable, linking it to the round brilliants as well as the original rough. The light and dark areas in topograph D are distributed somewhat differently due to the modified absorption behavior of X-rays in the Sunflower cut.

applying a search procedure with systematic rotational movements around the goniometer circles. A set of suitable symmetrically equivalent reflections

such as 220 , $\bar{2}\bar{2}0$, $\bar{2}\bar{2}0$, and $\bar{2}20$ eventually is located and then is precisely aligned using the X-ray detector mounted on circle E.

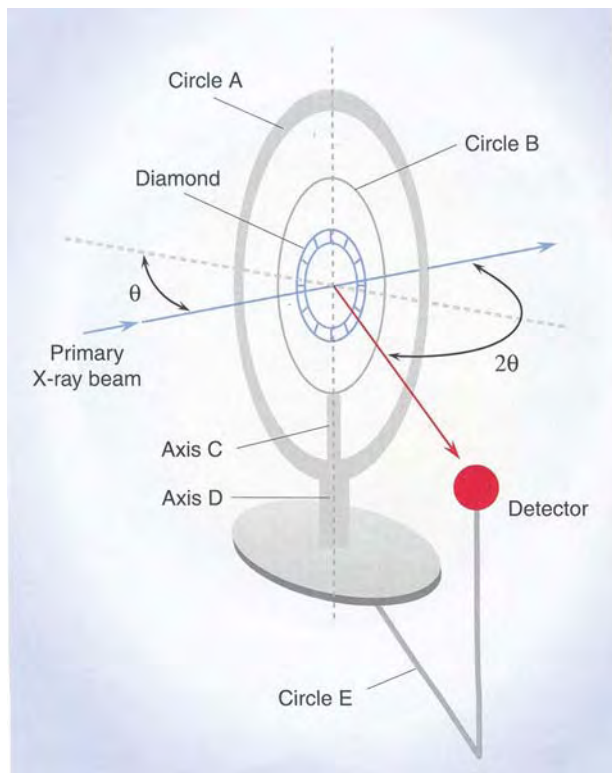


Figure 18. A five-circle goniometer was used to crystallographically align the diamonds prior to recording X-ray topographs. The five circles are preferably driven by computer-controlled motors. The diamond is attached in the center of the goniometer with its table facet perpendicular to the primary X-ray beam. The detector is used for adjusting, aligning, and measuring the reflecting position and the polar angles ρ and φ . To record a topograph, the detector is replaced by a camera or other imaging device.

This search procedure can be executed manually or, more readily, via fully automatic computer control with special software. In the end, the diamond is positioned so that a crystallographic reference vector such as a tetrad is oriented parallel to the goniometer's A-axis (around which the A circle rotates). The detector is then removed and replaced with a photographic plate or imaging assembly to record a topographic image.

Knowing the glancing angles of the 220-type Bragg reflections and now their positions, images using the four symmetrically equivalent Bragg reflections can be taken one at a time. Although they are taken of the same set of lattice defects, the topographs differ slightly because the defects have been projected onto the film from four different directions. Figure 16 shows a topograph where the pavilion facet edges are clearly seen, with the culet off-center.

PAST LIMITATIONS OF THE TECHNIQUE

The unique and hence unambiguous characterization of rough, partially cut, or fully cut gem diamonds by means of X-ray topography has been known for some years (Lang and Woods, 1976; Diehl, 1982; Sunagawa et al., 1998). Fingerprinting diamonds via X-ray topographic images of their lattice defects has been used to relate cut diamonds to their parent rough (Lang, 1975, 1978a, 1988; Lang and Woods, 1976; Sunagawa et al., 1998). So far, however, the method has not been applied systematically as a "passport" for individual fashioned diamonds, and the diamond trade has not yet seen widespread use of this fingerprinting technique, even for gem diamonds of high value. What are the reasons?

One reason is simply the difficulty of obtaining a well-defined topograph from a faceted diamond. Directing the monochromatic X-ray beam perpendicular to the table facet will not necessarily yield a Bragg reflection, since it is unlikely that this arbitrarily chosen orientation yields an angle θ that satisfies the diffraction condition. Even if a glancing angle is found, the beam will not necessarily diffract in the direction of the photographic plate. Therefore, one first has to solve the problem of precisely orienting the stone relative to the incident X-ray beam, which is done using X-ray diffraction and a goniometer.

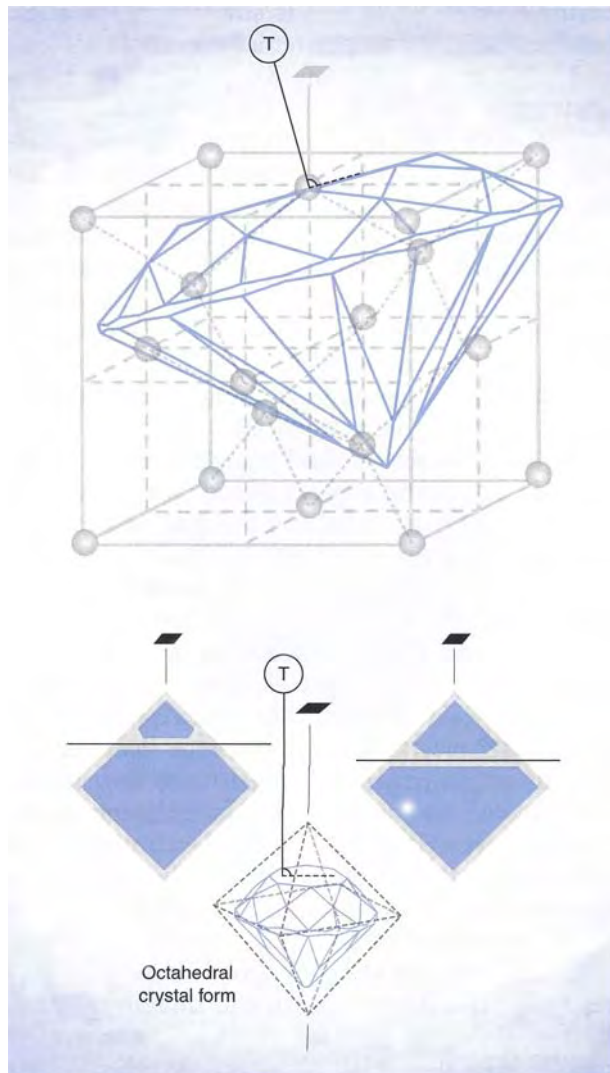
Moreover, due to the high crystallographic symmetry of the diamond lattice, there are many symmetrically equivalent Bragg reflections available to record an X-ray topograph. For example, there are 12 symmetrically equivalent type 220 reflections that share the same value for d_{220} and hence the Bragg angle θ_{220} . Thus, a complete characterization of a diamond requires the recording of at least 12 X-ray topographs (referred to as "mother topographs") in order to provide indisputable proof of identity when compared to a single ("daughter") topograph taken later for re-identification.

It is important to remember that a single lattice defect within a given diamond can have a variable appearance when viewed from different directions, just as a car looks different when viewed from above, below, and the side. Although each of the symmetrically equivalent Bragg reflections has the same diffraction condition, each also has a different projection orientation, which will cause the corresponding topographs to look different.

Even using the same Bragg reflection, the topograph projected along one direction may significantly differ from the topograph obtained in the reverse

direction, because of differences in the volume of the diamond that is penetrated by the X-rays. Imagine an extended lattice defect that penetrates the surface of the stone. The diffracted beam that carries the image through the volume of the stone will suffer from some absorption and scattering, so the projected image may appear somewhat blurred on the photo-

Figure 19. The diagram on top shows an example of how the table facet cuts through a diamond's crystal lattice. A line perpendicular to the table facet (T) forms angles with the three tetrads (axes of four-fold symmetry). Shown here is the tetrad that forms the smallest angle with T. The drawings below illustrate how octahedral diamond crystals are commonly sawn during preforming, in a direction that is approximately parallel to a cube direction.



graphic plate, and the low-contrast surface features may even become invisible. In the reverse direction, the defect image is generated just before the diffracted beam leaves the stone, so the image (and even the low-contrast surface features) will appear sharper on the photographic plate. So, using the Bragg reflection of type 220, 24 topographs may actually be needed to characterize a single diamond.

The execution of this procedure would require highly trained personnel and considerable effort in labor and time, so that the corresponding costs would be prohibitive. This is why X-ray fingerprinting of gemstones, although highly desirable for property protection, has not yet become commercially viable. So far, X-ray fingerprinting of diamonds, as well as other gem materials (Rinaudo et al., 2001), has remained a matter of research.

EXECUTION OF THE SIMPLIFIED ROUTINE

One way to make X-ray topography commercially viable would be to drastically reduce the number of mother topographs required to identify a faceted diamond. If the sample could be uniquely and reproducibly aligned in front of the X-ray source (e.g., relative to the table facet), only one mother topograph would be needed. This section describes such a procedure, as developed and patented by us (see Diehl and Herres, 1997; 1998). We used the table (as the most prominent facet of a cut diamond) to begin the alignment. Using X-ray diffraction, we started with the table perpendicular to the primary X-ray beam, and searched for the tetrad forming the smallest angle with the perpendicular T to the table facet (figure 19). This is the first part of the routine to determine the orientation of the table facet relative to the diamond lattice.

Many rough diamonds are octahedra or dodecahedra, which are sawn along a cube direction to yield a larger and a smaller rough diamond (again, see figure 19). The cross-sectional surfaces—which later become the table facets of the two gems—are thus nearly perpendicular to a tetrad of the diamond lattice. As a result, for many faceted diamonds, a tetrad is approximately perpendicular to the table facet (usually within 10°).

When this closest tetrad is selected as the crystallographic reference vector for recording topographs, the plane of the faceted diamond's girdle is projected onto the X-ray topograph with minimum distortion so that the projected area and thus the information content of the topograph are maximized. If a tetrad is

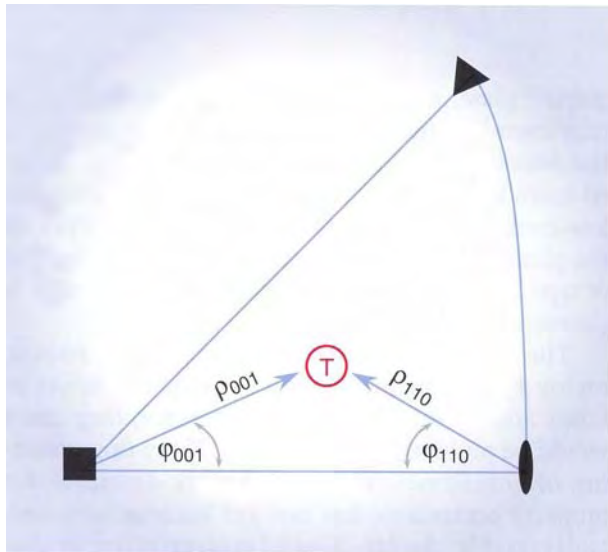


Figure 20. The position of the pole belonging to the perpendicular to the table facet (T) can be represented by the stereographic projection of this pole within the standard triangle *t*. If the chosen reference direction is a tetrad, the azimuth and polar distances are φ_{001} and ρ_{001} , respectively. If the reference direction is a diad, they are φ_{110} and ρ_{110} .

not found within a preset angular range, our automated procedure will then look for a diad. Since, in most cases, the crystal vector closest to the perpendicular T to the table facet will be a tetrad, we will describe the alignment procedure for this orientation. Figures 8 and 18 may help clarify the following description of the procedure we have developed.

To search for the diffraction condition for the set of 001 lattice planes to which the tetrad is perpendicular, the specimen is placed in the center of the goniometer and systematically moved using circles B and C. The detector finds and optimizes the signal for the strong 004 reflecting position, so that a tetrad is aligned perpendicular to circle A. This tetrad indicates the direction of one of the cubic coordinate axes, which we arbitrarily assign as a_3 (i.e., the vector [001] in the diamond lattice).

The second part of the alignment routine uses the 220 Bragg reflection to establish a unique orientation of the stone for taking the X-ray topograph—that is, we find and set the azimuthal orientation (see below) necessary to start the imaging. Circles D and E are set to include the Bragg angle of the diamond 220 reflection. Circles B and C remain fixed at the positions found before. The sample is rotated using circle A in order to find and optimize the signal for the 220-type reflecting positions.

The stereographic projection on the left in figure 8

illustrates that we should be able to find four 220-type reflecting positions (corresponding to the four diads at the rim). We now single out one of these four symmetrically equivalent reflections by optimizing only the 220-type reflection position of the set of 110 lattice planes, which has the perpendicular vector [110] that forms the smallest angle with T. We arbitrarily refer to this Bragg reflection as “220,” and this is the one used to record the mother topograph.

For diamonds cut from irregularly shaped rough, the table may be oriented quite differently from that of a gem derived from an octahedron or dodecahedron. This may lead to larger angles between T and the closest tetrad. In order to retain a large projected area of the stone (e.g., a circle in the case of a brilliant), it may be more practical to use a diad, instead of a tetrad, for the reference vector that is nearest to T. Since a tetrad has an angle of 45° with its neighboring diads, using a diad is advisable if the angle between T and the closest tetrad exceeds 22.5° .

In either case, after the X-ray diffraction alignment procedure is complete, the geometric relationship between T and the closest tetrad (or diad) is measured in terms of two crystallographic angles, namely the azimuth φ and the polar distance ρ (figure 20).

Imagine, with the help of figure 7, that this tetrad or diad coincides with the vertical line through the center of the sphere. T will then form a pole somewhere on the surface of the sphere. By definition, the stereographic projection of this pole will be found in the standard triangle *t* displayed in figure 8 and enlarged in figure 20.

As shown in the standard triangle of figure 20, the azimuth φ_{001} is the angle between two planes: the first defined by the tetrad and the diad, and the second containing the tetrad and T. The polar distance ρ_{001} is the angle between the tetrad and T. When using a diad, the assignment of φ_{110} and ρ_{110} is done in a similar way. Common ranges for φ and ρ are 0 – 45° and 0 – 22.5° , respectively. Using the goniometer and the X-ray detector, both angles can be recorded with high precision (usually to better than $1/10^\circ$).

This alignment routine determines how to orient a faceted diamond prior to taking the topograph. The two crystallographic angles—azimuth φ and polar distance ρ —uniquely define the position of the table facet with respect to the underlying diamond crystal lattice.

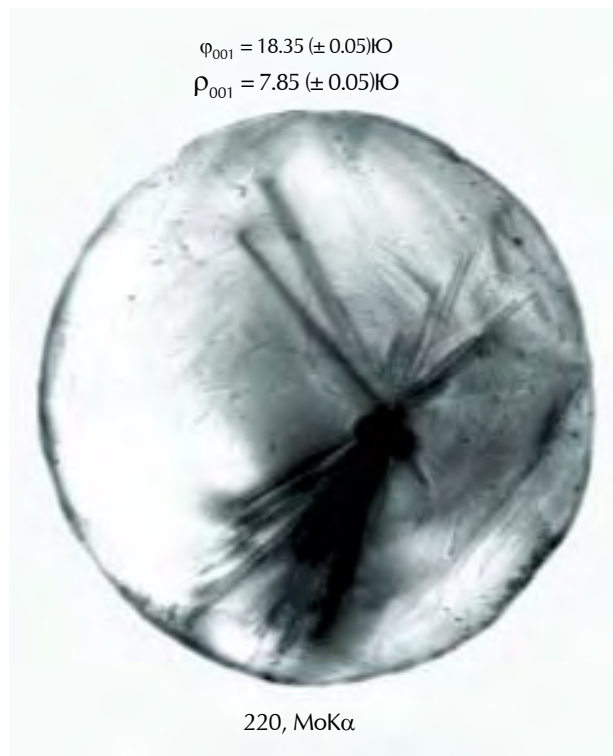
Finally, the mother topograph is recorded by replacing the detector with the imaging device. Because the orientation is unique, only one mother topograph is required. In the event that the identity

of a diamond needs to be verified, the same routine is executed by reproducing both crystallographic angles to record the new topograph. If it is the same stone, the alignment angles should be equal within the goniometer's tolerances ($\pm 0.2^\circ$), and the daughter topograph will show unique features that are recognizable in the mother topograph (again, see figures 16 and 17).

DISCUSSION

We have endeavored to present here a viable technique, together with its underlying principles, to render X-ray fingerprinting a practical tool for the identification of individual cut diamonds. The technique involves imaging the lattice defect structure of a faceted diamond under specific, well-defined, reproducible conditions. This is made possible by measuring the polar angles ϕ and ρ .

Figure 21. As illustrated here, a fingerprint generated by this X-ray topography routine could accompany a diamond grading certificate. The polar angles and X-ray topograph provide complementary information that is unique to a particular faceted diamond. (MoK α denotes the X-ray wavelength of highest intensity from a molybdenum target.)



Polar Angles ϕ and ρ . The azimuth ϕ and polar distance ρ are typically unique to every faceted diamond. Together, these two angles define the orientation of a specimen's table facet with respect to its crystal lattice in terms of a reference direction (nearest tetrad or diad). Within the alignment tolerances of the goniometer, both polar angles are reproducible and almost always unique. Therefore, although they are obtained as a "by-product" during the alignment procedure for taking topographs, the polar angles contribute further valuable information for fingerprinting a stone. Particularly in combination, the polar angles are highly characteristic in their own right. Being numerical values, they also may serve as searching parameters to quickly locate the potential mother topograph in a database. Using suitable software, the search can be performed automatically.

It is important to note that the polar angles would become useless for fingerprinting if the inclination angle of the table facet relative to the diamond crystal lattice is modified significantly. However, this would occur only if there were some significant reshaping of the stone, as well as appreciable loss of weight.

X-ray Topographs. The mother X-ray topograph provides a unique, archivable diamond fingerprint. Such fingerprints reproduced on microfilm could become an integral part of a diamond report (e.g., as in figure 21), with a digital copy archived separately. Should a stone be recovered after loss or theft, its "fingerprint" could be compared to that of the mother topograph to confirm identity.

Properly oriented, daughter and mother topographs from the same diamond will be identical with respect to the image characteristics stemming from internal defects. Even two diamonds cut from the same rough can clearly be differentiated, according to subtleties in their defect structure, as well as their polar angles. Complete reproduction of all details, such as polishing flaws and rough or damaged facet edges, would be achieved only if the diamond had not been repolished after the mother topograph was recorded. Significant recutting would be expected to remove some features of the fingerprint, while leaving the rest intact. If the table facet's inclination angle is changed by only a few degrees, a daughter topograph will differ only slightly from the mother topograph. Extensive reshaping would complicate the identification, although it is still possible in principle (see, e.g., figure 17). In the worst-case

scenario, multiple (up to 24) X-ray daughter topographs would be needed to prove that a diamond was recut from a particular stone. This also would require experience in interpreting the features visible on the topographs. Nevertheless, such effort would be worthwhile in exceptional cases.

The exposure time is an important consideration, since it affects topographic contrast. If the recording conditions are identical, mother and daughter topographs will be identical. The exposure time depends on the flux of X-rays. Efforts should be made to standardize the X-ray flux according to sample size, orientation, and the like.

In rare cases, a diamond's topographic fingerprint may not be diagnostic. For example, samples with a very low concentration of extended defects might yield only a few useful features. In contrast, diamonds with very high concentrations of defects could render X-ray topographs meaningless due to multiple superpositions of defects. In both cases, however, the polar angles might prove useful as identifiers. In unusual cases in which the reference direction is exactly perpendicular to the table facet, more than one mother topograph must be recorded. In such a case, a maximum of four topographs are needed if the reference direction is a tetrad, or a maximum of two for a diad. Nevertheless, only one daughter topograph will be needed for comparison.

What is the size range of diamonds that can be fingerprinted by X-ray methods? So far, we have been unable to obtain large diamonds for testing this technique; the largest sample weighed 2.31 ct and was 5.1 mm in thickness (figure 17). The penetration depth of X-rays into diamond depends on the energy of the incident X-rays. From data on absorption and extinction of X-rays when interacting with matter (see, e.g., Wilson, 1992), we have derived some reasonable estimates for acceptable stone sizes. Employing X-rays from a copper target, diamonds with a thickness of up to 3 mm can be topographed. For molybdenum and silver radiation, the maximum thicknesses are estimated at 8 mm and 12 mm, respectively. For thicker samples, the defect contrast would become weaker due to increasing absorption, and even larger sizes would not be expected to show distinctive topographs due to the superposition of too many defects (unless the defect concentration is low). Nevertheless, some fingerprinting of larger diamonds can be accomplished by using their polar angles and also by observing topographic features near the edges where the thickness is reduced.

APPLICABILITY TO THE GEM TRADE

To establish an X-ray topographic fingerprinting laboratory, a floor space of about 10 m² and the necessary means to run an X-ray generator (e.g., water cooling) are required. A minimum investment of approximately US\$50,000 is envisaged, to purchase an X-ray generator with a stationary anode, a multi-axes goniometer with stepping motors, computer, printer, and the like. A darkroom for film processing is not needed, as digital X-ray imagers with high sensitivity and acceptable resolution have become available (see, e.g., www.photonic-science.ltd.uk). This allows for short exposure times and the observation of topographs while the sample is still positioned in the goniometer. Costs for X-ray imaging systems are in the range of \$15,000–\$35,000, depending mainly on the size and resolution of the imaging chip.

Software development costs for computer automation of the equipment and programming are estimated at \$25,000. After a straightforward routine has been implemented, it should take 6–20 minutes to acquire each topograph. Operating expenses, outside of the space required, are relatively small, involving primarily water use (coolant), electricity, and salaries. Technical personnel need not have a scientific background because specific knowledge and expertise are incorporated into the software.

The routine described here can be executed in any laboratory competent in X-ray crystallography. Such laboratories are found in many research institutes that are active in materials science, solid-state physics, crystal chemistry, and earth sciences. Since the investment costs are relatively high and a secure infrastructure is required, only major gem laboratories would be expected to consider this X-ray fingerprinting procedure. Ideally, these laboratories would develop a workable agreement to share their databases over the Internet. The pole angles could serve as searching parameters to quickly locate mother topographs in a database.

The simplified routine for the X-ray diffractive/topographic characterization of faceted diamonds presented here considerably reduces the time, effort, and manpower needed for fingerprinting diamonds. The polar angle data and the mother topograph could make valuable additions to a diamond's certificate, providing added confidence for both the jeweler and the consumer.

ABOUT THE AUTHORS

Dr. Diehl (rodiehl@t-online.de) is senior scientist at the Fraunhofer Institute for Applied Solid-State Physics IAF in Freiburg, Germany, and is an advisory board member of the German Gemmological Association in Idar-Oberstein. Dr. Herres (nikolaus.herres@ntb.ch) is a lecturer at the Interstaatliche Hochschule für Technik NTB in Buchs, Switzerland.

ACKNOWLEDGMENTS: The authors express their sincerest thanks to Karl-Heinz Meng of Idar-Oberstein for providing diamond specimens for examination and development of the method described in this article. They are also deeply indebted to Lutz Kirste (Fraunhofer IAF) for his support in providing access to the equipment and for taking several of the X-ray topographs.

REFERENCES

- Bohm J. (1995) *Realstruktur von Kristallen*. Schweizerbart'sche Verlagsbuchhandlung, Stuttgart, Germany.
- Borchardt-Ott W. (1997) *Kristallographie*, 5th ed. Springer-Verlag, Berlin, Germany.
- Buerger M.J. (1967) *Elementary Crystallography*. Wiley, New York.
- Cullity B.D. (1978) *Elements of X-Ray Diffraction*, 2nd ed. Addison-Wesley, Reading, Massachusetts.
- Diehl R. (1982) Möglichkeiten der Edelsteindiagnose mit Hilfe der Röntgentopographie [Possibilities of gem identification using X-ray topography]. *Zeitschrift der Deutschen Gemmologischen Gesellschaft*, Vol. 31, pp. 3–22.
- Diehl R., Herres N. (1997) *Verfahren zur röntgenographischen Identifizierung von geschliffenen Diamanten [X-Ray Identification Method for Cut Diamonds]*. German patent DE 1963 1367, issued November 13.
- Diehl R., Herres N. (1998) Ein vereinfachtes Verfahren zur zweifelsfreien Identifizierung von geschliffenen Diamanten. *Gemmologie: Zeitschrift der Deutschen Gemmologischen Gesellschaft*, Vol. 47, No. 2, pp. 77–88.
- Frank F.C., Lang A.R. (1965) X-ray topography of diamond. In R. Berman, Ed., *Physical Properties of Diamond*, Clarendon Press, Oxford, England, pp. 69–115.
- Kelly A., Groves G.W., Kidd P. (2000) *Crystallography and Crystal Defects*, revised ed. Wiley, Chichester, England.
- Lang A.R. (1959) A projection topograph: A new method in X-ray diffraction microradiography. *Acta Crystallographica*, Vol. 12, pp. 249–250.
- Lang A.R. (1975) *Diamond Identification*. British patent 328/75, issued January 3.
- Lang A.R. (1978a) *Diamond Identification*. U.S. patent 4,125,770, issued November 14.
- Lang A.R. (1978b) Techniques and interpretation in X-ray topography. In S. Amelinckx et al., Eds., *Diffraction and Imaging Techniques in Material Science*, Vol. II, North-Holland, Amsterdam, pp. 623–714.
- Lang A.R. (1988) *Verfahren zur Identifizierung von Diamanten*. German patent DE 2559245 C2, issued May 26.
- Lang A.R. (1979) Internal Structure. In J.E. Field, Ed., *The Properties of Diamond*, Academic Press, London, pp. 425–469.
- Lang A.R., Woods G.S. (1976) Fingerprinting diamonds by X-ray topography. *Industrial Diamond Review*, March, pp. 96–103.
- Lang A.R., Moore M., Walmsley J.C. (1992) Diffraction and imaging studies of diamond. In J.E. Field, Ed., *Properties of Natural and Synthetic Diamond*, Academic Press, London, pp. 215–258.
- Laurs B.M., Ed. (2001) Gem News International: White House conference on “conflict” diamonds. *Gems & Gemology*, Vol. 37, No. 1, pp. 64–66.
- Martineau P.M., Lawson S.C., Taylor A.J., Quinn S.J., Evans D.J.F., Crowder M.J. (2004) Identification of synthetic diamond grown using chemical vapor deposition (CVD). *Gems & Gemology*, Vol. 40, No. 1, pp. 2–25.
- McKie D., McKie C. (1974) *Crystalline Solids*. Nelson, London.
- Moses T.M., Shigley J.E., McClure S.F., Koivula J.I., Van Daele M. (1999) Observations on GE-processed diamonds: A photographic record. *Gems & Gemology*, Vol. 35, No. 3, pp. 14–22.
- Rinaudo C., Capelle B., Navone R. (2001) A new method to identify a cut gemstone. *Gemmologie: Zeitschrift der Deutschen Gemmologischen Gesellschaft*, Vol. 50, No. 1, pp. 43–50.
- Smith J.G.C. (1999) *Diamond or Gemstone Marking by Plurality of Grooves*. European patent WO99/33671, issued July 8.
- Smith C.P., Bosshart G., Ponahlo J., Hammer V.M.F., Klapper H., Schmetzer K. (2000) GE POL diamonds: Before and after. *Gems & Gemology*, Vol. 36, No. 3, pp. 192–215.
- Sunagawa I. (1995) The distinction of natural from synthetic diamonds. *Journal of Gemmology*, Vol. 24, No. 7, pp. 485–499.
- Sunagawa I., Yasuda T., Fukushima H. (1998) Fingerprinting of two diamonds cut from the same rough. *Gems & Gemology*, Vol. 34, No. 4, pp. 270–280.
- Wallner, H.F., Vanier, D.J. (1992) *Gemstone Identification, Tracking and Recovery System*. U.S. patent 5,124,935, filed Nov. 30, 1990.
- Wilson A.J.C., Ed. (1992) *International Tables for X-Ray Crystallography, Vol. C*. Publ. for the International Union of Crystallography by Kluwer Academic Publishers, Dordrecht, The Netherlands.

For regular updates from the world of **GEMS & GEMOLOGY**, visit our website at:

www.gia.edu

2004

LAB NOTES

EDITORS

Thomas M. Moses, Ilene Reinitz,
Shane F. McClure, and Mary L. Johnson

GIA Gem Laboratory

CONTRIBUTING EDITORS

G. Robert Crowningshield

GIA Gem Laboratory, East Coast

Karin N. Hurwit, John I. Koivula, and
Cheryl Y. Wentzell

GIA Gem Laboratory, West Coast

Feathers in COPAL

Like its much older relative amber, gem-quality copal can be quite interesting when it contains unusual or photogenic inclusions, because of its excellent preservative nature and typically high degree of transparency. Recently, gem and mineral dealer Russell E. Behnke of Meriden, Connecticut, sent the West Coast laboratory a 41.59 ct freeform polished mass of fossil resin that measured approximately $44.66 \times 32.25 \times 9.80$ mm. The specimen had been mined, shaped, and polished in Boyacá, Colombia. Mr. Behnke wanted to know if it would be considered amber or the more recent fossil resin, copal. Both

amber and copal have been reported from Colombia (see Summer 1993 Gem News, pp. 135–136).

The light brownish yellow sample was transparent to translucent due to the presence of inclusions (figure 1). The refractive index was 1.54, and the specific gravity (determined hydrostatically) was 1.03. While the S.G. was slightly low for a fossil resin, this was not too surprising considering the numerous gas bubbles the piece contained.

As expected for either amber or copal, no absorption spectrum was observed with a desk-model prism spectroscope. When the piece was exposed to long-wave UV radiation,

we saw a moderate slightly chalky yellow fluorescence, while exposure to short-wave UV produced only a very weak yellow reaction.

In addition to the gas bubbles and insects typically seen in such material, magnification revealed a significant number of two-phase (liquid and gas) inclusions, some of which had moving gas phases. However, the most interesting inclusion, which was clearly visible even without magnification, was the upper portion of a bird's flight feather (again, see figure 1). Close examination with a gemological microscope and polarized light showed the details of the well-preserved feather as well as the presence of significant strain (figure 2).

In addition to the large flight feather, two tiny feather fragments (figure 3) were also observed. As with most inclusions, these were clearly visible only through the microscope.

Using magnification, we placed a tiny droplet of acetone on the edge of the specimen and allowed it to evaporate. The acetone produced a miniscule dull spot, and this spot proved to be sticky when it was lightly rubbed with the torn edge of a facial tissue. Such a reaction is indicative of copal,

Figure 1. This 41.59 ct freeform polished mass of copal resin from Boyacá, Colombia, contains bird feathers as inclusions.



Editor's note: The initials at the end of each item identify the editor(s) or contributing editor(s) who provided that item. Full names are given for other GIA Gem Laboratory contributors.

Gems & Gemology, Vol. 40, No. 1, pp. 58–65

© 2004 Gemological Institute of America

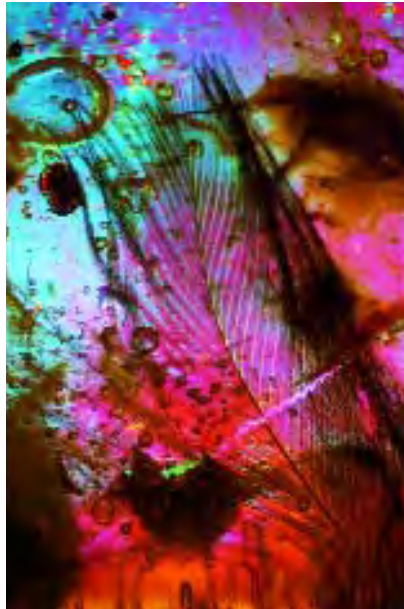


Figure 2. Feathers occur only rarely as inclusions in natural fossil resins. This flight feather is well preserved in its copal resin host. The use of crossed polarizers reveals the significant strain in this specimen. Magnified 2×.

since amber does not soften and get sticky in response to acetone. Therefore, through this microchemical confirmatory test, we established that this fossil resin was copal rather than amber.

John I. Koivula and Maha Tannous

Rare Type IIa Pink DIAMOND, with Green Radiation Stains

The color of some diamonds can be attributed to exposure to natural radiation. Green and brown radiation stains are occasionally observed on rough diamond surfaces or within fractures, but generally they do not contribute to the bodycolor of the diamond. Most of the diamonds in which such stains are seen are yellow, brown, or green. Rarely, brown radiation stains have been observed in blue type IIb diamonds (Fall 1991 Lab Notes, pp. 174–175).



Figure 3. Two tiny feather fragments were also discovered in the Colombian copal. Magnified 10×.

Recently, we examined a large pink diamond with green radiation stains located mainly within fractures. While much of the formation of radiation stains is not completely understood, this observation indicates that natural irradiation can and does occur with all types of diamond, regardless

Figure 4. This Faint pink 20.24 ct pear-shaped brilliant revealed many green radiation stains when examined with magnification. This is a rare feature in pink type IIa diamond, and it indicates that natural irradiation can occur in diamonds of all types.



of color and nitrogen/boron concentrations.

The 20.24 ct pear-shaped brilliant cut (31.62 × 17.73 × 3.70 mm) in figure 4 was color graded Faint pink. It fluoresced weak blue to both long- and short-wave UV radiation. No phosphorescence was observed. This stone had very few internal characteristics, but many fractures were present around the girdle. Though most were very shallow, a few larger ones penetrated as deep as 4 mm. Many small green radiation stains were visible along these fractures (figure 5). It is believed that these stains are caused by radioactive isotopes transported in fluids that enter surface-reaching fissures in the rough diamond (see, e.g., A.T. Collins, "Colour centres in diamond," *Journal of Gemmology*, Vol. 18, No. 1, 1982, pp. 37–75).

The stains in this diamond generally had well-defined boundaries. The radiation was not strong enough to affect the bodycolor of even this weakly colored pink stone, which was caused by a broad absorption around 550 nm. Spectroscopic analysis confirmed that this stone was type IIa, with extremely low concentrations of some point defects common in type IIa diamonds. While the combination of pink color and green radiation stains is rare, it represents proof that this stone was not HPHT treated. HPHT processing can create pink dia-

Figure 5. The green radiation stains in this faint pink diamond generally have well-defined boundaries. Length of this image is about 4 mm.



monds from brown ones, but the heat necessary to change the color of a type IIa diamond would also change the color of the radiation stains. Depending on the temperature used, the green stains could turn brown or perhaps even disappear entirely.

Wuyi Wang and Thomas Gelb

Two Yellow SYNTHETIC DIAMONDS

From the time they were first produced, synthetic diamonds have been a source of concern for the gem and jewelry industry. With the release into the market of gem-quality synthetic diamonds by Gemesis Corp. and other manufacturers, these concerns have grown considerably. In the Winter 2002 issue of *Gems & Gemology* (pp. 301–309), J. E. Shigley et al. described Gemesis yellow synthetic diamonds and the clues for their detection. Although identification may require advanced spectroscopic or luminescence equipment that is only available in a well-equipped gemological laboratory, in many cases the trained gemologist can make the separation based on standard gemological clues, such as metallic inclusions and color zoning. Such was the case with two yellow brilliants that were submitted to the East Coast laboratory for grading.

On examination with a microscope, both were immediately suspected of being synthetic. The first, a 0.99 ct round brilliant, had a very unusual inclusion under the center of the table (figure 6). When viewed from various angles, this pyramid-shaped inclusion was seen to be very dark gray to black with rounded edges—in contrast to the pyramidal or octahedral inclusions that may be seen in natural diamonds, which typically are transparent or white with flat surfaces and sharp edges. On the basis of its appearance, we concluded that this somewhat globular inclusion was a remnant of metallic flux, which is not uncommon in synthetic diamonds grown by a high pressure/high temper-

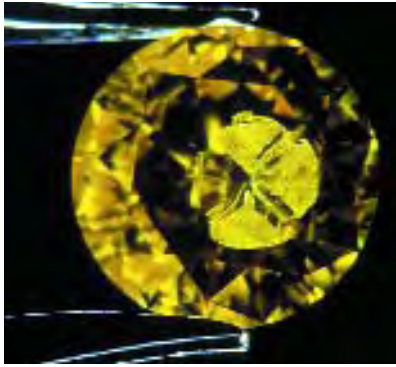


Figure 6. The rounded edges on this large inclusion in the table of a 0.99 ct yellow round brilliant are indicative of synthetic origin.

ature process. During this growth process, the carbon source is dissolved in a molten metal, or flux, typically composed of iron, nickel, and cobalt. This flux facilitates the movement of carbon atoms toward a host seed crystal, where they are deposited to form a larger crystal. Sometimes pieces of the molten material are trapped inside the growing synthetic diamond as inclusions, taking on diamond's octahedral crystal form while still exhibiting the melted appearance and rounded edges that are characteristic of a metallic

Figure 8. The presence of metallic inclusions caused this 1.41 ct synthetic diamond to be attracted by a magnet, from which it is suspended here. Magnetic inclusions are very rare in natural yellow diamonds.

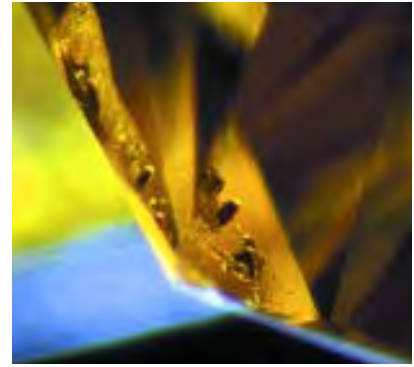
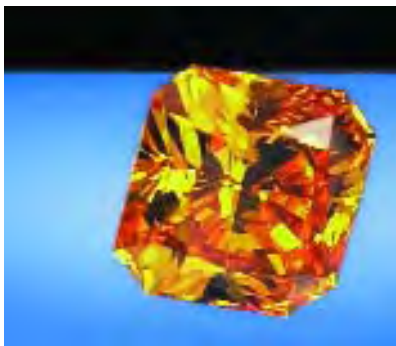
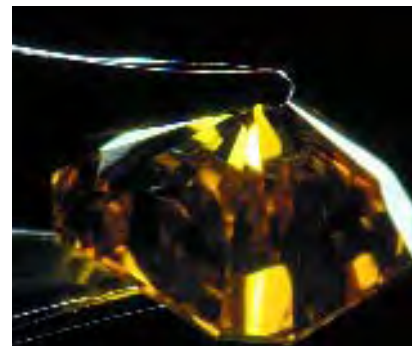


Figure 7. The rounded form and protrusions of this surface-reaching inclusion, seen touching the crown of a 1.41 ct yellow square modified brilliant, are similar to those that have been reported in commercial synthetic diamonds. Magnified 63×.

flux.

The second sample, a 1.41 ct square modified brilliant, also had a black inclusion. In this instance, the inclusion reached the crown surface, and had been partially polished away. The remnant visible at the surface did not look so unusual, but the internal portion was globular in appearance, with rounded, elongated protrusions

Figure 9. Color zoning, such as that visible through the pavilion of this 1.41 ct yellow square modified brilliant, is a good indication of synthetic origin. Magnified 10×.



penetrating a short distance into the diamond (figure 7). Again, such rounded black opaque inclusions are indicative of synthetic origin. As a further test, a strong magnet was used to verify that the inclusion was indeed metallic, as all three of the elements typically used in the flux are usually magnetic (figure 8). Further observation of this synthetic diamond revealed color zoning (figure 9) and a cloud of minute pinpoint inclusions. Both of these characteristics are typical of synthetic diamonds. We confirmed the synthetic origin of these two samples with the De Beers DiamondView luminescence imaging system.

Vincent Cracco and Joshua Sheby

HERDERITE Update

Herderite-hydroxyl-herderite [CaBePO₄(F,OH)] is a phosphate mineral series that can form excellent crystal specimens and, when sufficiently transparent, be faceted into attractive stones (with a Mohs hardness of 5–5½). In the Fall 1996 Lab Notes (p. 208), the West Coast laboratory reported on an “extraordinarily large” 38.91 ct herderite. With only one other confirmed example of gem herderite found in the literature (P. J. Dunn and W. Wight, “Green gem herderite from Brazil,” *Journal of Gemmology*, Vol. 15, No. 1, 1976, pp. 27–28), this member of the series historically has been considered quite rare. Since 1996, however, we have identified another five specimens of this gem material, ranging from 12.28 to 161.09 ct. The most recent was in November 2003, when Solari and Huntington Jewelers of Park Ridge, Illinois, submitted the 78.35 ct herderite, shown in figure 10. The largest of the six stones, which measured 57.9 × 27.4 × 17.1 mm, was submitted in May 2002 by the Gemological Center in Belo Horizonte, Minas Gerais, Brazil. Given the rarity of this material, these samples provided a unique opportunity to study the properties of gem-quality

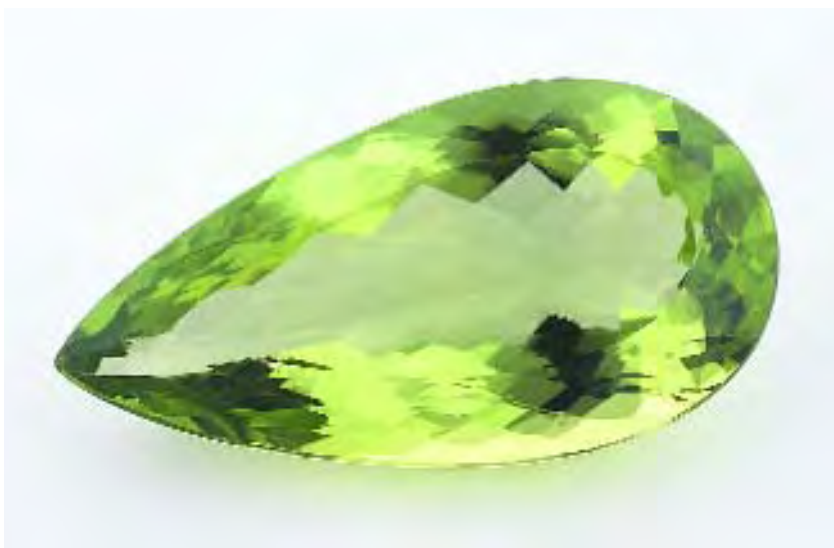


Figure 10. This 78.35 ct herderite (43.45 × 22.56 × 13.52 mm), reportedly from Minas Gerais, Brazil, is one of six large herderites examined by GIA since 1996.

herderite.

All six herderites, which were either pear shapes or emerald cuts, were yellowish green and had similar gemological properties. Magnification revealed strong doubling (due to birefringence that ranged from 0.029 to 0.031) and only a few internal features: pinpoint or needle-like inclusions that were isolated or in small clusters, as well as small two-phase inclusions, fractures, and coarse needles or growth tubes.

The R.I. values were consistent in five of the six samples, with $\alpha = 1.580$ and γ ranging from 1.609 to 1.611. One sample had slightly lower values: $\alpha = 1.578$ and $\gamma = 1.607$ –1.608. Specific gravity was very constant for all samples, at approximately 3.04. Each stone showed a line at 580 or 585 nm in the desk-model spectroscope. Pleochroic colors were recorded for four of the samples, the most common combination being yellow and yellowish green, with some reports of greenish yellow, green, or brownish green components.

Herderite displays a characteristic luminescence to X-rays; this property was checked on two of the samples,

and both luminesced strong orange or yellow-orange with prolonged phosphorescence. A property not found in the literature was the unusual luminescence to transmitted light from a strong light source such as that of a fiber-optic light: weak to medium violet in three stones; the luminescence was very weak blue in the fourth stone tested for this feature.

With all other properties being remarkably similar, it is interesting to note that the UV fluorescence varied considerably from stone to stone. The long-wave UV fluorescence ranged in intensity from inert to weak; of the five samples that did fluoresce, three displayed blue luminescence, one green-blue, and one violet. Moderate chalkiness was recorded in two instances. The short-wave UV fluorescence ranged from faint to weak, in the following colors: yellow, yellowish green, blue, greenish blue, green-blue, and violet. Weak to strong chalkiness was recorded for the same two samples as above.

Energy-dispersive X-ray fluorescence (EDXRF) analyses performed on four of the samples revealed Ca and P as major constituents in all, with

Mn, Pb, Sr, and Y as minor or trace elements. Fe was a trace or possible trace element in two of the samples.

The end-member species of herderite-hydroxyl-herderite are differentiated by mineralogists according to the ratio of fluorine to hydroxyl in the formula. Although these components are not detectable by routine analytical techniques found in most gemological laboratories, it is possible to estimate the composition of the herderite series by measuring the refractive indices, since the R.I. values systematically decrease with increasing fluorine content (see P. B. Leavens et al., "Compositional and refractive index variations of the herderite-hydroxyl-herderite series," *American Mineralogist*, Vol. 63, No. 4, 1978, pp. 913–917). The fluorine content of the previously confirmed gem-quality herderite was determined to be greater than its hydroxyl content (Dunn and Wight, 1976). Since the gemological properties of the six specimens we examined were consistent with this 5.90 ct Brazilian sample (R.I.'s of $\alpha = 1.581$ and $\gamma = 1.610$, with just a slightly lower S.G. value—3.02 vs. 3.04), it can be concluded that the additional specimens also fall within the fluorine-rich herderite side of the series, and may be the only other examples of rare and fine gem-quality herderite reported in literature.

Although Dunn and Wight (1976) did not provide any additional information on the locality of their herderite sample, two of the most significant deposits of large, well-formed crystals of hydroxyl-herderite in Brazil are the Virgem da Lapa and Golconda mines in Minas Gerais (P. J. Dunn et al., "Hydroxyl-herderite from Brazil and a guide to species nomenclature for the herderite/hydroxyl-herderite series," *Mineralogical Record*, Vol. 10, No. 1, 1979, pp. 5–11). The owner of the 161.09 ct herderite reported that it was from Ouro Verde, Minas Gerais; the herderite shown in figure 10 is also reportedly from Minas Gerais, although the specific locality is unknown. At the

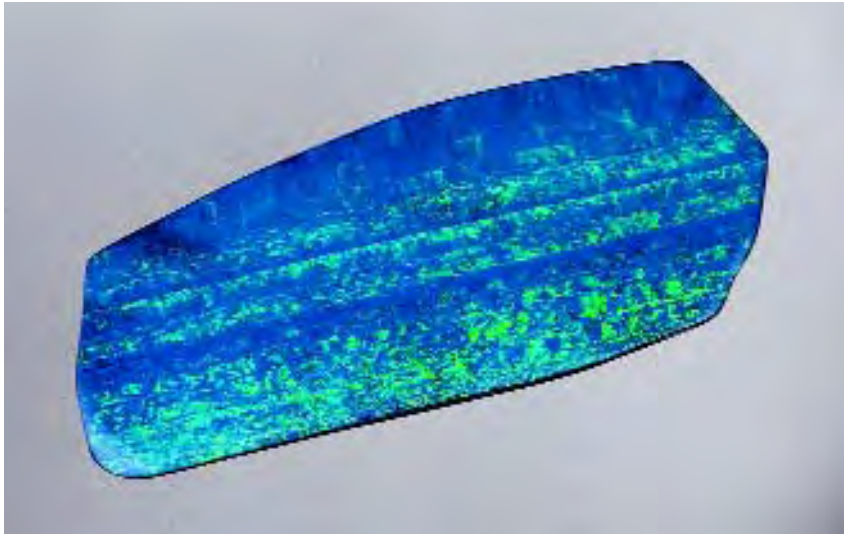


Figure 11. This 798.39 ct specimen was the largest opal doublet of such high quality ever seen in the laboratory.

time of this writing, no source information about the other samples examined at GIA was available. Given the number of large herderites submitted to the laboratory since 1996, it would be interesting to know whether the other stones also originated from Minas Gerais, perhaps from the same deposit as the largest herderite reported here.

CYW

Large OPAL Doublet

Recently, the West Coast laboratory had the opportunity to examine a large freeform opal doublet that was submitted by Christensen & Co. of South Australia. The doublet weighed 798.39 ct and measured $\sim 139.0 \times 57.5 \times 13.5$ mm (figure 11). Because of its size (none of the staff could recall seeing a larger one of such quality), we had to exercise extra special care in our examination.

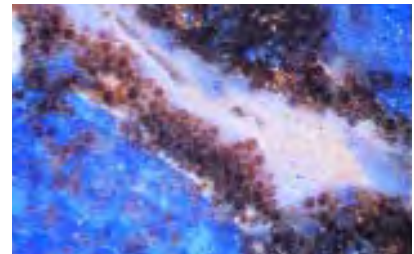
The top portion of the doublet consisted of a thin transparent-to-semi-transparent layer that showed play-of-color. The bottom portion consisted of a thicker translucent-to-opaque mottled brown-and-white layer that also displayed some play-of-

color. These two layers were joined by a black cement. Both top and bottom portions were reportedly from Andamooka, South Australia.

We obtained a typical opal R.I. of 1.46 from both the top and bottom layers, and an additional R.I. of 1.55 from some spots on the backing. The opal portions of both layers fluoresced a medium blue-white to long-wave ultraviolet radiation, with a weak blue-white reaction to short-wave UV. Both also displayed phosphorescence of the same color and relative strength to long- and short-wave UV.

Microscopic examination revealed

Figure 12. At 10 \times magnification, the unusual circular structure of the oolitic opal backing was readily apparent.



that the top layer was indeed natural opal, while the backing material consisted partly of natural oolitic opal, which is characterized by an unusual circular structure (figure 12; see also Summer 1982 Lab Notes, pp. 104–105). Magnification, along with the 1.55 R.I., indicated that there were also areas of quartz, probably chalcedony, in the backing material (see Spring 1986 Lab Notes, p. 50).

It was obvious that great care had been taken to create such a piece. The opal top was fairly thin for its size and was not perfectly flat. It had been carved to follow the natural contours of the vein in which it formed, and the backing mimicked the contours of the top layer almost perfectly.

Elizabeth P. Quinn

Three Rutilated QUARTZ Cat's-Eyes

Rutilated quartz is a popular gem material. In lower qualities, it can be found in abundance at gem and mineral shows, while good examples showing desirable features such as chatoyancy or starburst patterns of rutile are prized by collectors and jewelry designers. Three chatoyant rutilated quartz cabochons recently examined in the West Coast laboratory were particularly interesting because of the different colors presented in their eyes.

As illustrated in figure 13, the reflective chatoyant colors shown by these cabochons were “silvery” gray, “golden” yellow, and “coppery” red. The 13.70 ct silvery chatoyant stone measured 14.47–14.96 × 8.91 mm, while the 10.46 ct yellow cat's-eye measured 13.80–14.03 × 7.59 mm. Both stones were cut from Brazilian quartz by Falk Burger of Los Alamos, New Mexico. The silvery chatoyant cab was fashioned from material that has recently been sold as “platinum quartz” (see Winter 2003 Gem News International, p. 334).

The 24.22 ct cabochon showing red chatoyancy (14.98–15.64 × 12.51 mm) was cut by Kevin Lane Smith of

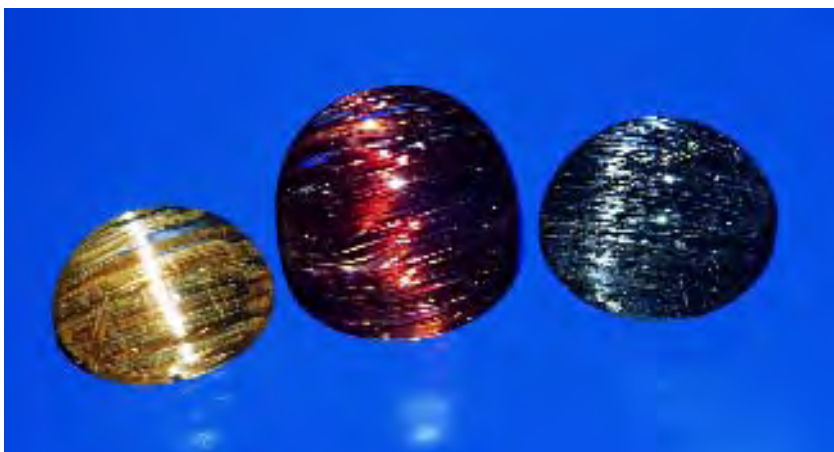


Figure 13. These rutilated quartz cabochons (10.46–24.22 ct) show three different colors of chatoyancy.

Tucson, Arizona, from rutilated quartz said to have come from Madagascar. Rutile of this color is known to come from other sources as well, including Brazil and North Carolina.

With magnification, the lengthwise striations and tetragonal cross section typical of rutile were visible on the inclusions, as was rutile's high luster compared to the surrounding quartz. Raman analysis confirmed that the chatoyancy-causing inclusions in all three gems were rutile.

While rutilated quartz showing a golden yellow color is relatively common, the silvery gray and coppery red colors are considerably more unusual. The presence of sufficient acicular rutile inclusions in parallel alignment and of a diameter suitable to produce chatoyancy in highly transparent quartz is even rarer in any color of rutile, but particularly so in gray and red.

John I. Koivula and Maha Tannous

SPURRITE

Since there are actually very few naturally colored purple gem minerals, receipt in the West Coast laboratory of four translucent purple beads (see, e.g., figure 14) immediately raised

suspicious of dyed quartzite or carbonate. However, when the beads were examined with magnification, they were found to be aggregates that contained numerous naturally colored, distinctly dichroic purple grains, which changed from a rich purple to very light purple or near colorless when the polarizer of the microscope was rotated. This identification was to be a greater challenge than initially expected.

We selected one of the beads (0.43 ct, 4.34–4.39 × 2.90 mm) for testing. With permission from the owner, Stephen Mauldin Stone Co. of Sandia Park, New Mexico, we exposed this bead to a minute amount of 10% HCl solution; it effervesced readily, indicating the presence of a carbonate. The purple grains displayed a higher resistance to the acid, while the interconnecting material was easily etched.

On the refractometer, the sample displayed a birefringence blink from approximately 1.64 (α) to 1.68 (γ). Some areas appeared to have a larger birefringence, while others gave a spot R.I. value close to 1.50; however, these secondary values were indefinite. The average S.G., obtained hydrostatically, was close to 2.96 although values as low as 2.85 were also obtained because of the small size of the bead.

The specimen displayed no visi-

ble spectrum and was inert to short-wave UV radiation. The long-wave UV luminescence was a faint "cobalt" blue.

The area of purple grains that was isolated by the acid etching was scraped for X-ray powder diffraction analysis. The resultant pattern matched that for the mineral spurrite, which is an uncommon, usually massive, biaxial negative, monoclinic mineral with the chemical composition $\text{Ca}_5(\text{SiO}_4)_2(\text{CO}_3)$ and a hardness of 5 on the Mohs scale (see, e.g., W. L. Roberts et al., *Encyclopedia of Minerals*, 2nd ed., Van Nostrand Reinhold, New York, 1990, pp. 808–809). To further isolate individual components for testing, the bead was immersed in the dilute HCl solution for several hours. It effervesced readily, and most of the sample dissolved, leaving a white pow-

dery residue. A white substance that remained intact was also scraped for X-ray powder diffraction, yielding a pattern that matched that of a combination of grossular and idocrase.

EDXRF, performed on the bead by senior research associate Sam Muhlmeister prior to its dissolution in acid, revealed Si and Ca as the major elements present, with a trace of Fe. The primary constituents were consistent with spurrite, but the lack of Al suggested that neither grossular nor idocrase was present. Further analysis of numerous areas of this and an accompanying bead found Al in some areas, but not in many others. The relative amounts of Al could not be determined, and Mr. Muhlmeister believed that its variable presence was due to the inhomogeneity of the material.

Raman analysis of the purple

grains yielded distinct spectra that contained possible carbonate peaks, but they did not match any reference spectra in the database (which did not include spurrite). The spectra of areas between the purple grains matched those of several carbonates in the database. None of the areas tested yielded any matches for grossular or idocrase.

The R.I. of this sample was consistent with that recorded for the mineral spurrite. The S.G. was slightly below but close to the value of 3.0 reported in the literature. The presence of a carbonate compound, the X-ray powder diffraction pattern, and the chemistry all confirmed that this material indeed consisted largely of spurrite. One of the X-ray diffraction patterns indicated the presence of additional minerals; however, since the identity of these minerals could not be confirmed by either EDXRF or Raman spectroscopy, it was necessary to conclude that the item was a rock consisting of spurrite and additional minerals. Petrographic testing would be necessary to characterize this material further.

In February 2001, the West Coast laboratory received a 7.19 ct partially polished piece of rough material that had similar properties to the aforementioned stones, and had a corresponding conclusion on the report. This entry's author tested (less extensively) another purple aggregate that was purchased as spurrite for the GIA stone collection at the 1997 Tucson gem show; it too had enough of the same properties to indicate that it was indeed spurrite (or at least its dimorphous counterpart, paraspurrite [discussed below]), reportedly from a deposit in the southwestern U.S.

To further compare these materials to each other and to the properties published in the literature for spurrite, cathodoluminescence was observed on two of the four beads as well as on the stone from the GIA collection. The published cathodolu-

Figure 14. Four purple beads that were reportedly from Guerrero State in southern Mexico proved to be rocks that consist primarily of spurrite plus additional minerals. Shown are two of the beads (0.85 ct total weight) along with a sample (19.02 ct) from GIA's collection, reported to be spurrite from the southwestern U.S.



minescence of spurrite is green (J. W. Anthony et al., *Handbook of Mineralogy*, Vol. II, *Silica, Silicates*, Part 2, Mineral Data Publishing, Tucson, Arizona, 1995, p. 748); however, the two beads luminesced pinkish orange, and the stone from the GIA collection luminesced orange. Given that the spurrites seen in the lab were aggregates with other minerals, it is possible that the additional components influenced the cathodoluminescence.

Spurrite may be white, gray, purple, or purple-gray, and is the product of low-pressure, high-temperature metamorphism along the contact between carbonate rock, most commonly limestone, and mafic magma. The best-known source localities include northern Mexico and Ireland, but it also occurs in Scotland, the U.S. (Riverside County, California; Luna County, New Mexico; and Lewis and Clark, and Meagher counties, Montana), Turkey, Israel, Japan, New Zealand, Siberia, and elsewhere in Russia (Anthony et al., 1995). The owner of the samples received for testing said they came from Guerrero State in southern Mexico, a location that was not reported in the author's reference literature.

Paraspurrite, a pseudomorph of spurrite, has an identical chemical composition, closely related crystal structure, and similar gemological properties to those of spurrite. It has been found in Inyo County, California (A. A. Colville and P. A. Colville, "Paraspurrite, a new polymorph to spurrite from Inyo County, California," *American Mineralogist*, Vol. 62, 1977, pp. 1003–1005). The two minerals may be distinguished by measurement of their unit-cell parameters. The X-ray powder diffraction patterns are similar, with paraspurrite exhibiting additional reflections and different line intensities in the pattern. Paraspurrite also has different associated minerals, which may be observed in thin section.

In addition to the samples dis-

cussed in this entry, another spurrite was observed by GIA laboratory staff at the 1986 Tucson gem show (Summer 1986 Gem News, pp. 114–115); however, the four beads reported here represent only the second instance that this material has been submitted by a client to the laboratory for identification. CYW

Bicolored Cat's-eye TOURMALINE

Cat's-eye tourmaline and bicolored tourmaline are well known to gemologists. The bicolored gems are usually faceted to display the component colors, or cut as polished slabs as in the case of green and red so-called watermelon tourmaline. Cat's-eyes are always fashioned as cabochons to showcase the reflective nature of the chatoyancy-causing bundles of parallel growth tubes. However, it is unusual to have bicolouration and chatoyancy together in the same stone.

Just such a specimen was recently examined in the West Coast laboratory. The 9.77 ct bicolored cat's-eye tourmaline (16.84 × 11.16 × 5.71 mm) was cut by Falk Burger of Los Alamos, New Mexico. The rough material, which came from Brazil, was bicolored blue and green perpendicular to the length of the crystal.

The cabochon was cut as a cushion shape with one end green and the other blue (figure 15). When it was tilted under a single point source of light, such as a fiber-optic illuminator, a single sharp eye was observed to drift back and forth across the stone, changing from blue to green depending on the portion of the stone in which it was observed. However, as shown in figure 15, when two light sources were used, a green eye and a blue eye could be seen simultaneously.

Magnification revealed that the chatoyancy was caused by reflection from a combination of two micro-features. As expected, numerous fine growth tubes extending lengthwise in



Figure 15. This 9.77 ct Brazilian cat's-eye tourmaline shows two different colors of chatoyancy at the same time when illuminated by two separate light sources.

the cabochon were in large part responsible for the phenomenon. Also playing a part in the chatoyant effect, however, was a naturally striated unpolished base, which was the rough surface of the original tourmaline crystal.

Over the years, we have seen numerous bicolored tourmalines as well as many cat's-eye tourmalines. This is the first time, however, that we have seen these two varieties of tourmaline used so effectively in combination to create a very unusual gem.

John I. Koivula and Maha Tannous

Erratum: Euclase Specimen

Ms. Claudia Piñeros, the owner of the euclase specimen described in the Spring 2003 Lab Notes (p. 42), has informed us that the specimen was actually found in the course of exploration for emeralds in Pauna, Colombia (not in Brazil as was reported in that entry). *Gems & Gemology* regrets the error.

PHOTO CREDITS

Maha Tannous—1, 11, 13, and 15; John I. Koivula—2, 3, and 12; Wuyi Wang—4 and 5; V. Cracco—6, 7, and 9; Elizabeth Schrader—8; C. D. Mengason—10 and 14.



EDITOR

Brendan M. Laurs (blaur@gia.edu)

CONTRIBUTING EDITORS

Emmanuel Fritsch, *IMN, University of Nantes, France* (fritsch@cnrs-immn.fr)

Henry A. Hanni, *SSEF, Basel, Switzerland* (gemlab@ssef.ch)

Kenneth V. G. Scarratt, *AGTA Gemological Testing Center, New York* (kscarratt@email.msn.com)

Karl Schmetzer, *Petershausen, Germany* (schmetzerkarl@hotmail.com)

James E. Shigley, *GIA Research, Carlsbad, California* (jshigley@gia.edu)

Christopher P. Smith, *GIA Gem Laboratory, New York* (chris.smith@gia.edu)

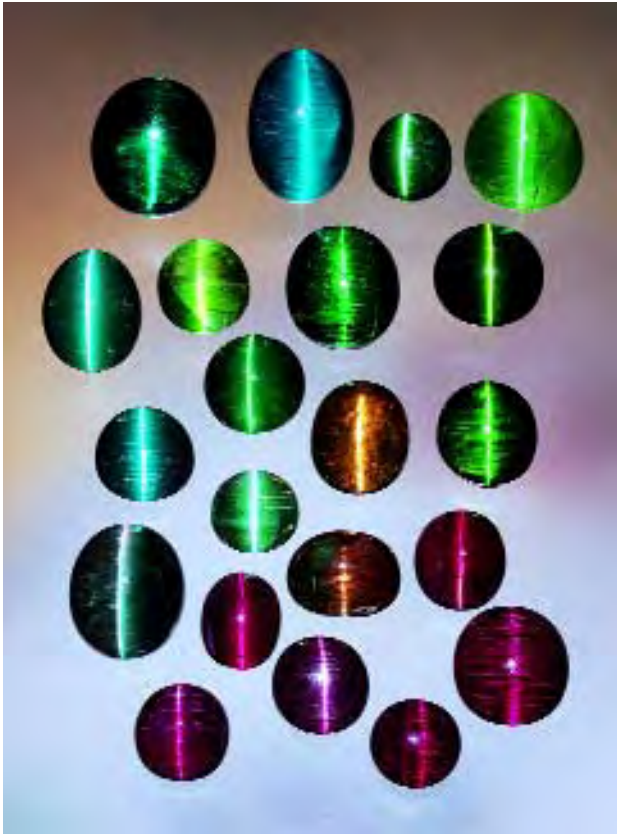
Tucson Report 2004

The annual gem and mineral shows in Tucson, Arizona, showcased a spectacular variety of products. In addition to large quantities of common gems from traditional localities, the shows remain an excellent source of rare and unusual items for the collector. One example was a spectacular suite of cat's-eye tourmaline from Brazil that was brought to our attention by Michael Kazanjian of Kazanjian Bros., Beverly Hills, California (figure 1). Although few new items debuted at this year's show, we saw additional production of interesting materials from several sources, as well as some new developments in synthetic and treated gems. Some of these items are described below, and others will be included in the upcoming Summer 2004 GNI section. *G&G* thanks our many friends who shared information with us this year.

COLORED STONES AND ORGANIC MATERIALS

Yellow cat's-eye beryl from Brazil. At the GJX show, Robert Van Wagoner of Maui Gems, Haiku, Hawaii, had a few cabochons of brownish yellow cat's-eye beryl from Brazil (see, e.g., figure 2). Mr. Van Wagoner first sold this material at the June 2003 JCK show, but only recently did he obtain specific information on it. According to his source in Brazil, the material was mined from a pegmatite in the Padre Paraíso area, which is located 85 km north of Teófilo Otoni in Minas Gerais State. Only a small amount of gem-quality rough was obtained, ranging from translucent to semitransparent. The cat's-eye cabochons typically weigh 5 to 20 ct, although larger stones are believed to exist. Reportedly the yellow color in about 60% of the material was produced by irradiation in a linear accelerator.

Figure 1. This remarkable suite of cat's-eye tourmaline (6.36–36.75 ct) is part of a larger collection of such stones, all from Brazil, that was purchased at one of the Tucson gem shows by Michael Kazanjian. Photo © GIA and Harold & Erica Van Pelt.



Some additional information was provided by Steve Perry of Steve Perry Gems, Davis, California, who also has sold these cat's-eye beryls. His source indicated that a small amount of the material was mined in March 2003. Mr. Perry indicated that both "golden" beryl and aquamarine are produced from this region.

BML

Update on demantoid and cat's-eye demantoid from Iran.

During the Tucson show, one of these contributors (MD) showed GIA personnel two cabochons of cat's-eye demantoid from Kerman Province, southern Iran. Based on the experience of this contributor, who regularly visited the deposit from early 2001 to November 2003, this report provides an update on the mining and production of the demantoid from this area, as well as the appearance of the chatoyant material. The gemological properties and color range of this Iranian demantoid were described in the Spring 2002 Gem News International section (p. 96).

The site is located at 28°19'N and 57°45'E, between the villages of Bagha Borch and Soghan, which lie approximately 150 km south of the town of Jiroft. Travel from Tehran to Jiroft takes about 16 hours, although considerable delays may be encountered along the highway, which is heavily patrolled to prevent drug smuggling. The journey onward from Jiroft to the site requires three hours of driving on a rough road.

The mining area (figure 3) is situated approximately 1,500 m above sea level, and consists of several tunnels and small pits scattered across an area of approximately 500 m². Mining is done by hand, mostly in December–March when the weather is cooler. The workings range from 2 to 8 m deep, and about 10 miners are active during the cool season.

The demantoid crystals are hosted by regionally metamorphosed asbestiform rocks. The garnets range from yellowish green to dark "emerald" green, and faceted stones are known up to 7 ct, although they typically weigh about 0.7 ct. Round nodules up to three grams, mostly in dark green and orangy yellow, have also been found, as well as large, well-crystallized translucent specimens on the order of 5 cm in diameter. Approximately 20 kg of rough was extracted during the 2003–2004 season. Of this, 1.5 kg was facet-quality, with about 200 grams yielding stones of more than 2 ct in good color and clarity.

Editor's note: Interested contributors should send information and illustrations to Brendan Laurs at blaurs@gia.edu (e-mail), 760-603-4595 (fax), or GIA, 5345 Armada Drive, Carlsbad, CA 92008. Original photos will be returned after consideration or publication.

GEMS & GEMOLOGY, Vol. 40, No. 1, pp. 66–86
© 2004 Gemological Institute of America

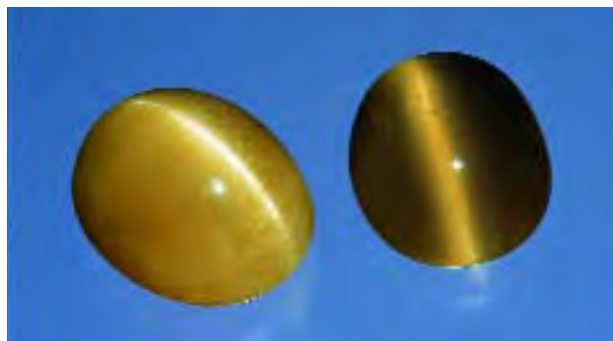


Figure 2. These brownish yellow cat's-eye beryls from Brazil have sharp "eyes" and range from translucent (left, 15.17 ct) to semitransparent (right, 11.47 ct). Courtesy of Maui Gems; photo by Maha Tannous.

Chatoyant demantoid from this area was first encountered by one of these contributors (MD) in November 2003. Approximately 35 grams of crystals and crystal fragments were collected, some of which were polished into cabochons of 5–10 ct (figure 4). A few chatoyant demantoid crystals also were noted, such as the 41.73 ct specimen in figure 4. The chatoyancy is caused mainly by

Figure 3. Demantoid garnets from Iran have been mined in shallow workings such as this tunnel, which Makhmout Douman visited in November 2003. Although this tunnel proved uneconomic, other workings on nearby hills have yielded significant quantities of the garnets. Photo by R. Sadeghi.

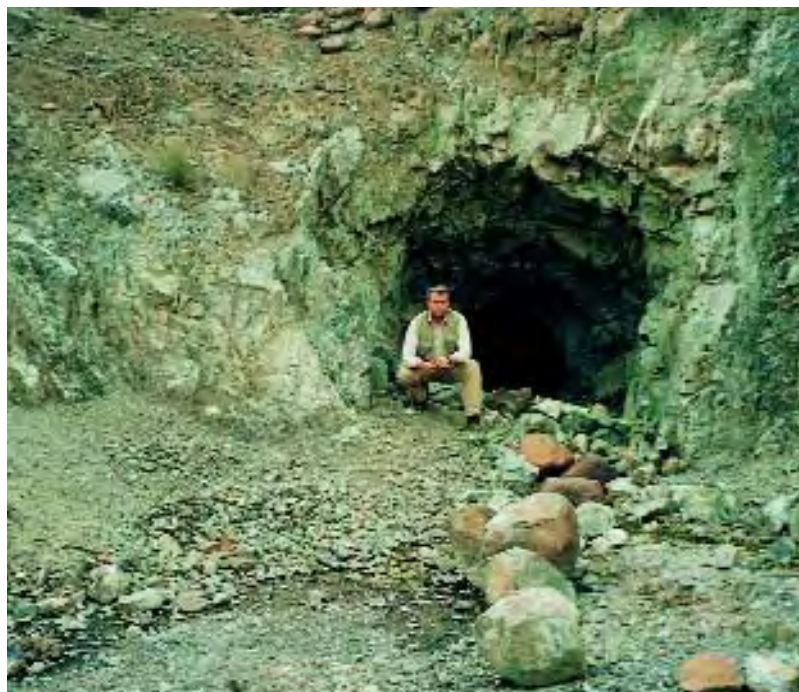




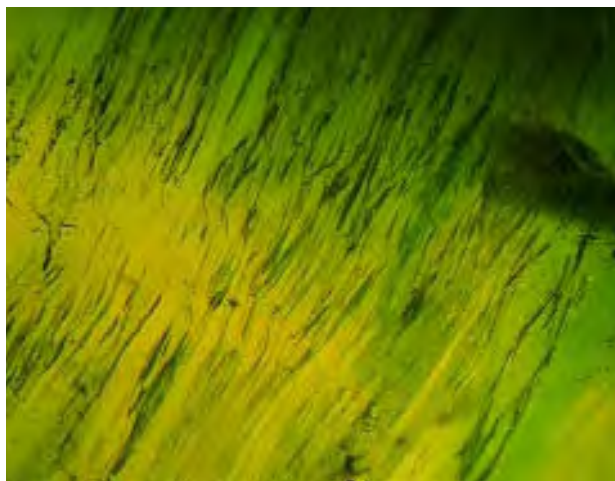
Figure 4. Some of the Iranian demantoids are chatoyant, such as the 7.06 and 5.00 ct examples shown here. The 41.73 ct composite crystal also contains the chatoyancy-causing fibers. Photo © GIA and Jeff Scovil.

concentrations of parallel fibers (figure 5) that are, based on their appearance, possibly chrysotile or byssolite.

Makhmout Douman (makhmout@arzawa.com)
Arzawa Mineralogical Inc., New York

Dona Dirlam
Liddicoat Gemological Library, GIA, Carlsbad

Figure 5. Parallel to semi-parallel fibers (possibly chrysotile or byssolite), together with associated oriented micro-cracks, are responsible for the chatoyancy seen in some of the demantoid garnets from Iran. Photograph by John I. Koivula; magnified 20×.



Blue omphacite from Guatemala. A small number of rough and polished specimens of a new dark blue omphacite “jade” were displayed by Ventana Mining Co. (Los Altos, California) at the Pueblo Inn and by Leher Designs (San Rafael, California) at the GJX show and at the Westward Look Resort. Ideally $(Ca,Na)(Mg,Al)Si_2O_6$, omphacite is a member of the pyroxene group, and is composed of a solid solution of jadeite and calcic clinopyroxene (e.g., diopside) with subordinate aegirine.

The material was first recovered by one of these contributors (WRR) in June 2003, and so far it has been found in a relatively restricted part of a claim held by Ventana Mining Co. The deposit is located in the Quebrada Seca area, near Carrizal Grande in Jalapa Department, Guatemala. (For information on recent jadeite discoveries in this area, see the Winter 2002 Gem News International, pp. 352–353.) The blue omphacite occurs as fine veins that cross-cut large alluvial boulders of greenish blue jadeite that were situated near outcrops consisting of blueschist, eclogite, and jadeite. Because the veins are rather narrow (i.e., from 2 to 20 mm thick), the material lends itself to small cabochons and carvings.

Three of the four oval cabochons shown in figure 6 were loaned to GIA for examination, and the following properties were determined by one of us (EPQ): color—mottled grayish greenish blue to mottled dark grayish greenish blue; diaphaneity—translucent; R.I.—spot readings of 1.67 to 1.68; S.G.—3.33–3.41 (measured hydrostatically); no Chelsea filter reaction; fluorescence—inert to long- and short-wave UV radiation; and no absorption features were observed with the desk-model spectroscope. Microscopic examination revealed that the stones had an aggregate structure with a mottled granular texture, irregular fractures, and nondescript white globular masses. In one of the cabochons, small transparent near-colorless crystals were observed. FTIR spectroscopy did not detect any polymer impregnation. Although not identified in these particular cabochons, the blue omphacite from Guatemala has been reported to contain minor amounts of phengite and sphene, and traces of zircon, monazite, allanite, and rutile (G. E. Harlow, “Blue omphacite in jadeitites from Guatemala and Japan: Crystal chemistry and color origin,” Geological Society of America Annual Meeting, Seattle, Washington, November 2–5, 2003, http://gsa.confex.com/gsa/2003AM/finalprogram/abstract_65497.htm).

Electron-microprobe analyses of a fourth blue cabochon by one of us (GEH) revealed that it was composed predominantly of omphacite. Backscattered-electron imagery of the cabochon and of another blue vein sample (figure 7) showed strong compositional zoning within the individual omphacite grains. Expressed in terms of jadeite and diopside components, the average composition of the omphacite in the cabochon was $Jd_{55}Di_{39}$ (range $Jd_{30-87}Di_{9-62}$; see figure 8). The compositional range of another sample of the same type of blue omphacite was $Jd_{38-77}Di_{22-47}$. In both cases, small amounts of hedenbergite



Figure 6. These cabochons (approximately 0.35 ct each) of blue omphacite show the distinctive color of this new material from Guatemala. Courtesy of Ventana Mining Co.; photo © Lee-Carraher Photography, San Francisco, California.

and aegirine components also were present. In the cabochon, total iron (reported as FeO) averaged 1.23 wt.%, with a range of 0.4–1.9 wt.%; titanium averaged 0.29 wt.% TiO_2 , with a range of 0.03–1.5 wt.%.

Vis-NIR spectroscopy of another sample of the blue omphacite by one of these contributors (GRR) showed a transmission window in the visible region centered near

Figure 7. This backscattered-electron image is of a vein of blue omphacite cutting greenish blue jadeite. The omphacite is visible as the lighter area in the center, whereas the surrounding jadeite appears much darker. The minute bright spots are zircon grains, and the black spots are quartz. Note the compositional zonation shown by individual pyroxene grains of the omphacite; the lighter areas correspond to more Fe, and the darker areas have more Ti.

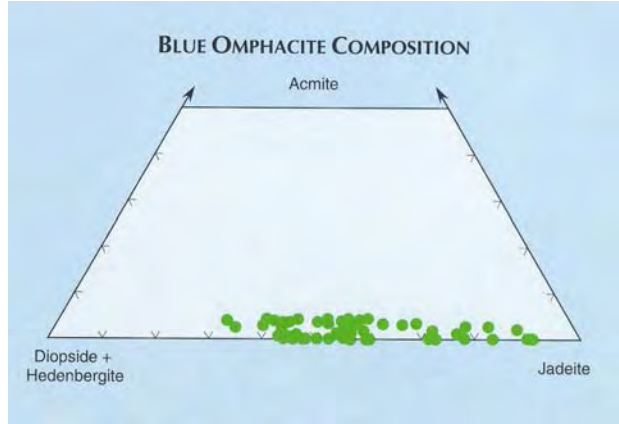
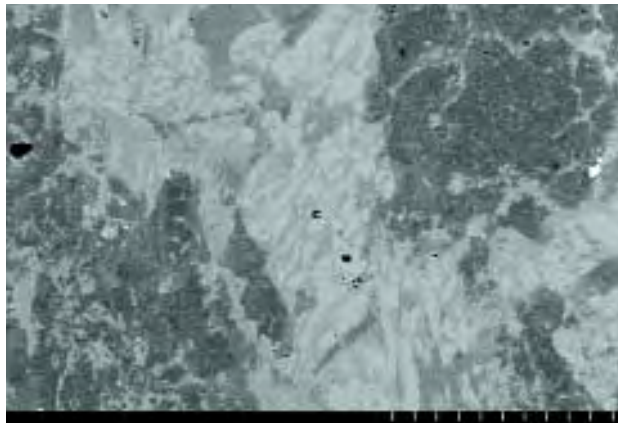


Figure 8. The blue omphacite was composed of strongly zoned grains of the jadeite-diopside series, as revealed by electron microprobe analysis.

500 nm (figure 9). This feature was defined by a sharp absorption band at 438 nm—superimposed on a tail that rises in intensity toward shorter wavelengths—and a broader band system that reaches its maximum at about 712 nm. The 438 nm feature arises from Fe^{3+} , and the broad band system correlates to the interaction of Fe^{2+} and Fe^{3+} . The broad features at longer wavelengths arise from Fe^{2+} . In contrast, a sample of green jadeite from Guatemala showed absorption bands due to Cr^{3+} that define the transmission window near 530 nm (again, see figure 9). The absorption was modified by features from both Fe^{3+} (sharp feature at 438 nm) and broader features below 900 nm from Fe^{2+} .

The absorption spectra show that the color of the green jadeite is due primarily to Cr^{3+} , whereas the blue omphacite is colored by iron—at least in part. Since the depth of the

Figure 9. These Vis-NIR absorption spectra show that the blue omphacite is dominated by iron-related features, whereas the green Guatemalan jadeite has absorptions related to chromium and subordinate iron.

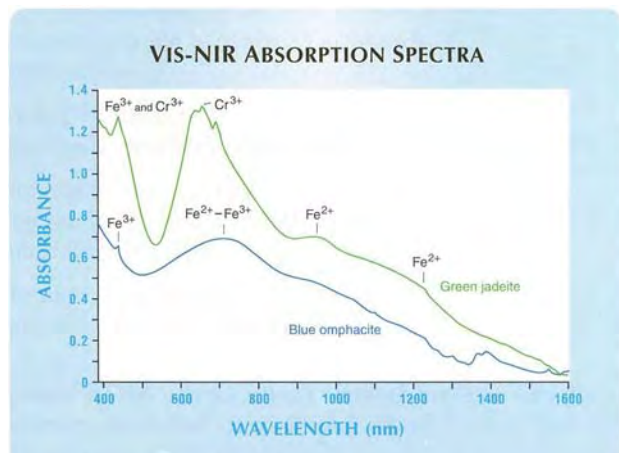




Figure 10. These cultured pearls (8.5–9 mm in diameter) were selected to show the range of color commercially available from southern Japan. Note how the colors of some of the cultured pearls resemble those seen in the shell of the *P. margaritifera* oyster in which they are cultured. Cultured pearls courtesy of A&Z Pearls, and shell donated by A&Z Pearls and Tasaki Shinju Co. (GIA Collection no. 30484); photo by Maha Tannous.

blue color showed a direct relation to titanium content in the samples analyzed, it appears that Ti^{4+} may also play a role in the coloration. The exact cause of the unusual blue color in this omphacite will remain unknown until further work is done to characterize the absorption features.

Although blue omphacite also has been found in Japan and Canada (Harlow, 2003), this new Guatemalan omphacite represents the first occurrence of gem-quality material.

George E. Harlow (gharlow@amnh.org)
American Museum of Natural History
New York

Elizabeth P. Quinn
GIA Gem Laboratory, Carlsbad

George R. Rossman
California Institute of Technology
Pasadena, California

William R. Rohtert
Hermosa Beach, California

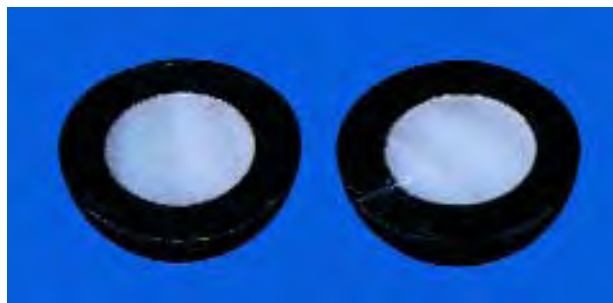
Black cultured pearls from Japan. At the AGTA show, Avi Raz of A&Z Pearls, Los Angeles, had some recently harvested black cultured pearls from the southernmost

region of Japan. They were cultured in *Pinctada margaritifera* oysters at farms owned by Tasaki Shinju Co. in the Oshima Straits, at Ikomo Bay, and at Yakiuchi Bay of the Amami Oshima Islands. The oysters are smaller than those from French Polynesia, as the Amami Oshima islands are at the northernmost habitat limit for this species (where colder waters slow the oysters' growth and metabolism).

According to Shodai Tasaki of Tasaki Shinju Co., the hatchery-bred oysters are nucleated at three to four years of age with small beads (i.e., 4.5–6.0 mm in diameter). Harvesting takes place after two to three years, in September–October. The cultured pearls are reportedly produced in a variety of colors, such as “peacock,” gray, “silver,” “gold,” and reddish purple, in sizes ranging from 6 to 14 mm, with 7–8 mm being the most common. According to Japanese researchers, the relatively cold water results in a finer surface texture and superior luster, similar to Akoya cultured pearls. The first commercial harvest occurred in 1993; however, annual production is still less than 20,000 cultured pearls and a similar-sized crop is expected in September–October 2004. Due to their small size and high production cost, quantities of these black cultured pearls will likely remain limited.

Mr. Raz loaned GIA 14 of the cultured pearls (8.5–9 mm in diameter; see, e.g., figure 10). These samples were near-round to round, and one had been cut in half. The colors included light greenish yellow and light gray to dark gray, with overtones varying from weak to moderate reddish purple and green. Such variations in overtone and color are typical of black cultured pearls from French Polynesia, and resemble those seen in shells from the host *P. margaritifera* oyster (again, see figure 10). The nacre thickness of the sliced sample averaged 1.5 mm (figure 11), with very slight variations. X-radiography of the other cultured pearls showed similar nacre thickness. UV-Vis reflectance spectra of these samples exhibited an absorption feature at 700 nm, which is characteristic of the *P. margaritifera* oyster. Other sig-

Figure 11. The nacre thickness of this sliced black cultured pearl from Japan averaged 1.5 mm. Courtesy of A&Z Pearls; photo by Maha Tannous.



nificant absorptions occurred at 405 and 495 nm. Fluorescence to long-wave UV radiation was also typical of this species, with the darker samples exhibiting a reddish brown luminescence.

Shane Elen (selen@gia.edu)
GIA Research, Carlsbad

New ruby production from Malawi. At the AGTA show, Columbia Gem House of Vancouver, Washington, had some recently produced untreated rubies and pinkish orange sapphires from Chimwadzulu Hill, Malawi. The deposit is located about 150 km southeast of the capital, Lilongwe, and only 5 km from the Mozambique border. Chimwadzulu Hill consists primarily of a metamorphosed ultramafic intrusive complex exposed over an area of about 1 km², and is surrounded by various Precambrian metasedimentary rocks. The corundum is found in deeply weathered iron-rich soil and is easily liberated by standard washing processes. Because of the long winter rainy season, the mining period lasts from April to October. The mine was closed during the late 1980s and early 1990s before being reopened in 1994 by a U.K. company (for more on the history and geology of this mine, see Spring 2000 Gem News, pp. 71–73). Since the beginning of 2003, systematic prospecting and an expansion in mining have significantly improved the quality and quantity of the production.

According to Eric Braunwart, president of Columbia Gem House, there are approximately 70 people working at the mine. They have been producing up to 1 kg of cuttable ruby rough per month, yielding mostly small, calibrated gemstones up to ³/₄ ct. There are a significant number of fine stones from 1 to 3 ct, but those above 3 ct are rare. The largest faceted ruby known from the deposit was a 16 ct pinkish red heart-shaped gem. Since most of the material being mined has no obvious rutile inclusions and is attractively colored, heat treatment is not necessary.

Unlike earlier mining efforts, no facet-grade blue sapphire has been recovered so far. Mr. Braunwart estimates that the mine will yield approximately 5 kg of cuttable rough per month of ruby and pinkish orange sapphire once a new processing plant, currently under construction, is built. He also predicts that almost half of the pinkish orange gems will grade “padparadscha” without the need for heat treatment.

This contributor examined three of the rubies (1.50–3.78 ct; figure 12). Selected to show the range of colors available, they were pinkish red, slightly orangy red, and purplish red, with obvious red to orangy red pleochroism. All contained boehmite along twinning planes, a typical inclusion scene in East African rubies. Microscopic examination also revealed short rutile needles and platelets in the largest stone. The refractive indices (1.762–1.770) obtained from the three samples were also comparable to the properties reported in the literature for these rubies (see, e.g., U. Henn et al., “Red and orange corundum [ruby and padparadscha] from Malawi,” *Journal of Gemmology*, Vol. 22, No. 2, 1990, pp. 83–89).



Figure 12. These untreated rubies (1.50–3.78 ct) were recently mined from the Chimwadzulu Hill deposit in Malawi. Courtesy of Columbia Gem House; photo by Maha Tannous.

Columbia Gem House and its jewelry-manufacturing subsidiary are marketing this untreated material as “Nyala ruby,” after the rare Nyala antelope that is native to the game reserve close to the mine. This product is being sold under the company’s “Fair Trade Gems” initiative, which was launched at this year’s Tucson gem show. This program supports a clean environment, employee-friendly policies, and complete product integrity from mine to market. The strict chain of custody also ensures non-treatment designations where appropriate, and eliminates the possible introduction of undisclosed treated gems or synthetics into the supply chain. To the benefit of locals in the Chimwadzulu Hill area, the company has built a school and is providing medical insurance for all mine personnel.

Edward Boehm (joebgem@aol.com)
JOEB Enterprises, Solana Beach, California

Pink to pink-orange spinel from Tanzania. At the GJX show, Menahem Sevdermish of Advanced Quality, Ramat Gan, Israel, had some attractive spinel from a new find in the Mahenge region of south-central Tanzania. His stock consisted of about 2,000 carats of faceted stones (ranging up to 3 ct) and 1 kg of rough. According to Mr. Sevdermish, the new spinel discovery occurred in August 2003, although ruby and pink-to-red spinel have been mined from this area for several years (see Summer 1993 Gem News, pp. 136–137). Several kilograms of rough spinel were recovered, ranging from pink to pink-orange to brownish red. Most notable are the pink-orange stones, with a color similar to that of some “padparadscha” sapphires. He also indicated that the material is mined from alluvial and eluvial deposits, and is not heated or subjected to any other forms of treatment. The rough typically consists of small octahedra or broken fragments that weigh 0.1–2 grams; less than 30% is facetable, and the remainder is bead- or cabochon-quality, in Mr. Sevdermish’s experience.

Some of the rough has made its way to Asian markets. According to Scott Davies of American-Thai Trading (Bangkok), some dealers in Bangkok have been marketing



Figure 13. These spinels (0.68–2.28 ct) show the range of color of the new material being mined in the Mahenge region of Tanzania. Courtesy of Advanced Quality; photo by Maha Tannous.

the faceted orange-pink stones as spinel from Vietnam's Luc Yen region. Mr. Davies reported that the largest stone he has cut weighed 3.39 ct, and that stones containing eye-visible inclusions can make attractive rose cuts.

Mr. Sevdemish loaned GIA six Mahenge spinels (0.68–2.28 ct) that were representative of the range of color for this material: purplish pink, pink, orangy pink, red-orange, and orangy red (figure 13). Gemological properties obtained by one of us (EPQ) showed refractive indices ranging from 1.710 to 1.712 and (hydrostatic) specific gravity values of 3.60–3.63. There was no birefringence or pleochroism, as expected for a singly refractive gem material, but all samples displayed weak anomalous double refraction when viewed between crossed polarizing filters. Long-wave UV radiation produced a red fluorescence, which ranged from weak to moderately strong for the various samples. With short-wave UV radiation, the orangy red to red-orange spinels were inert, but the three pink stones fluoresced very weak to weak orangy red. When examined with a desk-model spectroscope, all samples showed several absorption lines in the red region (typical of Cr³⁺) and a weak band from 520 to 590 nm. Microscopic examination revealed that all of the spinels contained stringers of particles, three of them had clouds throughout, two had fractures, and one had a "fingerprint." The stones did not exhibit any transmission luminescence, as has been documented previously for pink Tanzanian spinel (see the Summer 1990 Lab Notes, pp. 156–157).

The properties of these stones are generally consistent with those listed for spinel by R. Webster (*Gems*, 5th ed., revised by P. Read, Butterworth-Heinemann, Oxford, England, 1994, pp. 142–145), although the R.I.'s recorded for these stones are just slightly lower.

Elizabeth P. Quinn (equinn@gia.edu)
GIA Gem Laboratory, Carlsbad
BML

Large tsavorite and green grossular from Tanzania. At the GLDA show in the Radisson Hotel, Axel Henn of Idar-Oberstein, Germany, had several large examples of tsavorite and green grossular from the tanzanite deposit in Merelani, Tanzania. According to Mark and Eric Saul of Swala Gem Traders, Arusha, Tanzania, the garnets were recovered in three "pockets" from December 2002 to February 2003. About 2.5 kg of rough tsavorite and green grossular were recovered as well-formed crystals (figure 14) and fragments. Many of the stones were relatively clean and of large size. The smaller stones were typically light green, while the larger ones were a vivid green. Where present, eye-visible inclusions consisted of "fingerprints" (mostly in smaller rough) and mineral inclusions (probably pyrite; in the larger pieces).

The Sauls also reported that most of the production was purchased by only a few parties, with the majority sold in Idar-Oberstein and the remainder in Bangkok. In addition to one 100+ ct, one 50+ ct, and four 20+ ct faceted stones, they also cut and sold a half-dozen examples in the 20–55 ct range and at least 10 weighing 10–20 ct. A few cabochons weighing 50–100 ct also were cut.

Most of the rough purchased by Mr. Henn was faceted in August–November 2003. The largest tsavorite he had in Tucson weighed 72 ct, although even larger ones have been faceted by his firm (e.g., 88 and 144 ct).

Mr. Henn arranged for one of us (WMM) to examine an

Figure 14. Fine crystals of tsavorite and green grossular were recovered from Merelani, Tanzania, from late 2002 to February 2003. This specimen measures approximately 1.5 cm in diameter. From the collection of F. Lietard; photo © Jeff Scovil.



88.03 ct tsavorite at the East Coast laboratory. This oval modified brilliant was a strongly saturated yellowish green (figure 15). The refractive index was 1.731 and specific gravity was 3.60. No absorption features were visible with the desk-model spectroscope. Observation with the polariscope revealed anomalous double reaction, which is not uncommon in garnets. With magnification (up to 60×), the stone showed only some subtle straight, angular growth zoning. Although the R.I. value was within the accepted range for grossular—albeit slightly lower than the range given by R. Webster (*Gems*, 5th ed., p. 202) for material from East Africa—it was in a range that could overlap, in rare instances, with natural spinel. The green color was not at all typical for natural spinel with this R.I., but combined with the stone's unusually large size and lack of inclusions, we performed Raman analysis to further confirm the stone's identity as grossular.

One particularly interesting aspect of this tsavorite was its UV fluorescence. Although the moderate orange long-wave UV fluorescence was not uncommon, when exposed to short-wave UV radiation the stone fluoresced a weak greenish yellow with straight, angular zones of weak-moderate orange, some of which corresponded to the growth zoning seen with the microscope. Even more unusual were two concentrically zoned "spots" of fluorescence. The stronger of these is shown in figure 16. Closer observation of this area with the De Beers DiamondView instrument (see figure 16, inset) revealed that the "spot" was not actually round, but was characterized by angular zones that corresponded to the growth zoning and the orange short-wave fluorescence.

Coincidentally, in August 2003 *Gems & Gemology* was informed about similar unusual fluorescence characteristics in Tanzanian tsavorite by Kaushal P. Mehta, who is a laboratory gemologist in Bangkok. He reported that a 65.72 ct sample fluoresced moderate orange to long-wave and moderate yellow to short-wave UV radiation. EDXRF spectroscopy yielded a composition that was typical for tsavorite. Mr. Mehta subsequently learned that tsavorite from the recent Tanzanian production commonly shows this unusual fluorescence.

Wendi M. Mayerson (wmayerson@gia.edu)
GIA Gem Trade Laboratory, Carlsbad

BML

SYNTHETICS AND SIMULANTS

Color-change glass, imitating alexandrite. At the G&LW show at the Holidome, House of Williams of Loveland, Colorado, had numerous faceted pieces of color-change glass. According to Michael Williams, this alexandrite imitation has been around for several years, and was trademarked as "Zandrite" about three years ago. Although the material is not new, the lack of published technical information prompted this report.

This contributor acquired a transparent 4.45 ct modi-

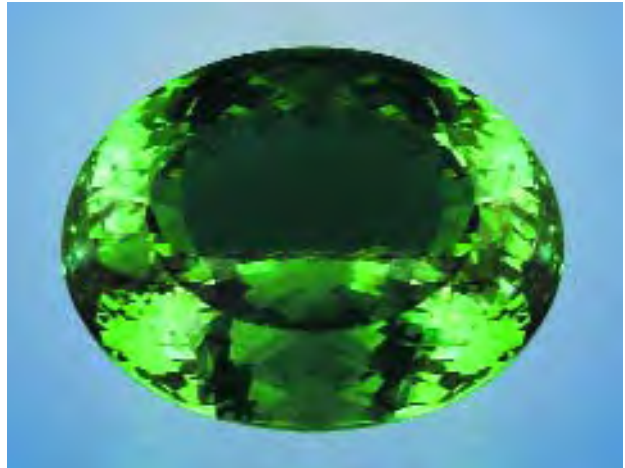
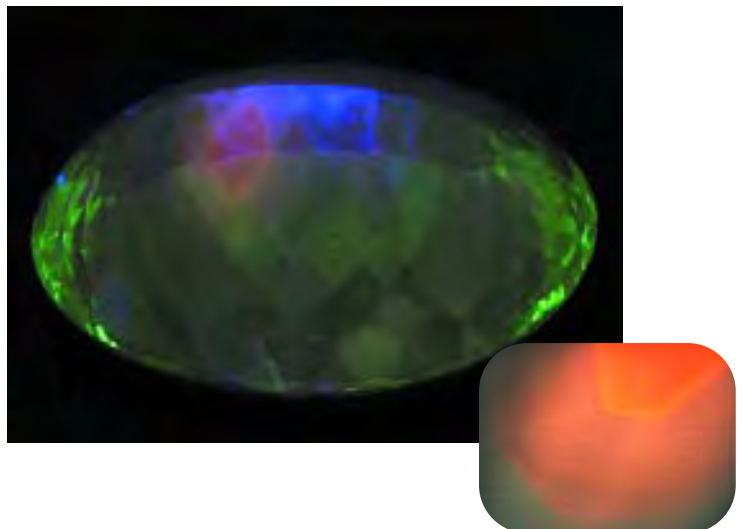


Figure 15. This 88.03 ct tsavorite provides a fine example of the notable size and transparency of the new material from Merelani. Courtesy of Henn GmbH; photo by Elizabeth Schrader.

fied oval brilliant that had an attractive (almost pastel) color change. In sunlight and daylight-equivalent light sources, it was slightly bluish green (figure 17, left); in incandescent light, it was purplish pink (figure 17, right). The R.I. was 1.521, and the S.G. (taken hydrostatically) was 2.66. The sample displayed no birefringence or pleochroism, as expected of an amorphous material, although it did display weak anomalous double refraction. There was no reaction to the Chelsea filter, but the sample fluoresced very weak bluish green to long-wave UV

Figure 16. Unusual fluorescence behavior was shown by the 88.03 ct tsavorite, as evident here in short-wave UV radiation. When viewed in the De Beers DiamondView instrument, the fluorescent "spot" was seen to consist of angular zones (see inset). These patches corresponded to the growth zoning and the orange short-wave UV fluorescence of this feature. Photos by Elizabeth Schrader.



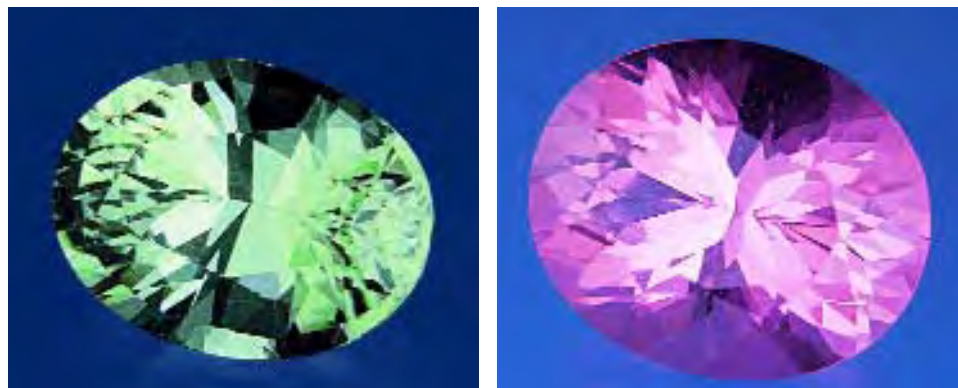
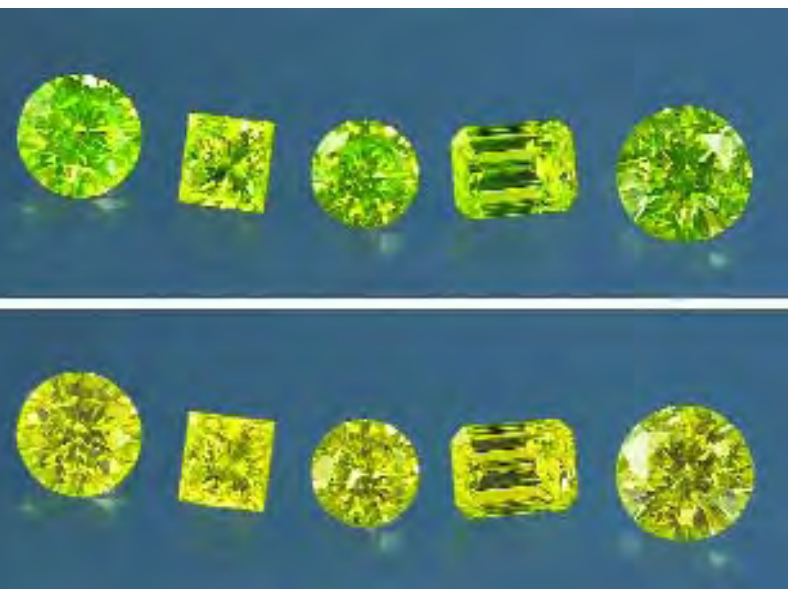


Figure 17. This 4.45 ct oval modified brilliant is color-change glass. In daylight-equivalent fluorescent light, the sample is a slightly bluish green (left). With incandescent light, the color changes to an attractive purplish pink (right). Photos by Maha Tannous.

radiation (and was inert to short-wave UV). The material had a rare-earth spectrum, visible with the desk-model spectroscope, that consisted of strong absorption lines and bands at 435, 440–450, 465, 476, 480, 483, 510, 520–535, 560–595, 600, and 660 nm, with weak lines at 500, 550, and 610 nm. EDXRF spectroscopy performed by senior research associate Sam Muhlmeister found Si, Na, K, Ca, Zn, and Nd. This composition, together with the visible spectrum, indicates that Nd is responsible for the coloration; this is consistent with information that was subsequently provided by Mr. Williams.

Elizabeth P. Quinn

Figure 18. Commercial production of highly saturated green-yellow diamonds is being done with HPHT treatment, specifically to show a change in color appearance in different light sources. Due to strong green fluorescence from the H3 center, these diamonds (here, 0.50–1.16 ct) appear greener in daylight-equivalent fluorescent light (top) than in incandescent light (bottom). Courtesy of Lucent Diamonds; photos by Elizabeth Schrader.



TREATMENTS

Commercial production of HPHT-treated diamonds showing a color shift. More than half a dozen mechanisms are known to cause a green hue in naturally colored diamonds. These include irradiation, H₂- and hydrogen-related absorption, and chameleon behavior. However, “chartreuse,” or green-transmitter, diamonds are very different in terms of color origin, as their green color results not from a selective absorption, but from fluorescence that is related to the H₃ defect (zero-phonon line at 503 nm). The H₃ system absorbs blue and violet light and emits green light that is slightly lower in energy. These diamonds, which appear predominantly yellow in incandescent light, can emit such strong green light in fluorescent or natural lighting conditions that in some cases this green transmission dominates the color of the diamond. I. Reinitz and T. Moses (Summer 1997 Lab Notes, p. 136) pointed out that highly saturated combinations of yellow and luminescent green are quite rare in natural-color diamonds. A historical example is an intense greenish yellow 2.15 ct diamond that reportedly once belonged to Pedro II, the emperor of Brazil during the mid-19th century (see Spring 1997 Lab Notes, pp. 54–55).

However, while rare in natural-color diamonds, this color-causing mechanism can routinely be produced in the laboratory by annealing certain brown diamonds at high pressure and high temperature (I. M. Reinitz et al., “Identification of HPHT-treated yellow to green diamonds,” Summer 2000 *Gems & Gemology*, pp. 128–137). At the 2004 Tucson gem show, Alex Grizenko of Lucent Diamonds, Lakewood, Colorado, informed these contributors that his company has started commercial production of green-transmitter HPHT-treated diamonds, at approximately 500 carats per month, to showcase the different hues these diamonds display in different lighting conditions (figure 18). They range from less than 1 ct to over 8 ct. Both rough and faceted diamonds from Australia and Russia are being annealed to 2,100–2,500°C at elevated pressures.

Spectroscopic analysis of 12 faceted samples (0.50–1.36 ct) supplied by Mr. Grizenko revealed properties similar to those reported by Reinitz et al. (2000); all were type IaA/B and showed widely different amounts of nitrogen. A very strong H₃ center and a relatively weak H₂ were detected in all tested samples.

As the green color component is due to fluorescence of the H3 system, which absorbs blue and violet light, it follows that the intensity of the green color varies according to the light source. Thus, these stones appear greener in natural daylight or blue-rich daylight-equivalent fluorescent light (which also contains some ultraviolet content) than in standard incandescent or spot lighting (figure 18). The strength of the color shift varied significantly from sample to sample, as shown in the diamonds selected for figure 18. This variation in color appearance is very different from the well-known alexandrite effect, which is caused by selective absorption.

Many factors in a diamond can affect H3 fluorescence. While the concentration of this defect largely determines the intensity of fluorescence, A-aggregates of nitrogen can significantly quench luminescence from H3 and N3 centers, which may help explain the varying intensity of the green component from one HPHT-treated diamond to another. Nevertheless, this process makes what is a difficult-to-obtain color—and color shift—in untreated natural diamonds available in a range of sizes and qualities in treated stones.

*Wuyi Wang (wuyi.wang@gia.edu) and Tom Moses
GIA Gem Laboratory, New York*

CONFERENCE REPORT

Accredited Gemologists Association conference. About 100 people attended the AGA conference on synthetic diamonds, held February 4 at the Marriott University Park hotel in Tucson.

Tom Chatham of Chatham Created Gems, San Francisco, said that synthetic diamond production of all types (mostly industrial) totals about 600 million carats per year, but in general it is still cheaper to mine gem-quality diamonds than produce them synthetically. He told the audience that Chatham is working with an Asian manufacturer to produce about 400 carats monthly in four colors: pink, yellow, blue, and green. Most of the faceted goods weigh approximately 1 ct, although some are up to 1.5 ct. Colorless synthetic diamonds are still too expensive to produce profitably, he said.

Dr. Robert Linares of Apollo Diamond Co., Boston, outlined the production of synthetic diamonds by chemical vapor deposition, and stressed that both the jewelry and high-technology industries require diamond of high purity and large size. Apollo will be expanding production by adding new equipment that can quadruple output. CVD

synthetic diamond, he said, is identical to natural diamond in structure. "It has the same four C's, though CVD [synthetic] diamond is often clearer and harder."

Carlos Valeiras of Gemesis Corp., Sarasota, Florida, told the audience that his company has taken the BARS process of producing synthetic diamonds by HPHT "to the next level," resulting in high quality and attractive color. He said that it takes 80–100 hours to grow 1 ct crystals and that the process is very difficult, "so it is unlikely there will be many producers coming into the market." He announced that Gemesis was ready to expand its production to commercial quantities—the majority being equivalent to Fancy Intense yellow and Fancy Vivid orange, and faceted into princess and Asscher cuts. All of their synthetic diamonds over 0.25 ct will be laser inscribed; those over 1.0 ct will carry EGL grading reports.

Alex Grizenko of Lucent Diamonds, Lakewood, Colorado, predicted that the future diamond market will consist of three segments: mined diamonds, synthetic diamonds, and "restored" (treated) diamonds. He said that his company produces a variety of colors including reds, which are subjected to beta (electron) radiation and HPHT annealing. Lucent also has a partnership with LifeGem (Elk Grove, Illinois), which creates synthetic diamonds from human remains (see Spring 2003 Gem News International, p. 62). "This is certainly a specialty product, but one with great potential," he said.

Shane McClure of the GIA Gem Laboratory, Carlsbad, explained a number of common identification techniques for synthetic diamonds, including distinctive color zoning, metallic (flux) inclusions, and UV fluorescence patterns. **Dr. Henry Hänni** of the SSEF Swiss Gemmological Institute, Basel, noted that most synthetic diamonds are type Ib, though a small minority are type IIb, which are much more difficult to detect. They do, however, display the same growth patterns in the De Beers DiamondView instrument as are shown by type Ib synthetics. **Branko Deljanin** of EGL USA, Vancouver, Canada, reported that CVD synthetic diamonds can often be identified by weak yellow fluorescence to long-wave UV radiation and moderate to strong yellow-green fluorescence to short-wave UV. He added that they can also show a characteristic Raman photoluminescence peak at 575 nm, but for CVD material that has been subjected to HPHT annealing to remove brown color, a 637 nm peak can be diagnostic.

*Russell Shor (russell.shor@gia.edu)
GIA, Carlsbad*

GNI Regular Features

DIAMONDS

Update on proprietary diamond cuts. An updated version of the chart of proprietary diamond cuts, which originally appeared in the Winter 2002 issue of *Gems & Gemology* (see T. W. Overton, "Legal protection for proprietary dia-

mond cuts," pp. 310–325), is now available in the *Gems & Gemology* Data Depository (www.gia.edu/pdfs/diamond_cuts.pdf). Following is a brief summary of recent developments in the legal protection of diamond cuts.

Consistent with other major changes in the diamond

market, the trends identified by Overton (2002) have accelerated in the last year. New branded cuts are being introduced every month (see, e.g., figure 19), and nearly all of them have been protected by trademark, patent, or both. Between January 2003 and January 2004, the U.S. Patent and Trademark Office (USPTO) issued 59 patents and published five applications for gemstone cuts (compared to 29 patents from January 2000 to January 2001); this represents a 127% increase in just three years.

The U.S. officially joined the Madrid Protocol (see Overton, 2002) in November 2002. This allows U.S. trademark holders to enjoy trademark protection in any member country by filing an international registration application with the USPTO or WIPO (World Intellectual Property Organization).

Beginning in January 2003, the European Community (EC) Office for Harmonization in the Internal Market began accepting design registrations (see Overton, 2002). This contributor is aware of a number of diamond cut designs that enjoy EC design protection (these are indicated on the updated chart). The maximum 25-year term of an EC design registration, compared to the 14-year term of a U.S. design patent, makes this a protection method that should not be overlooked despite its limited geographic reach.

There also may be protection available beyond that of traditional patent and trademark. At least one "mainstream" cut design, the Elara, is now protected by U.S. copyright registration (H. B. Rockman, "Obtaining U.S. copyright registration for the Elara square cut-cornered bril-

liant diamond," Fall 2003 *Gems & Gemology*, pp. 210-213). (Another design, the rather fanciful "Buddha" cut, also has copyright registration.) This should have manufacturers exploring copyright protection for their designs, given the much longer term of copyright (currently 95 years for works-for-hire versus 14 or 20 years for a patent) and the much simpler application procedure.

Last year also saw what this contributor believes to be the first lawsuit over a diamond cut patent. In August 2003, a U.S. federal court in Chicago held the design patent for the Elara cut, owned by Kuwayama Europe and Elara Diamond USA, unenforceable as a result of a dispute with another manufacturer, National Diamond Syndicate. This lawsuit has been discussed in more detail in various trade publications (see V. Gomelsky, "Elara diamond design patent invalidated by court," *National Jeweler*, Vol. 97, No. 18, 2003, pp. 28, 30; I. Solotaroff, "Brand name: Chicago," *Modern Jeweler*, Vol. 102, No. 11, 2003, pp. 42-44, 105-107).

Twenty-seven new cuts have been added to the chart. Of these, 20 are believed to be protected by patent (or pending applications), while an equal number have registered trademarks. Thirteen are protected by both trademark registration and patent, six have registered trademarks but no patents, and seven appear to have patents but unregistered trademarks.

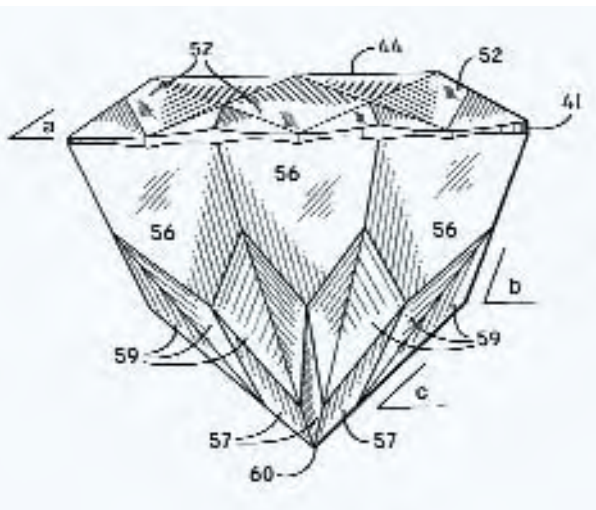
Although several cuts (which this contributor believes are obsolete) have been removed from the chart, and several more (which this contributor believes are basically the same cut) were condensed into single entries, the number of identified cuts on the chart rose from 81 to 101. A strong trend toward patent protection is now apparent: 64 of 101 are believed to be patented or patent pending. Somewhat less than half (42) enjoy both patent protection and trademark registration. (These numbers do not include the Elara, because of the court decision mentioned above.)

It is safe to say that patent protection is now the rule rather than the exception, and the benefits afforded by patent and trademark are an increasingly important element of diamond branding.

This contributor thanks the numerous diamond manufacturers who responded with information on their proprietary cuts.

*Thomas W. Overton (toverton@gia.edu)
GIA, Carlsbad*

Figure 19. The Solei cut, a modified round brilliant design created by Michael Schachter and Uri Peleg for Diamco of New York, was one of the new diamond cuts for which patents were issued in 2003. This drawing is taken from the patent application.



A diamond exhibiting a spectacular phantom. This contributor recently encountered a natural diamond exhibiting a spectacular phantom cloud of cuboid shape. The phantom was particularly visible when the 0.20 ct Fancy grayish greenish yellow diamond was viewed with dark-field illumination (figure 20). Phantom clouds are rarely seen in diamonds and are often indistinct, although some good examples were recorded by J. I. Koivula (*The Micro World of Diamonds*, Gemworld International, Northbrook, Illinois, 2000). While phantoms are frequently

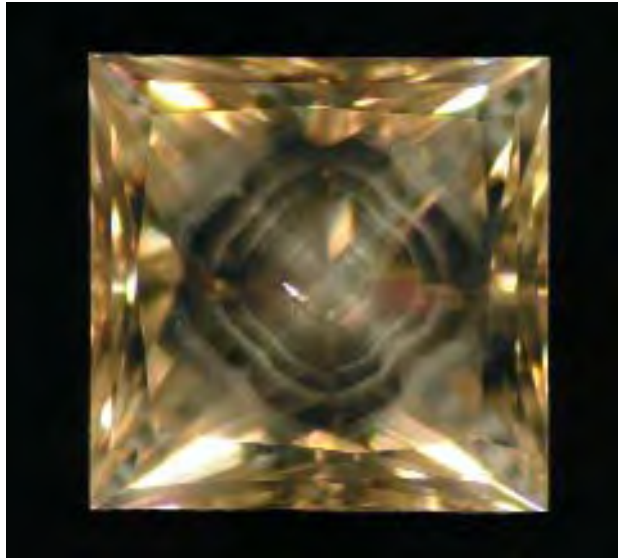


Figure 20. With darkfield illumination, this 0.20 ct diamond displays a most unusual phantom cloud. Photomicrograph by T. Hainschwang; magnified 20 \times .

associated with an elevated hydrogen content, this is not always the case, as rare type Ib diamonds with high nitrogen content may also exhibit such inclusions; some examples have been described by this contributor (T. Hainschwang, "Classification and color origin of brown diamonds," *Diplôme d'Université de Gemmologie*, University of Nantes, France, 2003).

Typically, these clouds exhibit a cuboid shape and are formed by very small particles of unknown nature. Depending on the viewing direction, such clouds may appear to have hexagonal symmetry (see, e.g., *Gem Trade Lab Notes*: Spring 1999, pp. 42–43, and Fall 2000, pp. 255–256). In the diamond described here, the cloud displayed numerous distinct layers with a cross-like feature in the center, forming an overall flower-like pattern. The cross-shaped parts of the cloud separate the octahedral sectors, whereas the "flower-petal" portions lie along dodeca-

hedral directions (see W. Wang and W. Mayerson, "Symmetrical clouds in diamond—The hydrogen connection," *Journal of Gemmology*, Vol. 28, No. 3, pp. 143–152). The diamond exhibited homogeneous strong chalky blue fluorescence to long-wave UV radiation and medium chalky greenish blue fluorescence (and weak yellow phosphorescence) to short-wave UV.

FTIR spectroscopy performed on a Perkin-Elmer Spectrum BXII spectrometer revealed that this diamond was a type IaA/B with high nitrogen and hydrogen contents, and was thus typical for a diamond with phantom inclusions. In addition to showing hydrogen-related features (see E. Fritsch and K. Scarratt, "Gemmological properties of type Ia diamonds with an unusually high hydrogen content," *Journal of Gemmology*, Vol. 23, No. 8, 1993, pp. 451–460), the spectrum included a triplet of peaks at 1546, 1518, and 1500 cm^{-1} ; in the experience of the author this triplet is frequently observed in hydrogen-rich diamonds and thus also may be associated with this impurity.

A Vis-NIR transmission spectrum was recorded using an SAS2000 spectrophotometer, with the stone immersed in liquid nitrogen. The low-temperature spectrum showed characteristic absorptions associated with high hydrogen and nitrogen contents, as well as nickel impurities (figure 21; see K. Iakoubovskii and G. J. Adriaenssens, "Optical characterization of natural Argyle diamonds," *Diamond and Related Materials*, Vol. 11, 2001, pp. 125–131). Some of the observed peaks (e.g., at 894 nm) have not yet been described in the literature.

This contributor has found that many "straw" yellow to "olive" yellow diamonds with such spectra exhibit a chameleon-like color change when heated to approximately 200°C ("Characterization of hydrogen rich diamonds from Argyle/Australia with Vis/NIR—and photoluminescence—spectroscopy," www.gemlab.net/research1_1.htm). However, the color change is unlike that seen in typical chameleon diamonds, as it is mainly characterized by increases in saturation and in the green color component.

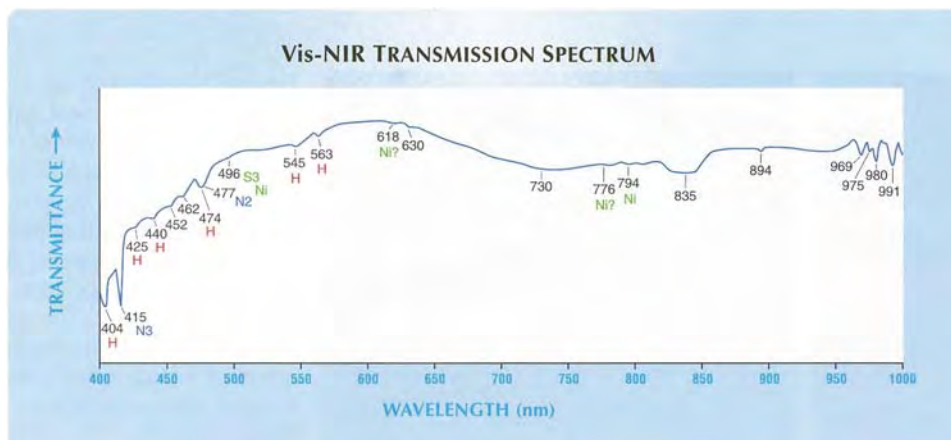


Figure 21. The low-temperature Vis-NIR transmission spectrum of the 0.20 ct diamond shows absorptions due to nitrogen (N3, N2), hydrogen, and nickel impurities.



Figure 22. This necklace of lustrous black beads proved to be black (horn) coral with a polymer coating. Photo by H. A. Hänni, © SSEF.

In this contributor's experience, typical chameleon diamonds show a more distinct change in color from "olive" to orangy yellow, and the Vis-NIR and FTIR spectra of such stones also are very different. Thus it appears that there are two different groups of diamonds exhibiting a chameleon effect—those with a more yellow stable color and those with an "olive" stable color.

Based on its properties, the 0.20 ct diamond described here could potentially show chameleon behavior (i.e., with the more yellow stable color). However, this diamond did not change color when heated on a hot plate. This was not surprising since only a small percentage of such hydrogen-rich "yellow" diamonds exhibit the chameleon behavior.

At first sight, this small diamond appeared to be just a commercial "olive" yellow diamond, but the microscope revealed an amazing internal treasure.

*Thomas Hainschwang (gemlab@adon.li)
Gemlab Gemological Laboratory
Vaduz, Principality of Liechtenstein*

COLORED STONES AND ORGANIC MATERIALS

Black horn coral coated with artificial resin. A client recently submitted a black bead necklace to the SSEF Swiss Gemmological Institute for identification. He had purchased a number of these necklaces from a Chinese supplier, who represented them as black coral. He became concerned when testing by another lab indicated the material was plastic.

The necklace contained 27 beads that measured 14 mm in diameter (figure 22). The specific gravity (determined hydrostatically on one bead) was 1.325, and the R.I. was approximately 1.56. Both of these values are consistent with those expected for black coral.

Black coral (also called horn coral) typically shows characteristic curved growth lines and concentric cracks that are oriented parallel to the long axis of the branches. These features were not present in the beads of the necklace. However, scattered reddish brown reflections were apparent, as is typical for black coral, and linear arrays of tiny holes or spots were seen on some of the spheres. A dark gray surface color was seen with strong fiber-optic light, and minute bubbles were found sporadically. It became clear that instrumental analysis would be necessary for a proper identification.

EDXRF spectroscopy of a few of the beads revealed characteristic elements for black coral: chlorine, bromine, and iodine. A Fourier-transform infrared spectrum of one of the beads was compared to a reference spectrum of black coral, and the peaks showed a full agreement. However, a Raman spectrum from the surface of one of the beads showed a 1605 cm^{-1} peak, indicating the presence of a polymer.

We informed the client of our identification of the beads as black horn coral coated with an artificial substance, and asked for permission to cut one of the beads in half. In cross-section, we could see the extent and result of the treatment (figure 23). A coating consisting of several very thin layers covered the surface of the beads. Fissures and cracks were sealed by the artificial resinous

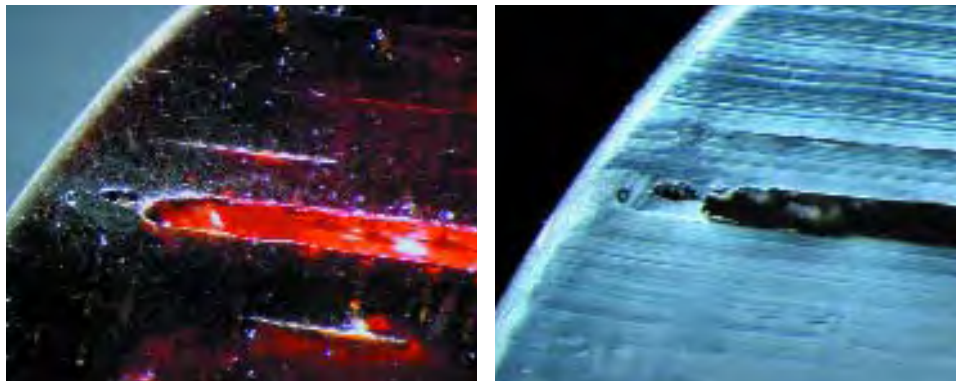


Figure 23. In these cross-sections of a black coral bead, the outer portion of one of the characteristic cracks is filled by a polymer; note the trapped bubbles. In transmitted light (left), the polymer appears gray along the thin surface layer. In reflected light (right), the polymer and bubbles are even more apparent. Width of both photos is 3 mm. Photos by H. A. Hänni, © SSEF.

substance, creating a very smooth appearance, which explained the lack of typical surface structures for black coral. This example demonstrates, once again, how only a combination of tests can safely identify the nature and treatment of gem materials.

HAH

Petroleum inclusions in quartz from Pakistan: A photo-essay. Hydrocarbon inclusions are quite fascinating, to the point that some gems are specifically cut with them for sale to collectors. Most fluid inclusions containing hydrocarbons, typically in quartz and fluorite, consist mainly of liquid natural petroleum and methane gas, sometimes with water as an immiscible liquid. Opaque black to dark brown translucent bituminous material may also be present, usually within the fluid inclusions as a solid daughter phase, but also as isolated solid inclusions within the host. Such bituminous organic solids are usually lumped under the general heading of asphaltite, the group name for solid bituminous hydrocarbons, unless a more specific analysis has been done.

At the Munich gem and mineral show in October 2002, Michael and Patricia Gray of Graystone Enterprises and Coast-to-Coast Rare Gems (Missoula, Montana) obtained a large parcel of more than 400 quartz crystals with fluid inclusions of natural petroleum that ranged from very light yellow (the smaller inclusions) through bright yellow to yellowish brown. Many of these fluid inclusions also contained dark brown to black solid phases of asphaltite. Asphaltite inclusions also were noted as solids within the quartz itself. All 400 quartz crystals were provided to these contributors for examination. Herb Obodda (H. Obodda, Short Hills, New Jersey) and Hussain Rezayee (All Access Co. Ltd., Bangkok) also loaned several similar crystals from this new find.

Of the more than 400 specimens examined during this study, a representative sample of seven crystals ranging from 0.99 to 6.28 ct is shown in figure 24. Some of the crystals were of suitable quality for faceting (figure 25) although according to Mr. Gray, their heat sensitivity makes this somewhat difficult: If they get too hot, they are prone to cracking, which will subsequently drain any inclusions that rupture and breach the surface.

Magnification revealed that the hydrocarbon fluid inclusions contained two different immiscible liquids: (1) a yellow portion that was natural petroleum, and (2) a colorless aqueous fraction that was situated along some edges of the negative crystals. The gas bubbles were primarily methane, while one or more black asphaltite solid phase(s) were also present (figure 26, left). The odor of motor oil or kerosene was apparent when a crystal from this contributor's collection was cracked or crushed, and in the presence of a flame, the liquid and gas released were seen to be flammable.

On exposure to long-wave UV radiation, the yellow petroleum in most of these fluid inclusions luminesced either bright yellow or bright blue (figure 26, right),

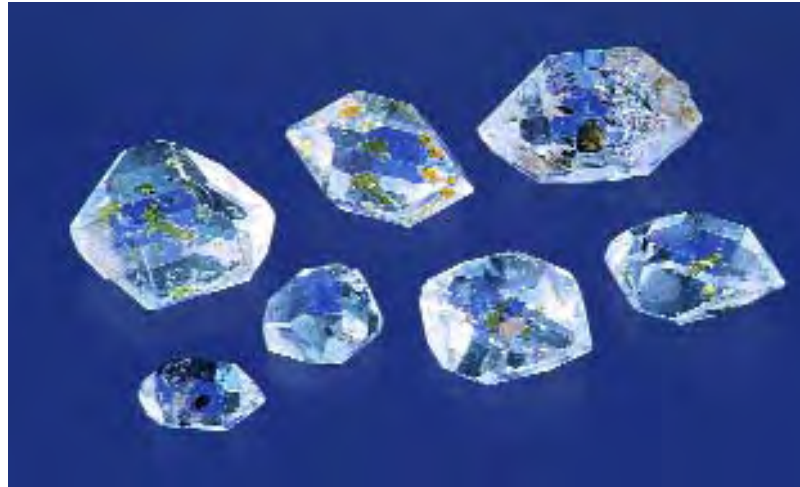


Figure 24. These seven quartz crystals (0.99–6.28 ct) all contain fluid inclusions composed of various hydrocarbons and water. They are representative of more than 400 Pakistani quartz crystals examined for this report. Photo by Maha Tannous.

although orange was also observed in a few samples. Much weaker fluorescence, or no reaction, was seen with short-wave UV. No phosphorescence was noted in any of the samples examined. This characteristic luminescence is useful in the identification of natural petroleum-containing fluid inclusions.

As shown in figure 27, another curious identifying characteristic of the yellow liquid in these fluid inclusions is that when they were illuminated from the side with an incandescent fiber-optic light source, they showed a slightly bluish green to green transmission luminescence.

During the examination of these quartz crystals, a few

Figure 25. Measuring 16.75 mm long, this 9.23 ct quartz crystal shows the intriguing natural beauty of these petroleum-rich rock crystals from Pakistan. The 2.33 ct faceted stone illustrates that gems can be cut from some of these crystals, although their sensitivity to heat requires great caution. Courtesy of Graystone Enterprises; photo by Maha Tannous.



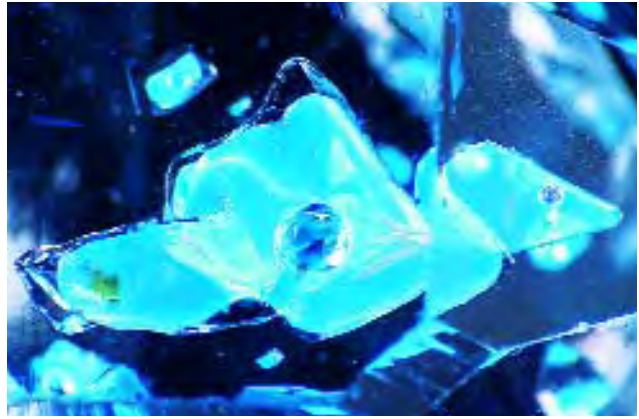
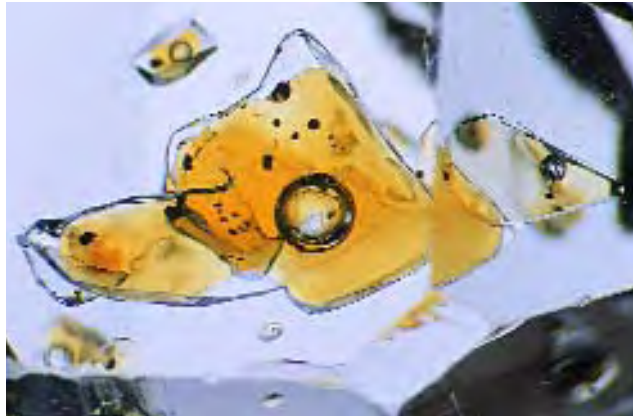


Figure 26. As shown on the left, the hydrocarbon inclusions in the Pakistani quartz crystals were observed to contain two immiscible liquids—a yellow portion (natural petroleum) and a colorless fraction (water) along some edges of the negative crystals. The gas bubbles are primarily methane. A black bituminous asphaltite solid phase also is present. When exposed to long-wave UV radiation, the petroleum in most of these fluid inclusions glows either bright yellow or (as shown on the right) bright blue, although orange also was observed in a few samples. This luminescence is characteristic of such fluid inclusions, and helps identify them. Photomicrographs by John I. Koivula; magnified 5 \times .

oddities also were noted. Four of them contained black bituminous material that moved freely within the petroleum. The most impressive of these was a 4.42 ct, 12.59-mm-long crystal that contained a spherical globule of petroleum, half filled with tiny black asphaltite particles that moved freely (figure 28), coating the meniscus between the petroleum and the aqueous solution surrounding it. The strangest inclusion, shown in figure 29, was a trigonal negative crystal that seemed to be lined with a brown bituminous film and small black blebs of asphaltite.

The geographic locality of these crystals has been variously represented as Baluchistan, Pakistan; Kandahar,

Afghanistan; or “somewhere in China.” Considering that Baluchistan is also known for the production of fluorite with oil-bearing fluid inclusions (A. H. Rankin et al., “Unusual, oil-bearing inclusions in fluorite from Baluchistan, Pakistan,” *Mineralogical Magazine*, Vol. 54, 1990, pp. 335–342), it would not be surprising if these quartz crystals came from that area, as well. The location of the petroleum-bearing quartz deposit was subsequently confirmed as Baluchistan by Mr. Obodda, and also by Farooq Hashmi (Intimate Gems, Jamaica, New York), both of whom recently visited Pakistan.

John I. Koivula (jkoivula@gia.edu) and Maha Tannous
GIA Gem Laboratory, Carlsbad

Figure 27. Another curious identifying characteristic of yellow petroleum inclusions is that when they are illuminated with a white light fiber-optic source from the side, they show slightly bluish green transmission luminescence. Photomicrograph by John I. Koivula; magnified 5 \times .



INSTRUMENTS AND TECHNIQUES

New Swarovski triplet loupe. Swarovski Optik has been producing high-quality binoculars and telescopes for over 50 years. Recently, they have expanded their product line with a newly developed loupe. As can be seen in figure 30, this loupe has a gray matte finished lens holder and a black housing, and is connected to an adjustable lanyard.

The lens is an asymmetrical Taylor-Cook triplet (three optical elements) with 10 \times magnification. The design of this triplet results in a thinner and smaller lens system, resulting in a lighter overall weight (by approximately 30%) compared to similar commercial loupes. The loupe has a field of view of 20 mm and a free working distance of 18.2 mm. The optical surfaces have a high-grade coating to avoid hindering reflections, and to improve chromatic neutrality and the hardness of the optical surface. For best performance, the loupe should be positioned 20 mm away from the subject and approximately 15 mm away from the eye, depending on the eyesight of the user. The view is unidirectional; the loupe

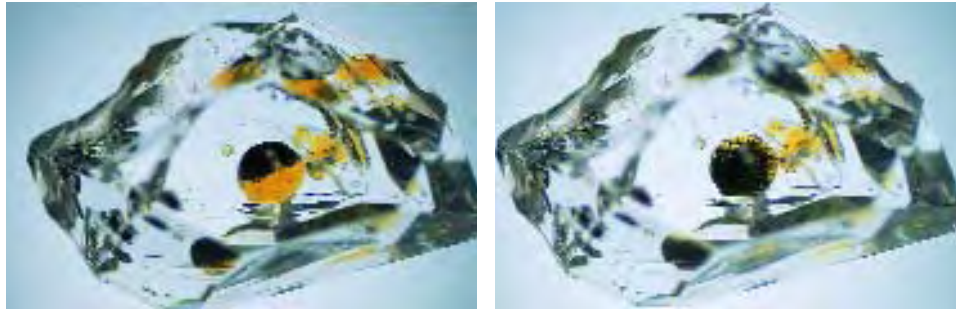


Figure 28. Four of the petroleum-containing quartz crystals had black bituminous material that was free to move within the petroleum. The movement of the bitumen is readily apparent in these photos of a 12.59-mm-long crystal. Photos by John I. Koivula.

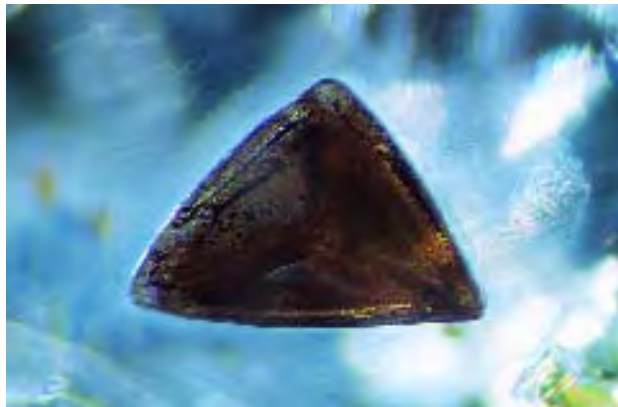


Figure 29. The strangest inclusion encountered in the hydrocarbon-included quartz crystals from Pakistan was this trigonal negative crystal that appeared to be lined with a brown bituminous film and randomly decorated with small black spots of asphaltite. Photomicrograph by John I. Koivula; magnified 10 \times .

works best with the recessed grip toward the user.

We have noticed that this loupe performs differently from traditional 10 \times triplet loupes. A ring covering the perimeter of the lens creates a slightly more limited field of view, but at the same time acts as an aperture creating a larger depth of view. As a result, the center of the image is sharper than in the traditional 10 \times triplet loupes, but the aperture design shields the periphery. Therefore, for optimal results the object being examined should be in the center of the field of view. This is a slight adjustment for those accustomed to other loupes, but is quite comfortable after a few minutes of use. The loupe is therefore very useful for observing inclusions, but the more limited view does not allow for clearly observing an entire stone if it is larger than 8–10 mm.

Overall, this new loupe is a welcome tool for jewelers and gemologists, offering excellent optics and ergonomics.

Tom Moses (tmoses@gia.edu)
GIA Gem Laboratory, New York

Ron Geurts
T.T. Consulting N.V.
Antwerp, Belgium

CONFERENCE REPORTS

Diamond presentations at the Australian Diamond Conference. Approximately 200 people attended the annual Australian Diamond Conference, which was held in Perth on December 1–2, 2003, and comprised 28 presentations and a concluding panel discussion. The mood of the conference attendees was buoyant and optimistic. Following the opening address by the Honorable Richard Court, former premier of Western Australia, **James Picton**, diamond analyst with W. H. Ireland, London, emphasized that if the predicted 4% annual rise in demand for diamond rough continues for the next decade, by 2012 there

Figure 30. This newly developed 10 \times loupe from Swarovski Optik has several innovative features, including an ergonomic design and a much lighter lens. Photo by Elizabeth Schrader.



will be a shortfall of US\$3.5 billion that cannot be met by the present rate of discovery. This will further increase the price of rough and fuel more diamond prospecting. **Bill McKechnie** of the De Beers Group, Johannesburg, South Africa, said that in 2004 De Beers plans to spend US\$6.3 million on diamond exploration in Australia, which is unchanged from 2003. This represents 8% of their world annual budget, versus 40% in Canada, 9% in South Africa, 32% elsewhere in Africa, 7% in India, 2% in Russia, and 2% elsewhere. He said that 2002 was a good year for rough sales and 2003 was very good.

Veston Malango of the Ministry of Mines and Energy, Windhoek, Namibia, said that his government's new mining act and mineral exploration policy was well received by the international mining community. A new NamGem diamond cutting factory, which is 100% owned by Namdeb, recently opened in Windhoek. Seven other privately owned factories have opened since 1999. **Ashok Damarapurshad** of the Ministry of Minerals and Energy, Johannesburg, South Africa, said that the new mining act requiring incorporation of Black Economic Empowerment groups in every mining project was generally well received. At present there are 37 diamond mining operations in South Africa, of which 16 are mining kimberlites, 12 are alluvial, and seven are beach deposits. Of the kimberlites, nine are pipes and seven are fissures. South African diamond production for 2003 is estimated at 10.1 Mct (down from 2002 = 11.1 Mct), worth US\$950 million (up from 2002 = \$900 million).

Many speakers reported on the results and progress of their respective companies. **David Jones** and **Peter Danchin** of Kimberley Diamond Co., Perth, presented the latest news on the Ellendale diamond mine. First-year production (i.e., July 2002 through June 2003) was 51,819 carats, at an average value of US\$159/ct and an average ore grade of about 9 carats/100 tonnes (cpht) recovered from the western area of pipe 9. The mine produces a relatively high proportion of fancy yellows. Recent results from a bulk sample in the eastern area of pipe 9 indicated an average grade of 9.25 cpht and an average size of 0.41 ct. The latest sale in Antwerp of last year's production generated US\$310/ct. Prospecting and ore reserve calculations were greatly improved by using the 2.5-m-diameter Bauer drill rig, which provides 10 tonne samples for each meter drilled. An in-ground value of US\$450 million has been calculated for a mine life of 13 years.

Colin Williams of Argyle Diamonds, Perth, indicated that alluvial operations at the Argyle mine ceased at the end of 2002, and the mine now produces about 30 Mct annually. All rough is sold direct to the market except for pinks, which are retained and sold as polished tenders. Argyle production by volume is 5% gem, 70% near gem, and 25% industrial; by color, 72% brown, 27% near colorless to light yellow, and <1% pink to red. Widening of the open pit by stepping back the west wall in 2000 has extended its life to 2007. An A\$70 million study to be

completed in 2005 is investigating the feasibility of an underground mine, which would extend mine life to 2020 at 5 million tonnes of ore per year and a diamond recovery at about half the current level.

Tom Reddicliffe of Striker Resources, Perth, reported on the latest results from Seppelt 5 in North Kimberley, which is connected by a 2.5-km-long kimberlite dike to Seppelt 2. Both pipes yielded grades in excess of 200 cpht. Many diamonds exceeding 2 ct were recovered, the largest being 8.5 ct, near colorless, and gem quality. Investigations have begun into the feasibility of an open pit plus underground mine for Seppelt 2 and 5. Striker also has acquired the Merlin Orbit properties. These consist of six tenements totaling 1,800 km² surrounding the former Merlin diamond mine, which operated from 1998 to 2002 and is fully owned by Rio Tinto. The Merlin Orbit leases contain many promising targets resembling the known Merlin pipes, which were found by Mr. Reddicliffe when he was exploration manager for Ashton Mining. Striker also acquired a three-year usage of the Rio Tinto kimberlite indicator mineral database for nearly the entire Kimberley region.

Several South African properties also were reviewed. **Charles Mostert** of Crown Diamonds, Perth, introduced this new diamond mining company, which was created through a merger of previous alluvial miner Majestic Resources (Australia) and Messina Investments (South Africa). Two operating fissure mines in South Africa, Messina and Star, produced 31,700 carats in 2002, of which 90% were gem quality. The Messina mine is located in the Bellsbank area, 80 km northwest of Kimberley, and the Star mine is located in Orange Free State near Welkom. A 52.51 ct gem-quality diamond was recovered from a Crown Diamonds mining operation in November 2003. In the same month, Crown completed negotiations to purchase the Helam fissure mine in the western Transvaal region. Future plans include upgrading the production of all three mines to reach 250,000 carats/year by 2006. **Wolf Marx** of Tawana Resources, Melbourne, discussed their Daniel project (owned 30% by Tawana, which can earn up to 40%, the remainder owned by BHP), a buried alluvial channel 7 km long and 2 km wide, which is 6 km down slope from the Finsch mine. It is estimated that about 1,400 m of the Finsch pipe has been eroded, with many of the diamonds transported through the Daniel channel. The bedrock is dolomite and contains many pot holes, which form ideal diamond repositories. **Karl Simich** of Namakwa Diamonds, West Perth, said that 1% of an onshore diamond deposit on the Atlantic coast of Namaqualand has been estimated to contain 411,000 carats with a value of \$100/ct. Environmental plans were approved, and Namakwa may be the first diamond mining company to be granted a license under the new mining legislation in South Africa.

Pamela Strand of Shear Minerals, Edmonton, Canada, gave a review of that company's exploration in the Churchill

diamond project, located on the west side of Hudson Bay, where in two years' fieldwork 18 kimberlites have been found, some of which are diamondiferous. Many other speakers discussed their exploration projects, but none of them had reached advanced stages.

A. J. A. "Bram" Janse (*archonexpl@iinet.net.au*)
Archon Exploration Pty. Ltd.
Perth, Western Australia

"Science of Gem Materials" session at the MRS meeting.

In December 2003, for the first time, the large Materials Research Society meeting in Boston, Massachusetts, included a session on gem materials. Conference abstracts are available at www.mrs.org/meetings/fall2003/program/AbstractBookII.pdf, and summaries of some of the presentations from this two-day session are provided below.

Dr. Jeffrey Post of the Smithsonian Institution, Washington, D.C., described the U.S. national gem collection; notable pieces include the Blue Heart (30.62 ct) and Hope (45.52 ct) diamonds (see Winter 2003 Gem News International, pp. 322–325), a giant Brazilian topaz crystal (weighing approximately 50 kg), and the 127 ct Portuguese diamond with very strong blue fluorescence.

Dr. Reza Abbaschian of the University of Florida, Gainesville, and colleagues discussed recent progress in the growth of synthetic diamonds by Gemesis Corp. (Sarasota, Florida). Yellow crystals up to 3–3.5 ct are produced routinely. The largest crystal grown to date weighed about 5 ct, which should cut a 3.5 ct synthetic diamond; 10 ct crystals are reportedly possible. For near-colorless synthetic diamonds, slow growth is needed (less than 2 mg/hour); a 1 ct crystal requires 100 hours to grow. By comparison, colored synthetic diamonds (e.g., yellow and blue) grow faster, at about 16 mg/hour.

Branko Deljanin of EGL USA, Vancouver, Canada, and colleagues discussed the jewelry-quality synthetic diamonds that Apollo Diamond Co. has grown using chemical vapor deposition (CVD). Single-crystal synthetic diamond films 1–2 mm thick are grown on diamond seeds, and the films are then sawn off with a laser. Brown, "colorless," and blue samples have been grown. They contain traces of nitrogen, hydrogen, and/or silicon, and are types IIa or IIb. CVD synthetic diamonds often show four growth sectors, and microscopic examination revealed inclusions parallel to the seed plate but no graining. In addition to their brown or orange cathodoluminescence, spectral characteristics were described. HPHT annealing of CVD synthetic diamond resulted in a near-colorless product with blue or violet cathodoluminescence and a stronger 637 nm than 575 nm photoluminescence (PL) peak.

Matthew Hall of the GIA Gem Laboratory, New York, and colleagues discussed HPHT annealing of gray-blue type IIb diamonds. Through experiments, they found that annealing reduces the gray component of these diamonds and produces a blue color, sometimes at the Fancy Intense

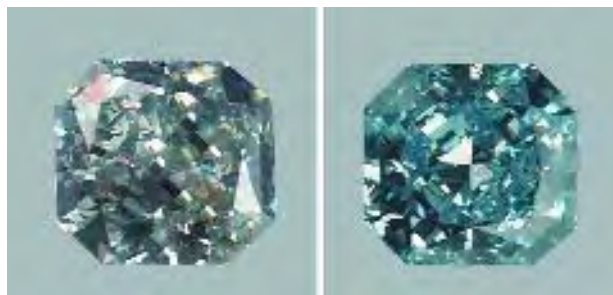


Figure 31. A GIA laboratory study has shown that HPHT annealing of some type IIb diamonds can reduce the gray component and produce blue color, as illustrated by this approximately 0.65 ct diamond before (left) and after (right) HPHT treatment. Photos by Elizabeth Schrader.

or Fancy Vivid level. (According to Mr. Hall, before HPHT annealing, some of the boron in such diamonds is compensated by hydrogen. The treatment process makes this boron available to cause absorption in the mid-IR to higher-wavelength portion of the visible spectrum, producing the blue color.) Although the saturation of their color was altered by the treatment, their tone (lightness or darkness) did not change appreciably (figure 31). The diamonds show characteristic infrared and PL spectral features.

This contributor (and colleagues) discussed GIA's computer modeling of the appearance aspects of a faceted diamond. Several additional brightness and fire metrics have been developed for round brilliants (based on different assumptions about environments and observer conditions), and about 50,000 observations of actual diamonds have been performed to identify the metrics that best agreed with various observers' perceptions of brightness and fire under standardized conditions. The patterns of light and dark seen in round brilliants were found to affect people's decisions as to what makes a good-looking diamond; these pattern effects can also be calculated.

Dr. Lee Groat of the University of British Columbia, Vancouver, and colleagues discussed gem beryl localities in Canada: emerald from Regal Ridge in the Yukon Territory (described in the Spring 2002 Gem News International [GNI], pp. 93–94), dark blue aquamarine from the Yukon (see Winter 2003 GNI, pp. 327–329), and green beryl from Lened, just across the border in the Northwest Territories. The Lened skarn occurs in the vicinity of a tungsten mine and tin-tungsten deposit, as well as a spodumene-bearing pegmatite, but there is no granite exposed in the area. The green beryl is transparent but very pale, with crystals reaching 30 × 5 mm. It is colored by vanadium, not chromium, although some Fe³⁺ is also present as a chromophore.

Dr. Alain Cheillett of CNRS, Vandoeuvre-les-Nancy, France, and colleagues discussed the occurrence of deuterium (a heavy isotope of hydrogen) in emeralds, and its use for determining emerald sources. With infrared spectroscopy, they have developed a database for emeralds from 46 deposits. **Dr. John Rakovan** of Miami University,

Oxford, Ohio, discussed the role of surface structure in the incorporation of rare-earth elements in sector-zoned fluorite. For fluorite from Long Lake, New York, sector zoning shows up with irradiation. The blue color of some fluorite from Bingham, New Mexico, is unstable to sunlight. **Margaret Broz** of the University of Minnesota, Minneapolis, and co-authors discussed hardness and surface-contact properties of gems and minerals. Depth-sensitive indentation (DSI) behavior can be determined from measurements with Vickers and Berkovich devices; these produce measurements of hardness, toughness, stiffness, and bulk modulus. The Mohs hardness scale is nonlinear relative to the DSI hardness scale: Minerals with high Mohs values have much greater measured hardnesses than one would expect from the measured values of minerals with lower Mohs values. **Kenneth Scarratt** of the AGTA Gemological Testing Center, New York, described different types of natural and cultured pearls (freshwater, saltwater, black, and “golden”) from various bivalve mollusks, as well as non-nacreous “pearls” (conch, melo, etc.) from gastropods.

Dr. Laurence Galois of the University of Paris, France, and colleagues examined neolithic jewels containing variscite ($\text{AlPO}_4 \cdot 2\text{H}_2\text{O}$) from Er-Grah and Luffagh (two sites in Brittany, France), both dating from 4400–3900 BC. When compared to variscite from various other European sources, the best spectral match for the Luffagh jewel was nearby Pannecé, but for the Er-Grah piece, Sarrabus in Sicily was the best match. Consequently, it appears that trade routes covered a large area of southern Europe at the time. **Vera Borisovna Kovalevskaja** of the Institute of Archaeology, Moscow, traced gem trade routes to the Scythians and Samartians in the Caucasus, Central Asia, and eastern Europe during the first millennium AD. The gems included amber, topaz, emerald, agate, carnelian, jet, and lapis. Beads came from India via Iran and the Volga River to the steppes; gems and jewelry from Byzantium came via the Red Sea to Europe; and amber spread south and southeast from the Baltic. Locally cut beads can be distinguished from Indian-cut beads by differences in cutting styles and in the quality of the material.

Drs. Peter Heaney and Donald Fisher, both of Penn State University, University Park, Pennsylvania, compared the chatoyant gems tiger’s-eye and pietersite. Tiger’s-eye quartz typically occurs as seams up to a few centimeters thick in banded iron formations; most is mined near Griquatown in South Africa. Although tiger’s-eye was formerly explained as quartz pseudomorphs after crocidolite (riebeckite) asbestos fibers, in fact the quartz is granular and includes wisps of oxidized crocidolite; these parallel fibrous inclusions cause the chatoyancy. Pietersite is always brecciated; this quartz gem occurs as silicified nodules in limestone, near Windhoek, Namibia. Again, the quartz did not replace crocidolite; instead, the original siliceous material in

these nodules was fibrous chalcedony, occurring with hematite. The quartz replacement of chalcedony reorganized the hematite into segregations, and sodium metasomatism caused hematite and chalcedony to react to form crocidolite (and granular quartz).

Dr. Emmanuel Fritch of IMN, Nantes, France, and colleagues discussed the microstructure of play-of-color and common opals. Mineralogists distinguish opal-A (which is X-ray amorphous) from opal-CT (which shows cristobalite and/or tridymite lattice spacings in its X-ray diffraction pattern). Australian sedimentary opal-A owes its play-of-color to 200 nm array elements; this gem mainly consists of silica, with the holes between the intergrown spheres organized in an array. Volcanic-related opal-CT may not show play-of-color. Examples include fire opal (from Brazil, Kazakhstan, Mexico, and Ethiopia); pink opals showing fibrous opal microstructures and colored by palygorskite microfibers (from Peru and Mexico); opals with microscopic platelets; and those with “lepispheres”—resembling tiny gypsum roses—of cristobalite-like opal-CT. All these have spheroids of silica of about the same size, 20–40 nm. **Dr. Orlin Velev** of North Carolina State University, Raleigh, summarized the research his group has done on opal-structured materials. Controlled crystallization is necessary to create the opal microstructure. In their laboratory experiments, colloidal polymer spheres were “crystallized” in an organized fashion to create play-of-color; spheres 100–1000 nm in diameter resulted in play-of-color effects in materials such as plastic films, graphite, and gold.

*Mary L. Johnson (mary.johnson@gia.edu)
GIA Gem Laboratory, Carlsbad*

Sinkankas tourmaline symposium. The 2nd Annual John Sinkankas Memorial Symposium was co-hosted by the San Diego Mineral & Gem Society and GIA on April 10, 2004. The all-day event took place at GIA’s headquarters in Carlsbad, where approximately 120 attendees were treated to seven presentations on tourmaline. Each participant received an informative proceedings volume that contained excerpts of some of the presentations, selections from previous publications on tourmaline, and a bibliography.

After opening remarks by convener **Roger Merk** (Merk’s Jade, San Diego, California), **Dr. William B. “Skip” Simmons** of the University of New Orleans reviewed the complex chemical variations and the 14 currently recognized species of the tourmaline group, which are divided into alkali (e.g., elbaitite), calcic (e.g., liddicoatite), and X-site vacant (e.g., rossmanite) tourmalines. He then took the audience on a “virtual field trip” to the Transbaikalia Malkhanski pegmatites near Lake Baikal in Siberia, Russia. At the most important deposit, the Mokhovaya pegmatite, gem-quality tourmaline in a variety of colors has been systematically mined from a large open cut since the early 1990s.

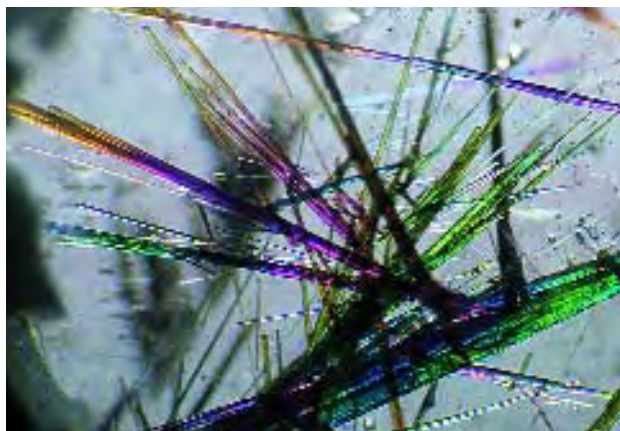


Figure 32. Needle-like inclusions of tourmaline (probably schorl) in this sample of quartz from Governador Valadares, Brazil, show brilliant interference colors between partially crossed polarizing filters. Photomicrograph by John I. Koivula; magnified 5 \times .

Si Frazier of El Cerrito, California, reviewed the common crystal forms of tourmaline, provided simple diagrams to illustrate the angular relationships between various pyramidal forms, and showed interesting examples of tourmaline inclusions in quartz. **Jesse Fisher** of UK Mining Ventures, San Francisco, summarized important tourmaline localities of the world. Some of the most significant producers of gem-quality tourmaline include Minas Gerais, Brazil (the Araçuaí area and the region around Teófilo Otoni and Governador Valadares), eastern Afghanistan (e.g., the Paprok, Mawi, and Darre Pech areas), and southern California (e.g., the Himalaya and Tourmaline Queen mines).

Meg Berry of Mega Gem, Fallbrook, California, provided useful insights on faceting tourmaline. She emphasized the importance of polishing tourmaline lengthwise on the wheel to avoid stress fracturing, and explained how emerald cuts of bicolored stones and those with a “closed” (or dark-colored) c-axis should be faceted with steeply inclined ends (i.e., at least 75°). **William Larson** of Pala International, Fallbrook, California, then described some of the historic literature on tourmaline, including rare manuscripts dating back to the 18th century.

John Koivula of the GIA Gem Laboratory in Carlsbad reviewed the inclusions and optical phenomena in gem-quality tourmaline. Growth tubes, negative crystals, various solid-liquid-gas assemblages, and distinctive color zoning may be found in tourmaline, whereas tourmaline has been documented as inclusions in minerals such as apatite, beryl, cassiterite, quartz (figure 32), pezzottaite, and topaz. The visibility of minute inclusions can be enhanced with certain lighting conditions, such as shadowing, fiber-optic illumination, or the use of polarizing filters.

Dr. George Rossman of the California Institute of Technology, Pasadena, gave the closing presentation, on

the coloration of tourmaline. The most common chromophores are Fe²⁺, Fe³⁺, Ti⁴⁺, Mn²⁺, and Mn³⁺, although Cr³⁺, V⁵⁺, and Cu²⁺ can also cause color. Multiple coloration mechanisms can be present in a single sample, and post-crystallization color modifications can occur through exposure to ionizing radiation (gamma rays) in the pegmatitic environment or laboratory (i.e., colorless Mn²⁺ converted to pink Mn³⁺).

The theme of next year’s Sinkankas symposium will be beryl.

BML

ANNOUNCEMENTS

Dr. Henry A. Hänni receives AGA Bonanno Award. SSEF Swiss Gemmological Institute director (and GNI contributing editor) Dr. Henry A. Hänni has received the Accredited Gemologists Association’s Antonio C. Bonanno Award for Excellence in Gemology. This award recognizes people in the gemological field who have made significant contributions to the field or defended and upheld gemological standards in ways that benefit the gem and jewelry community. Dr. Hänni was honored for his nearly 30 years as a leading gemological researcher and educator, and his contributions to gem treatment reporting standards.

Dr. George R. Rossman receives Feynman Prize. Dr. George R. Rossman, professor of mineralogy at the California Institute of Technology in Pasadena and a longtime member of the *G&G* editorial review board, has been named the recipient of Caltech’s most prestigious teaching honor, the Feynman Prize for Excellence in Teaching. The award, given to an outstanding faculty member each year, recognizes “exceptional ability, creativity, and innovation in both laboratory and classroom instruction.” Dr. Rossman has taught mineralogy at Caltech for more than 30 years.

Conferences

JCK Show—Las Vegas. Held at the Venetian Resort & Hotel on June 3–8, 2004, this show will also host a comprehensive educational program beginning June 3. Scheduled seminars will cover industry trends, diamond sales and marketing strategies, legal issues for retailers and manufacturers, and developments in gemology. AGTA will also be offering seminars focusing on color and fashion on June 3 at the AGTA Pavilion. To register, call 800-257-3626 or 203-840-5684. Visit <http://jckvegas2004.expoplanner.com>.

Jewelry Camp 2004. The 25th Annual Antique & Period Jewelry and Gemstone Conference will be held July 17–24 at Hofstra University, Hempstead, New York. The program covers hands-on jewelry examination techniques, methods of construction, understanding materials used

throughout history, and the constantly changing marketplace. Visit www.jewelrystcamp.org, call 212-535-2479, or e-mail jwlrystcamp@aol.com.

Geoscience Africa 2004. Hosted by the University of the Witwatersrand in Johannesburg, South Africa, July 12–16, this conference will feature a symposium titled “Kimberlites, Diamonds and Mantle Petrology.” Field trips to the Premier diamond mine and alluvial diamond deposits along the Orange River will be offered. Visit www.wits.ac.za/geoscienceafrica.

International Geological Congress. The 32nd Session of the International Geological Congress will take place August 20–28, 2004, in Florence, Italy. Symposia are planned that will cover such topics as gem materials, inclusions in minerals, and mineral spectroscopy. Visit www.32igc.org/default1.htm.

5th European Conference on Mineralogy and Spectroscopy. Held September 4–8, at the University of Vienna, Austria, this meeting will be held in conjunction with the 6th European Mineralogical Union School on Spectroscopic Methods in Mineralogy, which takes place from August 30 to September 8. Students will gain exposure to optical (UV-Vis-NIR) and luminescence spectroscopy, vibrational spectroscopy (Raman and infrared), Mössbauer spectroscopy, nuclear magnetic resonance spectroscopy (NMR), and X-ray absorption spectroscopy (XANES and EXAFS). Visit www.univie.ac.at/Mineralogie/ECMS2004 and www.univie.ac.at/Mineralogie/EMU_School.

Gems of Pacific continental margins. The International Association on the Genesis of Ore Deposits will host a symposium titled “Gem Deposits Associated with the Pacific Continental Margins” at the Interim IAGOD Conference on Metallogeny of the Pacific Northwest: Tectonics, Magmatism & Metallogeny of Active Continental Margins. The conference will take place September 11–19, in Vladivostok, Russia. Visit www.fegi.ru/IAGOD.

Diamond 2004. A review of the latest scientific and technological aspects of natural and synthetic diamond (as well as related materials) will take place at the 15th European Conference on Diamond, Diamond-like Materials, Carbon Nanotubes, Nitrides & Silicon Carbide, September 12–17, 2004, in Riva del Garda, Italy. Visit www.diamond-conference.com.

ICAM 2004 in Brazil. The 2004 International Congress on Applied Mineralogy will be held in Águas de Lindóia, Brazil, September 19–22, 2004, and will include a special session on gem materials. Pre- and post-conference field trips will tour colored gemstone and diamond deposits in

the Ouro Preto and Diamantina areas, as well as agate and amethyst mines in Rio Grande do Sul State. Visit www.icam2004.org.

Hong Kong Jewellery & Watch Fair. Held at the Hong Kong Convention and Exhibition Centre on September 19–22, this show will also host GIA GemFest Asia 2004 on September 20, and an educational seminar given by the Gemmological Association of Hong Kong on September 21, in addition to several jewelry design competitions. Visit <http://www.jewellerynetasia.com/exhibitions/default.asp?siteid=5&lang=1>.

Exhibits

GIA Museum exhibits in Carlsbad. *Magic, Myths, and Minerals*, a traveling exhibition of Chinese jades from the Smithsonian Institution’s Arthur M. Sackler Gallery, will be on display in GIA’s Museum Gallery, from May 24 to October 31, 2004. In addition, the exhibit *All Natural, Organically Grown Gems* will share the Museum Gallery space until October 31. New pieces continue to be added to *From the Vault: Gifts to Our Collection*, on view in the Rotunda through December 2004. Contact Alexander Angelle at 800-421-7250, ext. 4112 (or 760-603-4112), or e-mail alex.angelle@gia.edu.

ERRATA

1. Regarding the Summer 2001 Gem News International entry on “Canary” tourmaline (pp. 151–152), it has subsequently come to our attention that this material was produced from an existing deposit near the city of Chipata in Zambia, not far from the Malawi border (see, e.g., K. Schmetzer and H. Bank, “Intensive yellow tsilaisite [manganese tourmaline] of gem quality from Zambia,” *Journal of Gemmology*, Vol. 14, No. 3, 1984, pp. 218–223). Tourmaline from this locality also has been incorrectly reported by suppliers as being from Tumbuka, Mozambique (see March 2001 *Jewellery News Asia*, p. 209), although more recent publications correctly refer to Zambia as the source (see April 2004 *Jewellery News Asia*, pp. 128, 138, 140).
2. The article “Gem-quality synthetic diamonds grown by a chemical vapor deposition (CVD) method” in the Winter 2003 issue contained an incorrect reference. The reference for De Beers Industrial Diamonds et al. (2001) should have been:

Vagarali S.S., Webb S.W., Jackson W.E., Banholzer W.F., Anthony T.R., Kaplan G.R. (2003) *High Pressure/High Temperature Production of Colorless and Fancy-colored Diamonds*. U.S. patent application 20030143150, filed January 8.

Gems & Gemology regrets the error.

The
Dr. Edward J. Gübelin
 MOST VALUABLE ARTICLE

Award

Gems & Gemology is pleased to announce the winners of this year's Dr. Edward J. Gübelin Most Valuable Article Award, as voted by the journal's readers. Our special thanks to the many G&G readers who participated in this year's voting.

The first-place article was "Beryllium Diffusion of Ruby and Sapphire" (Summer 2003), an in-depth report on Be-diffused corundum and the gemological and other tests that can help identify it. Receiving second place was "Gem-Quality Synthetic Diamonds Grown by a Chemical Vapor Deposition (CVD) Method" (Winter 2003), which presented a complete description and identifying characteristics of Apollo Diamond Inc.'s facetable, single-crystal type IIa CVD synthetic diamonds. Third place was awarded to "Photomicrography for Gemologists" (Spring 2003), which reviewed the fundamentals of gem photomicrography and discussed the newest techniques in the field.

The authors of these three articles will share cash prizes of \$2,000, \$1,000, and \$500, respectively. Following are brief biographies of the winning authors.

Congratulations also to Hector Nick Hernandez of San Antonio, Texas, whose ballot was drawn from the many entries to win a three-year subscription to *Gems & Gemology* and a copy of *Legacy of Leadership: A History of the Gemological Institute of America*.

First Place

BERYLLIUM DIFFUSION OF RUBY AND SAPPHIRE

John L. Emmett, Kenneth Scarratt, Shane F. McClure, Thomas Moses, Troy R. Douthit, Richard Hughes, Steven Novak, James E. Shigley, Wuyi Wang, Owen Bordelon, and Robert E. Kane

John L. Emmett received a bachelor's degree in physics from the California Institute of Technology and a Ph.D. in physics from Stanford University. Dr. Emmett is a former associate director of the Lawrence Livermore National Laboratory and a co-founder of Crystal Chemistry. He consults on laser applications, heat treatment, and other aspects of gemology. **Kenneth Scarratt** has 30 years of experience as a laboratory gemologist. He is currently laboratory director for the AGTA Gemological Testing Center in New York City. Previously laboratory director at AIGS in Bangkok and GAGTL in London, Mr. Scarratt has published extensively in gemological journals throughout the world. **Shane F. McClure** is director of Identification Services at the GIA Gem Laboratory in Carlsbad, California. Mr. McClure is well known for his articles on gem identification and is an editor of *G&G's* Lab Notes section. **Thomas Moses** is vice president of Identification and Research at the GIA Gem Laboratory in New York. Mr. Moses, who attended Bowling Green University, is also an editor of the Lab Notes section and a member of the *G&G* Editorial Review Board. **Troy R. Douthit** (not pictured) is a principal of Crystal Chemistry in Los Altos,



John L. Emmett



Kenneth Scarratt



Shane F. McClure



Thomas Moses



Richard Hughes



Steven Novak



James E. Shigley



Wuyi Wang



Owen Bordelon



Robert E. Kane

California. **Richard W. Hughes** is a leading authority on corundum and the author of *Ruby & Sapphire*. Mr. Hughes is webmaster at Pala International's Palagems.com, and his writings can also be found on his personal Web site, Ruby-Sapphire.com. **Steven Novak** is manager of the Dynamic SIMS group at Evans East, East Windsor, New Jersey, a contract analytical laboratory specializing in surface analysis. He has a bachelor's degree from the University of Maryland, a master's degree from Virginia Tech, and a Ph.D. from Stanford University, all in geology. **James E. Shigley** is director of GIA Research in Carlsbad. Dr. Shigley is the author of numerous articles on diamonds and other gemstones and is a contributing editor to *G&G*. He received a bachelor's degree in geology from the University of California, Berkeley, and a doctorate in geology from Stanford University. **Wuyi Wang** is a research scientist for GIA Research and Identification in New York. He holds a Ph.D. in geology from the Tsukuba University in Japan, and has considerable experience in studying diamond geochemistry. **Owen Bordelon** is a former captain in the U.S. Army Airborne Rangers and a pilot. He holds an M.A. in music theory and composition and a J.D. in law. Based in New Orleans, he designs and builds optical-electronic scientific instruments for the AGTA-GTC and other laboratories. **Robert E. Kane** is president and CEO of Fine Gems International in Helena, Montana, and a member of the *G&G* Editorial Review Board since 1981. With more than 25 years of gemological experience, Mr. Kane is well known for his many articles on diamonds, colored stones, and gem identification.

Second Place

GEM-QUALITY SYNTHETIC DIAMONDS GROWN BY A CHEMICAL VAPOR DEPOSITION (CVD) METHOD

Wuyi Wang, Thomas Moses, Robert C. Linares, James E. Shigley, Matthew Hall, and James E. Butler

Wuyi Wang, **Thomas Moses**, and **James Shigley** are profiled in the first-place entry. **Robert C. Linares** (not pictured) is chairman of Apollo Diamond Inc. in Boston. A graduate of Fairleigh Dickinson (M.B.A.) and Rutgers University (Ph.D. in materials science), Dr. Linares has a long history of research in advanced semiconductor and telecommunications technologies, with a more recent focus on creating products from synthetic diamond. **Matthew Hall** is supervisor of analytical equipment at the GIA Gem Laboratory in New York. He holds a bachelor's degree in geology from Franklin and Marshall College and a master's in geology and geochemistry from the University of Maryland. **James E. Butler** is head of the Gas/Surface Dynamics Section of the Naval Research Laboratory in Washington, D.C. Dr. Butler has published over 190 papers in experimental chemical physics. He received a bachelor's degree from MIT and a Ph.D. from The University of Chicago, both in chemical physics.



Matthew Hall



James E. Butler



John I. Koivula

Third Place

PHOTOMICROGRAPHY FOR GEMOLOGISTS

John I. Koivula

John I. Koivula is chief research gemologist at the GIA Gem Laboratory in Carlsbad. A longtime contributor to *G&G*, Mr. Koivula is the author of *MicroWorld of Diamonds* and co-author of *Photoatlas of Inclusions in Gemstones*. He holds bachelor's degrees in chemistry and mineralogy-geology from Eastern Washington State University.

Challenge

The following 25 questions are based on information from the four 2003 issues of *Gems & Gemology*. Refer to the feature articles and “Notes and New Techniques” in those issues to find the **single best answer** for each question; then mark your choice on the response card provided in this issue. (Sorry, no photocopies or facsimiles will be accepted; contact the Subscriptions Department—dortiz@gia.edu—if you wish to purchase additional copies of this issue.) Mail the card so that we receive it no later than Monday, August 2, 2004. Please include your name and address. All entries will be acknowledged with a letter and an answer key **after the due date**.

Score 75% or better, and you will receive a GIA Continuing Education Certificate. If you are a member of the GIA Alumni Association, you will earn 10 Carat Points toward GIA’s Alumni Circle of Achievement. (Be sure to include your GIA Alumni membership number on your answer card and submit your Carat card for credit.) Earn a perfect score, and your name also will be listed in the Fall 2004 issue of *Gems & Gemology*. Good luck!

- In rubies and sapphires for which a surface-conformal layer of color is not evident, _____ may provide an important indication of the high heat required for Be-diffusion treatment.
 - specific gravity
 - birefringence
 - pleochroism
 - inclusions
- One strong indication for CVD-grown synthetic diamonds that can be seen with standard gemological testing is the presence of
 - cross-hatched bands of low-order interference colors.
 - non-diamond carbon inclusions.
 - metallic flux inclusions and negative crystals.
 - chalky blue short-wave UV fluorescence.
- When doing polarized light photomicrography, a filter that can dramatically reduce exposure times (thus diminishing the effects of vibration) and make dull, interference, or strain colors more vibrant is known as a
 - custom-made light diffuser.
 - translucent white filter.
 - first-order red compensator.
 - depth filter.
- Although red beryl has been reported from a number of locations, the only commercially important occurrence is in
 - Topaz Valley, Utah.
 - Ambatovita, Madagascar.
 - the Wah Wah Mountains, Utah.
 - Mogok, Myanmar (Burma).
- When a copyrighted work such as a gemstone design is comprised of individual, un-copyrightable elements,
 - copyright registration protects all elements of the design.
 - others may freely use those individual elements to create a similar design.
 - the copyright extends only to the design as a whole.
 - the copyright may not be enforceable.
- A study of black and dark gray diamonds from Siberia determined that they were colored primarily by inclusions of magnetite, native iron, and

- A. hematite.
B. graphite.
C. chromite.
D. ilmenite.
8. In 2003, the International Mineralogical Association recognized pezzottaite as a new member of the _____ group.
A. garnet
B. beryl
C. tourmaline
D. spinel
9. The largest Fancy red diamond graded by GIA as of 1997 is the
A. Hancock Red.
B. Moussaieff Red.
C. Heart of Eternity.
D. Millennium Star.
10. _____ clearly separates gem grandidierite from lazulite, the material otherwise closest in properties.
A. Refractive index
B. Iron content
C. Specific gravity
D. Birefringence
11. Prior to the recent identification of a 3.00 ct specimen of poudretteite from Myanmar, only seven crystals of the material were known to exist, from a single quarry in
A. Sri Lanka.
B. Thailand.
C. Brazil.
D. Canada.
12. The technique of _____ involves spreading on the gemstone a small drop of refractive index fluid with an R.I. close to that of the stone, so that scratches can be made effectively transparent.
A. total immersion
B. mirroring
C. quick polishing
D. shadowing
13. In the earliest reported gem corundum diffusion process, _____ was diffused into the stone, producing a thin blue outer layer.
- A. iron
B. titanium
C. vanadium
D. chromium
14. In 1971, Robert Crowningshield published the first gemological description of
A. synthetic diamonds.
B. synthetic rutile.
C. flux-grown synthetic emeralds.
D. HPHT-treated diamonds.
15. The brown color in some CVD-grown synthetic diamonds can be removed by
A. laser drilling and skillful polishing.
B. HPHT annealing.
C. fracture filling.
D. electron irradiation and annealing.
16. When faceted, the color of red beryl will vary depending on the orientation of the table to the c-axis because of the gem's
A. large amount of inclusions.
B. high refractive index and dispersion.
C. dichroism.
D. near-total absence of water in its chemical make-up.
17. The only major commercially available gem material that poudretteite would likely be confused with is
A. alexandrite.
B. amethyst.
C. tourmaline.
D. spinel.
18. To register a gemstone design with the U.S. Copyright Office (USCO), the designer must
A. file an application with the USCO.
B. pay a fee.
C. deposit a specimen of the design with the USCO.
D. all of the above.
19. Natural black diamonds from Siberia may be separated from artificially colored black diamonds on the basis of
A. electrical conductivity.
B. fluorescence.
C. magnetic properties.
D. thermal conductivity.
20. Pezzottaite has thus far been reported from
A. Madagascar.
B. Myanmar (Burma).
C. Afghanistan.
D. both a and c
21. Photomicrography using _____ can be extremely dangerous to your eyes.
A. ultraviolet illumination
B. transmitted light
C. polarized light
D. darkfield illumination
22. The first known transparent faceted grandidierite is from
A. Madagascar.
B. Vietnam.
C. Sri Lanka.
D. none of the above
23. Conclusive identification of Apollo CVD synthetic diamonds requires the use of
A. scanning electron microscopy.
B. long-wave ultraviolet luminescence.
C. magnetism.
D. advanced spectroscopic methods.
24. Analyses have indicated that the beryllium concentration in the diffused region of Be-diffused sapphires is approximately _____ parts per million atomic.
A. 10 to 35
B. 50 to 75
C. 135 to 160
D. 175 to 200
25. Natural blue-green to green color in diamonds such as the 5.51 ct Ocean Dream is due to
A. exposure to radiation in the earth.
B. a high hydrogen content.
C. small amounts of nitrogen.
D. plastic deformation of the diamond's atomic lattice.

EDITORS

Susan B. Johnson
Jana E. Miyahira-Smith
Stuart Overlin

Pearl Buying Guide: How to Evaluate, Identify and Select Pearls & Pearl Jewelry

By Renée Newman, 134 pp., illus., publ. by International Jewelry Publications, Los Angeles, 2004. US\$19.95*

The *Pearl Buying Guide* is a well-written, beautifully illustrated book designed to help retail customers, jewelry designers, and store buyers who lack specialized knowledge make informed buying decisions about the various types of pearls and pearl jewelry available on the market today.

Drawing heavily on the Gemological Institute of America's pearl description system, it covers the standard "price factors," including size, shape, color, luster, and nacre quality. There is a good discussion of the differences in price between, for example, South Sea, Tahitian black, and Chinese freshwater cultured pearls, as well as between full-round and mabe types. Particularly effective are the sections that help consumers evaluate the relative importance of these various factors and come to decisions that reflect their own needs, as well as provide tips on evaluating the quality of information offered by retailers. Additional sections cover pearl jewelry, caring for pearls, and the gemology of pearls.

Of considerable value to retail buyers will be the sections on cultured versus natural and imitation pearls as well as treatments. These are brief yet thorough, and could also form the basis for presentations to the public or sales training sessions. It is perhaps with the latter in mind that the author has included a section with quizzes for each chapter.

The book is distinguished by photographs reflecting the range of both traditional and more unusual pearls available on the market today. The photos are abundant and well chosen, and the use of a coated stock contributes to the exceptional quality of the reproduction.

I have only two complaints about the text: I found that the typeface and page layout made reading somewhat difficult, and the chapter presenting pearl history from the pearl's perspective was perhaps more clever as a concept than it really needed to be.

Overall, the *Pearl Buying Guide* will be a valuable addition to the retailer or designer's reference library. Consumers also will find this book a source of accurate and easy-to-understand information about a topic that has become increasingly complex in the last 10 years.

LISA SCHOENING

*Gemological Institute of America
Los Angeles*

Faszination Turmalin

By Paul Rustemeyer, 309 pp., illus., publ. by Spektrum Akademischer Verlag, Heidelberg, Germany, 2003 (in German). € 99.95

This book will delight the eyes of gemologists, crystallographers, collectors, and the art-loving general public alike. In it, the author provides a thorough description of the many different growth features, post-growth dissolution or etch features, and causes of color in this fascinating and extraordinarily multicolored group of silicates, which are chemically and structurally some of the most complex of gem minerals. But the author's

intended audience is not limited to scientists, as he avoids technical jargon. Aided by the clearly understandable diagrams, any interested layperson or collector will acquire an appreciation of the splendid diversity of forms and colors seen in tourmalines.

After an introduction that includes surprising evidence that even common "black" tourmalines are colorful in thin slices, the book goes on to cover the geologic origin and geographic distribution of tourmaline. Next are the chemistry, atomic structure, and physical and optical properties of the species in the tourmaline group, as well as tourmaline crystal growth processes and crystal shapes. It is in chapter 5, though, that the author gets into the true purpose of his book: the fascinating inner world of tourmaline crystals, mostly as illustrated by slices viewed with transmitted light. Here we find an explanation for the famous and valuable "Mercedes stars" that are seen in some tourmaline slices. Subsequent chapters explore the effects of structural (crystal lattice) flaws on tourmaline growth, broken crystals "healed" by later growth, and growth interrupted by foreign particles. Of special interest to gemologists is a section on the causes of chatoyancy in tourmaline.

These topics may give the impression of dry, technical subject matter. Yet, the phenomena being explained are expressed so much more colorfully

**This book is available for purchase through the GIA Bookstore, 5345 Armada Drive, Carlsbad, CA 92008. Telephone: (800) 421-7250, ext. 4200; outside the U.S. (760) 603-4200. Fax: (760) 603-4266.*

in tourmaline than in other gem minerals, and the relatively small amount of text is illustrated so profusely, that the reader will be aesthetically entertained while receiving a technical education. The book ends with a two-page list of references and a helpful index.

The subject matter in the main part of the book is covered exhaustively, and it would be hard to find any fault with it, although I personally would have liked to see at least one "watermelon" tourmaline depicted.

Although this book is written in German, the vast majority of the publication consists of color photos illustrating various aspects of the internal and external structure of tourmalines. In combination with the numerous accompanying diagrams, the didactic intent of each photo becomes self-explanatory, even for the linguistically challenged. The quality of the photographic reproduction, paper, printing, and binding are all first rate.

The author displays a profound knowledge and love of his subject, and readers will undoubtedly catch some of this passion themselves. Seldom does a book exhibit such a glorious interplay of art and science. Apart from enjoying the purely aesthetic pleasures of this book, gemologists who deal with tourmaline will find it of practical use in better understanding the complex internal aspects and growth features in this mineral group. Furthermore, creative jewelers may well find it a source of inspiration for expanding their ideas on what can be done with tourmalines.

ALFREDO PETROV
Peekskill, New York

Flux-Enhanced Rubies and Sapphires

By Ted Themelis, 48 pp., illus., publ. by Gemlab Inc., Bangkok, 2004. US\$20.00

Prolific gemstone author Ted Themelis has written yet another informative booklet, this time on the controversial topic of flux-enhancement heat treatment of rubies and sapphires. This treat-

ment is used to fill fractures and fissures in corundum to increase apparent clarity. It is the flux processing of Mong Hsu ruby that converts this low-grade material into gemstones.

The booklet opens with a background discussion, written partially in a question-and-answer format, that effectively serves to introduce the topic. This section is followed by one that explains fractures, fissures, and other defects and describes what fluxes do to these features. These two introductory sections place the topic in perspective.

The next section of the booklet, "Fluxes and Additives," attempts to explain the chemistry of this treatment but fails abysmally. If you have a background in inorganic chemistry it will amuse; if you don't, it will confuse. For example, it says of aluminum nitrate, "This chemical produces oxygen at the anode and hydrogen at the cathode," which actually describes what happens when electricity is run through water. The terminology and formulas of the chemicals border on the bizarre: "anhydrous chromium CrO_6 " should be chromic anhydride CrO_3 ; "aluminum fluorite" is used instead of aluminum fluoride; "chlorite" is routinely used for chloride; and "alumina nitrate" could refer to aluminum nitrate, or maybe ammonium nitrate, or maybe something else altogether. One particularly wonders, just what is an "alkali acid"? This section calls into question the chemical knowledge of the author, the editor, or both. Avoid it.

However, Mr. Themelis does make an important contribution when he shows the results of the many experiments he has personally conducted over several years. The majority of the book photographically illustrates the results of flux processing applied to many different types of ruby and sapphire. It is unclear whether the changes in color shown are caused by the heat treatment temperature, the flux, or both, so it would have been helpful if some of the samples also had been heat treated without flux for comparison. In most

cases, the clarity enhancements can be ascribed to the flux. The many photos effectively carry the topic quite independently of the text. The author champions the disclosure of flux processing, and indeed disclosure of all corundum processing, but realistically notes that it is rarely done.

This book should be on every gemologist's bookshelf, simply for the value of the "before and after" pictures of flux processing, which are unavailable anywhere else.

JOHN L. EMMETT
*Crystal Chemistry
Brush Prairie, Washington*

Tesouros de Arte e Devoção [Treasures of Art and Devotion]

By Artur Goulart de Melo Borges, 336 pp., illus., publ. by Fundação Eugénio de Almeida, Évora, Portugal, 2004 (in Portuguese). € 40.00

Tesouros de Arte e Devoção (Treasures of Art and Devotion) is the colorful catalog of the exhibition of the same name, the result of an ambitious project conducted by the Eugénio de Almeida Foundation to classify and inventory the artistic heritage of the Archdiocese of Évora, which was created in 1540 by Cardinal D. Henrique, son of King Manuel I of Portugal. This catalog also responds to the Vatican's urgent need to study and safeguard the rich artistic and historical legacy of the church as a whole. Inside are 130 of the most interesting religious artifacts encountered during research performed in 2002, including paintings, sculptures, liturgical artifacts, vestments, and jewelry.

Among the silver, gold, and gem-set pieces, there is special mention of altar service items such as chalices, pyxes, and monstrances (the latter two designed for storing and exhibiting the consecrated host, respectively), as well as altar crosses and holy images. There are also a significant number of costume jewelry pieces that feature votive paintings known as *ex votos*.

As a note of interest, this reviewer examined these jewels and identified

an array of gem materials used in Portuguese jewelry, particularly in the 18th century. Among them were greenish yellow chrysoberyl; amethyst; pinkish, Imperial, and yellow topaz; and a series of colorless gems (known commercially in Portugal as "minas novas") typical of the period: rock crystal, topaz, and beryl. All the stones were set with a colorless or colored foil back, and doublets and colored pastes were also encountered. Diamonds play a distinguished part in the collection, cut in both in rose and old-mine styles reminiscent of Portugal's diamond wealth during Brazil's colonial era.

Of particular interest is a rosary, dated from the 17th century, that holds paste "goldstone" beads and a diamond-set silver pendant with imitation pearls that correspond to the "Roman pearl" described in the literature.

The exhibition and this illustrated catalog are a testimony to the strength and commitment of Évora's Christian heritage. They provide valuable examples of the quality of Portuguese sacred art from the 16th to 18th centuries.

The book also includes a history of the archdiocese, the particular conditions that enabled the preservation of these items (namely their concealment during Napoleonic invasions in the early 19th century), and a section of bibliographic and documental sources.

RUI GALOPIM DE CARVALHO
*Portuguese Gemological Laboratory
Sintra, Portugal*

Glitter & Greed: The Secret World of the Diamond Cartel

By Janine Roberts, 374 pp., illus., publ. by The Disinformation Co., New York, 2003. US\$22.95

Author Janine Roberts, the producer of a 1994 documentary called *The Diamond Empire*, is a seasoned reporter who has spent years tracking down diamond stories. Unfortunately, hers is a world of endless conspiracies and machinations that overwhelm whatever legitimate, accurate information is presented in this book.

The work's 18 chapters cover a mix of historical and contemporary subjects—including "In Bondage—The Child and Adult Cutters of India," "How the Only US Diamond Mine Was Sabotaged," "Diamonds for Hitler," and "How Diamonds Were Made Rare"—that describe how De Beers (primarily) disenfranchised local tribal peoples, encouraged maltreatment of workers, and bullied every other potential player out of the rough diamond business. Regardless of a chapter's stated topic, Roberts inevitably turns the subject back into accounts of De Beers's master manipulations and stories of attempts to expel her from various diamond operations in Africa and India, and to suppress her documentary.

While these chapters contain a measure of truth, some information is long out of date. Take the issue of child labor in India, for example. Until the mid-to-late 1980s, many children *did* work in India's diamond-cutting industry, particularly in the "informal" cutting sector, where families often took contract work from large operations. But after pressure from several Indian firms, De Beers, and Argyle, the practice was nearly—albeit not completely—ended. A 1996 study commissioned by the Indian government, which was not mentioned by the author, pegged the total of diamond workers under age 15 at 3%. The author claims it is 16% and rising, repeating an unproven 1995 charge by the Belgian diamond workers' union as her source.

The book also contains a number of instances of sloppy writing. For example, in relating how CRA (now Rio Tinto) allegedly bullied aboriginal peoples off the area that would be developed into Australia's Argyle mine, she claims that Ernest Oppenheimer directed a "spring offensive" to secure De Beers's control over marketing Argyle's diamonds. While De Beers certainly did employ tough business tactics in securing the Argyle contract in 1981, the policy was not led by Ernest Oppenheimer, who died in 1957. On page 165, in a chapter discussing synthetic diamonds, the

author refers to a proposed 1994 deal between General Electric Co. and "Zoroski" to market large, gem-quality laboratory-created diamonds. The company she meant to refer to was D. Swarovski & Co. The meetings reportedly did take place, but GE could not produce clean, white synthetics cheaply enough to make the venture profitable. And later in that same chapter, she comes up with some funny science regarding diamond origins and a baffling quote she attributes to GIA that allegedly appeared in a 1987 issue of *Diamond Intelligence Newsletter*: "[N]atural diamond cannot be distinguished from polished [diamonds] . . . using loupe or microscope."

It is unfortunate that a talented reporter with the guts to chase down interesting stories undercuts her own work with mistakes, bias, and diatribes. On this basis, the book cannot be recommended except as a reflection of the extreme distrust with which some people hold De Beers and the diamond industry.

RUSSELL SHOR
*Gemological Institute of America
Carlsbad, California*

OTHER BOOKS RECEIVED

Minerals of Nevada. *By Stephen B. Castor and Gregory C. Ferdock, 560 pp., illus., publ. by the University of Nevada Press, Reno, NV, 2003, US\$75.00.* This reference guide to Nevada's mineral wealth was written for mineral and gem collectors, prospectors, and exploration geologists. The catalog of minerals lists the more than 840 that have been found in the state and the places where they occur. The variety and quality of these minerals is illustrated in 102 color photos, most of them by noted photographer Jeff Scovil. Complementing the catalog is a series of essays on the history of mining in Nevada, its geology, and tips for collectors. Also included are an extensive bibliography and a foldout map of mining districts and important mineral occurrences.

STUART OVERLIN

Gemological ABSTRACTS

2004

EDITOR

A. A. Levinson
University of Calgary
Calgary, Alberta, Canada

REVIEW BOARD

Jo Ellen Cole
Vista, California

Claudia D'Andrea
GIA Gem Laboratory, Carlsbad

Vladislav Dombrovskiy
GIA Gem Laboratory, Carlsbad

Michelle Walden Fink
GIA Gem Laboratory, Carlsbad

R. A. Howie
Royal Holloway, University of London

Alethea Inns
GIA Gem Laboratory, Carlsbad

Taijin Lu
GIA Research, Carlsbad

Wendi M. Mayerson
GIA Gem Laboratory, New York

Kyaw Soe Moe
GIA Gem Laboratory, New York

Keith A. Mychaluk
Calgary, Alberta, Canada

Joshua Sheby
GIA Gem Laboratory, New York

James E. Shigley
GIA Research, Carlsbad

Boris M. Shmakin
Russian Academy of Sciences, Irkutsk, Russia

Russell Shor
GIA, Carlsbad

Maha Tannous
GIA Gem Laboratory, Carlsbad

Rolf Tatje
Duisburg University, Germany

Christina Taylor
Boulder, Colorado

Sharon Wakefield
Northwest Gem Lab, Boise, Idaho

COLORED STONES AND ORGANIC MATERIALS

Be-minerals: Synthesis, stability, and occurrence in metamorphic rocks. G. Franz and G. Morteani, Chapter 13 in *Beryllium: Mineralogy, Petrology, and Geochemistry*, Vol. 50 of *Reviews in Mineralogy and Geochemistry*, 2002, pp. 551–589.

Metamorphic rocks and associated pegmatites are important sources for both major (e.g., beryl, chrysoberyl) and minor (e.g., phenakite) beryllium minerals used as gems. This exceptionally thorough review article on Be minerals in these rocks contains data of importance to gemologists in two areas: (1) the synthesis of Be gems; and (2) the occurrence of, and exploration for, natural Be gem materials.

Be minerals, including those used for gems, have been synthesized since the mid-19th century in various simple (e.g., $\text{BeO-Al}_2\text{O}_3$) and more advanced (e.g., $\text{BeO-MgO-Al}_2\text{O}_3\text{-SiO}_2\text{-H}_2\text{O}$) systems by a variety of techniques (e.g., hydrothermal, flux, fusion, sintering). This article discusses the results of this experimental work and limitations of the various techniques, as well as the synthetic minerals formed under different experimental conditions (e.g., pressure and temperature) and their stability in various natural environments (e.g., in hydrous solutions). The authors report that synthetic Be minerals are currently being manufactured, for both gem and industrial uses, by at least a dozen companies in five countries (France, U.S., Japan, Australia, and Russia). Russian production dominates the market, with about 500,000 carats of synthetic emeralds produced annually.

The geologic settings and mineralogical characteristics of Be mineralization in regional metamorphic terrains and hydrothermal occurrences are varied. An overview is present-

This section is designed to provide as complete a record as practical of the recent literature on gems and gemology. Articles are selected for abstracting solely at the discretion of the section editor and his reviewers, and space limitations may require that we include only those articles that we feel will be of greatest interest to our readership.

Requests for reprints of articles abstracted must be addressed to the author or publisher of the original material.

The reviewer of each article is identified by his or her initials at the end of each abstract. Guest reviewers are identified by their full names. Opinions expressed in an abstract belong to the abstracter and in no way reflect the position of Gems & Gemology or GIA.

© 2004 Gemological Institute of America

ed for the occurrence, origin, and geochemical characteristics of typical emerald, chrysoberyl and phenakite deposits—where a combined metasomatic-metamorphic process is important. Schist-type emerald deposits, which are known on all continents (except Antarctica), receive particular attention. Gradations exist between these Be deposits and those classified as hydrothermal. The Colombian emerald deposits are classified as “metamorphic-hydrothermal” and are similarly discussed.

Several avenues for future research and field data gathering are suggested. For example, the authors recommend that a comprehensive database be established that includes descriptions of associated minerals at Be occurrences, along with the geologic setting (mainly the metamorphic overprint, if any). Such information could go a long way toward better prediction of occurrences and the economic potential of Be mineral deposits. *KAM*

New interpretation of the origin of tiger’s-eye. P. J. Heaney and D. M. Fisher, *Geology*, Vol. 31, No. 4, 2003, pp. 323–326.

The classic explanation for the origin of the chatoyancy in tiger’s-eye has been pseudomorphism (i.e., the replacement of one mineral by another with the retention of the earlier mineral’s shape). This was first proposed in 1873 and has been adopted uncritically by contemporary mineralogists and gemologists. Quartz was thought to replace preexisting fibrous crocidolite asbestos, and these quartz fibers were assumed to be the source of the chatoyancy. However, based on new crystallographic and textural studies, this hypothesis is challenged.

If crocidolite silicification occurs by a fiber-for-fiber substitution, then tiger’s-eye should be composed of the chalcedony variety of quartz—but this is not the case. These authors believe that the texture of tiger’s-eye is consistent with formation by a discontinuous crack-seal mechanism. This vein-filling process involves the cracking of a crocidolite-bearing host rock followed by the deposition of columnar quartz crystals from silica-saturated fluids. Simultaneously, overgrowth on the pre-existing crocidolite grains occurs; these crocidolite overgrowths are subsequently encapsulated by the columnar quartz. Thus, fibrous crocidolite, and not quartz, is the cause of chatoyancy in tiger’s-eye. *JEC*

Paraiba-Turmalin mit Inversfarbwechsel [Inverse color-change Paraiba tourmaline]. R. Schultz-Güttler, *Gemmologie: Zeitschrift der Deutschen Gemmologischen Gesellschaft*, Vol. 52, No. 1, 2003, pp. 25–30 [in German with English abstract].

Color-change gems commonly appear blue or green in daylight and violet to red in incandescent light. This article describes a color-change Paraiba tourmaline that is apparently the first and only known natural gem that exhibits an “inverse” color change. The 1.5 ct stone is “amethyst”-colored in daylight and “steel” blue in incandescent light.

Until now, this kind of color change has only been reported for Nd-doped synthetic materials. However, UV-Vis spectroscopy did not reveal any absorptions related to Nd or other rare-earth elements, but only, as expected, those of Mn^{3+} (at 510 nm) and copper (at 688, 896, and 1440 nm). While the spectrum of this stone resembles that of a typical Paraíba tourmaline, the intensity of the Mn^{3+} band at 510 nm is much stronger. The author suggests that its peculiar color change is probably a function of the relative absorption intensities of manganese and copper. *RT*

Peridot with new types of inclusions. S. V. Sokolov, S. A. Yarmishko, and A. V. Fedorov, *Gemological Bulletin*, No. 3, 2002, pp. 49–54 [in Russian with English abstract].

Gem-quality peridot is known from the Kovdor massif in the Kola Peninsula (Russia), a large topographic and structural feature composed of ultramafic alkaline rocks. The host rocks are magmatic, but they have undergone recrystallization as well as metasomatic and hydrothermal processes. The yellowish green peridot occurs in the center of large crystals of forsterite (Mg_2SiO_4 ; a member of the olivine group). Electron-microprobe analysis showed that the peridot contains 11.6–12.3% of the fayalite (Fe_2SiO_4) component. S.G. ranges from 3.32 to 3.39, and R.I. values are $\alpha=1.654$ – 1.656 ; $\beta=1.669$ – 1.672 ; $\gamma=1.689$ – 1.690 (birefringence=0.034–0.035). Two types of inclusions were observed. At magnifications of 15–30 \times , crystallized multiphase melt inclusions consisting of phlogopite, olivine, magnetite, shortite, dolomite, and bradleyite were documented. At magnifications less than 15 \times , prismatic crystals of apatite and sometimes needles of amphibole could be seen.

The Kovdor peridots were compared to those from the Kugla deposit, in the Krasnoyarsk district (Russia), which occurs in a massif with the same type of ultrabasic alkaline rocks. Similar melt inclusions (consisting of phlogopite, dolomite, calcite, magnetite, and Fe-Ni sulfides) were found in the Kugla peridots, but there were no apatite inclusions. The authors conclude that the inclusions found in peridots from different geologic occurrences (e.g., kimberlites, basalts, and partially serpentinized ultramafic rocks) are distinctive, and therefore it is possible to determine the geologic origin of a peridot from its mineral inclusions. *BMS*

Ruby and sapphire provinces [and belts] of the world. E. P. Melnikov and M. A. Viktorov, *Gemological Bulletin*, No. 3, 2002, pp. 18–25 [in Russian with English abstract].

Russian geologists have classified gem corundum deposits into 12 genetic types based on their worldwide geographic occurrence and the geology of these areas (e.g., tectonic features, igneous and metamorphic events, volcanism, rock types, ages of major rock units, and geologic origin of economic gem deposits) on global, regional, and local

scales. Three are "provinces" (covering hundreds of thousands to millions of square kilometers): (1) Southeast Asia—China, Vietnam, Laos, Cambodia, Thailand; (2) South Asia—Myanmar, India, Nepal, Pakistan, Tajikistan; and (3) Karelia-Kola in Russia. Six are "belts," which are smaller, and usually elongate with folded and faulted rocks; they are found in Australia, China, Russia (e.g., the Ural Mountains), East Africa (also including Madagascar and South Africa), West Africa, and Brazil. Three are "areas," which are even smaller units (measured in thousands of square kilometers): Nigeria, Colombia, and the U.S. (North Carolina and Montana).

All deposits described in this paper are grouped into "monogenic" and "polygenic" types. Monogenic deposits are magmatic, pegmatitic, or metasomatic, whereas polygenic deposits have a metamorphic or metamorphic-metasomatic origin.

All 12 types of gem corundum deposits are described with details and, where possible, using a representative deposit. For example, historical data, a description of the corundum crystals, production figures, future economic potential, geologic origin, and a geologic cross-section are presented for the Koltashi deposit in the Urals, which is representative of the Ural belt. Such information is of practical value to anyone who is searching for gem corundum deposits. BMS

DIAMONDS

About mechanism of the fibrous structure appearing in cubic diamond crystals [sic]. V. M. Sonin, D. G. Bagryantsev, A. I. Chepurov, and J. M. Dereppe, *Proceedings of the Russian Mineralogical Society*, Vol. 132, Part 2, 2003, pp. 95–98 [in Russian with English abstract].

The growth of diamond crystals at high pressure in the Fe-Ni-C system was studied in terms of a temperature decrease of $\sim 1\text{--}2^\circ/\text{sec}$. A morphological transformation in octahedral crystals occurred with the growth of numerous tiny cubic sub-individuals on their faces. This may represent the formation mechanism of natural cubic diamond crystals with a fibrous structure, whereby sectors of cubic growth become enlarged while the octahedral growth sectors are declining. The main cause of this change in the growth mechanism is the sharp increase of supersaturation in the crystallization media provided by the falling temperature. RAH

Assessing the diamond potential of kimberlites from discovery to evaluation bulk sampling. L. Rombouts, *Mineralium Deposita*, Vol. 38, No. 4, 2003, pp. 496–504.

The economic potential of a kimberlite must be correctly evaluated before diamond mining can begin. The evaluation procedure normally consists of four stages. Since

financial expenditures tend to increase by an order of magnitude at each successive stage, it is critical that the diamond potential be correctly appraised before a decision is made to proceed to the next stage.

The first stage occurs even before individual kimberlite bodies have been discovered, when the geochemistry of a suite of indicator minerals (in particular, that of the pyrope garnets) gives a rough idea of the diamond potential of an area. In the next stage, when the kimberlite body has been found, a few hundred kilograms of the kimberlite rock is sampled to recover sufficient numbers of microdiamonds to allow an extrapolation of the size distribution of commercial-sized diamonds and a rough estimate of the diamond grade (expressed as carats per tonne of kimberlite) of the deposit. If the results of this stage are positive, a limited bulk sampling program (~ 200 tonnes of kimberlite) should be carried out in the third stage to determine the commercial-sized diamond grade. The goal of the fourth stage is to obtain a parcel containing $\sim 1,000$ rough diamonds to estimate the average commercial value (expressed as US\$ per carat) for the entire deposit. The evaluation of both the diamond grade and the commercial value can be supported by statistical analysis. JES

Determination of the kinetic parameters of growth of a diamond crystal by its inner morphology. A. I. Glazov and N. V. Ezhak, *Proceedings of the Russian Mineralogical Society*, Vol. 132, No. 3, 2003, pp. 80–83 [in Russian with English abstract].

The UV fluorescence patterns shown by diamond crystals reveal their zonal structure. In this study, changes in the relative growth rates of the cubic and octahedral faces could be visualized by observing the luminescence patterns in successive planes through a diamond crystal. Luminescence spectra provided information on the nature and distribution of impurities, which were found to influence the changes in crystal habit. Such observations provide insight into the physical and chemical history of a diamond's formation. RAH

Polishing diamond—A matter of wear. Part I. J. Chapman, *Rough Diamond Review*, No. 2, September 2003, pp. 39–41.

Polishing is the most labor intensive of the operations that transform a rough diamond into a faceted gem. It proceeds primarily by abrasion, in which atoms are successively torn away from a diamond's surface. Understanding the abrasion mechanism and the factors that influence it provide opportunities to reduce the faceting time. Of the several factors affecting abrasion, orientation of the diamond's crystal axes relative to the polishing direction of a facet is the most critical, because there are significant variations in hardness in different crystal directions. Those directions along which a diamond can be polished are called the "grain." This article discusses how to determine the grain,

and explains the meaning of the terms *2-point*, *3-point*, and *4-point* planes used in diamond polishing, as well as the directional (i.e., greatly differing) cutting characteristics associated with each of these planes. MWF

GEM LOCALITIES

Edle Steine vom Dach der Welt [Precious stones from the roof of the world]. *extraLapis*, No. 24, 2003, 96 pp. [in German].

This issue of *extraLapis* covers the gem wealth of Afghanistan, Pakistan, and the Himalayas. Most of the contributions are written by Dr. Vera M. F. Hammer, curator at the Museum of Natural History in Vienna. They deal with the history of gem production and trade in this region from the days of Alexander the Great to the present; more specifically, they describe the different types of gem deposits, their products, and production methods. The topics include: garnets ("Garnets instead of grenades"); pegmatite minerals (including tourmaline and topaz, but also rare minerals such as viitaniemiite); the aquamarine pegmatites of Nagar; deposits of sapphire, ruby, and spinel (Kashmir, Jegdalek, Hunza); lazurite/lapis lazuli and afghanite from Badakhshan; and (coauthored with Andreas Weerth) the minerals of the alpine-type fissures from the Tormiq Valley of Pakistan.

Other contributors include Herb Obodda, who gives an interesting report of his difficult travels into the Karakoram Mountains and to the bazaars of Kabul and Peshawar since 1972. Drs. Bernhard Grasemann and Erich Draganits describe how the Himalayas and their gem deposits were formed by the collision of the Indian subcontinent with Asia. Andreas Weerth and Michael Huber have compiled maps and a listing of the 100 most important mineral deposits in the region.

While all articles—as usual for *extraLapis*—are lavishly illustrated, the centerpiece of the volume is a 20-page photo gallery of superb mineral and gem specimens ranging from afghanite to zoisite. Sheer beauty! RT

Gem quality petalite from Myanmar (Burma). K. K. Win and T. Themelis, *Australian Gemmologist*, Vol. 21, No. 10, 2003, p. 409.

A brief report is given of gem-quality, colorless crystals of petalite from a tourmaline-bearing pegmatite at Khet-chal, Molo District, Momeik, Shan State, Myanmar. They have refractive indices of $\alpha=1.505$ and $\gamma=1.516$, and a specific gravity of ~ 2.39 . The expected faint absorption band around 454 nm was not detected, but a weak orange glow was observed with long-wave UV radiation. Water-worn pebbles of petalite also are found that display a characteristic waxy luster. RAH

Lapis lazuli from Sar-e-Sang, Badakhshan, Afghanistan. W. Heflik and L. Natkaniec-Nowak, *Gemmologie*:

Zeitschrift der Deutschen Gemmologischen Gesellschaft, Vol. 52, No. 1, 2003, pp. 11–24.

The famous lapis lazuli mines at Sar-e-Sang in northern Afghanistan are among the most ancient gem sources in the world, with mining extending back thousands of years. The present study was undertaken to reexamine material from this occurrence with several modern analytical techniques. Detailed observations using both optical and scanning electron microscopes revealed the complex mineralogical and structural nature of the rock. Chemical composition obtained by EDXRF spectroscopy is presented for the rock's constituents, including phlogopite, diopside, scapolite, lazurite, and pyrite. In addition, chemical analysis of major, minor, and trace elements was carried out using the electron microprobe, instrumental neutron activation analysis, and ICP-MS techniques. The authors conclude that the Sar-e-Sang lapis lazuli is a product of contact metamorphism that occurred in stages as the result of the intrusion of granitic rocks into weakly metamorphosed sediments (thought to be clays and carbonates). JES

Precious corals in Hawaii: Discovery of a new bed and revised management measures for existing beds. R. W. Grigg, *Marine Fisheries Review*, Vol. 64, No. 1, 2002, pp. 13–20.

Precious corals were first discovered in the Hawaiian Islands in the early 1900s, but it was not until the 1960s that commercial quantities were found and exploited. However, the recovery of Hawaiian corals has experienced an on-and-off history since that time. The corals are found at depths of 380–475 m, necessitating the use of remote-controlled or submersible vehicles for their recovery. This article describes recent efforts, undertaken as part of an attempt to revive this fishery, to evaluate by deepwater surveys the occurrence of precious corals (pink, red, and "golden") at two locations—the Makapuu bed off of the eastern coast of Oahu, and the Keahole Point bed along the western coast of the big island of Hawaii. A new bed, located on the Cross Seamount about 250 km south of Honolulu, also is described. The maximum sustained annual yield for precious corals from the Hawaiian Islands is estimated to be about 1800 kg, an amount sufficient to supply a small local industry. However, several factors (weather constraints, deep recovery depths, and costs versus benefits of the legally required selective coral harvesting) continue to limit the profitability of this fishery. JES

Prospecting methods for coloured gemstone deposits in Kenya. C. Simonet and S. Okundi, *African Journal of Science and Technology, Science and Engineering Series*, Vol. 4, No. 1, 2003, pp. 44–55.

In most countries, finding colored stone deposits is a largely primitive operation involving small groups of miners using simple methods, such as direct observation of gem minerals in rock outcrops or in river alluvium, and often mere luck. Such methods are slow, random, and not

always effective. Little use is made of either geologic information or modern prospecting techniques (i.e., systematic test pitting, geophysical and geochemical sampling, and remote sensing). In Kenya, because of the dryness of the region, it is particularly difficult to locate secondary (alluvial) gem deposits.

Currently, most gem occurrences in Kenya are primary deposits of corundum, garnet, and tourmaline that occur in igneous or metamorphic rocks that may or may not be exposed at the ground surface. These occurrences typically occupy a small area (meters to tens or hundreds of meters), which is an important factor that determines the scale at which prospecting measurements or sampling should be undertaken. The authors discuss the potential benefits and drawbacks of several modern prospecting methods, and the record of their limited utilization in Kenya. They emphasize that the selection of the exploration method employed depends on the geologic characteristics of the particular deposit. The use of modern exploration techniques at the Kisoli deposit (in the Taita-Taveta district)—which has been mined for ruby, rhodolite, and tourmaline—is described. It is concluded that modern prospecting methods can greatly improve the likelihood for the discovery of minable gem deposits, both secondary (alluvial) and primary, in Kenya and other areas of East Africa. *JES*

Sandawana set to increase emerald supply to market. F. Marsh, *ICA Gazette*, August 2003, pp. 12–13.

For 45 years, Zimbabwe's Sandawana mines have been the source of highly prized, bright green, 1–4 mm emeralds, which have been marketed to the watch, jewelry, and luxury products industries. Currently, the mines produce 15–20 kg of rough per month; 25,000 rough stones are sorted each day. Although production has been steady, a great increase in the availability of Sandawana emeralds is possible if a large stockpile of ore containing emeralds over 8 mm is processed in the future. In addition, the separation plant is being upgraded to increase production (from one to five tons of ore per hour). A modern cutting factory in Harare produces excellent-quality calibrated sizes, some as small as 0.05 ct.

Recently, commercial quantities of tantalum (a valuable metal used in the medical and electronics industries) have become available as a byproduct of the mining operation at Sandawana, making it economically feasible to extract emerald-bearing ore at lower depths. There is also potential for mining both diamonds and platinum in the area, which—if this occurs—will significantly accelerate the development of the region. *JS*

Trace elements in Thai gem corundums. S. Saminpanya, D. A. C. Manning, G. T. R. Droop, and C. M. B. Henderson, *Journal of Gemmology*, Vol. 28, No. 7, 2003, pp. 399–415.

To gain insight into their geologic origin, the authors

compared the trace-element compositions of gem corundums from several areas in Thailand and Laos to those from well-documented deposits throughout the world (e.g., Scotland, South Africa, and Zimbabwe). Analyses were performed by LA-ICP-MS and electron microprobe for 15 elements: V, Ni, Ga, Fe, Mn, Cr, La, Ti, Sn, Si, Y, Ta, Nb, W, and Cu. Altogether, analyses (including some from the literature) were obtained for 491 samples: 307 from Thailand-Laos and 184 from the rest of the world.

The most notable finding was that Thai gem corundums fall into two discrete populations with regard to gallium and chromium. The sapphires are rich in Ga (up to 0.10 wt.% Ga₂O₃) and poor in Cr (<0.05 wt.% Cr₂O₃), whereas the situation for rubies is the reverse, as they are rich in Cr (up to 0.56 wt.% Cr₂O₃) and poor in Ga (<0.01 wt.% Ga₂O₃). Using these and the remaining trace-element data, the authors concluded that the genesis of both sapphires and rubies in Thailand is related to metamorphism. The fact that the rubies are high in Cr and poor in Ga suggests that they formed in a pre-existing metamorphic rock of mafic composition. The Ga-rich and Cr-poor sapphires are believed to have formed in a syenitic metamorphic rock that was metasomatized by a highly evolved fractionated magma. Both originated from sources at the base of the thick continental crust or in the upper mantle and were later carried to the surface in alkali magmas that erupted as basalts. Rubies are always found with sapphires in Thailand but are dominant in the eastern part of the country, whereas sapphires are dominant in the west. *WMM*

INSTRUMENTS AND TECHNIQUES

Limitations of the pavilion depth rapid sight estimates method. G. Holloway, *Australian Gemmologist*, Vol. 21, No. 10, 2003, pp. 400–403.

The "rapid sight" estimates method (see R. T. Liddicoat, Fall 1962 *Gems & Gemology*, pp. 323–335; and Winter 1962–1963 *Gems & Gemology*, pp. 365–375) is commonly used for estimating the pavilion depth of round brilliant cut diamonds. It is based on visually estimating the size of the table reflection relative to the actual table size; larger reflections indicate a deeper pavilion. This article reports that the method has the potential to mislead in certain cases. Specifically, pavilion depth is overestimated when the table size is larger, and underestimated when the crown angle and girdle are steeper and thicker, respectively. The "nail-head" is the only round brilliant with proportions from which pavilion depth can be accurately predicted using the rapid sight estimates method. Examples are presented of round brilliants with a range of proportion parameters (crown angles, table sizes, and girdle thicknesses) that support these conclusions; the maximum error in the pavilion depth in these examples was 2.6%. *MWF*

Out of the stone age: The impact of technology on the gem trade. D. A. Yonick, *AJM*, December 2002, pp. 41–47.

Although it has been notoriously slow to change, the gem industry is now permeated by technology—from mining to marketing. This article presents examples of the progress.

Diamond mining companies are leaders in applying technology and now evaluate and mine deposits with high-tech equipment and recovery systems, saving a lot of money in the process. Colored-stone mining companies have been slower to adapt technology, but Afgem, a vertically integrated South African company, provides an example of embracing modern technology at its tanzanite mines in Tanzania. As a result, it has achieved higher daily processing volumes and recovery with lower operating costs.

Gem-cutting technology based on computer software has demonstrated great potential in mass production. Golay and Swarovski, among others, have successfully used automated gem-cutting processes to facet cubic zirconia and other synthetic gems, as well as natural stones, in a variety of shapes and sizes. Others have used technology for concave faceting. In the realm of gem enhancement, increasingly sophisticated techniques require gemologists and gem laboratories to use advanced analytical methods to detect some treatments. These methods include LA-ICP-MS and SIMS, both of which require specialized expertise.

Companies are now able to market their products across the globe via the Internet with greatly reduced overheads, passing the savings on to the consumer. As Internet connections evolve, buyers will be able to see more 3-D images, as well as have the tools to judge a gem's appearance in various lighting environments, with different combinations of metals and stones. *MT*

To the issue of polished diamond color determination [A comparison of color grading methods for faceted diamonds]. A. M. Bocharov and T. V. Shirokikh, *Gemological Bulletin*, No. 4, 2002, pp. 32–36 [in Russian with English abstract].

The authors report on the color grading of polished diamonds, using synthetic standards (created by the Crystal Co. in Smolensk, Russia), both visually (with the aid of the CIELUV system) and with a spectrophotometer. The factors that influenced color grading by each method were related to various parameters.

Color grades obtained by visual determination were influenced by the nature of the light source, spectral characteristics of the paper on which the diamonds were placed, the quantity and range of standards, the physiological state of the observers, and the quality of the CIELUV system. Other factors influenced color grades obtained with a spectrophotometer. These included incident light reflected from the table back to the light source, the type and quality of the facets, and the nature and abundance of

inclusions. Further, the path length of the light through a faceted stone was significant, especially with fancy cuts. Several formulas are presented for determining colors, and their purity, in faceted diamonds, as well as the relationship between angles of incidence and resulting color.

BMS

Using XAFS, EDAX and AFM in comparative study of various natural and synthetic emeralds. P. Parikh, N. L. Saini, S. Dalela, D. M. Bhardwaj, S. Fernandes, R. P. Gupta, and D. B. Garg, *Nuclear Instruments and Methods in Physics Research B*, Vol. 499, 2003, pp. 489–493.

This paper outlines a pilot study using X-ray absorption fine structure (XAFS) spectroscopy, energy-dispersive analysis through X-ray (EDAX) spectroscopy, and atomic force microscopy (AFM) to distinguish between natural and synthetic (flux grown) emeralds. The natural emeralds studied were from Zambia, Brazil, and Zimbabwe. Measurements on all samples were performed on crystal faces parallel to the [0001] plane.

XAFS spectroscopy yielded information on the valence of the Cr ion and distances between atoms within the crystal structure. Most of the Cr in the synthetic emerald was found in the octahedral site (as Cr³⁺). EDAX measurements showed that variations in elemental composition existed on the (0001) surface in each crystal. Notable differences were found for Cr (higher in flux-grown synthetic emeralds) and Na and Mg (higher in natural emeralds but with significant variations among the samples). AFM determined the areal atomic density of the surface of the emeralds; it is much higher for the synthetic emeralds. The authors conclude that EDAX and AFM show promise for differentiating between synthetic and natural emeralds; they also acknowledge that the XAFS method is impractical for the gem industry. *AI*

JEWELRY RETAILING

The biggest of them all. G. A. Beres, *New York Diamonds*, Vol. 77, July 2003, p. 36.

Zale Corp. is the largest retail jewelry chain in the U.S., with 2,200 stores and \$2.2 billion in annual sales. The company has announced a “return to its core roots” by strengthening its bridal program, which accounts for 40–45% of its sales. Tied into its renewed emphasis on bridal pieces is a commitment to branded diamonds. The company has its own Zale Diamond solitaire program, a new and exclusive 73-facet Gordon's Diamond Solitaire, and, in Canada, its People's Diamond Solitaire, the latter featuring diamonds mined and cut in that country. Its up-market division, Bailey Banks & Biddle, offers the Linz Diamond, a modified princess cut.

Zales requires vendors to adhere to strict quality control standards, and to provide a substantial amount of

merchandise on memo. The new push to branded goods is part of the company's strategy to reduce its past reliance on clearance/promotional items and build sales volume. The company also plans to go more heavily into direct sourcing, further reducing its dealings with domestic suppliers, wholesalers, and importers. RS

The next big thing. E. Blauer, *New York Diamonds*, Vol. 77, July 2003, pp. 24–30.

The De Beers Diamond Trading Company (DTC) is putting substantial promotional resources behind the right-hand ring, a category of jewelry intended for a woman's "non-designated" hand. Rings represent 28% of diamond jewelry sales, with an average price of \$701. The potential market, according to DTC research, is an "unserved" niche of self-purchasing, mature women between 45 and 65 years old that, it is claimed, totals 77 million. The DTC sought designs that would set these products apart from other rings on the market, including "negative" (open) spaces, and a "vertical" orientation that runs parallel to the finger. The rings contain diamonds that weigh at least 20 points, and are being advertised in luxury, fashion, and epicurean magazines with the tag line, "Women of the world, raise your right hand." RS

Volume drives the market. G. A. Beres, *New York Diamonds*, Vol. 77, July 2003, pp. 32–40.

Major jewelry chains, department stores, discount stores, and TV shopping channels now have the greatest effect on the diamond market. These operations exert tremendous control over every part of the diamond jewelry pipeline. Their impact is felt most keenly in four areas:

- *Limiting the pricing power of suppliers.* Volume retailers often dictate price points and demand that suppliers meet them. In addition, they have kept polished prices from rising, even though the price of rough has increased substantially.
- *Driving supplies of certain categories of goods.* When high-volume buyers lock into particular size, quality, and shape categories, these diamonds can become scarce.
- *Forcing suppliers to offer favorable terms.* This is accomplished by demanding memo programs, extended payments, and liberal return privileges.
- *Dictating diamond jewelry styles to the rest of the market.* Major retailers heavily promote and stock such De Beers-backed favorites as the "Three Stone Ring." Conversely, they focus so strongly on a few basic, heavily advertised items that innovation is often stifled.

These volume retailers have achieved such power because diamond suppliers have acquiesced to their demands in exchange for huge orders. Suppliers who do try to toughen their terms generally find themselves losing business to others who will comply. RS

SYNTHETICS AND SIMULANTS

Comparison of the color of synthetic polished diamonds with the concentration of basic diamond lattice impurity defects. M. S. Gorbatova and V. G. Vins, *Gemological Bulletin*, No. 4, 2002, pp. 29–31 [in Russian with English abstract].

A representative collection of 37 synthetic diamond crystals grown in the Ni-Fe-C system with a BARS apparatus were visually classified as yellow (16 samples), orange-yellow (9), orange (8), and "lemon" yellow (4). They contained the following types of impurity defects: isolated nitrogen atoms in substitution positions, pairs of nitrogen atoms, and "732 nm" (nitrogen-nickel centers). Absorption spectra were measured in the range of 400–550 nm in order to determine the location of the so-called secondary band edge.

Correlations were observed between color and the abundance of defects, between color and band edge, and between the latter and the abundance of defects. Although the correlations showed significant variance, the authors were able to draw certain conclusions.

The color of the orange synthetic diamonds was most intense when the abundance of isolated nitrogen defects was highest and that of paired nitrogen defects was lowest. A shift of the band edge from 470 to 435 nm correlated to a change of color from bright orange to "lemon" yellow. In the majority of the orange synthetic diamonds, the 732 nm defect was absent, which deviates from results published previously by the second author. The orange color of these synthetic diamonds can be correlated to a band edge of 470 nm. BMS

Diamonds find a friend in the semiconductor sector. A. Eisenberg, *New York Times*, March 11, 2004, p. G5 (www.nytimes.com/2004/03/11/technology/circuits/11next.html).

The production of synthetic diamonds by the chemical vapor deposition (CVD) method is spreading rapidly, partly in response to demand from high-tech industries, where the products have great potential for use as semiconductors. Apollo Diamond Inc., of Boston, announced last year that it had developed a method to create large single-crystal synthetic diamonds using this low-pressure process. Researchers at the Carnegie Institution of Washington reported they too have succeeded in producing thick single crystals (about 5 mm thick and 10 mm wide) by the CVD process that are harder than natural diamonds.

While researchers are now able to grow CVD diamonds much more quickly and easily, they have not yet succeeded in turning them into usable semiconductors. The main difficulty is that pure synthetic diamonds are natural insulators and must be doped to improve their electrical properties. Doping with boron turns them into p-type (positive) semiconductors, but transistors and diodes also need n-type (negative) semiconductor materi-

al. The manufacture of n-type synthetic diamonds has proved elusive. The search continues for a doping agent that will integrate fully into the diamond structure and yield the requisite n-type behavior. RS

Gemological properties of synthetic flux spinel. V. A. Deeva and Y. B. Shelementiev, *Gemmological Bulletin*, No. 3, 2002, pp. 9–17 [in Russian with English abstract].

The gemological properties of 21 crystals of flux-grown synthetic spinel, a relatively new product from the “Gold Triangular” Co. (Novosibirsk, Russia), were determined and compared to those of 22 natural spinel crystals from the Mogok area (Myanmar). Most of the samples were red or “rose,” although a few of the synthetic spinels were blue or violet.

The morphology of both sets of crystals, as well as their specific gravities and optical properties, were identical. Their inclusions, however, were distinctly different. Flux inclusions were observed in 13 of the synthetic spinels; platinum inclusions were identified in four. Fifteen of the natural spinels had inclusions consisting of apatite, graphite, carbonate, and opaque minerals, as well as gas-liquid inclusions, usually as negative crystals. Because about one-third of the samples did not contain inclusions of any kind, the samples also were studied by more advanced methods.

The chemical compositions of all samples in the red and “rose” color range were essentially identical except for their Zn and V contents, both of which were higher in the natural spinels: ZnO = 0.12–0.42 wt.% vs. ≤ 0.02 wt.% and V₂O₃ = 0.12–0.29 wt.% vs. ≤ 0.05 wt.%. Blue synthetic spinels had distinctive contents of Fe, Co, and Ni. Differences also were observed in the absorption spectra, with a characteristic peak at 540 nm in the natural spinels and at 550 nm in the synthetic samples. The best method for distinguishing between the natural and synthetic spinels was photoluminescence spectroscopy. The identifying characteristics in the PL spectra between 670 and 710 nm are explained by slight differences in crystal structure imperfections. BMS

Oh, these imitations again! A. V. Fedorov, *Gemmological Bulletin*, No. 4, 2002, pp. 37–38 [in Russian with English abstract].

Russian simulants of malachite, lapis lazuli, sugilite, rhodochrosite, and “blue tiger’s-eye” are described, along with simple methods by which they may be distinguished from their natural counterparts.

The malachite simulant is made of a rock composed of gibbsite that has been artificially colored and compressed. It appears similar to malachite from the Democratic Republic of Congo, but under magnification it is easily recognized as a simulant by the absence of a silky texture. In addition, the S.G. of this simulant is low (1.92–1.93) compared to that of malachite (~3.95).

Lapis lazuli and sugilite imitations are both made of artificially colored magnesite and look very similar to natural stones. However, the color distribution is often uneven, with the coarse-grained areas or veinlets lighter colored and sometimes gray or even colorless. The S.G. of this simulant is 2.81–2.85, whereas lapis lazuli is ~2.75 and sugilite is ~2.74.

Some beads and pendants sold as rhodochrosite are actually a talc-calcite aggregate. Talc is the source of the pink color; Mn is not present in the calcite. The S.G. of this simulant is about 2.73; rhodochrosite’s is significantly higher (~3.60).

Two rough specimens of a bluish gray, translucent synthetic material were sold as “rodusite” (a Russian trade name for silicified riebeckite asbestos, known in some places as “blue tiger’s-eye”). This simulant exhibited melt features and was found to be synthetic forsterite (a Mg olivine).

The author warns potential purchasers of inexpensive stones and jewelry to beware of imitations. Generally, visual inspection and S.G. determinations are sufficient to recognize simulants. The determination of R.I. and other optical properties is difficult because of the small grain size of these simulants and, in most cases, an absence of flat facets. BMS

Research on hydrothermal aqueous solution adapted to grow emerald crystals. Z. Chen, W. Zhou, J. Zeng, H. Huo, and C. Zhang, *Journal of Synthetic Crystals*, Vol. 32, No. 3, 2003, pp. 267–271 [in Chinese with English abstract].

Various hydrothermal techniques for growing synthetic emerald crystals suitable for lasers (with potential to be used as gems) have been investigated extensively for several decades. However, results have generally been disappointing, owing to the low optical quality and small size of the crystals. This study investigated three alkali and six acid hydrothermal solutions from which higher-quality crystals could possibly be grown. As a first step, the solubility of emerald was determined in each of the several potential solutions by measuring the weight loss of crushed synthetic emerald grains following treatment in an autoclave at various temperatures and pressures.

All of the alkali solutions were found to be unsuitable for the growth of high-quality synthetic emerald crystals, owing to the ubiquitous presence of tiny synthetic quartz and phenakite (Be₂SiO₄) crystals that crystallize on their surfaces. Among the acid solutions, emerald had the highest solubility in the H₂SO₄ solution, followed by a mixed solution (H₂SO₄ + [NH₄]₂SO₄). Based on these data, high-quality synthetic emerald crystals were hydrothermally grown from a 2.2N H₂SO₄ solution at 500–600°C, and pressures of 152–202.6 MPa. The authors believe that most gem-quality hydrothermal synthetic emerald crystals are grown from similar acid solutions, although published data on such syntheses are lacking. TL

TREATMENTS

A busca pela cor perfeita. Diamantes coloridos artificialmente ganham espaço no mercado [In search of the perfect color. Artificially colored diamonds gain market share]. *Diamond News*, No. 10, 2002, pp. 5–9 [in Portuguese].

Koss Fancy Colored Diamonds uses radiation from an electron accelerator (rather than the better-known neutron bombardment), in some cases followed by annealing, to alter the color of natural diamonds. They produce colors such as blue, "sky" blue, green, "canary" yellow, "gold," "cognac," orange, and black that are stable and uniform. To address safety concerns, Koss submitted seven color-altered diamonds to the Israeli National Atomic Energy Commission's Soreq Nuclear Research Center, which determined that these irradiated diamonds presented no sign of residual radiation that might present a health hazard. *David Kondo*

MISCELLANEOUS

Carats and sticks: Pursuing war and peace through the diamond trade. M. Kaplan, *New York University Journal of International Law and Politics*, Vol. 35, No. 3, 2003, pp. 559–617.

This article provides a very detailed review of the civil wars in Angola, Sierra Leone, and the Democratic Republic of the Congo, which had been sustained by trade in diamonds. The author describes the developing theory that the majority of civil wars are fought, at least in Africa, over commodities, rather than because of ideological, religious, or cultural differences.

The article provides an exhaustive account of the Kimberley Process, in which rough diamonds are certified at the mine source or export origin to ensure that they proceed through legitimate channels and are not sold by agents of rebel groups to support conflicts. The author cites criticisms of the Kimberley Process from non-governmental organizations, such as Global Witness, which claim that the process is too dependent on the good faith of the industry and participating governments to be effective. Further, many in the industry remain opposed to the concept of outside monitoring, and a number of governments of diamond producing nations are too corrupt to be trusted to effectively certify the legitimate origins of their diamonds.

The author argues that independent monitoring of diamond certification is the best method of ensuring that the Kimberley Process accomplishes its purpose of stopping the trade in conflict diamonds. Only then can diamonds be an agent for peace and development. *RS*

Co-option in Siberia: The case of diamonds and the Vilyuy Sakha. S. A. Crate, *Polar Geography*, No. 26, No. 4, 2002, pp. 289–307.

This article examines how nuclear testing, mining (for diamonds and other commodities such as oil and gold), and industrial development (e.g., construction of hydroelectric dams) have adversely affected the environment of Russia's Sakha Republic and the lives of the Vilyuy Sakha people, non-Russians who for centuries have forged a subsistence living by raising horses and other livestock.

The Sakha Republic, which is the source of nearly all of Russia's diamond production, is twice the size of Alaska. Diamonds were discovered there in 1954. And like most other development projects of the Soviet era, no heed was paid to environmental consequences. Diamond mining activities have polluted the Vilyuy River with traces of thallium and other toxins. Thallium was part of a compound used to separate rough diamonds from the kimberlite ore. In addition, during the 1970s and 1980s, a series of 11 underground nuclear tests near the river basin killed off large tracts of forest and made the permafrost radioactive in the surrounding area.

Several initiatives to clean up diamond operations and to reverse environmental damage were attempted. One was a 1993 joint venture between the Sakha government and Almazy-Rossii-Sakha (Alrosa) to fund remedial environmental programs for the Vilyuy region, including decontaminating the drinking water. Funding was supposed to be provided by taking 2% of the diamond revenues. The venture, Sakha-Almaz-Proinvest (SAPI), proved ineffective for a number of reasons, and eight years later it was folded into a government agency. However, that agency has yet to finance water purification systems to remove thallium and other chemicals from the drinking water.

Another initiative, comprised of Vilyuy people, called the Vilyuy Committee, lobbied the press and government about the region's environmental problems. One member, Pyotr Martinev, who had worked in the region's diamond operations, spearheaded a drive to delay development of several newly discovered kimberlite pipes that were located near villages. Mr. Martinev demanded that the mining operators adopt environmentally safe extraction processes and fulfill their promise to dedicate a percentage of their revenues to Vilyuy inhabitants. However, he died of cancer in 1997, and many original members of the Vilyuy Committee have been replaced by representatives of local industries. The author concludes with a suggestion that the Vilyuy may be able to obtain redress by allying and coordinating efforts with the Russian Association of Indigenous Peoples of the North (RAIPON) to influence government and world opinion. *RS*